DEVELOPMENT OF INNOVATIVE BIOENGINEERING APPROACHES FOR THE REGENERATION OF DENTAL ENAMEL

A Thesis Submitted to the
College of Graduate and Postdoctoral Studies
In Partial Fulfillment of the Requirements
For the Degree of Doctor of Philosophy
In the Division of Biomedical Engineering
University of Saskatchewan
Saskatoon

By

FATEMEH MOHABATPOUR

© Copyright Fatemeh Mohabatpour, May, 2022. All rights reserved

Unless otherwise noted, copyright of the material in this thesis belongs to the author

PERMISSION TO USE

In presenting this thesis/dissertation in partial fulfillment of the requirements for a Postgraduate degree from the University of Saskatchewan, I agree that the Libraries of this University may make it freely available for inspection. I further agree that permission for copying of this thesis/dissertation in any manner, in whole or in part, for scholarly purposes may be granted by Prof. Petros Papagerakis, Prof. Daniel Chen, Prof. Silvana Papagerakis, the professors who supervised my thesis/dissertation work or, in their absence, by the Head of the Department or the Dean of the College in which my thesis work was done. It is understood that any copying or publication or use of this thesis/dissertation or parts thereof for financial gain shall not be allowed without my written permission. It is also understood that due recognition shall be given to me and to the University of Saskatchewan in any scholarly use which may be made of any material in my thesis/dissertation.

Requests for permission to copy or to make other uses of materials in this thesis/dissertation in whole or part should be addressed to:

Head of the Division of Biomedical Engineering
57 Campus Drive,
University of Saskatchewan
Saskatoon, Saskatchewan S7N 5A9 Canada

OR

Dean
College of Graduate and Postdoctoral Studies
University of Saskatchewan
116 Thorvaldson Building, 110 Science Place
Saskatoon, Saskatchewan, S7N 5C9 Canada

Abstract

Dental enamel is the hard tissue that covers the tooth crown that is incapable of endogenous regeneration, once damaged, due to the loss of enamel secreting cells (i.e., ameloblast) following the tooth eruption. The current treatment options, including artificial filling materials, are of temporary solutions. This greatly raises the need of approaches to regenerate enamel, which, however, remains unachievable nowadays. To address this emerging need, this thesis aimed to develop novel bioengineering approaches for the regeneration of enamel tissue. The specific objectives are to develop (1) lipid-based gene delivery systems for *Tbx1* encoding genes to dental epithelial cell line, HAT-7 cells, (2) an ionically cross-linkable bioink composed of alginate and carboxymethyl chitosan for bioprinting of HAT-7 cells, (3) a covalently cross-linkable hydrogel consisting of oxidized alginate and carboxymethyl chitosan with injectability and self-healing properties as a cell carrier to incorporate HAT-7 cells, for enamel formation *in vitro*.

The first objective was to prepare and characterize a non-viral gene delivery system for the transfer of plasmid DNA encoding *Tbx1*. First, we prepared and characterized lipid-based nanoparticles that were based on two different cationic lipids: glycyl-lysine-substituted gemini surfactants with the 16-carbon tail and 1,2-dioleoyl-3-trimethylammonium-propane with three varying the ratios of cationic lipid nitrogen to pDNA phosphate (N/P ratios: 2.5, 5 and 10). The physicochemical properties and biological activities of these nanoparticles were examined in terms of particle size and zeta potential, morphology, DNA protection, cytotoxicity, and gene expression, with the results illustrating that the gemini surfactant-based nanaoparticles with the N/P ratio of 5 is the optimal formulation among those examined. Then, HAT-7 was transfected with the optimal formulation and cultured in 2D and 3D, photo-cross linkable gelatin methacrylate hydrogels, culture systems; followed by the assessment of ameloblast differentiation and enamel formation by evaluating the expression of ameloblast markers and by using mineralization assays. Results showed that the HAT-7 cells transfected with *Tbx1* gene were able to robustly express secretory and maturation ameloblast markers, have higher calcium deposition, and form more extensive mineralized nodules compared to control cells.

The second objective was to develop a bioink consisting of alginate and carboxymethyl chitosan for the fabrication of 3D HAT-7 cell-laden constructs by using three-dimensional extrusion

bioprinting for enamel tissue engineering applications. Alginate and carboxymethyl chitosan were mixed at three different mixture ratios (2-4, 3-3- and 4-2) and printed as porous scaffolds while being ionically crosslinked in calcium chloride bath (100 mM). Then, the physico-mechanical and biological properties of the 3D printed scaffolds were characterized in terms of structural features, swelling and degradation behavior, mechanical properties, cell viability, cell morphology, and mineralization. Results indicated that alginate 4%-carboxymethyl chitosan 2% hydrogels showed higher viscosity, slower degradation rate, lower swelling ability and higher compressive mechanical properties. HAT-7 cells showed a high percentage of viability, maintained their morphology and secreted alkaline phosphatase.

The third objective was to develop injectable self-healing hydrogels based on oxidized alginate and carboxymethyl chitosan for the use as a carrier of the dental epithelial stem cells for enamel regeneration applications. First, alginate was modified through oxidation reaction and chemically characterized. Then, oxidized alginate and carboxymethyl chitosan were mixed at three varying weight ratios (4:1, 3:1, 2:1) and in situ crosslinking occurred through Schiff base reactions, which was confirmed by chemical characterization. The physico-chemical and biological properties of the hydrogels were assessed in terms of gelation time, swelling ratio, structural, injectability, self-healing, antibacterial properties, cell morphology and viability, mineral deposition. The results indicated that hydrogels with the higher weight ratio of oxidized alginate had faster gelation time and lower swelling ability. Hydrogels formed highly porous structures and showed injectability and self-healing abilities, as well as antibacterial properties against two cariogenic bacteria. HAT-7 cells were able to maintain a high cell viability, without being affected by injection pressure, and could maintain their morphology, deposit minerals and secrete alkaline phosphatase.

Taken together, this thesis presents the development of methods for bio-enamel formation *in vitro* based on gene therapy and tissue engineering principles. The combination of optimized lipid-based system for T-box1 gene delivery and the developed hydrogel-based scaffolds may provide a foundation to develop the optimal conditions for enamel regeneration *in vitro* and *in vivo*.

Acknowledgements

I would like to sincerely acknowledge my supervisors, Prof. Petros Papagerakis, Prof. Daniel Chen and Prof. Silvana Papagerakis for providing me with their valuable guidance and support and countless opportunities throughout my doctoral study. I am also thankful to my PhD advisory committee members, Prof. Ildiko badea, Dr. Brian F. Eames, and Prof. Venkesh Meda for their valuable advice and recommendations.

I would like to acknowledge the financial support from the university of Saskatchewan (through the University of Saskatchewan Dean's scholarship and Biomedical Engineering Devolved Scholarship) and from Saskatchewan Health Research Foundation (SHRF) and College of Dentistry start-up financial support (PI: Prof. Petros Papagerakis), College of Medicine start-up funds (PI: Prof. Silvana Papagerakis).

I would like to extend my appreciation to members of Profs. Papagerakis' lab, Prof. Chen's lab and Prof. Baeda's lab and the undergraduate students for their significant contributions to my PhD research via their support and guidance: Mays Al-Dulaymi, Liubov Lobanova, Zahra Yazdanpanah, Adam McInnes, Ibrahim Hoja, Xiaoman Duan, Dough Bitner, Serena Liu, Brittany Scutchings, Davin Truong, Abdul El-Rabbany.

I would like to thank Dr. Ning Zhu and Adam Web and other staff at Canadian Light Source for their support for synchrotron-based X-ray imaging.

Lastly, I would like to express my deep gratitude to my dear parents, and my kind sister and her family for their unconditional love, care, and support throughout my life and during my doctoral study.

TABLE OF CONTENT

LIST OF FIGURES

LIST OF ATABLES

LIST OF ABBREVIATIONS

Abbreviation	Explanation
ACP	Amorphous calcium phosphate
AI	Amelogenesis imperfecta
ALN	Alendronate
Alg	Alginate
Alp	alkaline phosphatase
Ambn	Ameloblastin
AMELX	Amelogenin
AMTN	Amelotin
AOT	Surfactant bis (2 ethylhexyl) sulfosuccinate sodium salt
ATR	Attenuated total reflectance
beta-TCP	Beta tricalcium phosphate
Bmal1	Brain and muscle ARNT-like 1
BMP	Bone morphogenic protein
BRGD-PA	Branched RGD-peptide amphiphile
$CaCl_2$	Calcium chloride
CaF_2	Calcium fluoride
Car2	Carbonic anhydrase 2
CLS	Canadian Light Source
CMC	Critical micelle concentration
CMC	Carboxymethyl chitosan
CPP–ACP	Casein phosphopeptide-stabilized amorphous calcium phosphate
CRAC	Ca^{2+} release-activated Ca^{2+} channel
Cry1	Cryptochrome 1
DEJ:	Dentino-enamel junction
DESCs	human dental epithelial stem cells
DOPE	1,2-dioleoyl-sn glycerol-3-phosphoethanolamine
DOTAP	1,2-dioleoyl-3-trimethylammonium-propane
DPSCs	Dental pulp stem cells

Dspp	Dentin sialophosphoprotein
EAER	Electrically accelerated and enhanced remineralization
ELD	Electrolytic deposition
EMPs	Enamel matrix proteins
Enam	Enamelin
EOE	Enamel organ epithelial
EPD	Electrophoretic deposition
ERM	Epithelial cell rest of Malassez
Fe_2O_3 NPs	Iron oxide nanoparticles
FGF	Basic fibroblast growth factor
fs	Femtosecond pulsed lasers
fTCP	functionalized tricalcium phosphate
FTIR	Fourier Transform Infrared
GK	Glycyl-Lysine dipeptide
GelMA	Gelatin methacrylate
GS	Gemini surfactants
HAp	Hydroxyapatite
HEDTA	N-(2-hydroxyethyl) ethylene-diamine-N,N',N'-triacetic acid
HERS	Hertwig's epithelial root sheath
^{1}HNMR	Proton nuclear magnetic resonance spectroscopy
H_2O_2	Hydrogen peroxide
IL-7	Interleukin-7
iPSCs	Induced pluripotent stem cells
KLK4	Kallikrein-4
Lamp1	Lysosomal-associated membrane protein
MMP20	Matrix metalloproteinase-20
MTT	3-(4, 5-dimethylthiazol-2-yl)-2, 5-diphenyltetrazolium bromide
MTs	Melatonin receptors
NaF	Sodium fluoride
NBCe1	Sodium bicarbonate so-transporter
OAlg	Oxidized alginate

OCP	Octacalcium phosphate
Odam	Odontogenic ameloblast-associated protein
Orai1	Calcium release-activated calcium channel protein 1
PA	Peptide amphiphiles
PAMAM	Poly (amido amine)
PAMAM-COOH	Carboxyl-terminated PAMAM
PBS	Phosphate buffered saline
PCR	Polymerase chain reaction
PDL	Periodontal ligament
PEG	polyethylene glycol
PEGDA	PEG diacrylate
PEI	polyethyleneimine
Per	Period circadian regulator
PGA	Polyglycolate
P/G/L	pDNA/gemini surfactant/ helper lipids
PLGA	Poly (lactide-co-glycolide)
PLLA	Poly-L-lactate
PVP	Poly (vinylpyrrolidone)
qRT-PCR	quantitative Reverse Transcription Polymerase Chain Reaction
RA	Retinoic acid
RGD	Arginine-glycine-aspartic acid (Arg-Gly-Asp)
RGDS	Arginine-glycine-aspartic acid- serine (Arg-Gly-Asp-Ser)
rP172	Recombinant full length amelogenin
Runx2	Runt-related transcription factor 2
SCAP	Stem cells residing in the apical papillae apical papillae
SDF	Silver diamine fluoride
SEM	Scanning electron microscopy
SHED	Stem cells from human exfoliated deciduous teeth
SR	Swelling ratio
Stim1	Stromal-interacting molecule
Tbx1	T-box1

TDIs	Traumatic dental injuries
TEM	Transmission electron microscopy
WDR72	WD repeat-containing protein 72
W_{di}	Initial dry weight
W_s	Swollen weight
W_{df}	Final dry weight

Chapter 1: Introduction

1.1. Tooth histology, damage and current treatments

Tooth is made up of three main structures consisting of enamel, dentin and pulp (Figure 1.1). Enamel is the external layer of tooth that covers the crown that protects tooth from being damaged by mechanical, thermal and chemical stimuli [1–3]. Enamel is produced by differentiated dental epithelial stem cells, ameloblasts, which are lost during tooth eruption which makes enamel incapable of self-repair [4,5]. Enamel is more mineralized than dentin and dental pulp and thus functions as a protective cover for them [2]; however, enamel is also very brittle and it can break without the support of underneath dentin tissue which is more soft and flexible [6]. Dentin is an avascular tissue and is formed by differentiated dental mesenchymal stem cells (MSCs), the odontoblasts. Dentin exhibits a limited capacity for self-regeneration since cells existing in dental pulp tissue are able to induce dentin formation, even after tooth eruption [6–8]. The consecutive and mutual interactions among dental mesenchymal and epithelial stem cells are essential for tooth development and enamel formation[9]. Dental pulp is a soft tissue surrounded by dentin and has several functions including dentin formation and repair, nourishing the dentin, providing sensitivity for dentin tissue by nerves [6].

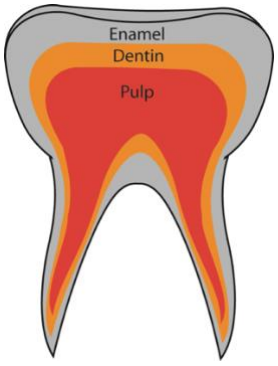

Figure 1.1. Tooth tissue is composed of three mains structures: enamel, dentin and pulp.

The functionality and vitality of the dental tissues can be destructively affected and even lost due to several incidents. Inherited disorders, periodontal disease, dental trauma, tooth decay, patient

neglect, poor oral health care or failure of prosthesis have been identified as leading causes of the damage or loss of dental tissues [8,10]. Amelogenesis imperfecta is a hereditary disorder which lead to enamel defects due to the disturbance of enamel development stages [11]. Dental caries as one of the most common infectious disease worldwide can be caused by acid production through cariogenic bacteria- sugar interactions which results in the demineralization of the dental enamel [12–15]. Dental trauma is the injuries that occur to enamel, dentin and pulp tissues due to incidents such as car accidents, sport injuries, physical activities and violence [16,17]. Tooth wear takes place when the mineralized substance of the tooth is lost due to the chemical and mechanical causes [18]. In addition, whole tooth loss, that was reported to affect 276 million people in the world, around 4.1% of global population, greatly reduces the quality life and overall health status of those affected [19].

The currently used methods for the clinical treatment of tooth damage or lost include fluoride therapy, dental restorative materials, endodontic therapy, auto- and allo-transplantation, and dental prosthesis. Fluoride therapy is a method that has been traditionally used to prevent or decrease the formation or promotion of dental caries; however, this method is more effective for the superficial carious lesions and the high concentration usage of fluoride could result in adverse side effects fluorosis [20,21]. Dental restorative materials including amalgam and composite resins have been commonly used to replace the lost or diseased dental tissues, even for deep carious lesions, to recover tooth functions [22]; however, tooth preparation for the replacement of dental tissues with dental fillings is invasive and needs several sittings, and they can be failed over time due to shrinkage, leakage or secondary cavity formation, which needs the replacement of the failed restoration materials [23]. Also, the restorative materials are not able to completely replicate the structural and functional properties of the tooth [24]. Endodontic therapy involves the removal of the infected or necrotic pulp followed by filling the root canals of the tooth with rubber-like materials. Although this method prevent bacteria to reinfect the tooth after treatment, the endodontically treated tooth loses its sensitivity and vitality and becomes brittle and incapable of responding to infections and sensing the irritation, which might lead to caries progression and even tooth extraction [10,25,26]. Tooth allotransplantation that involves the transplantation of a tooth from one person to another has become obsolete owing to histocompatibility issues and it was substituted with auto-transplantation [27]. On the other hand, dental auto-transplantation, that is

the transplantation of a tooth from one site to another in the same person, could potentially be adjusted to the jaw growth and thus considered a good option for restoring lost tooth in young-aged patients; nevertheless, it can cause donor site morbidity, blood loss and pain after the harvesting procedure [10,27]. Dental prostheses including implants, crown and bridges are used as a common practice for the replacement of lost dental tissues and they are able to only repair the dental tissues and not regenerate them and they often do not provide the same level of physiological functioning, durability and aesthetics as natural tooth [8]. Also, implants were found to be incapable of adjusting to the jaw growth that is of great importance for young-aged patients [27]. To overcome the aforementioned limitations associated with the current treatment approaches, novel materials and methods are required to improve the prevention and outcome of the treatments for tooth damage and loss.

1.2. Tooth tissue engineering

Tissue engineering as a newly emerging approach in modern medicine offers promises for developing the bioengineered tooth or tooth parts that can replace the currently used dental materials revolutionizing treatment options. Tissue engineering uses a combination of dental stem cells, scaffolds and signaling factors to regenerate either the whole tooth, or the individual parts of the tooth such as enamel, dentin, and dental pulp [10,28]. Stem cells that are undifferentiated cells can be obtained from dental or non-dental origins and be employed in tooth tissue engineering [29]. Dental epithelial stem cells (DESCs), periodontal ligament stem cells (PDLSCs), dental pulp stem cells (DPSCs), stem cells from human exfoliated deciduous teeth (SHED), stem cells from the apical papilla (SCAP) and dental follicle stem cells (DFSCs) are dental stem cells that have been identified to be used for tooth regeneration [30,31].

Scaffolds are 3D constructs that are designed to provide structural support that guides new tissue formation. For functional tissue engineering, scaffolds need to mimic the extracellular matrix of the natural tissue, have proper cell interaction properties, offer mechanical integrity, be biocompatible and biodegradable, and support cell functions such as adhesion, proliferation, and differentiation [24,32,33]. Scaffolds materials can be categorized into two main groups of natural and synthetic, both of which have been used for tooth tissue engineering [28]. Natural biomaterials (e.g., alginate, collagen, gelatin, chitosan) are compatible with cells and tissues and support cell

functions, but they have the risk of immunogenicity and cross-contamination from the source, and poor mechanical properties [34,35]. Synthetic biomaterials (e.g., ***p***olylactic acid (PLA), polyglycolic acid (PGA), poly (lactic-co-glycolic acid) (PLGA) and polycaprolactone (PCL)) have well-defined chemical structures and offers adjustable physicochemical properties and do not have the risk of immunogenicity that natural biomaterials have; however, they often lack biological activity to support cell functions [34,36,37]. Tooth and its surrounding supporting tissues have very complex anatomical structures with anisotropic mechanical characteristics and multicellular interactions; in addition, the growth factors are distributed heterogeneously that are all essential for proper function of dental tissues. Thus, conventional scaffold fabrication techniques such as porogen leaching and electrospinning are not able to mimic these complexities of dental tissues [38].Three dimensional (3D) printing allows fabrication of scaffolds with personalized anatomical designs and the desired shape, size and microarchitectures based on a computer-aided design (CAD) converted from x-rays, MRI or CT scans [39–41]. This technique also offers more control over porosity of the scaffolds and enables incorporation of living cells and growth factors in the construct [42,43]. 3D printing has been successfully used to fabricate scaffolds for regeneration of dental tissues including on periodontal (PDL) [44–46], dental bone [42] and also dentin [47–49]. The mixture of hydrogel and living cells (also called bioink in the literature) are used to fabricate 3D printed cell-laden constructs. However, there is a significant shortage of bioinks with desirable printability, mechanical and biological properties, particularly for tooth tissue engineering [50]. Injectable hydrogels have exhibited a remarkable potential application as carrier systems for cell or biomolecules in regenerative medicine [51–53]. They can be applied in a minimally invasive manner and are able to fill complex-shaped defects, that is particularly beneficial for dental defects with irregular size and shape [54–56]. However, the conventional injectable hydrogels often need the chemical crosslinkers to become gelled that can be toxic to cells. Also, hydrogels without self-healing ability have the susceptibility to be damaged under mechanical forces leading to losing their integrity in terms of their structural and functional properties, and inability to protect cells from mechanical damage, which could result in cell death or loss [57,58]. This resulted in the emergence of a new generation of hydrogels that possess injectability and self-healing characteristics to meet the requirements for cell/drug carriers [58,59]. Notably, the application of injectable self-healing hydrogels has not been explored for dental tissue regeneration. One aim of

*t*his thesis is to address these emerging needs for bioinks and injectable self-healing hydrogels for dental enamel regeneration.

1.3. Gene therapy

A wide variety of transcription factors (e.g. Runt-related transcription factor2 (Runx2), T-box transcription factor 1 (Tbx1), LIM homobox transcription factor-6, -7 (Lhx6, 7), paired box-9 transcription factor (Pax-9)) and growth factors (e.g. bone morphogenic proteins (BMPs), fibroblast growth factors (FGFs), transforming growth factors (FGFs), Hedgehog (Hh)) have been recognized to be expressed and play key roles during natural tooth development [10,60,61]. Therefore, design and development of multifunctional scaffolds that can act as localized delivery systems for signaling molecules and cells, in addition to their role as the structural support for tissue formation, can improve the efficiency of dental tissue engineering techniques [10]. However, growth factors often have short half-lives, they can undergo denaturation while being encapsulated, supraphysiological concentrations of growth factors, or even a combination of growth factors, might be required to produce the desired stimulation, they can be expensive and time-consuming [10,62]. Gene therapy can be integrated into tissue engineering with the aim of addressing challenges associated with using proteins and enhancing the expression of key factors that induct and guide tissue formation or suppress the expression of factors that have inhibitory effects, thereby modulating the differentiation of dental stem cells; in addition, the protein expression provided via gene delivery can last longer and be at sufficient concentrations [10,63]. Therefore, delivery of genes encoding transcription or growth factors, either from tissue engineering scaffolds or from viral/nonviral gene carriers, is a promising approach for dental tissue regeneration.Gene therapy is a method through which genes, either DNA or RNA, are transferred into cells to change the expression of the genes causing diseases or enhancing certain biological functions [64]. For tissue engineering applications, the gene of interest is able to express molecules such as growth factors, transcription factors and extracellular matrix components which are involved in the regenerative process of the tissues [65].

There are two different approaches for the delivery of the vectors: ex vivo and in vivo (Figure 1.2). In ex vivo technique, cells are isolated from the patient's body and cultured and then genetically modified using transfection with vectors and then re-injected into the body after selection and

amplification. Ex vivo approach can selectively target certain groups of cells to deliver the desired gene before transplantation of cells into the patient's body. This is in spite of the fact that in this method cells should be able to divide and therefore some cell populations which are postmitotic including neurons are not able to be targeted using this technique. In addition, transplantation of cells is more invasive compared to direct injection of gene vectors into the body in in vivo gene therapy. In in vivo approach, either vectors are directly entered into the patient's body, or they are attached to the scaffold and then implanted into the body. Although in vivo gene therapy is minimally invasive, simple, there are some limitations associated with this technique such as non-specific targeting of cells, inefficient gene delivery, cytotoxicity and immunoreaction [66,67]. For dentin/pulp regeneration, in vivo technique seems to be more effective when there is an adequate number of viable and non-infected cells, while ex vivo method can be employed when substantial inflammation exists [68]. Owing to the absence of ameloblasts in mature enamel in the erupted tooth, only ex vivo technique can be employed in which dental epithelial stem cells, derived from other sources such as epithelial rests of Malassez, are transfected with the gene of interest and then they are implanted in vivo. However, recognizing the importance and sufficiency of a gene or a combination of genes and choosing these genes to induce ameloblast differentiation and enamel formation through gene delivery approaches might be challenging in this area. Currently, there is a remarkable shortage of gene delivery systems that are primarily designed for the regeneration of dental tissues, particularly enamel. To address this knowledge gap, this study aimed to develop lipid-based nanoparticles to investigate the effect of the delivery of a gene encoding an ameloblast differentiation-inducing factor on enamel formation.

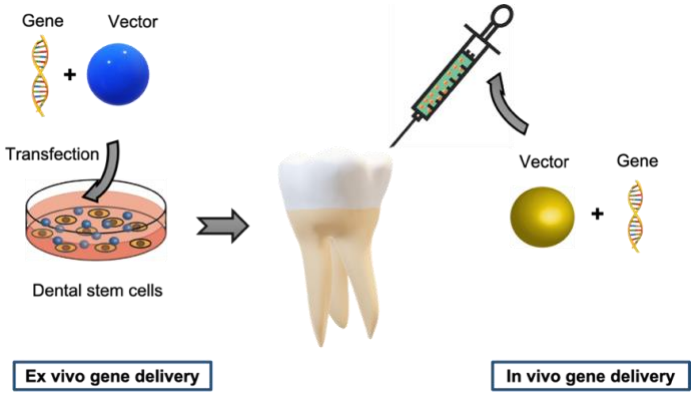

Figure 1.2. In vivo and ex vivo delivery of gene vectors.

1.4. Research objectives

By addressing the aforementioned research issues, the research presented in this thesis aimed to develop bioengineering approaches based on gene therapy and tissue engineering principles for the regeneration of dental enamel. The specific objectives of this study are presented as follows.

1. To develop a lipid-based gene delivery system for the transfer of a gene encoding T-box transcription factor 1 (*Tbx1*), which is a strong inducer of ameloblast differentiation, into a rat dental epithelial stem cell line, HAT-7 cells, for the guidance of these cells towards ameloblast differentiation and enamel formation *in vitro*. The planned research activities are to

    - Examine the effect of lipid composition and the ratio of cationic lipid nitrogen to pDNA phosphate (N/P ratio) on phsysico-chemical and biological performances of the lipid-based nanoparticles including particle size and zeta potential, morphology, DNA compaction and protection, cytotoxicity, and gene expression.
    - Investigate into the effect of *Tbx1* gene delivery (using the optimal formulation) on ameloblast differentiation, mineralization, and enamel-like tissue formation in two- and three-dimensional cell culture systems.

2. To develop a novel bioink composed of alginate and carboxymethyl chitosan with favorable properties for bioprinting of HAT-7 cells for enamel tissue engineering applications *in vitro*. Alginate is the most commonly used materials as bioink owing to the fast crosslinking with divalent ions. However, alginate has slow degradation rate and limited ability to interact with cells and support cell functions [69]. In addition, there is a lack of available bioinks that have been characterized primarily for dental tissue engineering. The planned research activities are to

    - Prepare the bioink with varying concentrations of alginate and carboxymethyl chitosan and then print it to create scaffolds.
    - Characterize the physico-mechanical properties of the printed scaffolds in terms of structure, swelling and degradation behavior.
    - Examine the biological performances of HAT-7 cells in the printed scaffolds in terms of call viability, morphology and mineral deposition.

3. To develop an injectable hydrogel system consisting of oxidized alginate and carboxymethyl chitosan as a cell carrier for enamel tissue engineering applications *in vitro*. The development of injectable hydrogels with appropriate structures and properties has been a challenging task, leaving many to be desired in terms of cytocompatibility, antibacterial and self-healing properties, and the ability to support dental stem cell functions. The planned research activities are to

- Synthesize and characterize the oxidized alginate that is a derivative of alginate with the ability to become covalently crosslinked with amino containing carboxymethyl chitosan.
- Prepare the covalently crosslinked hydrogels with three different weight ratios of oxidized alginate and carboxymethyl chitosan, and characterize them in terms of gelation time, swelling ratio, structural, injectability, self-healing, antibacterial properties,
- Assess the biological performances of HAT-7 cells in the self-crosslinked hydrogels in terms of call viability, morphology and mineral deposition.

1.5. Organization of this thesis

This dissertation is organized into six chapters including this chapter (**Chapter 1**), as an introduction, and four other chapters that are prepared in the form of manuscripts, and a final chapter presenting conclusions drawn from this research, along with the suggestions for future studies in the directions of this research.

Chapter 2 presents a comprehensive literature review on cell-free and cell-based approaches that have been under development for remineralization, regeneration, and repair of dental enamel tissue. In the first part of this chapter, the structure, properties, and development of dental enamel are discussed. Then, the second part discusses the clinical aspects that are required to be considered when designing and establishing new therapeutic methods for enamel regeneration. In the third section, the acellular approaches (including chemical solutions, electrodeposition, synthesis of artificial hydroxyapatite, laser-assisted mineralization, electrically accelerated and enhanced remineralization, immunization, organic matrix mimicking approaches) by which enamel is tried to be artificially synthesized or mineralized are described. In the next section, different cell sources that are available to be used for enamel tissue engineering and cell-based strategies, that can mimic

the natural enamel development process more precisely as compared to acellular techniques are explained. In the cellular approaches, epithelial cells can be stimulated to produce the enamel matrix using scaffold-free (including ameloblast differentiation-inducing factors, co-culture systems, microfluidic systems, chrono-dentistry) or tissue engineering techniques. In addition, the challenges that currently exist in the area of enamel regeneration and future perspectives are discussed for further studies in this field.

Chapter 3 describes the development of lipid-based systems to deliver *Tbx1*-encoding gene into HAT-7 cells to guide them towards differentiation into enamel secreting ameloblasts. Lipid-based nanoparticles were first prepared by using two different cationic lipid compositions: glycyl-lysine-substituted gemini surfactants with the 16-carbon tail and 1,2-dioleoyl-3-trimethylammonium-propane (DOTAP) at three selected nitrogen to phosphate ratios. The optimal formulation for *Tbx1* gene delivery was selected based on the physico-chemical and biological characterization of lipid nanoparticles and then used to transfect HAT-7 cells to induce ameloblast differentiation. *Tbx1*-transfected HAT-7 cells were then cultured in conventional two-dimensional cell culture systems and the photo-cross-linkable hydrogel, gelatin methacrylate and were allowed to differentiate. Then, the expression of ameloblast markers and mineralization were examined to investigate the effect *Tbx1* gene delivery on enamel-like tissue formation.

Chapter 4 presents the development of a bioink containing a blend of alginate and carboxymethyl chitosan for bioprinting of HAT-7 cell-laden hydrogel constructs for enamel regeneration applications**.** Hydrogel scaffolds were fabricated with three different concentrations of alginate to carboxymethyl chitosan using an extrusion-based bioprinting technique. Hydrogel solutions were crosslinked in the calcium chloride solution while printing, followed by further crosslinking in a higher concentration of calcium chloride solution after printing. The 3D printed scaffolds were characterized by examining their structural properties, swelling degree, degradation rate, mechanical properties. In addition, the viability and morphology of HAT-7 cells in 3D printed alginate-carboxymethyl chitosan hydrogel scaffolds and alkaline phosphatase production within the cell-laden constructs were assessed.

Chapter 5 describes the development of a self-cross-linkable hydrogel as an injectable self-healing cell carrier for potential use in enamel regeneration applications. First, oxidized alginate

was synthesized and characterized. Then, hydrogels were prepared by mixing oxidized alginate with carboxymethyl chitosan at three weight ratios. The formation of Schiff base linkages that led to covalent crosslinking between oxidized alginate and carboxymethyl chitosan was verified by chemical characterization of hydrogels. The effect of weight ratio of oxidized alginate to carboxymethyl chitosan on swelling ratio and gelation time was also investigated. The structural, injectability, self-healing properties of the hydrogels were assessed. In addition, the antibacterial activity of the hydrogels was tested against two cariogenic bacteria: *Streptococcus mutans* and *Streptococcus sobrinus*. HAT-7 cells were encapsulated in the hydrogels and cell viability and morphology, alkaline phosphatase production and calcium deposition were investigated.

Chapter 6 summarizes the conclusions drawn from this research and discusses the recommendations for future studies.

1.6. Contributions of the primary investigator

The manuscripts included in this dissertation are co-authored and the contributions of all authors are greatly appreciated and acknowledged. However, it is the mutual understanding of all authors that Fatemeh Mohabatpour, as the first author, is the primary contributor of the experimental research work included here.

References

[1] A. Gupta, Dental Biochemistry, in: Compr. Biochem. Dent., Springer, 2019: pp. 595–604.

[2] R.S. Lacruz, S. Habelitz, J.T. Wright, M.L. Paine, Dental enamel formation and implications for oral health and disease, Physiol. Rev. 97 (2017) 939–993.

[3] A.H. Carreon, P.D. Funkenbusch, Nanoscale properties and deformation of human enamel and dentin, J. Mech. Behav. Biomed. Mater. 97 (2019) 74–84.

[4] B. Jayasudha, H.K. Navin, K.B. Prasanna, Enamel regeneration-current progress and challenges, J. Clin. Diagnostic Res. JCDR. 8 (2014) ZE06.

[5] A.L. Kierszenbaum, L. Tres, Histology and Cell Biology: an introduction to pathology E-Book, Elsevier Health Sciences, 2015.

[6] A. Nanci, Ten Cate's Oral Histology Development, Structure, and Function, 8/e, Elsevier

India, 2012.

[7] G.T.-J. Huang, Dental pulp and dentin tissue engineering and regeneration–advancement and challenge, Front. Biosci. (Elite Ed). 3 (2011) 788.

[8] E. Battistella, S. Mele, L. Rimondini, Dental tissue engineering: a new approach to dental tissue reconstruction, in: Biomimetics Learn. from Nat., InTech, 2010.

[9] E.P. Chalisserry, S.Y. Nam, S.H. Park, S. Anil, Therapeutic potential of dental stem cells, J. Tissue Eng. 8 (2017) 2041731417702531.

[10] N. Monteiro, P.C. Yelick, Advances and perspectives in tooth tissue engineering, J. Tissue Eng. Regen. Med. (2016).

[11] W.K. Seow, Developmental defects of enamel and dentine: challenges for basic science research and clinical management, Aust. Dent. J. 59 (2014) 143–154.

[12] N. Tinanoff, Dental caries, in: Pediatr. Dent., Elsevier, 2019: pp. 169–179.

[13] Maintaining and Improving the Oral Health of Young Children, Pediatrics. 134 (2014) 1224 LP – 1229. https://doi.org/10.1542/peds.2014-2984.

[14] T. Walsh, H. V Worthington, A. Glenny, V.C.C. Marinho, A. Jeroncic, Fluoride toothpastes of different concentrations for preventing dental caries, Cochrane Database Syst. Rev. (2019).

[15] J.D.B. Featherstone, Dental caries: a dynamic disease process, Aust. Dent. J. 53 (2008) 286–291.

[16] H.C. Güngör, Management of crown-related fractures in children: an update review, Dent. Traumatol. 30 (2014) 88–99.

[17] S.S. Chandra, E. Choudhary, S. Chandra, Traumatic injuries to permanent anterior teeth among Indians: frequency, aetiology and risk factors., Endod. Pract. Today. 8 (2014).

[18] E.-J. Muts, H. van Pelt, D. Edelhoff, I. Krejci, M. Cune, Tooth wear: a systematic review of treatment options, J. Prosthet. Dent. 112 (2014) 752–759.

[19] J. Aida, Tooth Loss, in: M.A. Peres, J.L.F. Antunes, R.G. Watt (Eds.), Oral Epidemiol. A Textb. Oral Heal. Cond. Res. Top. Methods, Springer International Publishing, Cham, 2021: pp. 223–233. https://doi.org/10.1007/978-3-030-50123-5_13.

[20] A.C.B. Delbem, M. Bergamaschi, K.T. Sassaki, R.F. Cunha, Effect of fluoridated varnish and silver diamine fluoride solution on enamel demineralization: pH-cycling study, J. Appl. Oral Sci. 14 (2006) 88–92.

[21] K.G. Chhabra, P.J. Shetty, K.V. V Prasad, C.S. Mendon, R. Kalyanpur, The beyond measures: Non flouride preventive measures for dental caries, J Int Oral Heal. 3 (2011) 1–8.

[22] K.J. Chun, J.Y. Lee, Comparative study of mechanical properties of dental restorative materials and dental hard tissues in compressive loads, J. Dent. Biomech. 5 (2014).

[23] M. Kakkar, An alternative to filling and drilling-EAER, Int J Res Heal. Allied Sci. 2 (2016) 32–34.

[24] G.M. Ahmed, E.A. Abouauf, N. AbuBakr, C.E. Dörfer, K.F. El-Sayed, Tissue Engineering Approaches for Enamel, Dentin, and Pulp Regeneration: An Update, Stem Cells Int. 2020 (2020).

[25] L. Tan, J. Wang, S. Yin, W. Zhu, G. Zhou, Y. Cao, L. Cen, Regeneration of dentin–pulp-like tissue using an injectable tissue engineering technique, RSC Adv. 5 (2015) 59723–59737.

[26] K.S. Tan, V.S.H. Yu, S.Y. Quah, G. Bergenholtz, Rapid method for the detection of root canal bacteria in endodontic therapy, J. Endod. 41 (2015) 447–450.

[27] T. Nimčenko, G. Omerca, V. Varinauskas, E. Bramanti, F. Signorino, M. Cicciù, Tooth auto-transplantation as an alternative treatment option: a literature review, Dent. Res. J. (Isfahan). 10 (2013) 1.

[28] S. Sharma, D. Srivastava, S. Grover, V. Sharma, Biomaterials in tooth tissue engineering: a review, J. Clin. Diagnostic Res. JCDR. 8 (2014) 309.

[29] A.H.-H. Yen, P.T. Sharpe, Stem cells and tooth tissue engineering, Cell Tissue Res. 331 (2008) 359–372.

[30] M.M. Steindorff, H. Lehl, A. Winkel, M. Stiesch, Innovative approaches to regenerate teeth by tissue engineering, Arch. Oral Biol. 59 (2014) 158–166.

[31] C. Morsczeck, G. Schmalz, T.E. Reichert, F. Völlner, K. Galler, O. Driemel, Somatic stem cells for regenerative dentistry, Clin. Oral Investig. 12 (2008) 113–118.

[32] L. Zhang, Y. Morsi, Y. Wang, Y. Li, S. Ramakrishna, Review scaffold design and stem cells for tooth regeneration, Jpn. Dent. Sci. Rev. 49 (2013) 14–26.

[33] C.L. Granz, A. Gorji, Dental stem cells: The role of biomaterials and scaffolds in developing novel therapeutic strategies, World J. Stem Cells. 12 (2020) 897.

[34] K.M. Galler, R.N. D'Souza, J.D. Hartgerink, Biomaterials and their potential applications

for dental tissue engineering, J. Mater. Chem. 20 (2010) 8730–8746.

[35] S. Prasadh, R.C.W. Wong, Unraveling the mechanical strength of biomaterials used as a bone scaffold in oral and maxillofacial defects, Oral Sci. Int. 15 (2018) 48–55.

[36] M.B. Rahmany, M. Van Dyke, Biomimetic approaches to modulate cellular adhesion in biomaterials: A review, Acta Biomater. 9 (2013) 5431–5437.

[37] B. Guo, P.X. Ma, Synthetic biodegradable functional polymers for tissue engineering: a brief review, Sci. China Chem. 57 (2014) 490–500.

[38] Y. Ma, L. Xie, B. Yang, W. Tian, Three-dimensional printing biotechnology for the regeneration of the tooth and tooth-supporting tissues, Biotechnol. Bioeng. 116 (2019) 452–468.

[39] C.L. Ventola, Medical applications for 3D printing: current and projected uses, Pharm. Ther. 39 (2014) 704.

[40] P.C. Yelick, P.T. Sharpe, Tooth bioengineering and regenerative dentistry, J. Dent. Res. 98 (2019) 1173–1182.

[41] C.R. Silva, M. Gomez-Florit, P.S. Babo, R.L. Reis, M.E. Gomes, 3D functional scaffolds for dental tissue engineering, in: Funct. 3D Tissue Eng. Scaffolds, Elsevier, 2018: pp. 423–450.

[42] J. Park, S.J. Lee, H.H. Jo, J.H. Lee, W.D. Kim, J.Y. Lee, A. Su, Fabrication and characterization of 3D-printed bone-like β-tricalcium phosphate/polycaprolactone scaffolds for dental tissue engineering, J. Ind. Eng. Chem. 46 (2017) 175–181.

[43] L. Ning, X. Chen, A brief review of extrusion-based tissue scaffold bio-printing, Biotechnol. J. (2017).

[44] J.H. Kim, C.H. Park, R.A. Perez, H.Y. Lee, J.H. Jang, H.H. Lee, I.B. Wall, S. Shi, H.W. Kim, Advanced biomatrix designs for regenerative therapy of periodontal tissues, J. Dent. Res. 93 (2014) 1203–1211.

[45] C.H. Park, K.H. Kim, H.F. Rios, Y.M. Lee, W. V Giannobile, Y.J. Seol, Spatiotemporally controlled microchannels of periodontal mimic scaffolds, J. Dent. Res. 93 (2014) 1304–1312.

[46] E.M. Varoni, S. Vijayakumar, E. Canciani, A. Cochis, L. De Nardo, G. Lodi, L. Rimondini, M. Cerruti, Chitosan-Based Trilayer Scaffold for Multitissue Periodontal Regeneration, J. Dent. Res. (2017) 0022034517736255.

[47] Y. Wu, D.F.B. Azmi, V. Rosa, A.S. Fawzy, J.Y.H. Fuh, Y. San Wong, W.F. Lu, Fabrication of dentin-like scaffolds through combined 3D printing and bio-mineralisation, Cogent Eng. 3 (2016) 1222777.

[48] C. Ho, H. Fang, B. Wang, T. Huang, M. Shie, The effects of Biodentine/polycaprolactone three-dimensional-scaffold with odontogenesis properties on human dental pulp cells, Int. Endod. J. 51 (2018) e291–e300.

[49] J. Han, D.S. Kim, H. Jang, H.-R. Kim, H.-W. Kang, Bioprinting of three-dimensional dentin–pulp complex with local differentiation of human dental pulp stem cells, J. Tissue Eng. 10 (2019) 2041731419845849.

[50] A. Athirasala, A. Tahayeri, G. Thrivikraman, C.M. França, N. Monteiro, V. Tran, J. Ferracane, L.E. Bertassoni, A dentin-derived hydrogel bioink for 3D bioprinting of cell laden scaffolds for regenerative dentistry, Biofabrication. 10 (2018) 24101.

[51] R. Fang, W. Tian, X. Chen, Synthesis of injectable alginate hydrogels with muscle-derived stem cells for potential myocardial infarction repair, Appl. Sci. 7 (2017) 252.

[52] R. Fang, S. Qiao, Y. Liu, Q. Meng, X. Chen, B. Song, X. Hou, W. Tian, Sustained co-delivery of BIO and IGF-1 by a novel hybrid hydrogel system to stimulate endogenous cardiac repair in myocardial infarcted rat hearts, Int. J. Nanomedicine. 10 (2015) 4691.

[53] X. Bai, R. Fang, S. Zhang, X. Shi, Z. Wang, X. Chen, J. Yang, X. Hou, Y. Nie, Y. Li, Self-cross-linkable hydrogels composed of partially oxidized alginate and gelatin for myocardial infarction repair, J. Bioact. Compat. Polym. 28 (2013) 126–140.

[54] B. Chang, N. Ahuja, C. Ma, X. Liu, Injectable scaffolds: Preparation and application in dental and craniofacial regeneration, Mater. Sci. Eng. R Reports. 111 (2017) 1–26.

[55] W. Toh, Injectable hydrogels in dentistry: Advances and promises, Austin J. Dent. 1 (2014) 1001.

[56] H.J. Haugen, P. Basu, M. Sukul, J.F. Mano, J.E. Reseland, Injectable Biomaterials for Dental Tissue Regeneration, Int. J. Mol. Sci. 21 (2020) 3442.

[57] S. Talebian, M. Mehrali, N. Taebnia, C.P. Pennisi, F.B. Kadumudi, J. Foroughi, M. Hasany, M. Nikkhah, M. Akbari, G. Orive, Self-healing hydrogels: the next paradigm shift in tissue engineering?, Adv. Sci. 6 (2019) 1801664.

[58] Z. Wei, J. Zhao, Y.M. Chen, P. Zhang, Q. Zhang, Self-healing polysaccharide-based hydrogels as injectable carriers for neural stem cells, Sci. Rep. 6 (2016) 37841.

[59] N. Pathan, P. Shende, Strategic conceptualization and potential of self-healing polymers in biomedical field, Mater. Sci. Eng. C. 125 (2021) 112099.

[60] Y.D. Zhang, C. Zhi, Y.Q. Song, L.I.U. Chao, Y.P. Chen, Making a tooth: growth factors, transcription factors, and stem cells, Cell Res. 15 (2005) 301–316.

[61] J. Catón, H.-U. Luder, M. Zoupa, M. Bradman, G. Bluteau, A.S. Tucker, O. Klein, T.A. Mitsiadis, Enamel-free teeth: Tbx1 deletion affects amelogenesis in rodent incisors, Dev. Biol. 328 (2009) 493–505.

[62] F. Wegman, F.C. Öner, W.J.A. Dhert, J. Alblas, Non-viral gene therapy for bone tissue engineering, Biotechnol. Genet. Eng. Rev. 29 (2013) 206–220.

[63] L. De Laporte, L.D. Shea, Matrices and scaffolds for DNA delivery in tissue engineering, Adv. Drug Deliv. Rev. 59 (2007) 292–307.

[64] A. V Oliveira, A.M.R. da Costa, G.A. Silva, Non-viral strategies for ocular gene delivery, Mater. Sci. Eng. C. 77 (2017) 1275–1289.

[65] M. Nakashima, A. Akamine, The application of tissue engineering to regeneration of pulp and dentin in endodontics, J. Endod. 31 (2005) 711–718.

[66] TYPES OF GENE THERAPY, (n.d.). http://fbme.utm.my/ongsimei/2016/05/10/types-of-gene-therapy/.

[67] B. Nussenbaum, P.H. Krebsbach, The role of gene therapy for craniofacial and dental tissue engineering, Adv. Drug Deliv. Rev. 58 (2006) 577–591.

[68] P.C. Edwards, J.M. Mason, Gene-enhanced tissue engineering for dental hard tissue regeneration:(2) dentin-pulp and periodontal regeneration, Head Face Med. 2 (2006) 16.

[69] E. Axpe, M.L. Oyen, Applications of alginate-based bioinks in 3D bioprinting, Int. J. Mol. Sci. 17 (2016) 1976.

Chapter 2. Novel Trends, Challenges and New Perspectives for Enamel Repair and Regeneration to Treat Dental Defects

Fatemeh Mohabatpour[1,2], Xiongbiao Chen[1,3*], Silvana Papagerakis[1, 4*], Petros Papagerakis[1, 2*]

[1]Division of Biomedical Engineering, University of Saskatchewan, 57 Campus Dr., S7N 5A9, SK, Canada

[2]College of Dentistry, University of Saskatchewan, 105 Wiggins Rd, Saskatoon, S7N 5E4, SK, Canada

[3]Department of Mechanical Engineering, University of Saskatchewan, Saskatoon, 57 Campus Dr., S7N 5A9, SK, Canada

[4]Department of Surgery, College of Medicine, University of Saskatchewan, 107 Wiggins Rd B419, S7N 0W8, SK, Canada

[*]Corresponding authors:

Petros Papagerakis, petros.papagerakis@usask.ca

Xiongbiao Chen, xbc719@usask.ca

Silvana Papagerakis, silvana.papagerakis@usask.ca

Keywords: dental enamel defects, regenerative dentistry, synthetic enamel, tissue engineering, precision health, dental stem cells, biomaterials

This chapter focuses on all the possible approaches for enamel repair including cell-free and cell-based strategies and not only tissue engineering. These techniques might not be clinically relevant nowadays, but one day they can be. In addition, they can provide a comprehensive view on the different aspects of enamel remineralization or regeneration that if of great importance for the development of novel approaches for the treatment of enamel defects in future.

2.1. Abstract

Dental enamel is the hardest tissue in the human body, providing external protection for the tooth against masticatory forces, temperature changes and chemical stimuli. Once enamel is damaged/altered by genetic defects, dental caries, trauma, and/or dental wear, it cannot repair itself due to the loss of enamel producing cells following the tooth eruption. The current restorative dental materials are unable to replicate physico-mechanical, esthetic features and crystal structures of the native enamel. Thus, development of alternative approaches to repair and regenerate enamel defects is much needed but remains challenging due to the structural and functional complexities involved. This review paper summarizes the clinical aspects to be taken into considerations for the development of optimal therapeutic approaches to tackle dental enamel defects. It also provides a comprehensive overview of the emerging acellular and cellular approaches proposed for enamel remineralization and regeneration. Acellular approaches aim to artificially synthesize or re-mineralize enamel, whereas cell-based strategies aim to mimic the natural process of enamel development given that epithelial cells can be stimulated to produce enamel postnatally during the adult life. The key issues and current challenges are also discussed here, along with new perspectives for future research to advance the field of regenerative dentistry.

2.1. Introduction

Dental enamel, the external layer of the tooth, which covers the dental crown, is the hardest tissue in the human body [1]. It provides external protection for the tooth against masticatory forces, temperature changes, and the acidic oral environment made by bacteria and food [2]. Enamel, in its mature form, is composed of 95% inorganic materials (hydroxyapatite (HAp) crystals), 1% organic components and 3% water [1]. Enamel has an intricate hierarchical structure which varies from nano- to micro-scales (Figure 2.1) [3,4]. At the nanoscale level, HAp crystals, which have the chemical formula Ca_{10} $(PO_4)_6$ $(OH)_2$, display hexagonal morphologies which are well organized and grow in their C-axis of the crystal. Within the crystals, there are also some trace minerals such as fluoride, zinc, magnesium, sodium, which may vary in their concentration depending on the thickness of enamel and body exposure to minerals [1]. At the next microscale level, HAp crystals are tightly packed together and oriented into units so-called enamel rods or prisms [5,6]. The rods or prism structures are separated by interrods or inter-prismatic areas, which are composed of proteins, lipids, and randomly oriented crystals. The interfacial regions between rods although are softer, have a higher resistance to acid erosion compared to rods [7–9]. The prisms and inter-prism units vary in size depending upon the thickness of the enamel in a fashion that in the outer layers the prisms are smaller and the inter-prism areas are broader [10]. Owing to the hierarchical arrangements of the enamel structure and its chemical composition, enamel exhibits exceptional anisotropic mechanical properties [10].

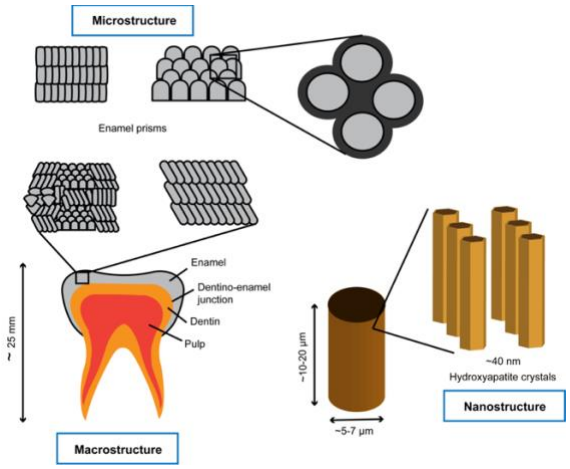

Figure 2.3. Structure of the dental enamel at macro, micro and nanoscale levels. Enamel repair and regeneration approaches need to take in consideration the complex enamel structure. This figure is redrawn from the reference [11].

Amelogenesis is a multi-stage process through which enamel is formed, and the process is chronometrically controlled by consecutive molecular pathways within the enamel forming cells, the ameloblasts. This process entails four different phases characterized based on the morphological and functional properties of ameloblasts: pre-secretory, secretory, transition and maturation [12,13]. Ameloblasts, which are originated from the inner enamel epithelium, regulate the amelogenesis process, produce organic matrix and control the arrangement of prisms and inter-prism regions [14].During the presecretory phase, pre-dentin is secreted by mesenchyme-derived odontoblasts at the future site of dentino-enamel junction (DEJ), and undifferentiated cells located in the inner enamel organ differentiate into pre-ameloblasts and produce proteins on top of the pre-dentin. The pre-ameloblasts degrade the basal lamina, which is present between pre-ameloblasts and developing dentin (deposited by differentiated dental papilla cells). Due to the basal lamina degradation, there is physical contact between future ameloblasts and odontoblasts, which provides inductive reciprocal epithelial-mesenchymal signalling that controls the formation of enamel and dentin. Then, the formation of crystallites starts in the enamel matrix. The newly secreted enamel is aprismatic with randomly oriented crystallites. [12,15,16]. During the secretory stage, ameloblasts elongate and acquire a cone-shaped process known as Tomes' process. During the secretory phase, the enamel matrix proteins are constantly produced and processed, and thus the enamel crystals grow in their length. The shape of the Tomes' process dictates the prismatic pattern of the enamel [10,15,17]. In addition, the thickness of the enamel start increasing at this stage, and about 30% of the secreted enamel is becoming mineralized [18]. During the transition step, there is a reduction in the secretion of the matrix proteins, and the loss of the Tomes' process occurs [17]. In the maturation stage, the enamel organic matrix is degraded by proteinases allowing crystals to grow in width and thickness in the space the matrix proteins have left behind. During the maturation stage, the ameloblasts change their morphology cyclically from ruffle ended to smooth ended cells to adjust their functions to the pH conditions intracellularly and extracellularly. Ameloblasts regulate the ion transport between cell and extracellular matrix, extracellular crystals form and grow, and finally, completion of enamel mineralization takes place by the progressive elimination of the matrix proteins and replacement of the extracellular space by enamel crystals [10,18].

After maturation stage is completed, ameloblasts undergo apoptosis during tooth eruption in the oral cavity; thus, it makes enamel incapable of spontaneous self-repair if damaged after the tooth eruption has been completed [6,19]. This feature is unlike the two other structural layers of the tooth, dentin and pulp, which both exhibit the ability to be regenerated by dental pulp cells existing in the pulp [20]. The traditional approaches employed to repair the damaged enamel are based on restorative dental materials, e.g., silver amalgam, resin composites and ceramics. These materials typically have different physical, mechanical, and esthetic features and crystal structures than the native enamel, thus limiting the enamel's functional recovery and structural restoration. To optimally address these aspects, the development of alternative therapeutic approaches to repair or even regenerate the damaged enamel is of great interest but remains challenging due to the complexities involved in matching the properties of the native enamel [21]. This review discusses the clinical requirements need to be taken into considerations in the development of new therapeutic interventions in order to promote enamel tissue regeneration and repair. It also presents a critical review of the state-of-the-art methods that have been reported to restore, remineralize and regenerate enamel tissue by acellular and cellular-based approaches. We also highlight the potential application of these techniques as therapeutic options to address the enamel defects caused by genetic defects such as amelogenesis imperfecta (AI), dental caries, enamel fractures due to trauma, dental wear. Moreover, we summarize the main limitations of the current approaches, the complexities that are needed to be addressed as well as novel perspectives for optimal restorative dentistry developments in the field of enamel repair and regeneration.

2.2. Clinical needs for novel therapeutic approaches to repair and regenerate dental enamel

2.2.1. Amelogenesis imperfecta

Amelogenesis imperfecta is a genetic disorder which causes enamel defects due to abnormal formation of the enamel in primary and/or permanent teeth [22,23]. In fact, defects of the enamel, ranging from minor anomalies in color or diffuse opacities, to the complete absence of enamel, can occur as a result of the disturbance in any stage of amelogenesis process due to genetic anomalies [19,26]. The disruption in the secretory phase may impact the quantity of the enamel, whereas any changes in the maturation phase can influence its mineralization quality [27].There

exist three main types of enamel defects which include: hypoplasia, hypo-calcification and hypo-maturation. Hypoplastic defects arise from the insufficient or the defective formation of the enamel organic matrix and the crystallite elongation influencing the thickness and the smoothness of the enamel. These defects can cause various changes in the enamel's structure ranging from very thin or completely missing, smooth or rough surface, and also create pits and grooves linearly dispersed on its surface [28,29]. Hypomineralized or hypocalcified defects can be formed due to the alterations occurring during the calcification step of the amelogenesis process which may result in inadequate transport of Ca^{2+} ions into the forming enamel [30]. Although the hypomineralized enamel has a normal thickness, it is soft and weak in structure [31], which causes the enamel to chunk and to get swiftly worn away exposing the underlying dentin [32]. Hypomaturated defects occurs owing to the imperfect elimination of the organic matrix during the maturation step which affects the crystallites' growth and render the enamel brittle [27,32]. Although the hypomaturated enamel is normal in size, it is inadequately mineralized, mottled and rough and thus very susceptible to chip away from the dentin [32,33]. Complex restorative systems using a combination of tissue engineering and materials science can provide new cures for genetically dysplastic dental enamel. An in-depth knowledge of enamel dental defects is necessary for optimal design and validation of novel therapeutic approaches.

2.2.2. Dental caries

Dental caries, also known as tooth decay, are among the most common chronic infectious diseases which can cause demineralization of the dental enamel by acids generated through interactions between cariogenic bacteria (predominantly streptococci and the lactobacilli species) and sugars in the food [34–37]. After being produced by the bacteria in the biofilm, the acids diffuse into the tooth in all directions and dissolve the acid soluble minerals in the enamel structure and cause demineralization. This is a dynamic process that entails the repeated cycles of demineralization and remineralization (the re-deposition of minerals). Once the demineralization process advances over remineralization, it can cause cavitation and formation of caries lesions [37,38]. Prior to the cavitation, white spot lesions are formed as the first clinical sign of tooth decay, which can be arrested or reversed by remineralization [37]. The decay progression occurs differently in the enamel and the dentin. It takes first place in the enamel by the dissolution of the hard tissue by acid attack and then progresses in the dentin by demineralization of minerals and also degradation

of the organic matrix containing collagen type I [39]. Caries affect both primary and permanent teeth in individuals throughout life. The vulnerability of teeth to decays is the highest after the eruption because enamel maturation is still incomplete, and then teeth become more resistant over time [38]. Dental caries is considered the leading cause of oral pain and tooth loss [40]. The formation of tooth decay depends on tooth vulnerability, salivary flow rate, and duration of the availability of the carbohydrates necessary for the fermentation of the biofilm bacteria [41]. Saliva plays a protective role against caries formation by buffering the acids, inhibiting demineralization and promoting remineralization by being a reservoir of calcium and phosphate minerals, and also by providing antibacterial elements [37]. Fluoride, dietary control of sugar intake, sealants and remineralizing therapy can be used for the prevention of dental caries or the management of the initial-stage or moderate lesions [38,42]. The standard treatment of advanced tooth decay, the extensive lesions, includes tooth preparation by removing the portions of the decayed tooth by using drills and then replacing them by restorative materials such as amalgam or composite resins. This process is considered an invasive method, requires the use of anesthetic injections and drilling and needs several sittings, which can cause dental phobia in some patients. In addition, the restorative materials require to be replaced after 7-12 years owing to the shrinkage, leakage or new cavity formation [43]. New approaches combining tissue engineering methods can largely improve biological control of dental caries.

2.2.3. Dental trauma

Traumatic dental injuries (TDIs) or dental trauma are a type of injury which involves teeth or other soft and hard tissues in the oral region, and they influence both primary and permanent teeth [44,45]. It is considered one of the most frequent oral health problems with a prevalence of 6%-37% and can be caused by car accidents, sport injuries, physical activities and violence. Although TDIs occur more commonly in preschool, school-age children and young adolescents, people at any age, and not only those with poor health, can be affected [46,47]. The dental injuries to the hard tissues include enamel infraction and crown fractures, which are classified as uncomplicated (enamel, enamel-dentin) and complicated (enamel-dentin-pulp) crown fractures [46]. These injures can cause not only physical and economic consequences but also a psychological burden. As a result, the management and the treatment of the injuries are of great importance, from both aesthetic and functionality points of view. Emergency management should be taken into

consideration at the time of injuries since time has a great influence on the recovery outcome [44,48]. The enamel infraction is the least severe form of TDIs and microcracks are appearing throughout the thickness of the enamel. No treatment is required in most cases of enamel infraction, and sealing by using adhesive systems is the treatment employed [49,50]. Uncomplicated crown fractures can be treated based on the amount of the lost tissue. Contouring, reattaching the fractures' part using adhesive systems and restoring using a composite resin are used for less severe cases. For fractures with exposed dentinal tubules which are in direct contact with pulp, the infection-related necrosis of pulp can be avoided by protecting the dentin [50,51]. Treatment options for the complicated crown fractures with the exposed pulp, include direct pulp capping, pulpotomy (vital pulp), pulpectomy (endodontic treatment) or extraction, depending on the amount of the exposed pulp, the time interval between the fracture and the clinical examination and the stage of the root development [52,53]. Overall, the outcome of TDIs is ranged from adequate to poor and new strategies and approaches are greatly needed.

2.2.4. Enamel wear

Tooth wear occurs when the hard tissue of the tooth, enamel, or dentin, are lost through attrition, abrasion, and erosion. Dental attrition is caused by physical contacts between two teeth with no contribution from foreign materials. Dental abrasion can be generated as a result of interactions among teeth and foreign substances through processes such as tooth-cleaning or tooth-brushing [54]. On the other hand, tooth erosion is the chronic loss of minerals on the tooth surface resulting from acidic dissolution and/or chelation without the contribution of bacteria [54–56]. The prevalence of enamel erosion was reported 36.6% among the 15-18 years old individuals and 61.9% among 55-60 years old group [57]. The origin of the acidic substances can be intrinsic, such as vomiting and acid reflux, or extrinsic such as dietary, acidic drugs or industrial fumes. While the hydrochloric acid originated from gastric substance is able to cause demineralization and loss of the tooth surface, acids present in the diet, such as soft drinks, fruits and sour foods, are the main cause of tooth erosion [55,58]. The degree of erosion varies based on different factors such as pH, concentration and exposure period of the acid, titratable acidity and the mineral content [58]. Saliva plays an important role in modifying the erosion process in a way that a low or decreased salivary flow can lead to a higher vulnerability to the erosion damage [55]. Enamel, dentin and filling materials can be influenced by dental erosion [55]. When enamel is exposed to

acid substances, softening process takes place through which mineral loss occurs in a layer reaching up to a few micrometers under the tooth surface. As softening process advances and reaches the superficial enamel, the layer of the enamel, which was under acid dissolution, is entirely lost. Enamel can be worn due to the erosion in two ways, including direct elimination of enamel through complete dissolution or generation of a fine softened layer with a higher susceptibility to mechanical wear. When dentin is exposed to acids, the junction between the peritubular and the inter-tubular dentin is dissolved; subsequently, the peritubular dentin is lost, tubule lamina is broadened, and at the end, a superficial layer composed of demineralized collagen is produced [54]. The erosion in dentin can lead to hypersensitivity, pulp exposure and tooth fracture. Filling materials such as glass ionomer cements and restorative composites can be degraded due to acid exposure as well [55]. Sealing and small composite fillings are used for the treatment of dental erosion [59]. Novel materials and techniques are necessary to improve the prevention strategies treatment options for dental erosion and related complications. A strategy has been proposed to add antibacterial molecules into dental composites to prevent secondary dental caries while restoring enamel structures [60–62].

2.2.5. Enamel discoloration

The color of the tooth is naturally shaded with the darker in the gingival to the lighter in the incisal part of the tooth. It is mainly determined by the color and the thickness of the dentin, which is yellow to brown. The color, thickness, translucency and degree of mineralization of the enamel have also an impact on the tooth color. Tooth discoloration causes various esthetic issues for which patients seek dental care and it can also lead to psychological trauma. Discoloration of the tooth can be categorized into three groups: intrinsic and extrinsic discolorations and stain internalization. Intrinsic discoloration is defined as the deposition of chromogens in the bulk of tooth as a result of alterations in the structural composition or the thickness of the hard tissues. There exist different factors that can cause intrinsic discoloration, including metabolic diseases (e.g., congenital erythropoietin porphyria), inherited (e.g., amelogenesis imperfecta and dentinogenesis imperfecta), traumatic, and the process of aging, which makes the color of the tooth darker and yellow. The extrinsic discoloration, which is divided into direct and indirect staining, is defined as the deposition of the chromogens on the surface of the tooth or in the pellicle layer. The direct staining, arising from the dietary sources, such as drinking tea or coffee, smoking, medicines,

results in the incorporation of the compounds in the pellicle layer, whereas the indirect staining can occur due to the chemical reaction with agents such as metal salts or cationic antiseptics on the surface of the tooth. Stain internalization refers to the insertion of the extrinsic stain into the tooth via dental defects or dental trauma, which can be caused by dental caries, restorative materials, dental wear and gingival recession. Based on the cause, tooth discoloration can be treated by prophylaxis for extrinsic discoloration and bleaching, microabrasion, veneers or crowns for intrinsic discoloration and bleaching and restoration using composite or veneers and crowns for stain internalization [63,64]. Methods of superficial enamel remineralization may be able to improve tooth color and diminish shortcomings of the current methods. A deep understanding of the amelogenesis will provide the necessary tools to design the best optimal options.

2.2.5. Sex differences

The sex of the patient is another important factor which needs to be considered when designing personalized therapies for enamel repair. The prevalence rate of dental caries is significantly higher in women compared to men, which might be due to the earlier tooth eruption, snacking during food preparation and female sex hormones and pregnancy [65–67]. Permanent dentition exhibits a sex difference of 3-5%, with women showing to be more advanced compared to men in the timing of the completion of the crown formation and the permanent teeth eruption for all tooth types except the third molar. Sex differences also exist in size and morphology of the tooth crown, which is mainly under genetic control, hormonal effects as well as environmental effects. The effect of genetic factors is more influential compared to other factors due to the early and swift formation of the tooth during embryonic development [68]. Although female and male teeth are similar in terms of the overall structure and morphology, minor variations like those in dental size are able to suggest the sex differences, which are reported to be in the range of 1% and 7% with larger teeth in men. Thanks to these variations, dimensions of the teeth can be measured using morphometric devices and then be used for sex determination and identification of unknown persons in forensics. Studies suggested that the canines exhibit the highest degree of sex dimorphism and the sex difference is greater in buccolingual diameters than mesiodistal ones [69,70]. Men have shown to have greater tooth crown size and more dentin compared to women [71]. The dentin area, DEJ length and bi-cervical diameters were shown to be larger in male molars than female counterparts; however, the enamel thickness is remarkably greater in women [69]. In

addition, the presence of specific amelogenin proteins in the enamel protein matrix obtained from males, which were not found in females revealed the sex dimorphism either in amelogenin expression or in post-secretory amelogenin processing [16,72]. Hormones are also deemed to have substantial impacts on ameloblasts and amelogenesis in the maturation stage and result in sex dimorphism in the mineralization and the quality of the enamel [73,74]. Knowledge of sex differences in enamel formation is necessary for designing personalized treatment options for enamel defects.

2.3. Novel Trends and state of the art approaches for enamel repair and regeneration

2.3.1. Acellular approaches

2.3.1.1. Chemical solutions

One of the methods that has been traditionally employed to prevent dental caries and to remineralize enamel is fluoride therapy. As fluoride exists in saliva at a very low concentration, around the sub-ppm level, it is considered an inherent remineralization solution. Even the low level of fluoride is able to disrupt the demineralization process and enhance the rate of remineralization [75–77]. Under acidic (cariogenic) pH, between 4.5 and 5.5, which is produced as a result of the conversion of the carbohydrates to acids via bacteria in the plaque biofilm, the level of phosphate ions in the biofilm becomes lower than normal, and hydroxyapatite in the enamel are dissolved to recreate the balance. In the presence of fluoride, hydroxyl groups (OH^-) are replaced with fluoride ions (F^-) in the crystal lattice and the fluorapatite is produced, which has a lower solubility and a higher resistance against demineralization under acidic condition compared to hydroxyapatite (Figure 2.2a) [75,78]. Hence, the dissolution of the enamel is diminished, and the loss of calcium and phosphate ions in the enamel is inhibited by retrieving in the form of fluorapatite [75]. However, the high concentration of fluoride can exhibit detrimental impacts owing to the potential risk of fluorosis (the brown and mottled teeth) [79,80]. In addition, for the formation of each unit cell of the fluorohydroxyapatite, two fluoride ions, ten calcium ions and six phosphate ions are required; thus, the shortage of calcium and phosphate ions acts as a limiting factor for enamel remineralization using fluoride therapy [81]. In addition to topical use, fluoride can be used systemically from other sources including mother's milk (that contains a very low concentration

of fluoride), respiration and dietary intake such as fluorinated drinking water, milk, salt, and fluoride supplements in the forms of tablets, drops [82,83]. Although caries preventive effects of the fluoride have been reported to be provided mainly through local topical application (post-eruptive effect), the systemic administration of fluoride could have the pre-eruptive effect and led to dental fluorosis in the case of excessive use of fluoride during the time of tooth development [84,85]. A layer of fluorapatite deposited on the surface is more stable against further demineralization and inhibits the permeation of calcium and phosphate ions needed to recreate the carious lesions underneath the surface layer [86]; as a result, fluoride therapy is greatly efficient on the smooth surface lesions, and its effectiveness is limited in the case of pit and fissure caries [79,80]. The remineralization can be increased by providing calcium and phosphate minerals; but, calcium phosphate ions are unable to be combined with fluoride ions in dental products since fluoride ions have the tendency to react with calcium ions and create insoluble products such as calcium fluoride (CaF_2), which results in loss of bioavailable fluoride ions [87–89]. To overcome this challenge, one approach is using a dual-compartment dentifrice containing sodium fluoride (NaF) in one of the compartments and dicalcium phosphate dihydrate in the other, which showed the increased fluoride delivery and a higher anticaries efficiency compared to dentifrice containing only NaF, when they were mixed prior to treatment [88]. Two calcium phosphate technologies, including casein phosphopeptide-stabilized amorphous calcium phosphate (CPP–ACP) and functionalized tricalcium phosphate (fTCP) were also developed to provide bioavailable and stable calcium, phosphate and fluoride ions and enhance the remineralization of enamel subsurface lesions [87]. Nevertheless, the protection of the enamel provided by applying fluoride and calcium phosphate nanocrystals is limited to about outer ~30 μm of the tooth. The structural and mechanical properties of the formed HAp is also inferior to those of the native enamel [90]. A simple chemical method based on using a calcium phosphate solution together with the chelating agent, N-(2-hydroxyethyl)ethylene-diamine-N,N',N'-triacetic acid (HEDTA) followed by adding KF solution, revealed the ability to directly regenerate the enamel under near-physiological conditions (37℃, 1 atm, pH 6.0) through retarding the nucleation and enhancing the growth of the crystals with the lengths greater than 10 μm. The hexagonal crystals of the fluorapatite are formed after the addition of fluoride ions to the solution and incorporation of the ions into the HAp lattice. However, the process takes several days, which restricts clinical applications of this method, and also, the chelating agent, HEDTA, is not safe to be consumed by the patient; thus, a device is

required to be designed to separate the mineralization solution from the oral environment. Furthermore, only prism-like structures, without inter-prism regions, are able to be reconstructed using this approach [91]. The calcium phosphate compounds with bundles of aligned HAp fibers similar to the dental enamel were produced by applying a solution containing the surfactant bis (2 ethylhexyl) sulfosuccinate sodium salt (AOT), water, and oil. The surfactant AOT was used as the structure-directing agent to regulate the nucleation and the growth of calcium phosphates [7]. Still, the function of formed calcium phosphate materials is limited, and also the presence of chemicals such as AOT can lead to excessive biological effects [92]. Silver diamine fluoride (SDF) is a colorless solution of ammonia and silver fluoride that is employed as an FDA cleared product for caries management. This solution can be used either on the decayed lesion in order to arrest caries or on the part of the tooth with no caries to prevent decay formation. SDF was revealed to be able to arrest the decays in primary teeth, treat tooth hypersensitivity, inhibit pit and fissure decays in the erupting permanent teeth, sterilize the infected root canals and to prevent root caries in elderlies [39,93]. It also inhibits both the demineralization of the dentin tissue and the degradation of the dentin matrix. In addition, the antibacterial features of the SDF prevents the progression of cariogenic biofilms. As one drawback of this solution, carious lesions get stained and become black after treatment with SDF, which might be unsatisfactory for patients [94]. Recently, a biomimetic regenerative solution based on calcium phosphate ion clusters, as the building block of amorphous calcium phosphate (ACP), and HAp, has been developed, which is able to induce the epitaxial crystal growth through the crystalline-amorphous mineralization once applied to a carious lesion. This solution, which is made by mixing calcium and phosphate minerals with trimethylamine in an ethanol solution, could repair the enamel up to the thickness of 2.7 µm with a structure identical to the structure of the native enamel [95].

2.3.1.2. Electrodeposition

Electrodeposition, also known as electrochemical deposition, is a simple and inexpensive method through which a uniform layer is deposited on the substrates under an electrical field [96]. Electrolytic deposition (ELD) and electrophoretic deposition (EPD) are the two main categories of electrodeposition. In the ELD, the metal ions are electrochemically reduced, or the colloidal particles are generated as a result of cathodic reactions, and then they are transferred to the electrode where a layer is formed, while in EPD, the charged particles in a liquid suspension are

moved towards the electrode (Figure 2.2.b) [96]. The ELD produces thinner layers of coating juxtaposed with the EPD [97]. The ELD method was shown the ability to induce precipitation of both self-assembled amelogenin proteins and CaP at the same time under physiological conditions to improve the crystal growth and enhance mechanical properties of the enamel-mimicking composite coatings [98]. The advantage of this technique is that calcium phosphate or HAp can be coated on substrates even with porous or irregular structures at a relatively low temperature with the controllable crystallinity [99,100]. Furthermore, the gradual increase in the local pH around the cathode is able to induce the self-assembly of amelogenin proteins as well as the supersaturation of CaP and the nucleation of crystals on the cathode [101,102]. Nevertheless, the high electric field condition used in the process prevents the potential of this technique for translation into clinical applications [103].

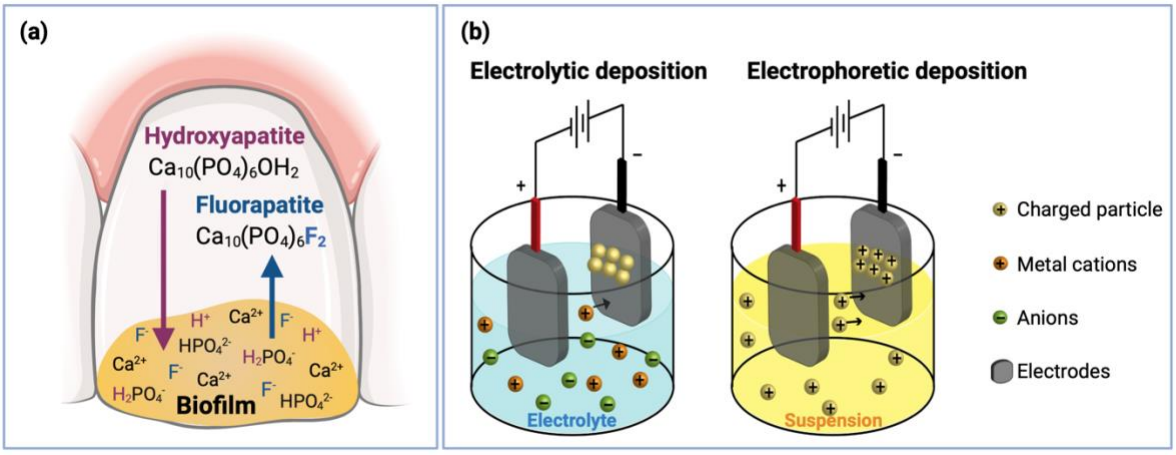

Figure 2.4. (a) The mechanism of demineralization inhibition by fluoride, this figure was drawn with Biorender.com. (b) Electrodeposition methods: Electrolytic deposition (ELD) and Electrophoretic deposition (EPD). Superficial enamel repair and remineralization can be achieved chemically. This type of approaches can prevent dental caries, repair enamel microcracks and improve enamel caries prevention strategies.

2.3.1.3. Inorganic pastes

Dental pastes, which contain inorganic components such as HAp, can be applied to form the synthetic enamel and to repair the early caries lesions by the growth of nanocrystalline structures without any need for prior excavation [104,105]. As the repair steps using the inorganic paste are shown in Figure 2.3, the HAp nanocrystals in the enamel are dissolved in the initial step;

afterwards, in the middle step, the enamel apatite crystals swiftly start re-growing, and new HAp crystals nucleate as a result of the presence of ionic species in the extremely acidic pH of the mother solution (pH<2). In the final step, the layer of newly grown HAp crystals, with the high crystallinity and identical crystallographic orientations, are created in the interface, while in the dense paste, the crystals are randomly oriented and low crystalline owing to the high supersaturation. Thus, the mechanical and physiochemical characteristics of the newly synthesized HAp are maintained in roughly 20 μm thickness of the interface also, no prism structures were observed [105]. Moreover, the high concentration of hydrogen peroxide (H_2O_2) is used in the paste formulation to form the oxygen bubbles in the surrounding environment needed for the generation of the micro-convention, which help with the nucleation and the growth of crystals [105]. Therefore, clinical applications of the inorganic pasts are limited due to the fact that the acidity of the condition and the usage of H_2O_2 are able to cause inflammation when they are placed on the gum [104].

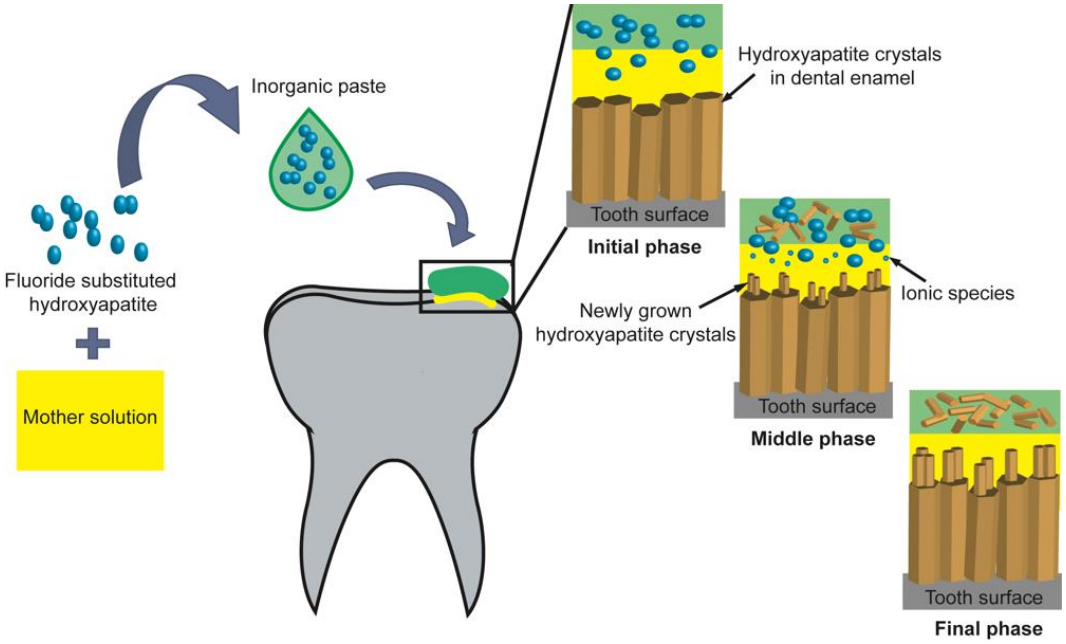

Figure 2.5. The repair steps using inorganic pastes: (1) Initial phase: the dissolution of hydroxyapatite (HAp) crystals in the original dental enamel. (2) Middle phase: the re-growth of the enamel HAp and nucleation of the new HAp crystals. (3) Final phase: the creation of the synthetic enamel in the interface and randomly oriented crystals in the dense paste. Based in part on the reference [105].

2.3.1.4. Synthesis of artificial enamel-like hydroxyapatite

Since there exist no enamel forming cells after the completion of the tooth eruption, one of the methods for the enamel restoration is to synthesize the artificial enamel HAp. The techniques by which HAp can be synthesized are categorized into two main groups: solid-state and wet-state methods [106]. In the solid-state approaches, the reactions among the raw materials such as $CaHPO_4$ and CaO powders are performed by thermal treatments and produced stoichiometric HAp with the well-crystallized structures. However, high temperatures (higher than 700 ℃) and a long period of treatment times are needed. Moreover, the resultant products are in the form of the sintered bulk, which requires to be milled or ground into nano-sizes using techniques such as direct ball milling, the plasma spraying [106]. While, nanoHAp can simply be synthesized via the wet-state approaches, including the wet chemical precipitation, the homogeneous precipitation, the micelle-templated precipitation, the emulsion method, the hydrothermal conversion, the hydrothermal crystal growth, and the sol-gel method, under comparatively low temperatures [106,107]. Nevertheless, the crystallinity and the Ca/P ratio of the products are at lower levels compared to HAp produced by solid-state methods. There exist some post-treatment techniques, such as hydrothermal treatment or calcination, that can be used to form the well-crystallized HAp [106]. One of the most effective methods is the hydrothermal approach by which the morphology and the architecture of the HAp can be regulated as a result of its potential to instigate nucleation and growth of HAp crystals [108]. However, the stringent conditions applied in these methods, such as the high temperature, the pressure, the low acidity, the high concentration of the surfactants, confine the potential of this approach for clinical applications [109].

2.3.1.5. Rotary evaporation

Rotary evaporation is a simple and efficient technique that can be used to control crystal growth and regenerate the enamel-like structures on various types of substrates, including dental enamel, dentin, titanium sheets and polyethylene sheets. Unlike other techniques such as hydrothermal approaches and hydrogel systems, which offer a very low speed of HAp crystal growth (less than 1 μm per day) and the limited thickness of the regenerated layer, the rotary evaporation is able to provide the rapid production of highly organized structures with a controllable thickness. In this technique, HAp crystals are grown in the remineralizing solution containing calcium and

phosphate and fluoride minerals with silk fibroin, which was employed as a modulator of crystal growth due to its similarity to amelogenin structure, under rotary evaporation. The regenerated enamel-like crystals produced using this method exhibited the microstructure (crystal size, morphology, organization) and mechanical features similar to those of native enamel [110].

2.3.1.6. Laser assisted mineralization

Lasers have been broadly used in the field of dentistry for cutting soft tissues and whitening. Owing to their photothermal effects, lasers are able to assist in crystal growth by warming the local area converting the reaction environment to the hydrothermal oven, which renders them suitable for enamel repair applications. Lasers accelerate the mineralization of the dental enamel and regulate the growth of HAp crystals in the regions, which can prevent the creation of dental calculus. However, the diode laser source can overheat the pulp and kill the nerve cells existing in this layer. Therefore, more studies are needed in order to validate the effectiveness of changing the laser source [5]. Furthermore, femtosecond pulsed lasers (fs) were used to remineralize the dental enamel by sintering the synthetic fluorapatite powder consisting of iron oxide nanoparticles (Fe_2O_3 NPs) in chitosan applied on the surface of the eroded enamel. Fe_2O_3 NPs were able to absorb laser photons like a thermal antenna and to distribute the heat locally to fluorapatite crystals, and induce densification into a dense layer which was attached to the native enamel [111].

2.3.1.7. Electrically accelerated and enhanced remineralization

Electrically accelerated and enhanced remineralization (EAER) is an innovative clinical approach for the remineralization of dental caries in a fast and efficient manner with no need for drilling or filling. This method can be used for the repair of the full depth of the initial-stage or moderate carious lesions through a painless process without any need for injections, drills or restorative materials. In addition, this method preserves the healthy part of the tooth during the process, which can lead to maintaining the tooth integrity, and it can also be employed to whiten teeth. The procedure uses a small “healing hand piece” that is put on the decayed surface of the tooth and includes two steps: first, the remineralizing agent reservoir in the form of the paste or liquid is placed on the carious lesions, and then an electric field is applied for a short time to accelerate the movement of the mineral agents to the lesion [43,112].

2.3.1.8. Immunization against cariogenic bacteria

Caries vaccines are another approach that has been developed for the prevention of dental caries over the last 40 years. Streptococcus mutans and Streptococcus sobrinus are the main targets in the development of the caries vaccines [113]. The immunization against cariogenic bacteria can be achieved either actively or passively. Active immunization uses target antigens to induce the production of endogenous antibodies by host's immune system [113,114]. Active vaccines are more effective and long-lasting; however, they can evoke harmful immune reactions that might be fatal [115]. Passive immunization involves administration of exogenous antibodies that provides a safer option; nevertheless, it provides less effective and temporary immunity and thus repeated administrations are needed [113,114]. Moreover, non-human antibodies used in passive vaccines often induce immune reactions [116]. The antigen-binding fragments (Fabs) that was synthesized against Streptococcus mutans and Streptococcus sobrinus by using recombinant DNA technology could prevent caries formation in a rat model and have the potential advantage to be engineered for passive immunization in order to prevent immune responses to non-human antibodies [116]. Further studies are required to investigate the long-term efficacy of vaccines for caries therapy in future. In addition, it is hypothesized that a combination of enamel matrix proteins and antibodies might be able to treat the dental caries in a carious tooth while inhibiting further progression of the caries by blocking cariogenic bacteria.

2.3.1.9. In situ remineralization/regeneration of enamel by mimicking the functions of organic matrix

The native enamel apatite is initially formed in the gel-like microenvironment containing different proteins such as amelogenin, and then the organic molecules are mostly degraded or eliminated over time as the enamel becomes mature [103]. Proteins in the enamel organic matrix provide a framework which structurally support the formation and the growth of crystals during the enamel development [117]. The physicochemical properties of the gel-like organic materials can mimic the native enamel matrix more accurately juxtaposed with aqueous solution-based systems and control the manner of the crystal growth [118]. Thus, one of the approaches for inducing enamel mineralization and regeneration is to mimic the role of organic matrices [109,119].

2.3.1.9.1. Recombinant enamel matrix proteins

The enamel extracellular matrix consists of proteins and proteases, which are secreted in a time-controlled manner based on different genes and signalling pathways, plays a pivotal role in the mineralization of the enamel. The main enamel matrix proteins (EMPs) expressed by ameloblasts include amelogenin, enamelin, ameloblastin and amelotin, among which amelogenin is the most essential in the enamel mineralization [120]. The mechanism of the role of amelogenin in the mineralization has been investigated by means of recombinant amelogenin. Amelogenin and its self-assembly regulate the crystallization of calcium and phosphate, the crystal size and the orientation and the elongation of apatite crystals within prism structures [87,121,122]. It has been indicated that the recombinant full length amelogenin (rP172) is able to enhance the formation of organized needle-like fluoridated HAp crystals under physiological conditions in a dose-dependent manner. The inclusion of the fluoride with amelogenin is also important for the crystal packing density and remineralization. In situ remineralization of the enamel by this technique can be applied for early caries lesions; nevertheless, the clinical application of this approach is confined due to the fact that expression and purification of amelogenin are hard and highly costly [123].

2.3.1.9.2. Dendrimers

Dendrimers are highly branched spherical shaped polymers with a well-defined structure consisting of a central core enclosed by repetitive branches [124]. This group of polymers, known as biomimetic artificial proteins, has been employed as models for proteins in biomedical applications due to their narrow size distributions, the dimensional length scaling. They can act as amelogenin analogues to mimic the function of the organic matrix for the enamel mineralization [125,126]. Poly (amido amine) (PAMAM) was the first synthetic dendrimer that has been used for the enamel mineralization by crystallization of HAp. The size and the shape of the HAp can be controlled by functional groups, generations and the concentration of the dendrimer. The carboxyl-terminated PAMAM (PAMAM-COOH) self-assembled like amelogenin and resembled its structure [126]; however, for in situ regeneration or mineralization, PAMAM dendrimers are required to have a higher adsorption affinity to the enamel surface [109]. To increase the binding ability, PAMAM-COOH dendrimer was conjugated to a HAp-anchored agent, alendronate (ALN), shown to be capable of adsorbing on the surface of the enamel and recreating nanorod-like HAp crystals with uniform sizes and shapes and the perpendicular orientation on the surface of the

acid-etched enamel when incubated in the artificial saliva for up to 4 weeks and recovered about 95.5% of the hardness of the original enamel [109]; however, the commercialization and clinical applications of the ALN-PAMAM-COOH are restricted due to its complex synthesis process.

2.3.1.9.3. Self-assembling peptides

Self-assembled peptides are structures which can be created by a bottom-up technique as a result of non-covalent interactions consisting hydrogen bonds, electrostatic interactions, hydrophobic interactions, van der Waals interactions, and also π–π stacking forces between small molecules, which are mostly peptide amphiphiles (PA) [127–129]. The structure of PA includes a tail group of dialkyl chain as a hydrophobic part which is linked to a head group containing a peptide group, as a hydrophilic part [128]. PA can spontaneously form nanostructures in aqueous conditions, and the self-assembly process can be induced by changes in pH, the concentration or the number of divalent ions [130]. The shape of nanostructures formed from self-assembling peptides is contingent upon chemical (e.g. sequence, charge, concentration, etc.) and physical (e.g. size and shape of peptides, etc.) characteristics [131]. The application of self-assembling peptides in the enamel regeneration is advantageous owing to the formation of fibrous structures with the high aspect ratio (the diameter and the length are in nanometer and micrometer size ranges) and the presence of well-defined surface functional groups, which periodically repeat in the structure and help with the mineral nucleation. Additionally, the dynamically stable 3D environment produced by fibrils can modulate the deposition and the growth of crystals, and these peptides can be injected in the form of fluids and then in situ gelation occurs, which makes these structures appropriate for filling cavities with irregular shapes [132]. The self-assembling peptide named P11-4 (Ace-Gln-Gln-Arg-Phe-Glu-Trp-Glu-Phe-Glu-Gln-Gin-NH_2) exhibits a high binding capacity for calcium ions which can help with the nucleation and form the needle-shaped HAp crystals and remineralize the enamel. Nevertheless, the proteolytic degradation of self-assembling peptides may affect their effectiveness on the tooth surface and confine their clinical applications [133,134].

2.3.1.9.4. Hydrogels

Hydrogels are 3D structures of hydrophilic polymers which can absorb a large amount of aqueous solutions and encapsulate biological agents [135]. Gelatin hydrogel was used to simulate enamel formation owing to similarities between structural and chemical characteristics of gelatin and the

enamel matrix. Gelatin provides nucleation sites, and its ionotropic properties allow inorganic ions, which are introduced in the gel through diffusion, to be oriented with organic molecules. A double-diffusion chamber can supply the buffered calcium and phosphate/fluoride solutions into the gelatin gel to prevent the quick precipitation of calcium phosphates [136]. The spherical fluorapatite-gelatine aggregates with needle-shaped sub-units and similar chemical and morphological properties to those of the natural enamel are able to be formed within weeks [137]. Nevertheless, the level of the fluoride in aggregates was higher than the enamel, and the crystals were shorter in their length [138]. Furthermore, gelatin is a thermosensitive material which is in a solution state at a physiological temperature, 37℃; as a result , the reaction should be performed at 25℃ to maintain the gelatin in the gel state [136]. To elevate melting temperature of gelatin up to 40℃, gelatin was supplemented with glycine [138]; but it can cause biosafety issues in a long time during which the gel is present in buccal cavity [118]. Agarose gel, which has the sol-gel transition temperature around 60 ℃, was used to address the challenge with gelatin. The results showed that the prism-like structures with hexagonal HAp crystals were formed in the newly formed tissue, which has similar mechanical properties to the enamel. Still, hydrogels were employed as a simplified model for enamel regeneration. Organic components, such as enamel proteins and proteinases can be incorporated into hydrogels (3.1.9.5 and 3.1.9.6) in order to emulate the organic matrix more precisely [118]. In addition, by incorporating antimicrobial and bioactive agents such as silver-doped bioactive glass [139], antimicrobial GKIIKLKASLKLL-NH2 (GL13K) peptides [140] and antibiotics [141,142], antimicrobial hydrogels can be fabricated to induce mineralization or regeneration in dental tissues while preventing bacterial infections or treating cariogenic bacteria.

2.3.1.9.5. Enamel matrix protein containing hydrogels

The more promising hydrogel-based approach can be obtained by incorporation of amelogenin proteins in the hydrogel in order to regulate the crystallization, the growth, and the orientation of HAp crystals [10]. The cyclic treatment of a mixed-species oral biofilm model by means of an amelogenin (rP172)-releasing hydrogel system based on agar, which contains calcium, phosphate and fluoride minerals, during several days significantly enhanced the microhardness of the remineralized enamel compared to the control group without amelogenin and fluoride. No cytotoxic effects were exhibited on periodontal ligament cells. Agar is a non-ionic polysaccharide

with a low propensity for maintaining amelogenin, which renders it suitable for releasing proteins and ions. However, the hardness of the remineralized enamel was lower than that of the native enamel. To promote the crystal packing density by using this system, enzymes such as enamelysin and KLK4 can be added using a time delayed delivery system for the elimination of the extra amelogenin between crystals [143]. Another amelogenin containing system for enamel repair was developed based on the chitosan hydrogel, which exhibits unique antimicrobial and adhesion properties. Amelogenin was self-assembled in the chitosan hydrogel, which stabilized Ca-P clusters in hydrogel and controlled their arrangement into linear chains fused with enamel crystals and formed into co-aligned crystals that attached to the native enamel as clusters were growing. Using the chitosan hydrogel system, a dense interface was formed between the enamel and regrown crystals resulted in the enhanced bonding between the repaired layer and the tooth surface, which can promote the endurance of the treatment and prevent the formation of secondary caries. In addition, hardness and elastic modulus were significantly increased after applying the hydrogel system to the etched enamel; but the levels were still lower than those of the native enamel owing to the lack of prism and inter-prism structures [10,122]. Further research is needed to perfect these systems for clinical applications.

2.3.1.9.6. Electrospun mats

The electrospun materials have been used in various dental applications, including tooth regeneration and wound dressing for oral mucosal lesions [144]. Amorphous calcium phosphate/poly(vinylpyrrolidone) (ACP/PVP) fibrous membranes produced by the electrospinning technique were able to shield the tooth and act as a metastable reservoir of calcium and phosphate ions. When used in the presence of artificial saliva containing fluoride ions, the electrospun mats get hydrated and provide a mineralizing hydrogel which can guide and enhance enamel remineralization by crystalizing fluoridated hydroxyapatite (500 nm in thickness). In addition, the exposed dentin tubules were able to be plugged after applying the ACP/PVP electrospun mat. As a result, the dentin hypersensitivity can be decreased using this approach [145].

2.3.1.10. Enamel matrix protease delivery systems

The enamel organic matrix guides the crystal formation and gradually undergoes degradation by the effect of the proteolytic enzymes, which hydrolyze the peptide bonds in proteins. These

proteases mainly include matrix metalloproteinase-20 (MMP20 known as enamelysin) and enamel matrix serine protease 1 (KLK4) [146,147]. MMP20 is involved in the processing of the enamel matrix and the cleavage of the amelogenin during the secretory stage, which is of great importance in the crystal elongation. KLK4 degrades proteins in the enamel matrix during the maturation stage [146,148]. Several studies have developed enzyme delivery systems for other biomedical applications such as cancer therapy [149–152]; however, there is no study on the treatment of enamel hypo-maturation using delivery of proteolytic enzymes. It is hypothesized that the delivery of KLK4 and MMP20 might help with the removal of the organic matrix and alleviate the symptoms of enamel hypo-maturation.

2.3.2. Cellular approaches for enamel regeneration

Although considerable progress has been made using acellular approaches, an innovative method that can be applied directly on the tooth surface in the oral cavity and mimic structural and mechanical properties of the dental enamel and produce several micrometer-sized HAp crystals is still required to be developed [90,153]. Since the native enamel is produced by ameloblasts prior to the tooth eruption, the regeneration of the enamel by cells seems promising as it can mimic the natural enamel development process, and the properties of the produced enamel can be much more similar to those of native tissue.

Different dental cell sources for enamel regeneration

There exist different cell sources that can be used to regenerate the dental enamel as described below:

2.3.2.1. Primary enamel organ epithelial (EOE) cells

Unlike the mature enamel, the enamel organ epithelium in the unerupted tooth contains ameloblast-like cells that can be used as the cell source to regenerate enamel. Primary epithelial-like cells from the tooth bud are in either polygonal or stellate morphologies, and express amelogenin. However, they exhibit a relatively slow growth rate [154,155]. In fact, *in vitro* culture of EOE cells for a long time while maintaining their primary phenotypes is difficult [156]. There are also two main challenges for culturing EOE cells: first, the disruption of their growth when

contaminated with dental mesenchymal cells and second, their terminal differentiation after several passages [156]. Moreover, these cells cannot be accessible after tooth eruption; as a result, alternative cell sources are required to be used for adults without any unerupted tooth.

2.3.2.2. Epithelial cell rest of Malassez

Epithelial cell rest of Malassez (ERM) are epithelial cells with stem cell characteristics derived from Hertwig's epithelial root sheath (HERS) in the periodontal ligament (PDL), which are the connective tissue connecting tooth root to the alveolar bone [157,158]. ERM is entailed in tooth-root formation, and it is considered the only dental-origin epithelial cells in adult teeth since it stays in PDL in adulthood to retain the tissue homeostasis [159–161]. These cells, which can be obtained either from HERS in root tip before the completion of the root formation or from ERM in the root surface after the tooth extraction, have the potential to differentiate into ameloblasts [162,163]. Adult human epithelial stem cells derived from hERM in a by-product of the surgical extraction of the wisdom teeth can be utilized as an easily accessible autologous donor source of epithelial stem cells [164].

2.3.2.3. Human skin keratinocytes

Human keratinocytes can be isolated from the epidermal layer of the skin and be used as non-dental epithelial cell source to produce dental enamel. These cells, that are easily accessible and can be expanded quickly in culture, have the potential for clinical applications. Human keratinocyte cell sheets have shown the ability to differentiate into enamel-producing ameloblasts, induced by with mouse embryonic dental mesenchyme and fibroblast growth factor 8 (FGF8) [165]. However, the relatively low induction rate of ameloblast differentiation in these cells prevent them from being used as an ideal cell source for future development of bioengineered teeth [166]. The treatment with FGF8 and Sonic hedgehog (SHH) [167] or low temperature culture [166] have found to significantly increase the rate of ameloblastic differentiation in human keratinocyte stem cells.

2.3.2.4. Ameloblast-like cell lines

Ameloblast-like cell lines are produced by insertion of the viral oncogenes, which makes dental derived cells immortalized with the ability to constantly proliferate and demonstrate an ameloblast-like gene profile [168]. These cells allow scientists to conduct research on molecular and cellular events occurring during amelogenesis and enamel regeneration without any need for animals as the source for cell-isolation [169]. LS8 is a mouse-derived cell line that can be used as a cellular model for the secretory phase of amelogenesis since it highly expresses amelogenin, ameloblastin, enamelin, and *Mmp20*; however, they are unable to generate calcified nodules [169–171]. ALC is another mouse-derived cell line for mimicking the ameloblasts in the maturation phase, and it expresses amelogenin, odontogenic ameloblast-associated protein (*Odam*), *Klk4*. In addition, this cell line has a very high alkaline phosphatase activity and is able to form calcified nodules [169,170,172]. HAT-7 is a dental epithelial cell line which is originated from the apical bud of the rat incisors [173,174]. Immunocytochemical studies have shown that HAT-7 cells display ameloblast traits such as the expression of the secretory phase markers, including amelogenin and ameloblastin [175], as well as the maturation-stage ameloblast markers such as *Klk4* and amelotin [173]. SF2 is another dental epithelial cell line derived from rat incisors and can be considered for analyzing the fate of the epithelial cells, the adhesion to the matrix and the interactions with dental mesenchymal stem cells [176]. Recently, two immortalized epithelial cell lines (EOE-2M and EOE-3M) were developed from the mouse EOE. These cells were able to maintain their ability for proliferation after 30 passages and express the enamel specific markers, including amelogenin, ameloblastin, KLK4, MMP20; as a result, they can be used to study events taking place during both secretory and maturation stages [168].Although mouse and rat cell lines can provide useful tools for studying enamel repair and regeneration, these cell lines cannot be used for human enamel repair.

2.3.2.5. Induced pluripotent stem cells

Induced pluripotent stem cells (iPSCs) can be derived from the differentiated adult cells via insertion of the specific four embryonic transcription factors— *Oct3/4, Sox2, Klf4, c-Myc,* and *Nanog* [177]. iPSCs are able to be produced from different dental cells, including stem cells residing in apical papillae (SCAP), dental pulp stem cells (DPSCs), stem cells from human

exfoliated deciduous teeth (SHED), third molars, and fibroblasts derived from the oral mucosa, gingiva and periodontal ligament. iPSCs can be used as an unlimited cell source for dental epithelial cells without the ethical issues and the risk of the immunorejection that the embryonic stem cells might have [178]. It was shown that the putative epithelial progenitors could be generated by iPSCs cultured on collagen-coated dishes in the presence of bone morphogenic protein (BMP)-4 and retinoic acid (RA) [179]. It was also indicated that iPSCs are able to differentiate into the enamel producing ameloblasts when co-cultured with dental epithelial cell line SF2 [180] or ERM cells [181]. However, the epigenetic memory of iPSCs from their original phenotype, which exists in iPSCs even after reprogramming, confines their ability for differentiation and also, there is a risk of tumor formation by the remained undifferentiated cells in the target cells [178]. Another potential disadvantage could be the multiple differentiation steps needed to guide iPSCs from an under differentiated stage to enamel-producing cells.

Scaffold-free strategies

During tooth development, ameloblasts are programmed to differentiate and produce enamel through receiving signals from growth factors, transcription factors, extracellular matrix as well as signals from mesenchymal cells. One approach to create the enamel can be achieved by controlling the differentiation of the enamel producing cells using the signalling pathways**.**

2.3.2.6. Ameloblast differentiation inducing factors

T-box1 (Tbx1) belongs to the family of Brachyury-related family transcription factors whose alteration or absence could lead to DiGeorge syndrome, a genetic disease that influence the development of organs including heart, face, parathyroid and teeth [182]. Tbx1 was found to be a stimulator of ameloblasts differentiation, proliferation as well as enamel deposition. The deletion of Tbx1 in a mouse model led to the absence of the enamel and the ameloblasts, decrease in cell proliferation and lower amelogenin expression, as well as the different levels of hypo-mineralization and hypo-plasticity [182]. Tbx1 expression in dental epithelium was found to be linked to the expression of fibroblast growth factor (FGF) which play an essential role in the function of ameloblast specification, survival and proliferation [183]. Globoside, which is also highly expressed during tooth development, has shown the ability to accelerate the ameloblast

differentiation by promoting the expression of the enamel matrix proteins and the expression of epiprofin and the regulation of runt-related transcription factor 2 (*Runx2*) expression when exogenously administrated in HAT-7 cells, while it has no effect on cell proliferation [184]. AmeloD transcription factor also has a pivotal role in tooth morphogenesis through controlling the expression of E-cadherin and epithelial–mesenchymal interactions. Deletion of AmeloD in a mouse model caused hypoplasia and the formation of the small-sized tooth and hindered the migration of cells [185]. Knockout of the nuclear factor 1-C also revealed the formation of the structurally defective enamel and diminished the ameloblast differentiation via regulating the osterix pathway [186]. Moreover, TGF-β-1 can enhance mineralization and maturation of enamel by regulating the expression of RUNX2 and WD repeat-containing protein 72 (WDR72) [187]. It was also demonstrated that TGF-β-1, BMP-2-soaked apatite and interleukin-7 (IL-7) are able to induce the ameloblasts differentiation [188]. Basic fibroblast growth factor (FGF-2) is another factor which affect the ameloblast differentiation and the secretion of the enamel matrix [189]. A comprehensive system of transcription and growth factor time-controlled delivery to lead differentiation of stem cells to enamel producing cells is still missing.

2.3.2.7. Co-culture systems

Another essential factor for enamel regeneration is epithelial-mesenchymal interactions which naturally occurs during tooth development. One method for inducing the ameloblast differentiation and enamel formation through providing such signals is based on two- or three- dimensional (2D or 3D) co-culture systems (Figure 2.4) [190–194]. Transwell systems offer non-contact co-culture models in which one type of the cells are seeded in the permeable insert, with the pore size of 0.4 μm, and placed on top of wells plated with the other cell type [195,196]. In this model, soluble signalling molecules secreted from each cell type act as inducers which affect the function of the other cells without the direct cell-cell contact [197,198]. Although these systems are simple and easy to use, they provide a 2D monolayer of cells which differs from the in vivo condition in terms of the cell functions, morphology and gene expression [199]. A 3D *in vitro* co-culture system based on collagen membrane in two different non-contact and indirect contact fashions was developed for inducing ameloblast differentiation in HAT-7 cells through interactions with dental mesenchymal stem cells. Results showed that direct cell-cell interactions are important for ameloblast differentiation. However, the collagen membrane allows only biomolecules smaller

than 12.5 kDa to move through it [190]. The development of a 3D co-culture microenvironment which mimics *in vivo* tissue structures with the natural cell morphogenesis has still remained a challenge [199].

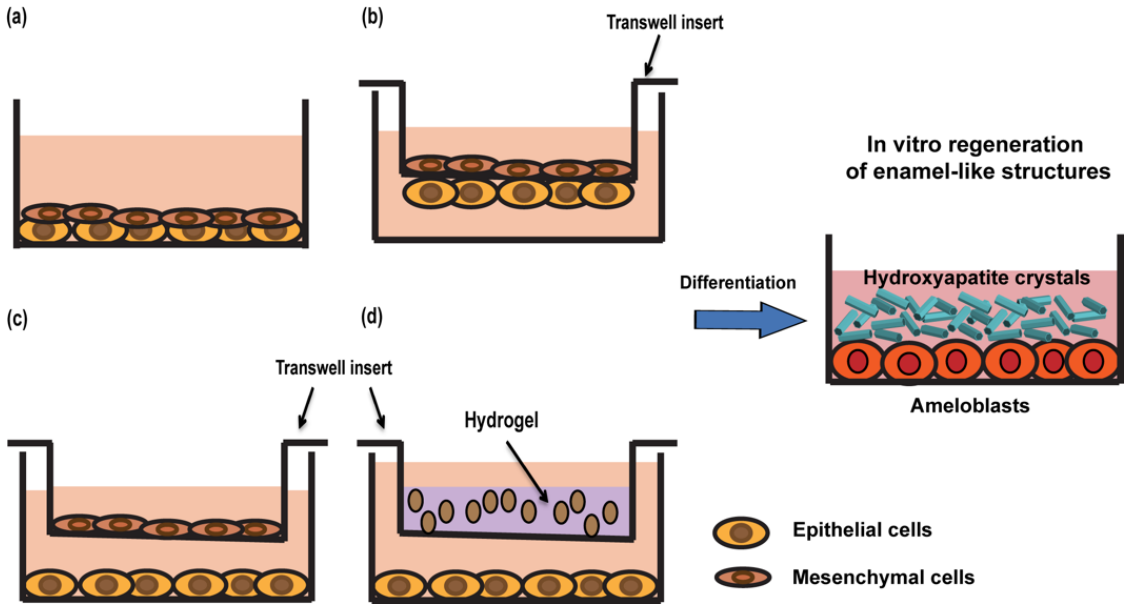

Figure 2.6. Different co-culture systems: (a) 2D non-contact model, (b) 2D indirect contact model, (c) direct contact model, (d) 3D non-contact model. These developed models can be used to study the importance of epithelial-mesenchymal signalling for ameloblast differentiation and enamel formation and mineralization. Advanced co-cultures methods could be used in the future to regenerate dental enamel in vitro.

Another approach which has been developed for this purpose is the reconstitution of the tooth germ by the tissue re-aggregation techniques through which dental mesenchyme and dental epithelium, or single cells derived from them, are re-combined and the epithelial-mesenchymal interactions commence the tooth formation and control cell differentiation and morphogenesis (Figure 2.5a-b) [200–202]. Tooth crowns with bone and soft tissues were regenerated when mesenchymal cells from non-dental sources were re-associated with the embryonic oral epithelium and transplanted in the renal capsule. In addition, tooth structures were formed after transplanting the embryonic tooth primordia into the jaw, which confirms the feasibility of replacing the lost or missing tooth with the artificial tissue primordia in the jaw [201]. Collagen gel has also been used to form the recombinant tooth germ [203–205] or the tooth bud [206], and it can provide the appropriate cell compartmentalization among epithelial and mesenchymal cells which is of great importance in both *in vitro* organ culture and *in vivo* implantation (Figure 2.5c) [203].

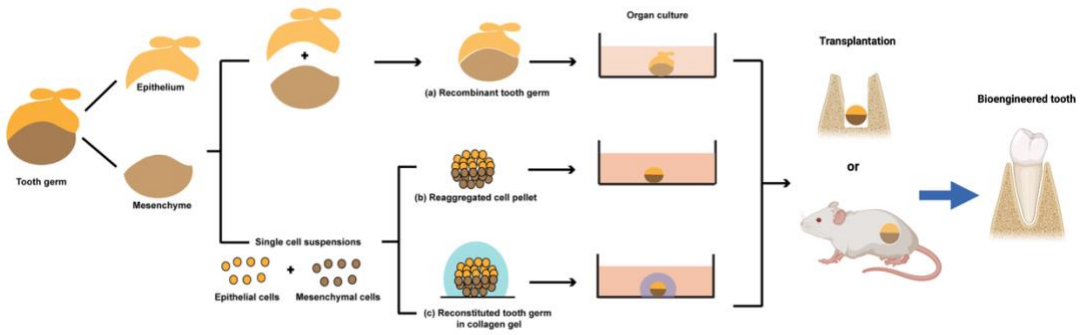

Figure 2.7. Scaffold-free approaches for bioengineering of the tooth germ through mesenchymal-epithelial interactions. Epithelium and mesenchyme are separated and then re-associated (a), epithelial and mesenchymal single cells derived from the tooth germ are combined by making pellets (b) or by using collagen hydrogels (c). The reconstituted tooth germ using (a), (b) and (c) techniques are cultured for a specific period followed by transplantation of the engineered tooth germ into the jaw (orthotopic) or in the renal capsule environment. These methods are used to study the potential of stem cells/signaling molecules combinations to regenerate physiological enamel. This pre-clinical step proof-of-concept step may provide foundation for future clinical applications that involve scaffold-free approaches. Some elements of this figure were generated with Biorender.com.

2.3.2.8. Microfluidic "tooth on chip" systems

Microfluidics and organ-on-chip systems are devices on which different types of laboratory experiments can be run in the micro scale and they are recently developed in order to imitate the human models for pre-clinical studies more accurately compared to the traditional systems such as 2D cell culture systems or the animal models. The merits of this technology include the need for only small volume of the reagents, high efficiency, reproducibility, the potential for designing integrated systems [207,208]. Unlike the traditional co-culture systems in which two types of cell populations are grown in the same media that might not provide the appropriate conditions for one type of cells to preserve their physiological functions, in microfluidic systems cells can be cultured in different media [209]. Organ-specific components such as epithelial or mesenchymal cells or tissues can be grown on the various chambers which exist in such devices. The molecular cues are able to cross between the chambers, and the systemic blood circulation can be mimicked by controlling the flow of the appropriate media. In addition, the physiological and pathological processes in the organs and immune responses can be modelled in such devices by the insertion of the mechanical forces, which mimic the physiological movements and the electrical stimuli, and

by the integration of the circulating immune cells or living microbiomes [207]. In the field of dentistry, microfluidic co-culture systems have been developed for the first time to model the interactions between the embryonic trigeminal ganglia and the postnatal tooth germs and to study tooth innervation [210]. Other microfluidic systems which have been engineered in this field include those for salivary glands, oral mucosa and dental biofilm, dentinal tubules (for studying odontogenesis), pulp-dentin-biomaterials interface (for studying the response of pulp cells to various dental materials) [211]. Microfluidic 3D systems to study enamel repair and regeneration will further advance this field.

Chronodentistry

The circadian biological clock, which is defined as an adjustment to daily changes (24 h cycle), modulates different physiological and cellular processes in living organisms [212]. The circadian clock can be disrupted by specific lifestyles and behavioral choices such as shift works, irregular meals and alcohol and drug abuse [213,214]. Several pieces of evidences have led to the hypothesis that enamel development is under circadian control, including the modulation of the development of other mineralized tissues such as bone by the circadian clock, the daily growth patterns (so-called cross-striations) in enamel, and the circadian matrix deposition during the secretory stage and the alternation between smooth- and ruffle-ended ameloblasts which occurs every 8 hours during the maturation stage [212,215]. The clock genes (period circadian regulator 2 (*Per2*) and brain and muscle ARNT-like 1 (*Bmal1*)) were shown to be expressed in synchronized ameloblast-like LS8 cells. Amelogenin expression was significantly diminished during the night period while the expression of other genes involved in the tooth development such as enamel matrix endocytosis (lysosomal-associated membrane protein (*Lamp1*)), bicarbonate transport (sodium bicarbonate so-transporter (*NBCe1*)) and bicarbonate production (carbonic anhydrase 2 (*Car2*)) was elevated [216]. The oscillation of the major clock genes (circadian locomotor output cycles kaput (*Clock*), *Bmal1*, *Per1*, *Per2*) was also reported in synchronized HAT-7 cells at both RNA and protein levels. The expression levels of amelogenin and *Klk4* were upregulated by overexpression of *Bmal1*, as a positive modulator of the circadian rhythm, while downregulated by overexpression of cryptochrome 1 (*Cry1*), as a negative modulator of the circadian clock, suggesting that the secretory and maturation phases of amelogenesis are regulated in a circadian manner [215]. Significant delays were observed in melatonin receptors (MTs) and amelogenin expression as well

as the enamel development when neonatal mice were in all-night or all-day conditions. The newborn mice that were in all day environment also revealed a delay in the development of enamel with immature histological features. In addition, the enamel formation was delayed in mouse babies whose mothers had circadian disruption during pregnancy. This suggests that the circadian clock is a vital factor for the enamel to be normally developed during pre- and post-natal phases [217]. In addition, expression of clock genes takes place during the ameloblast differentiation [218–220] and controls the enamel secretion and expression of ameloblast genes, including amelogenin and enamelin and *Klk4* and the key transcription factor, *Runx2* [221]. The disruption of the store-operated calcium entry (SOCE) was found to affect the expression of the ameloblasts' clock genes [222]. Although the field of chronodentistry is still far from clinical applications, the regulation of the enamel deposition by circadian clock suggests that control of circadian rhythms in cell-based systems and also acellular ions/proteins delivery might improve the efficiency and the outcome of the therapeutic approaches for repair of enamel defects and dental enamel regeneration.

Scaffold-based strategies (Enamel tissue engineering)

Tissue engineering (TE) is an interdisciplinary area for regeneration of the lost or damaged tissues by using a combination of cells, scaffolds and signalling molecules (Figure 2.6) [223]. Differentiation of dental epithelial SF2 cells into ameloblasts and their mineralization were shown to be increased when grown in 3D cultures as spheroids [176]. Therefore, regeneration of the enamel tissue using scaffold-based strategies seems as a promising approach [224]. Scaffolds have been made from both synthetic and natural biomaterials in the forms of sponges, hydrogels, and meshes for regeneration of enamel or enamel-dental tissues complexes [225]. Scaffolds provide support for dental tissue formation through providing cell-matrix signals and ideally should be able to mimic the ECM, interact with cells and support cell proliferation and differentiation, degrade over time, have proper mechanical properties and allow diffusion of nutrients and waste products and also cells and growth factors [224,225].

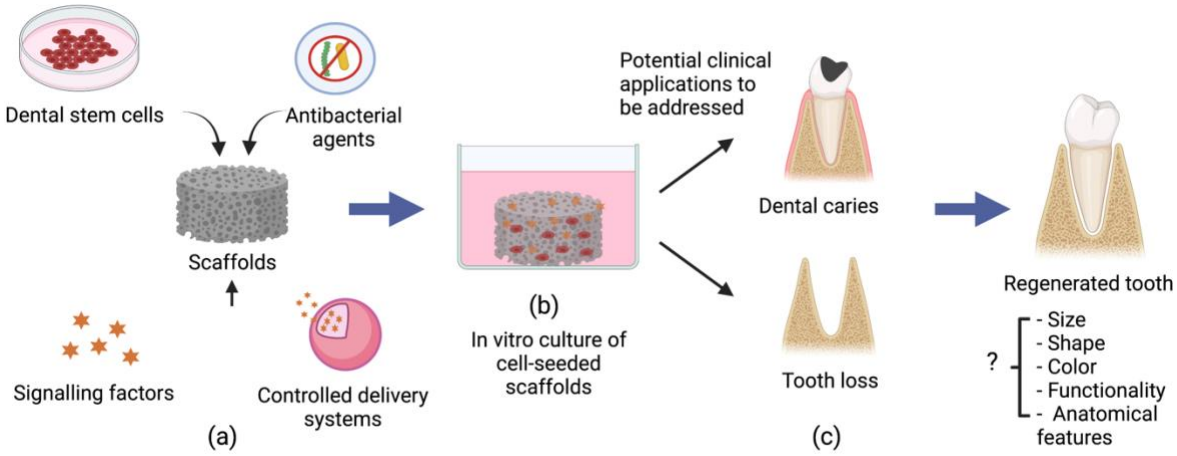

Figure 2.8. Scaffold-based strategies. (a) Three main elements of enamel tissue engineering including dental stem cells, signalling molecules, (b) cells are seeded onto the scaffolds loaded with signalling molecules and cultured in vitro to become mature, (c) the tissue engineered dental enamel is transplanted into the jaw for whole tooth applications or into dental cavities for enamel and/or joint enamel/dentin repair. Scaffold-based strategies may provide opportunities to incorporate controlled delivery systems for long term signaling molecules delivery and/or for delivery of anti-bacterial molecules that can be used in a caries environment. Some elements of this figure were generated with Biorender.com.

In the first study reported on the development of the bioengineered whole tooth crowns, single cell suspensions obtained from dissociated porcine third molar tooth buds were seeded on collagen-coated polyglycolate/poly-L-lactate (PGA/PLLA) and poly(lactide-co-glycolide) (PLGA) scaffolds, which were fabricated in the shape of human incisors and molars and transplanted onto the omentum of athymic rats. The reconstructed teeth contained enamel, dentin, pulp, and HERS- and cementoblasts-like tissues, and they were notably small (2× 2 mm) and did not match the size and shape of the biodegradable scaffolds [226]. In the next attempt, they revealed that cell suspensions of rat molar tooth buds could also be employed for the regeneration of the tooth crown in a shorter period of time compared to cells from the porcine molar tooth buds in the previous study, owing to the different natural growth patterns of the tooth in these two animals. It was shown that both PGA and PLGA scaffolds were able to support tooth growth [227]. In addition, the transplantation of the rat tooth bud cells seeded on the biodegradable PGA/PLLA and PLGA scaffolds into the mandible of the rat could regenerate small-sized tooth crowns containing dentin, enamel, pulp, and PDL. Hence, the bioengineered teeth showed the ability to replace the missing tooth by implanting the tissue engineered constructs at the location of the lost or the missing tooth in the jaw. However, the tooth grown in the fresh tooth extraction location in the jaw was less

organized in comparison to those grown in the omentum, which shows the need for further studies to improve the process of the implantation of the bioengineered tooth in the jaw [228]. A sequential cell-seeding approach was also shown to be useful for facilitating tooth regeneration and modulating the morphology of the tissue engineered constructs. In this method, the mesenchymal cells are seeded on the collagen sponge scaffolds at a high density, and epithelial stem cells are subsequently seeded on top of seeded mesenchymal cells so that these two cell populations are in direct contact [192].

When LS8 and primary EOE cells were grown within branched arginine-glycine-aspartic acid - peptide amphiphile nanofibrous structures (BRGD-PA), or injected into embryonic mouse incisors, they revealed increased differentiation into ameloblasts and a higher proliferation as well as enhanced matrix production and mineralization [229]. Furthermore, the transplantation of the incisor primordia, which were injected with BRGD-PA, in the renal capsule of the mice for a longer time, 8 weeks, showed the formation of the enamel pearls and mineralized nodules. In fact, BRGD-PA surrounding the EOE provides an artificial matrix and induces ameloblast differentiation as a result of cell-matrix interactions, which resemble signals from dental mesenchyme in the natural tooth development [230]. Subcutaneous transplantation of PLLA nanofibrous scaffolds, co-seeded with hERM-derived dental epithelial stem cells and human dental pulp stem cells, onto the back of the nude mice, resulted in the formation of the acinar and secretory epithelial-like structures without mineralized areas after 6 weeks. Additionally, the fully-formed heterotopic ossicles with the structure of enamel, dentin, cementum and bone, enclosed with cartilage tissue, as well as lipid-laden adipocytic clusters were observed in co-transplants after 10 weeks [164]. Scaffold based approaches provide also the opportunity to integrate anti-bacterial molecules with active ingredients that will activate cellular repair and regeneration signaling pathways similar to the systems used for dentin regeneration [60,139,231–233]. A summary of the scaffold-based strategies for enamel regeneration is summarized below (Table 2.1).

Table 2.1. Enamel regeneration using tissue engineering approaches

Scaffold type	**Scaffold material**	**Cell or animal studies**	**Signaling factors**	**Tissue type**	**References**
Porous scaffold made by solvent casting and porogen leaching	Collagen coated PGA/PLLA and PLGA scaffolds	*In vitro* Single cell suspension from dissociated porcine third molar tooth buds *In vivo* Omenta of athymic rats	-	Tooth crown consisting of enamel, dentin and pulp	[226]
Porous scaffold made by solvent casting and porogen leaching	PGA/PLLA and PLGA scaffolds	*In vitro* Single cell suspension from dissociated rat third molar tooth buds *In vivo* Omenta of syngeneic adult rats	-	Tooth crown consisting of enamel, dentin and pulp	[227]
Porous scaffold made by solvent casting and porogen leaching	Collagen coated PGA/PLLA and PLGA scaffolds	*In vitro* Single cell suspension from dissociated pig third molar tooth buds *In vivo* Omenta of athymic adult rat	-	Hybrid tooth-bone tissues containing enamel, pulp, dentin and bone	[234]
Porous scaffold	Gelfoam® Absorbable gelatin Dental Sponge strips, Upjohn/Pfizer Inc. PGA/PLLA scaffolds	*In vitro* Dental stem cells derived from enamel and pulp organs *In vivo* Mandible of female Yucatan mini pigs	-	Hybrid tooth-bone tissues containing enamel, pulp, dentin and bone, cementum, periodontal ligament	[235]
Porous scaffold made by solvent casting and porogen leaching	PGA/PLLA and PLGA scaffolds	*In vitro* Rat tooth bud cells *In vivo* Mandible of adult rat hosts and grown	-	Tooth crowns containing dentin, enamel, pulp, and PDL	[228]
Porous scaffold	Collagen sponge from NIPRO Corporation (Osaka, Japan) and PGA fiber mesh	*In vitro* Dissociated tooth cells from porcine third molar *In vivo* Omentum of immunocompromised rats	-	Enamel-dentin	[236]
	BRGD-PA	*In vitro*	-	Enamel	[229]

PA-based self-assembled nanofibers		The ameloblast-like cell line (LS8) / EOE Ex vivo The embryonic mandibular incisors (incisor primordia) from timed pregnant Swiss Webster mice			
PA-based self-assembled nanofibers	The branched RGDS peptide amphiphiles (bRGDS PA)	Ex vivo The embryonic mandibular incisors (incisor primordia) from timed pregnant Swiss Webster mice *In vivo* The kidney capsules of host mice Transplantation into the alveolar socket of pigs	-	Enamel	[230]
Nanofibers	PLLA	*In vitro* hDESCs/ human DPSCs	-	Enamel, cementum, dentin, and bone	[164]
Porous scaffolds	Beta tricalcium phosphate (beta-TCP)/collagen Particles	*In vitro* The tooth germ cells from SD rats *In vivo* Transplantation under SD rat's kidney capsule	Recombinant human BMP-2	Enamel-dentin	[237]
Fiber mesh	Collagen coated PGA fiber meshes	*In vitro* Cells of embryonic tooth germs *In vivo* Kidney capsule in adult mice	-	Enamel-covered dentin tissue	[238]
Fiber mesh	Collagen coated PGA fiber meshes	*In vitro* Tooth germ from porcine third molar *In vivo* Implantation in rat omentum	-	Enamel-covered dentin Cementum-covered dentin	[239]
Sponge scaffolds	Collagen	*In vitro* Mesenchymal cells so that they formed appropriate interactions in the scaffold *In vivo* Omentum of the rats	-	Enamel-dentin	[192]
		In vitro			

Sponge scaffolds	Collagen	Odontogenic epithelial cells and dental mesenchymal cells	-	Enamel-dentin comple	[240]

2.4. Current Challenges and Future perspectives for dental enamel defects

Although there is an urgent need for enamel regeneration and repair, the concept of enamel tissue engineering is still in its infancy, and numerous challenges and complexities are involved. For instance, the morphogenetic characteristics of the dental crown shape are far different from the shape of regenerated enamel-dentin complexes, which is either linear or circular with enamel inside the dentin (Iwatsuki et al., 2006). In addition, the arrangement of the enamel prims is somewhat irregular in comparison to the native enamel (Sumita et al., 2006). The size of the regenerated crowns is small and does not match the size of the scaffolds (Duailibi et al., 2008; Young et al., 2002). In addition, the complicated posttranslational protein processing needed for the crystal growth and the unique way of ameloblasts' movements through which HAp crystals are patterned into the enamel rods add more complexities to the engineering of the enamel tissue (Ahmed et al., 2020). As a result, further studies are required to be performed on how to regenerate the enamel tissue with controlled shape and size (Monteiro and Yelick, 2016).

Acellular and cellular approaches, which are discussed in this paper, need to be personalized based on individual characteristics and disease-specific traits as briefly discussed below (Table 2.2). For example, the methods which can imitate the organic matrix, including recombinant EMPs, dendrimers, self-assembling peptides, hydrogels, electrospun mats and EMP releasing systems, could be utilized in the case of enamel with a decreased thickness (hypoplasia). For hypo-mineralized enamel and tooth erosion, the methods that produce the inorganic phase of the enamel (HAp crystals) can be employed. These methods consist of chemical solution, inorganic paste, artificial HAp, rotary evaporation, electrodeposition, EART and laser-assisted mineralization. For hypo-maturation, which is caused by the deficient removal of the organic matrix via proteases, we hypothesize that proteases delivery systems can be applied to help with eliminating the matrix. In addition, initial or moderate carious lesions can be treated by chemical solution, inorganic paste, laser, EAER, electrodeposition, rotary evaporation, electrodeposition and organic matrix mimicking approaches, whereas the extensive lesions can be treated by tissue engineering and cell-

based strategies. Likewise, the enamel fracture due to dental trauma can be treated by tissue engineering and cell-based strategies. Lasers, EAER and tissue engineering and cell-based strategies can be potentially employed for tooth discoloration. Whole tissue engineering techniques and cell-based strategies can be used in the case of complete enamel absence.

Table 2.2. Different types of enamel defects, symptoms, causes and potential treatment options.

Defect	Symptoms	Causes	Potential treatment methods
Hypoplasia	Decreased thickness or full absence of enamel	Defect in the organic matrix formation	- Tissue engineering and cell- based strategies - Organic matrix mimicking approaches including recombinant EMPs, dendrimers, self-assembling peptides, hydrogels, electrospun mats and EMP releasing systems
Hypo-mineralization	- Normal thickness - Soft and weak	Defect in calcification during the maturation step	- Chemical solution - Inorganic paste - Artificial HAp - Electrodeposition - Laser-assisted mineralization - EAER - -Rotary evaporation
Hypo-maturation	- Normal thickness -Brittle with mottled appearance	Defect in removal of organic matrix	- Delivery systems for proteases (MMP20 and KLK4)
Dental caries	- Cavitation - Oral pain	Acid attack from interactions between sugar in the food and bacteria	- Chemical solution - Inorganic paste - Laser-assisted mineralization - EAER - Rotary evaporation - Organic matrix mimicking approaches including recombinant EMPs, dendrimers, self-assembling peptides, hydrogels, electrospun mats and EMP releasing systems

			- Tissue engineering and cell- based strategies
Dental trauma	- Enamel infraction - Crown fractures	Injury due to accident, physical activities or violence	- Tissue engineering and cell- based strategies -
Tooth erosion	Mineral loss from the tooth surface	Acidic dissolution or chelation due to vomiting, acid reflux, diet or industrial fumes	- Chemical solution - Inorganic paste - Artificial HAp - Electrodeposition - Rotary evaporation - Laser-assisted mineralization - EAER
Tooth discoloration	Change in color of the tooth (brown, yellow, black, grey)	- Intrinsic (Aging, metabolic or inherited diseases, trauma) - Extrinsic (diet, smoking, medicines, metal salts) - Stain internalization (caries, restorations, tooth wear)	- Laser-assisted mineralization - EAER - Tissue engineering and cell- based strategies

2.5. Conclusions

Despite encouraging first results achieved by several efforts which have been made in enamel repair and regeneration field, more research is required to recreate dental enamel with a quality similar to natural enamel and to control regenerative enamel size and shape [241–243]. Also, novel models are needed for preclinical testing prior application into the clinical practice [244,245]. Tooth is an intricate tissue formed as a result of a wide variety of biomolecular signals and gene expressions, and knowing more about the signalling pathways engaged in the natural tooth development is of great importance for enamel regeneration [225]. Accordingly, although considerable progress has been made with dental mesenchymal tissues cells resulting in repair and regeneration of dental mesenchymal tissues [246], there is a very limited number of studies available using human dental epithelial stem cells which differentiate to enamel-secreting ameloblasts producing regenerated human enamel. In contrast with the majority of other tissues in the human body, endogenous enamel regeneration is impossible because ameloblasts are lost by apoptosis prior to tooth eruption [233]. As a consequent, acellular methods and exogenous stem

cell approaches appear to be the only possibilities to re-create the lost or diseased enamel. There exist some challenges in acellular approaches, including scalability (from micro- to milli-meters) and fabrication of the enamel, with its structural hierarchy and both prism and interprismatic regions and mechanical properties similar to enamel, directly in the site of the defective enamel in the buccal environment [21,90,120,247]. In addition, the differentiation of dental stem cells into enamel-producing cells is considered another existing challenge in cell-based strategies.

The mechanism of epithelial-mesenchymal and cell-scaffold interactions needs to be further investigated as such interactions guide the morphology of the dental tissues and mineralization while defining the size and shape of the tooth [226,248]. More advanced co-culture models can also be developed based on microfluidic and organ-on-a-chip and cell patterning systems [199,249]. Moreover, to mimic the mesenchymal-epithelial signalling, the co-culture of dental epithelial stem cells and dental mesenchymal stem cells within a dual-compartment 3D printed scaffold will allow molecular signalling between the two cell types and will support the differentiation of the cells into enamel-forming ameloblasts and dentin-secreting odontoblasts and result in jointly regenerated enamel and dentin. In addition, the types of materials and designs that have been used to fabricate tissue engineering scaffolds for enamel regeneration are very limited, as illustrated in Table 2.1. Scaffolds with alternative materials (e.g. antibacterial materials) and various structural and architectural properties such as pore sizes, interconnectivity, and degradation rate need to be developed to ameliorate the formation of the dental enamel with the intended size and shape [228]. Considering the advances in nanotechnology [250–252] and 3D printing [253–256], it seems that more innovative structures can be fabricated to direct the interactions between mesenchymal and epithelial cells and also control cell proliferation and differentiation [233,248]. A combination of scaffolds, especially 3D printed scaffolds constructing anatomically shaped tooth with a desired size and shape [257], using delivery systems for controlled release of growth factors and genetic materials might be a promising method to stimulate stem cells differentiation and promote enamel regeneration. Lastly, more investigations on the effect of the circadian clock on dental stem cells can ameliorate enamel regeneration as this internal clock mechanism can promote the coordinated stem cells differentiation steps needed resulting in tissue regeneration that mimics a physiological pattern similar to natural enamel deposition and mineralization [258].

Acknowledgements

The authors gratefully acknowledge the Saskatchewan Health Research Foundation (SHRF) financial support (PI: PP), Colleges of Dentistry and College of Medicine start-up funds to PP and SP, respectively, and the University of Saskatchewan Dean's scholarship and Biomedical Engineering Devolved Scholarship (to FM).

Authors' contribution: Conceptualization, F.M, S.P, X.C, P.P; Resources, S.P, X.C, P.P; Writing-Original Draft, F.M; Writing-Review & Editing, F.M, S.P, X.C, P.P; Supervision, S.P, X.C, P.P.

References

[1] A. Gupta, Dental Biochemistry, in: Compr. Biochem. Dent., Springer, 2019: pp. 595–604.

[2] E. Battistella, S. Mele, L. Rimondini, Dental tissue engineering: a new approach to dental tissue reconstruction, in: Biomimetics Learn. from Nat., InTech, 2010.

[3] N. Biswas, A. Dey, S. Kundu, H. Chakraborty, A.K. Mukhopadhyay, Orientational effect in nanohardness of functionally graded microstructure in enamel, J. Inst. Eng. Ser. D. 93 (2012) 87–95.

[4] C.M. Saratti, G.T. Rocca, I. Krejci, The potential of three-dimensional printing technologies to unlock the development of new'bio-inspired'dental materials: an overview and research roadmap, J. Prosthodont. Res. 63 (2019) 131–139.

[5] M. Sun, N. Wu, H. Chen, Laser-assisted Rapid Mineralization of Human Tooth Enamel, Sci. Rep. 7 (2017) 9611.

[6] B. Jayasudha, H.K. Navin, K.B. Prasanna, Enamel regeneration-current progress and challenges, J. Clin. Diagnostic Res. JCDR. 8 (2014) ZE06.

[7] C.E. Fowler, M. Li, S. Mann, H.C. Margolis, Influence of surfactant assembly on the formation of calcium phosphate materials—A model for dental enamel formation, J. Mater. Chem. 15 (2005) 3317–3325.

[8] J. Ge, F.Z. Cui, X.M. Wang, H.L. Feng, Property variations in the prism and the organic sheath within enamel by nanoindentation, Biomaterials. 26 (2005) 3333–3339.

[9] R. Tang, L. Wang, C.A. Orme, T. Bonstein, P.J. Bush, G.H. Nancollas, Dissolution at the

nanoscale: self-preservation of biominerals, Angew. Chemie. 116 (2004) 2751–2755.

[10] Q. Ruan, J. Moradian-Oldak, Amelogenin and enamel biomimetics, J. Mater. Chem. B. 3 (2015) 3112–3129.

[11] N. Biswas, A. Dey, S. Kundu, H. Chakraborty, A.K. Mukhopadhyay, Mechanical properties of enamel nanocomposite, ISRN Biomater. 2013 (2013). Creative Commons Attribution 3.0 License.

[12] J.D. Bartlett, Dental enamel development: proteinases and their enamel matrix substrates, ISRN Dent. 2013 (2013).

[13] J.T. Wright, I.A. Carrion, C. Morris, The molecular basis of hereditary enamel defects in humans, J. Dent. Res. 94 (2015) 52–61.

[14] C.E. Smith, A. Nanci, Overview of morphological changes in enamel organ cells associated with major events in amelogenesis., Int. J. Dev. Biol. 39 (2003) 153–161.

[15] B.K.B. Berkovitz, G.R. Holland, B.J. Moxham, Oral Anatomy, Histology and Embryology E-Book, Elsevier Health Sciences, 2017.

[16] R.W. Brand, D.E. Isselhard, Anatomy of Orofacial Structures E-Book: A Comprehensive Approach, Elsevier Health Sciences, 2017.

[17] R.S. Lacruz, S. Habelitz, J.T. Wright, M.L. Paine, Dental enamel formation and implications for oral health and disease, Physiol. Rev. 97 (2017) 939–993.

[18] G. Varga, B. Kerémi, E. Bori, A. Földes, Function and repair of dental enamel–Potential role of epithelial transport processes of ameloblasts, Pancreatology. 15 (2015) S55–S60.

[19] A.L. Kierszenbaum, L. Tres, Histology and Cell Biology: an introduction to pathology E-Book, Elsevier Health Sciences, 2015.

[20] J.S. Colombo, A.N. Moore, J.D. Hartgerink, R.N. D'Souza, Scaffolds to control inflammation and facilitate dental pulp regeneration, J. Endod. 40 (2014) S6–S12.

[21] Y. Zhou, Y. Zhou, L. Gao, C. Wu, J. Chang, Synthesis of artificial dental enamel by an elastin-like polypeptide assisted biomimetic approach, J. Mater. Chem. B. 6 (2018) 844–853.

[22] A.D. İzgi, E. Kale, R. Niğiz, Amelogenesis imperfecta: rehabilitation and brainstorming on the treatment outcome after the first year, Case Rep. Dent. 2015 (2015).

[23] P.J. Slootweg, Dental pathology, Springer, 2007.

[24] A. Tariq, M.A. Ansari, Z. Memon, Developmental Enamel Defects: A Review, JPDA. 22

(2013) 245.

[25] H.M. Wong, Aetiological factors for developmental defects of enamel, Austin J. Anat. (2014).

[26] T. Kanchan, M. Machado, A. Rao, K. Krishan, A.K. Garg, Enamel hypoplasia and its role in identification of individuals: A review of literature, Indian J. Dent. 6 (2015) 99.

[27] P.M. Yamaguti, R.N. Cabral, Developmental Defects of Enamel, in: Pediatr. Restor. Dent., Springer, 2019: pp. 93–116.

[28] A.R. Ogden, R. Pinhasi, W.J. White, Gross enamel hypoplasia in molars from subadults in a 16th–18th century London graveyard, Am. J. Phys. Anthropol. Off. Publ. Am. Assoc. Phys. Anthropol. 133 (2007) 957–966.

[29] A. Bloch-Zupan, H. Sedano, C. Scully, Dento/oro/craniofacial anomalies and genetics, Elsevier, 2012.

[30] W.K. Seow, Developmental defects of enamel and dentine: challenges for basic science research and clinical management, Aust. Dent. J. 59 (2014) 143–154.

[31] K. Gadhia, S. McDonald, N. Arkutu, K. Malik, Amelogenesis imperfecta: an introduction, Br. Dent. J. 212 (2012) 377.

[32] H.Q. Tran, L. Jenssen, Classification of severe tooth discolorations and treatment options, (2011).

[33] I. Brignall, S.B. Mehta, S. Banerji, B. J Millar, Aesthetic composite veneers for an adult patient with amelogenesis imperfecta: a case report, Dent. Update. 38 (2011) 594–603.

[34] N. Tinanoff, Dental caries, in: Pediatr. Dent., Elsevier, 2019: pp. 169–179.

[35] Maintaining and Improving the Oral Health of Young Children, Pediatrics. 134 (2014) 1224 LP – 1229. https://doi.org/10.1542/peds.2014-2984.

[36] T. Walsh, H. V Worthington, A. Glenny, V.C.C. Marinho, A. Jeroncic, Fluoride toothpastes of different concentrations for preventing dental caries, Cochrane Database Syst. Rev. (2019).

[37] J.D.B. Featherstone, Dental caries: a dynamic disease process, Aust. Dent. J. 53 (2008) 286–291.

[38] N.B. Pitts, D.T. Zero, P.D. Marsh, K. Ekstrand, J.A. Weintraub, F. Ramos-Gomez, J. Tagami, S. Twetman, G. Tsakos, A. Ismail, Dental caries, Nat. Rev. Dis. Prim. 3 (2017) 1–16.

[39] I.S. Zhao, S.S. Gao, N. Hiraishi, M.F. Burrow, D. Duangthip, M.L. Mei, E.C. Lo, C. Chu, Mechanisms of silver diamine fluoride on arresting caries: a literature review, Int. Dent. J. 68 (2018) 67–76.

[40] R.H. Selwitz, A.I. Ismail, N.B. Pitts, Dental caries, Lancet. 369 (2007) 51–59.

[41] P. Moynihan, P.E. Petersen, Diet, nutrition and the prevention of dental diseases, Public Health Nutr. 7 (2004) 201–226.

[42] D.T. Zero, M. Fontana, E.A. Martínez-Mier, A. Ferreira-Zandoná, M. Ando, C. González-Cabezas, S. Bayne, The biology, prevention, diagnosis and treatment of dental caries: scientific advances in the United States, J. Am. Dent. Assoc. 140 (2009) 25S-34S.

[43] M. Kakkar, An alternative to filling and drilling-EAER, Int J Res Heal. Allied Sci. 2 (2016) 32–34.

[44] R. Lam, Epidemiology and outcomes of traumatic dental injuries: a review of the literature, Aust. Dent. J. 61 (2016) 4–20.

[45] S. Petti, U. Glendor, L. Andersson, World traumatic dental injury prevalence and incidence, a meta-analysis—One billion living people have had traumatic dental injuries, Dent. Traumatol. 34 (2018) 71–86.

[46] H.C. Güngör, Management of crown-related fractures in children: an update review, Dent. Traumatol. 30 (2014) 88–99.

[47] S.S. Chandra, E. Choudhary, S. Chandra, Traumatic injuries to permanent anterior teeth among Indians: frequency, aetiology and risk factors., Endod. Pract. Today. 8 (2014).

[48] I. Viduskalne, R. Care, Analysis of the crown fractures and factors affecting pulp survival due to dental trauma, Stomatologija. 12 (2010) 109–115.

[49] S. Olsburgh, T. Jacoby, I. Krejci, Crown fractures in the permanent dentition: pulpal and restorative considerations, Dent. Traumatol. 18 (2002) 103–115.

[50] S. Olsburgh, I. Krejci, Pulp response to traumatic crown fractures, Endod. Top. 5 (2003) 26–40.

[51] N. Arhun, A. Arman-Ozcirpici, M. Ungor, O.P. Ozsoy, Dental Caries, Tooth Fracture and Exposed Dental Pulp: The Role of Endodontics in Orthodontic Treatment Planning and Mechanotherapy, Integr. Clin. Orthod. (2012) 283–312.

[52] F. Ojeda-Gutierrez, B. Martinez-Marquez, S. Arteaga-Larios, M.S. Ruiz-Rodriguez, A. Pozos-Guillen, Management and followup of complicated crown fractures in young

patients treated with partial pulpotomy, Case Rep. Dent. 2013 (2013).

[53] N. Zubaidah, Management of horizontal crown fracture caused by traumatic injury with endorestoration treatment, Dent. J. (Majalah Kedokt. Gigi). 44 (2011) 154–158.

[54] M. Addy, R.P. Shellis, Interaction between attrition, abrasion and erosion in tooth wear, in: Dent. Eros., Karger Publishers, 2006: pp. 17–31.

[55] S. Wongkhantee, V. Patanapiradej, C. Maneenut, D. Tantbirojn, Effect of acidic food and drinks on surface hardness of enamel, dentine, and tooth-coloured filling materials, J. Dent. 34 (2006) 214–220.

[56] J. Vlacic, I.A. Meyers, L.J. Walsh, Laser-activated fluoride treatment of enamel as prevention against erosion, Aust. Dent. J. 52 (2007) 175–180.

[57] S. Zimmer, G. Kirchner, M. Bizhang, M. Benedix, Influence of various acidic beverages on tooth erosion. Evaluation by a new method, PLoS One. 10 (2015) e0129462.

[58] K.S.F. de MESQUITA-GUIMARÃES, C. Scatena, M.C. Borsatto, A.L. Rodrigues-Junior, M.C. Serra, Effect of foods and drinks on primary tooth enamel after erosive challenge with hydrochloric acid, Braz. Oral Res. 29 (2015).

[59] A. Lussi, T. Jaeggi, M. Schaffner, Prevention and minimally invasive treatment of erosions., Oral Health Prev. Dent. 2 (2004) 321.

[60] X. Chatzistavrou, J.C. Fenno, D. Faulk, S. Badylak, T. Kasuga, A.R. Boccaccini, P. Papagerakis, Fabrication and characterization of bioactive and antibacterial composites for dental applications, Acta Biomater. 10 (2014) 3723–3732.

[61] X. Chatzistavrou, S. Velamakanni, K. DiRenzo, A. Lefkelidou, J.C. Fenno, T. Kasuga, A.R. Boccaccini, P. Papagerakis, Designing dental composites with bioactive and bactericidal properties, Mater. Sci. Eng. C. 52 (2015) 267–272.

[62] X. Chatzistavrou, A. Lefkelidou, L. Papadopoulou, E. Pavlidou, K.M. Paraskevopoulos, J.C. Fenno, S. Flannagan, C. González-Cabezas, N. Kotsanos, P. Papagerakis, Bactericidal and bioactive dental composites, Front. Physiol. 9 (2018) 103.

[63] M. Sulieman, An overview of tooth discoloration: extrinsic, intrinsic and internalized stains, Dent. Update. 32 (2005) 463–471.

[64] S.T. Manuel, P. Abhishek, M. Kundabala, Etiology of tooth discoloration-a review, Etiol. Tooth Discoloration-a Rev. 18 (2010) 56–63.

[65] J.R. Lukacs, L.L. Largaespada, Explaining sex differences in dental caries prevalence:

Saliva, hormones, and “life-history” etiologies, Am. J. Hum. Biol. Off. J. Hum. Biol. Assoc. 18 (2006) 540–555.

[66] J.R. Lukacs, Sex differences in dental caries experience: clinical evidence, complex etiology, Clin. Oral Investig. 15 (2011) 649–656.

[67] L. Doyal, S. Naidoo, Why dentists should take a greater interest in sex and gender, Br. Dent. J. 209 (2010) 335–337.

[68] A.H.W. Chan, Sexual Dimorphism of Modern Tooth Crown Tissues, (2007).

[69] T.M. Sabóia, P.N. Tannure, R.R. Luiz, M. de Castro Costa, J.M. Granjeiro, E.C. Küchler, L.S. Antunes, Sexual dimorphism involved in the mesiodistal and buccolingual dimensions of permanent teeth, Dent. 3000. 1 (2013) 2–6.

[70] L.H. Luna, Canine sex estimation and sexual dimorphism in the collection of identified skeletons of the University of Coimbra, with an application in a Roman cemetery from Faro, Portugal, Int. J. Osteoarchaeol. 29 (2019) 260–272.

[71] W. Monalisa, G. Kokila, H.D. Sharma, P.A. Gopinathan, O.M. Singh, S. Kumaraswamy, Sexual dimorphism of enamel area, coronal dentin area, bicervical diameter and dentinoenamel junction scallop area in longitudinal ground section, J. Oral Maxillofac. Pathol. JOMFP. 22 (2018) 423.

[72] E.P. Chalisserry, S.Y. Nam, S.H. Park, S. Anil, Therapeutic potential of dental stem cells, J. Tissue Eng. 8 (2017) 2041731417702531.

[73] K. Jedeon, S. Loiodice, K. Salhi, M. Le Normand, S. Houari, J. Chaloyard, A. Berdal, S. Babajko, Androgen receptor involvement in rat amelogenesis: an additional way for endocrine-disrupting chemicals to affect enamel synthesis, Endocrinology. 157 (2016) 4287–4296.

[74] S. Houari, S. Loiodice, K. Jedeon, A. Berdal, S. Babajko, Expression of steroid receptors in ameloblasts during amelogenesis in rat incisors, Front. Physiol. 7 (2016) 503.

[75] O.Y. Yu, M.L. Mei, I.S. Zhao, E.C.-M. Lo, C.-H. Chu, Effects of fluoride on two chemical models of enamel demineralization, Materials (Basel). 10 (2017) 1245.

[76] J. Hicks, F. Garcia-Godoy, C. Flaitz, Biological factors in dental caries: role of remineralization and fluoride in the dynamic process of demineralization and remineralization (part 3), J. Clin. Pediatr. Dent. 28 (2004) 203–214.

[77] J.A. Cury, L.M.A. Tenuta, Enamel remineralization: controlling the caries disease or

treating early caries lesions?, Braz. Oral Res. 23 (2009) 23–30.

[78] P.M. Koenigs, R. V Faller, Fundamentals of Dentifrice: Oral Health Benefits in a Tube, Contin. Dent. Educ. (2013).

[79] M. Goswami, S. Saha, T.R. Chaitra, Latest developments in non-fluoridated remineralizing technologies, J. Indian Soc. Pedod. Prev. Dent. 30 (2012) 2.

[80] K.G. Chhabra, P.J. Shetty, K.V. V Prasad, C.S. Mendon, R. Kalyanpur, The beyond measures: Non flouride preventive measures for dental caries, J Int Oral Heal. 3 (2011) 1–8.

[81] G. Acharya, P. Agrawal, G. Patri, Recent biomimetic advances in rebuilding lost enamel structure, J. Int. Oral Heal. 8 (2016) 527.

[82] Y. Şener, G. Tosun, F. Kahvecioğlu, A. Gökalp, H. Koc, Fluoride levels of human plasma and breast milk, Eur. J. Dent. 1 (2007) 21.

[83] D. Kanduti, P. Sterbenk, B. Artnik, Fluoride: a review of use and effects on health, Mater. Sociomed. 28 (2016) 133.

[84] F.C. Sampaio, S.M. Levy, Systemic fluoride, Fluoride Oral Environ. 22 (2011) 133–145.

[85] F. V Zohoori, N. Omid, R.A. Sanderson, R.A. Valentine, A. Maguire, Fluoride retention in infants living in fluoridated and non-fluoridated areas: effects of weaning, Br. J. Nutr. 121 (2019) 74–81.

[86] S. Lata, N.O. Varghese, J.M. Varughese, Remineralization potential of fluoride and amorphous calcium phosphate-casein phospho peptide on enamel lesions: An in vitro comparative evaluation, J. Conserv. Dent. JCD. 13 (2010) 42.

[87] P. Shen, D.J. Manton, N.J. Cochrane, G.D. Walker, Y. Yuan, C. Reynolds, E.C. Reynolds, Effect of added calcium phosphate on enamel remineralization by fluoride in a randomized controlled in situ trial, J. Dent. 39 (2011) 518–525.

[88] R.J. Sullivan, J. Masters, R. Cantore, A. Roberson, I. Petrou, M. Stranick, H. Goldman, B. Guggenheim, A. Gaffar, Development of an enhanced anticaries efficacy dual component dentifrice containing sodium fluoride and dicalcium phosphate dihydrate., Am. J. Dent. 14 (2001) 3A-11A.

[89] F. Meyer, B.T. Amaechi, H.-O. Fabritius, J. Enax, Overview of calcium phosphates used in biomimetic oral care, Open Dent. J. 12 (2018) 406.

[90] A.A. Volponi, L.K. Zaugg, V. Neves, Y. Liu, P.T. Sharpe, Tooth Repair and

Regeneration, Curr. Oral Heal. Reports. 5 (2018) 295–303.

[91] Y. Yin, S. Yun, J. Fang, H. Chen, Chemical regeneration of human tooth enamel under near-physiological conditions, Chem. Commun. (2009) 5892–5894.

[92] H. Chen, Z. Tang, J. Liu, K. Sun, S. Chang, M.C. Peters, J.F. Mansfield, A. Czajka-Jakubowska, B.H. Clarkson, Acellular synthesis of a human enamel-like microstructure, Adv. Mater. 18 (2006) 1846–1851.

[93] B.Y. Liu, E.C.M. Lo, C.M.T. Li, Effect of silver and fluoride ions on enamel demineralization: a quantitative study using micro-computed tomography, Aust. Dent. J. 57 (2012) 65–70.

[94] S.S. Gao, I.S. Zhao, N. Hiraishi, D. Duangthip, M.L. Mei, E.C.M. Lo, C.H. Chu, Clinical trials of silver diamine fluoride in arresting caries among children: a systematic review, JDR Clin. Transl. Res. 1 (2016) 201–210.

[95] C. Shao, B. Jin, Z. Mu, H. Lu, Y. Zhao, Z. Wu, L. Yan, Z. Zhang, Y. Zhou, H. Pan, Repair of tooth enamel by a biomimetic mineralization frontier ensuring epitaxial growth, Sci. Adv. 5 (2019) eaaw9569.

[96] A. Gao, R. Hang, L. Bai, B. Tang, P.K. Chu, Electrochemical surface engineering of titanium-based alloys for biomedical application, Electrochim. Acta. (2018).

[97] Y. Wang, Manganese dioxide based composite electrodes for electrochemical supercapacitors, (2012).

[98] Y. Fan, Z. Sun, R. Wang, C. Abbott, J. Moradian-Oldak, Enamel inspired nanocomposite fabrication through amelogenin supramolecular assembly, Biomaterials. 28 (2007) 3034–3042.

[99] C. Lei, Y. Liao, Z. Feng, Kinetic model for hydroxyapatite precipitation on human enamel surface by electrolytic deposition, Biomed. Mater. 4 (2009) 35010.

[100] Y. Fan, R. Wang, J. Moradian-Oldak, Fabrication of enamel-mimicking mineralization composite coating induced by electrolytic deposition (ELD) system, MRS Online Proc. Libr. Arch. 1008 (2007).

[101] I. Zhitomirsky, Cathodic electrodeposition of ceramic and organoceramic materials. Fundamental aspects, Adv. Colloid Interface Sci. 97 (2002) 279–317.

[102] J. Moradian-Oldak, W. Leung, A.G. Fincham, Temperature and pH-dependent supramolecular self-assembly of amelogenin molecules: a dynamic light-scattering

analysis, J. Struct. Biol. 122 (1998) 320–327.

[103] C. Cao, M. Mei, Q. Li, E. Lo, C. Chu, Methods for biomimetic mineralisation of human enamel: a systematic review, Materials (Basel). 8 (2015) 2873–2886.

[104] K. Yamagishi, K. Onuma, T. Suzuki, F. Okada, J. Tagami, M. Otsuki, P. Senawangse, Materials chemistry: a synthetic enamel for rapid tooth repair, Nature. 433 (2005) 819.

[105] K. Onuma, K. Yamagishi, A. Oyane, Nucleation and growth of hydroxyapatite nanocrystals for nondestructive repair of early caries lesions, J. Cryst. Growth. 282 (2005) 199–207.

[106] M. Okada, T. Matsumoto, Synthesis and modification of apatite nanoparticles for use in dental and medical applications, Jpn. Dent. Sci. Rev. 51 (2015) 85–95.

[107] K.R. Deshmukh, Synthesis and Characterization of Fluorescent Hydroxyapatite Nanoparticles and Their Applications in Bioimaging and Plasmid Delivery, (2016).

[108] X. Wang, Y. Sun, K. Lin, Facile synthesis of dental enamel-like hydroxyapatite nanorod arrays via hydrothermal transformation of hillebrandite nanobelts, J. Mater. Chem. B. 3 (2015) 7334–7339.

[109] D. Wu, J. Yang, J. Li, L. Chen, B. Tang, X. Chen, W. Wu, J. Li, Hydroxyapatite-anchored dendrimer for in situ remineralization of human tooth enamel, Biomaterials. 34 (2013) 5036–5047.

[110] S. Wang, L. Zhang, W. Chen, H. Jin, Y. Zhang, L. Wu, H. Shao, Z. Fang, X. He, S. Zheng, Rapid regeneration of enamel-like-oriented inorganic crystals by using rotary evaporation, Mater. Sci. Eng. C. (2020) 111141.

[111] A.D. Anastasiou, S. Strafford, C.L. Thomson, J. Gardy, T.J. Edwards, M. Malinowski, S.A. Hussain, N.K. Metzger, A. Hassanpour, C.T.A. Brown, Exogenous mineralization of hard tissues using photo-absorptive minerals and femto-second lasers; the case of dental enamel, Acta Biomater. 71 (2018) 86–95.

[112] N.B. Pitts, J.P. Wright, Reminova and EAER: keeping enamel whole through caries remineralization, Adv. Dent. Res. 29 (2018) 48–54.

[113] M. Patel, Dental caries vaccine: are we there yet?, Lett. Appl. Microbiol. 70 (2020) 2–12.

[114] B. Arora, V. Setia, A. Kaur, M. Mahajan, H.K. Sekhon, H. Singh, Dental caries vaccine: An overview, Indian J. Dent. Sci. 10 (2018) 121.

[115] Y. Abiko, Passive immunization against dental caries and periodontal disease:

development of recombinant and human monoclonal antibodies, Crit. Rev. Oral Biol. Med. 11 (2000) 140–158.

[116] M.K. Alam, L. Zheng, R. Liu, S. Papagerakis, P. Papagerakis, C.R. Geyer, Synthetic antigen-binding fragments (Fabs) against S. mutans and S. sobrinus inhibit caries formation, Sci. Rep. 8 (2018) 1–9.

[117] T. Baumann, T.S. Carvalho, A. Lussi, The effect of enamel proteins on erosion, Sci. Rep. 5 (2015) 15194.

[118] Y. Cao, M.L. Mei, Q.-L. Li, E.C.M. Lo, C.H. Chu, Agarose hydrogel biomimetic mineralization model for the regeneration of enamel prismlike tissue, ACS Appl. Mater. Interfaces. 6 (2013) 410–420.

[119] J.E. Nör, Buonocore memorial lecture: tooth regeneration in operative dentistry, Oper. Dent. 31 (2006) 633–642.

[120] J. Moradian-Oldak, Protein-mediated enamel mineralization, Front. Biosci. a J. Virtual Libr. 17 (2012) 1996.

[121] Q. Ruan, D. Liberman, R. Bapat, K.B. Chandrababu, J.-H. Phark, J. Moradian-Oldak, Efficacy of amelogenin-chitosan hydrogel in biomimetic repair of human enamel in pH-cycling systems, J. Biomed. Eng. Informatics. 2 (2016) 119.

[122] Q. Ruan, Y. Zhang, X. Yang, S. Nutt, J. Moradian-Oldak, An amelogenin–chitosan matrix promotes assembly of an enamel-like layer with a dense interface, Acta Biomater. 9 (2013) 7289–7297.

[123] Y. Fan, Z. Sun, J. Moradian-Oldak, Controlled remineralization of enamel in the presence of amelogenin and fluoride, Biomaterials. 30 (2009) 478–483.

[124] E. Abbasi, S.F. Aval, A. Akbarzadeh, M. Milani, H.T. Nasrabadi, S.W. Joo, Y. Hanifehpour, K. Nejati-Koshki, R. Pashaei-Asl, Dendrimers: synthesis, applications, and properties, Nanoscale Res. Lett. 9 (2014) 247.

[125] S. Svenson, D.A. Tomalia, Dendrimers in biomedical applications—reflections on the field, Adv. Drug Deliv. Rev. 64 (2012) 102–115.

[126] M. Chen, J. Yang, J. Li, K. Liang, L. He, Z. Lin, X. Chen, X. Ren, J. Li, Modulated regeneration of acid-etched human tooth enamel by a functionalized dendrimer that is an analog of amelogenin, Acta Biomater. 10 (2014) 4437–4446.

[127] J.M. Holzwarth, P.X. Ma, 3D nanofibrous scaffolds for tissue engineering, J. Mater.

Chem. 21 (2011) 10243–10251.

[128] L.T.H. Nguyen, S. Chen, N.K. Elumalai, M.P. Prabhakaran, Y. Zong, C. Vijila, S.I. Allakhverdiev, S. Ramakrishna, Biological, chemical, and electronic applications of nanofibers, Macromol. Mater. Eng. 298 (2013) 822–867.

[129] M. Rivas, L.J. del Valle, C. Alemán, J. Puiggalí, Peptide Self-Assembly into Hydrogels for Biomedical Applications Related to Hydroxyapatite, Gels. 5 (2019) 14.

[130] M.E. Furth, A. Atala, Tissue engineering: future perspectives, in: Princ. Tissue Eng. (Fourth Ed., Elsevier, 2014: pp. 83–123.

[131] L. Sun, C. Zheng, T.J. Webster, Self-assembled peptide nanomaterials for biomedical applications: promises and pitfalls, Int. J. Nanomedicine. 12 (2017) 73.

[132] A. Firth, A. Aggeli, J.L. Burke, X. Yang, J. Kirkham, Biomimetic self-assembling peptides as injectable scaffolds for hard tissue engineering, (2006).

[133] N. Philip, State of the Art Enamel Remineralization Systems: The Next Frontier in Caries Management, Caries Res. 53 (2019) 284–295.

[134] J. Kirkham, A. Firth, D. Vernals, N. Boden, C. Robinson, R.C. Shore, S.J. Brookes, A. Aggeli, Self-assembling peptide scaffolds promote enamel remineralization, J. Dent. Res. 86 (2007) 426–430.

[135] F. Ketabat, M. Pundir, F. Mohabatpour, L. Lobanova, S. Koutsopoulos, L. Hadjiiski, X. Chen, P. Papagerakis, S. Papagerakis, Controlled Drug Delivery Systems for Oral Cancer Treatment—Current Status and Future Perspectives, Pharmaceutics. 11 (2019) 302.

[136] S. Busch, U. Schwarz, R. Kniep, Morphogenesis and structure of human teeth in relation to biomimetically grown fluorapatite− gelatine composites, Chem. Mater. 13 (2001) 3260–3271.

[137] S. Busch, U. Schwarz, R. Kniep, Chemical and structural investigations of biomimetically grown fluorapatite–gelatin composite aggregates, Adv. Funct. Mater. 13 (2003) 189–198.

[138] S. Busch, Regeneration of human tooth enamel, Angew. Chemie Int. Ed. 43 (2004) 1428–1431.

[139] Y.Y. Wang, X. Chatzistavrou, D. Faulk, S. Badylak, L. Zheng, S. Papagerakis, L. Ge, H. Liu, P. Papagerakis, Biological and bactericidal properties of Ag-doped bioactive glass in a natural extracellular matrix hydrogel with potential application in dentistry, Eur Cell Mater. 29 (2015) 342–355.

[140] Z. Ye, X. Zhu, I. Mutreja, S.K. Boda, N.G. Fischer, A. Zhang, C. Lui, Y. Qi, C. Aparicio, Biomimetic mineralized hybrid scaffolds with antimicrobial peptides, Bioact. Mater. 6 (2021) 2250–2260.

[141] H. Aksel, F. Mahjour, F. Bosaid, S. Calamak, A.A. Azim, Antimicrobial activity and biocompatibility of antibiotic-loaded chitosan hydrogels as a potential scaffold in regenerative endodontic treatment, J. Endod. 46 (2020) 1867–1875.

[142] P.W. McIntyre, J.L. Wu, R. Kolte, R. Zhang, R.L. Gregory, A. Bruzzaniti, G.H. Yassen, The antimicrobial properties, cytotoxicity, and differentiation potential of double antibiotic intracanal medicaments loaded into hydrogel system, Clin. Oral Investig. 23 (2019) 1051–1059.

[143] Y. Fan, Z.T. Wen, S. Liao, T. Lallier, J.L. Hagan, J.T. Twomley, J.-F. Zhang, Z. Sun, X. Xu, Novel amelogenin-releasing hydrogel for remineralization of enamel artificial caries, J. Bioact. Compat. Polym. 27 (2012) 585–603.

[144] M. Zafar, S. Najeeb, Z. Khurshid, M. Vazirzadeh, S. Zohaib, B. Najeeb, F. Sefat, Potential of electrospun nanofibers for biomedical and dental applications, Materials (Basel). 9 (2016) 73.

[145] J. Fletcher, D. Walsh, C.E. Fowler, S. Mann, Electrospun mats of PVP/ACP nanofibres for remineralization of enamel tooth surfaces, CrystEngComm. 13 (2011) 3692–3697.

[146] V. Uskoković, Amelogenin in enamel tissue engineering, in: Eng. Miner. Load Bear. Tissues, Springer, 2015: pp. 237–254.

[147] Y. Lu, P. Papagerakis, Y. Yamakoshi, J.C.-C. Hu, J.D. Bartlett, J.P. Simmer, Functions of KLK4 and MMP-20 in dental enamel formation, Biol. Chem. 389 (2008) 695–700.

[148] R. Sidaly, M.A. Landin, Z. Suo, M.L. Snead, S.P. Lyngstadaas, J.E. Reseland, Hypoxia increases the expression of enamel genes and cytokines in an ameloblast-derived cell line, Eur. J. Oral Sci. 123 (2015) 335–340.

[149] N. Mokhtari, M. Vaidyanathan, S. Esener, Y.-S. Yeh, Nanoparticle-mediated enzyme delivery for application in cancer therapy, Drug Target Rev. 4 (2017) 38–41.

[150] S. Yan, L. Yang, L. Lu, Q. Guo, X. Hu, Y. Yuan, Y. Li, M. Wu, J. Zhang, Improved pharmacokinetic characteristics and bioactive effects of anticancer enzyme delivery systems, Expert Opin. Drug Metab. Toxicol. 14 (2018) 951–960.

[151] I.P. de Sousa, B. Cattoz, M.D. Wilcox, P.C. Griffiths, R. Dalgliesh, S. Rogers, A.

Bernkop-Schnürch, Nanoparticles decorated with proteolytic enzymes, a promising strategy to overcome the mucus barrier, Eur. J. Pharm. Biopharm. 97 (2015) 257–264.

[152] S.N. Dean, K.B. Turner, I.L. Medintz, S.A. Walper, Targeting and delivery of therapeutic enzymes, Ther. Deliv. 8 (2017) 577–595.

[153] S. Proksch, K.M. Galler, Scaffold Materials and Dental Stem Cells in Dental Tissue Regeneration, Curr. Oral Heal. Reports. 5 (2018) 304–316.

[154] P.K. Den Besten, C.H.E. Mathews, C. Gao, W. Li, Primary culture and characterization of enamel organ epithelial cells, Connect. Tissue Res. 38 (1998) 3–8.

[155] M.J. Honda, Y. Shinmura, Y. Shinohara, Enamel tissue engineering using subcultured enamel organ epithelial cells in combination with dental pulp cells, Cells Tissues Organs. 189 (2009) 261–267.

[156] K. Honda, Masaki and Hata, Enamel Tissue Engineering, in: 2010. https://doi.org/10.5772/8586.

[157] Y. Wang, L. Lv, X. Yu, T. Zhang, S. Li, The characteristics of epithelial cell rests of Malassez during tooth eruption of development mice, J. Mol. Histol. 45 (2014) 1–10. https://doi.org/10.1007/s10735-013-9527-2.

[158] H. Nam, J.-H. Kim, J.-W. Kim, B.-M. Seo, J.-C. Park, J.-W. Kim, G. Lee, Establishment of Hertwig's epithelial root sheath/epithelial rests of Malassez cell line from human periodontium, Mol. Cells. 37 (2014) 562.

[159] N.C.F. Fagundes, B.C.L. Nogueira, J. Valladares Neto, D. Normando, R.R. Lima, Epithelial rests of Malassez: from latent cells to active participation in orthodontic movement, Dental Press J. Orthod. 22 (2017) 119–125.

[160] J. Xiong, K. Mrozik, S. Gronthos, P.M. Bartold, Epithelial cell rests of Malassez contain unique stem cell populations capable of undergoing epithelial–mesenchymal transition, Stem Cells Dev. 21 (2011) 2012–2025.

[161] W. Ono, N. Sakagami, S. Nishimori, N. Ono, H.M. Kronenberg, Parathyroid hormone receptor signalling in osterix-expressing mesenchymal progenitors is essential for tooth root formation, Nat. Commun. 7 (2016).

[162] S.P. Priya, A. Higuchi, S.A. Fanas, M.P. Ling, V.K. Neela, P.M. Sunil, T.R. Saraswathi, K. Murugan, A.A. Alarfaj, M.A. Munusamy, Odontogenic epithelial stem cells: hidden sources, Lab. Investig. 95 (2015) 1344.

[163] Y. Shinmura, S. Tsuchiya, K. Hata, M.J. Honda, Quiescent epithelial cell rests of Malassez can differentiate into ameloblast-like cells, J. Cell. Physiol. 217 (2008) 728–738.

[164] M. Athanassiou-Papaefthymiou, P. Papagerakis, S. Papagerakis, Isolation and characterization of human adult epithelial stem cells from the periodontal ligament, J. Dent. Res. 94 (2015) 1591–1600.

[165] B. Wang, L. Li, S. Du, C. Liu, X. Lin, Y. Chen, Y. Zhang, Induction of human keratinocytes into enamel-secreting ameloblasts, Dev. Biol. 344 (2010) 795–799.

[166] Y. Song, B. Wang, H. Li, X. Hu, X. Lin, X. Hu, Y. Zhang, Low temperature culture enhances ameloblastic differentiation of human keratinocyte stem cells, J. Mol. Histol. 50 (2019) 417–425.

[167] X. Hu, J.-W. Lee, X. Zheng, J. Zhang, X. Lin, Y. Song, B. Wang, X. Hu, H.-H. Chang, Y. Chen, Efficient induction of functional ameloblasts from human keratinocyte stem cells, Stem Cell Res. Ther. 9 (2018) 1–13.

[168] M. MacDougall, O. Mamaeva, C. Lu, S. Chen, Establishment and characterization of immortalized mouse ameloblast-like cell lines, Orthod. Craniofac. Res. 22 (2019) 134–141.

[169] J. Sarkar, E.J. Simanian, S.Y. Tuggy, J.D. Bartlett, M.L. Snead, T. Sugiyama, M.L. Paine, Comparison of two mouse ameloblast-like cell lines for enamel-specific gene expression , Front. Physiol. . 5 (2014) 277.

[170] E. Le Norcy, J. Lesieur, J. Sadoine, G.Y. Rochefort, C. Chaussain, A. Poliard, Phosphorylated and non-phosphorylated Leucine Rich Amelogenin Peptide differentially affect ameloblast mineralization, Front. Physiol. 9 (2018) 55.

[171] E.A. Riksen, A.K. Stunes, A. Kalvik, B.I. Gustafsson, M.L. Snead, U. Syversen, S.P. Lyngstadaas, J.E. Reseland, Serotonin and fluoxetine receptors are expressed in enamel organs and LS8 cells and modulate gene expression in LS8 cells, Eur. J. Oral Sci. 118 (2010) 566–573.

[172] A. Nakata, T. Kameda, H. Nagai, K. Ikegami, Y. Duan, K. Terada, T. Sugiyama, Establishment and characterization of a spontaneously immortalized mouse ameloblast-lineage cell line, Biochem. Biophys. Res. Commun. 308 (2003) 834–839. https://doi.org/https://doi.org/10.1016/S0006-291X(03)01467-0.

[173] E. Bori, J. Guo, R. Rácz, B. Burghardt, A. Földes, B. Kerémi, H. Harada, M.C. Steward,

P. Den Besten, A. Bronckers, Evidence for bicarbonate secretion by ameloblasts in a novel cellular model, J. Dent. Res. 95 (2016) 588–596.

[174] S. Kawano, M. Saito, K. Handa, T. Morotomi, T. Toyono, Y. Seta, N. Nakamura, T. Uchida, K. Toyoshima, M. Ohishi, H. Harada, Characterization of Dental Epithelial Progenitor Cells Derived from Cervical-loop Epithelium in a Rat Lower Incisor, J. Dent. Res. 83 (2004) 129–133. https://doi.org/10.1177/154405910408300209.

[175] S. Kawano, T. Morotomi, T. Toyono, N. Nakamura, T. Uchida, M. Ohishi, K. Toyoshima, H. Harada, Establishment of Dental Epithelial Cell Line (HAT-7) and the Cell Differentiation Dependent on Notch Signaling Pathway, Connect. Tissue Res. 43 (2002) 409–412. https://doi.org/10.1080/03008200290000637.

[176] M. Tadaki, T. Anada, Y. Shiwaku, T. Nakamura, M. Nakamura, M. Kojima, T. Arai, S. Fukumoto, O. Suzuki, A 3D culture model study monitoring differentiation of dental epithelial cells into ameloblast-like cells, RSC Adv. 6 (2016) 62109–62118.

[177] K. Takahashi, S. Yamanaka, Induction of pluripotent stem cells from mouse embryonic and adult fibroblast cultures by defined factors, Cell. 126 (2006) 663–676.

[178] N. Malhotra, Induced pluripotent stem (iPS) cells in dentistry: a review, Int. J. Stem Cells. 9 (2016) 176.

[179] M. Sakurai, R. Hayashi, T. Kageyama, M. Yamato, K. Nishida, Induction of putative stratified epithelial progenitor cells in vitro from mouse-induced pluripotent stem cells, J. Artif. Organs. 14 (2011) 58–66.

[180] M. Arakaki, M. Ishikawa, T. Nakamura, T. Iwamoto, A. Yamada, E. Fukumoto, M. Saito, K. Otsu, H. Harada, Y. Yamada, Role of epithelial-stem cell interactions during dental cell differentiation, J. Biol. Chem. 287 (2012) 10590–10601.

[181] K. Yoshida, J. Sato, R. Takai, O. Uehara, Y. Kurashige, M. Nishimura, I. Chiba, M. Saitoh, Y. Abiko, Differentiation of mouse iPS cells into ameloblast-like cells in cultures using medium conditioned by epithelial cell rests of Malassez and gelatin-coated dishes, Med. Mol. Morphol. 48 (2015) 138–145.

[182] J. Catón, H.-U. Luder, M. Zoupa, M. Bradman, G. Bluteau, A.S. Tucker, O. Klein, T.A. Mitsiadis, Enamel-free teeth: Tbx1 deletion affects amelogenesis in rodent incisors, Dev. Biol. 328 (2009) 493–505.

[183] T.A. Mitsiadis, A.S. Tucker, C. De Bari, M.T. Cobourne, D.P.C. Rice, A regulatory

relationship between Tbx1 and FGF signaling during tooth morphogenesis and ameloblast lineage determination, Dev. Biol. 320 (2008) 39–48.

[184] T. Nakamura, Y. Chiba, M. Naruse, K. Saito, H. Harada, S. Fukumoto, Globoside accelerates the differentiation of dental epithelial cells into ameloblasts, Int. J. Oral Sci. 8 (2016) 205.

[185] Y. Chiba, B. He, K. Yoshizaki, C. Rhodes, M. Ishijima, C.K.E. Bleck, E. Stempinski, E.Y. Chu, T. Nakamura, T. Iwamoto, The transcription factor AmeloD stimulates epithelial cell motility essential for tooth morphology, J. Biol. Chem. 294 (2019) 3406–3418.

[186] D.S. Lee, S.Y. Roh, J.-C. Park, The Nfic-osterix pathway regulates ameloblast differentiation and enamel formation, Cell Tissue Res. 374 (2018) 531–540.

[187] X. Liu, C. Xu, Y. Tian, Y. Sun, J. Zhang, J. Bai, Z. Pan, W. Feng, M. Xu, C. Li, RUNX2 contributes to TGF-β1-induced expression of Wdr72 in ameloblasts during enamel mineralization, Biomed. Pharmacother. 118 (2019) 109235.

[188] R. Coin, Y. Haïkel, J. Ruch, Effects of apatite, transforming growth factor β-1, bone morphogenetic protein-2 and interleukin-7 on ameloblast differentiation in vitro, Eur. J. Oral Sci. 107 (1999) 487–495.

[189] T. Tsuboi, S. Mizutani, M. Nakano, K. Hirukawa, A. Togari, Fgf-2 regulates enamel and dentine formation in mouse tooth germ, Calcif. Tissue Int. 73 (2003) 496–501.

[190] A. Matsumoto, H. Harada, M. Saito, A. Taniguchi, Induction of enamel matrix protein expression in an ameloblast cell line co-cultured with a mesenchymal cell line in vitro, Vitr. Cell. Dev. Biol. 47 (2011) 39–44.

[191] W. Zhang, I.P. Ahluwalia, P.C. Yelick, Three dimensional dental epithelial-mesenchymal constructs of predetermined size and shape for tooth regeneration, Biomaterials. 31 (2010) 7995–8003.

[192] M.J. Honda, S. Tsuchiya, Y. Sumita, H. Sagara, M. Ueda, The sequential seeding of epithelial and mesenchymal cells for tissue-engineered tooth regeneration, Biomaterials. 28 (2007) 680–689.

[193] T. Morotomi, S. Kawano, T. Toyono, C. Kitamura, M. Terashita, T. Uchida, K. Toyoshima, H. Harada, In vitro differentiation of dental epithelial progenitor cells through epithelial–mesenchymal interactions, Arch. Oral Biol. 50 (2005) 695–705.

[194] Y. Liu, S. Rayatpisheh, S.Y. Chew, M.B. Chan-Park, Impact of endothelial cells on 3D

cultured smooth muscle cells in a biomimetic hydrogel, ACS Appl. Mater. Interfaces. 4 (2012) 1378–1387.

[195] X. Shi, L. Xiong, L. Xiao, C. Meng, G. Qi, W. Li, Downregulation of caveolin-1 upregulates the expression of growth factors and regulators in co-culture of fibroblasts with cancer cells, Mol. Med. Rep. 13 (2016) 744–752.

[196] H.-K. Lee, J.-W. Park, Y.-M. Seo, H.H. Kim, G. Lee, H.-S. Bae, J.-C. Park, Odontoblastic inductive potential of epithelial cells derived from human deciduous dental pulp, J. Mol. Histol. 47 (2016) 345–351.

[197] J. Renaud, M.-G. Martinoli, Development of an insert co-culture system of two cellular types in the absence of cell-cell contact, JoVE (Journal Vis. Exp. (2016) e54356.

[198] D.P.E. Herzog, E. Dohle, I. Bischoff, C.J. Kirkpatrick, Cell communication in a coculture system consisting of outgrowth endothelial cells and primary osteoblasts, Biomed Res. Int. 2014 (2014).

[199] M. Rothbauer, H. Zirath, P. Ertl, Recent advances in microfluidic technologies for cell-to-cell interaction studies, Lab Chip. 18 (2018) 249–270.

[200] H. Yamamoto, E.-J. Kim, S.-W. Cho, H.-S. Jung, Analysis of tooth formation by reaggregated dental mesenchyme from mouse embryo, Microscopy. 52 (2003) 559–566.

[201] A. Ohazama, S.A.C. Modino, I. Miletich, P.T. Sharpe, Stem-cell-based tissue engineering of murine teeth, J. Dent. Res. 83 (2004) 518–522.

[202] M. Ono, M. Oshima, M. Ogawa, W. Sonoyama, E.S. Hara, Y. Oida, S. Shinkawa, R. Nakajima, A. Mine, S. Hayano, S. Fukumoto, S. Kasugai, A. Yamaguchi, T. Tsuji, T. Kuboki, Practical whole-tooth restoration utilizing autologous bioengineered tooth germ transplantation in a postnatal canine model, Sci. Rep. 7 (2017) 44522.

[203] K. Nakao, R. Morita, Y. Saji, K. Ishida, Y. Tomita, M. Ogawa, M. Saitoh, Y. Tomooka, T. Tsuji, The development of a bioengineered organ germ method, Nat. Methods. 4 (2007) 227.

[204] E. Ikeda, R. Morita, K. Nakao, K. Ishida, T. Nakamura, T. Takano-Yamamoto, M. Ogawa, M. Mizuno, S. Kasugai, T. Tsuji, Fully functional bioengineered tooth replacement as an organ replacement therapy, Proc. Natl. Acad. Sci. 106 (2009) 13475–13480.

[205] M. Oshima, M. Mizuno, A. Imamura, M. Ogawa, M. Yasukawa, H. Yamazaki, R. Morita,

E. Ikeda, K. Nakao, T. Takano-Yamamoto, Functional tooth regeneration using a bioengineered tooth unit as a mature organ replacement regenerative therapy, PLoS One. 6 (2011) e21531.

[206] W. Zhang, B. Vázquez, P.C. Yelick, Bioengineered post-natal recombinant tooth bud models, J. Tissue Eng. Regen. Med. 11 (2017) 658–668.

[207] G. Orsini, P. Pagella, A. Putignano, T.A. Mitsiadis, Novel biological and technological platforms for dental clinical use, Front. Physiol. 9 (2018) 1102.

[208] K.-J. Kang, S.M. Ju, Y.-J. Jang, J. Kim, Indirect co-culture of stem cells from human exfoliated deciduous teeth and oral cells in a microfluidic platform, Tissue Eng. Regen. Med. 13 (2016) 428–436.

[209] P. Pagella, S. Miran, T. Mitsiadis, Analysis of developing tooth germ innervation using microfluidic co-culture devices, JoVE (Journal Vis. Exp. (2015) e53114.

[210] P. Pagella, E. Neto, L. Jiménez-Rojo, M. Lamghari, T.A. Mitsiadis, Microfluidics co-culture systems for studying tooth innervation, Front. Physiol. 5 (2014) 326.

[211] C.M. França, A. Tahayeri, N.S. Rodrigues, S. Ferdosian, R.M.P. Rontani, G. Sereda, J.L. Ferracane, L.E. Bertassoni, The tooth on-a-chip: a microphysiologic model system mimicking the biologic interface of the tooth with biomaterials, Lab Chip. 20 (2020) 405–413.

[212] K. Janjić, H. Agis, Chronodentistry: the role & potential of molecular clocks in oral medicine, BMC Oral Health. 19 (2019) 1–12.

[213] S.A. Bae, M.Z. Fang, V. Rustgi, H. Zarbl, I.P. Androulakis, At the interface of lifestyle, behavior and circadian rhythms: Metabolic implications, Front. Nutr. 6 (2019) 132.

[214] A.K. De Nobrega, L.C. Lyons, Drosophila: An emergent model for delineating interactions between the circadian clock and drugs of abuse, Neural Plast. 2017 (2017).

[215] L. Zheng, Y.J. Seon, M.A. Mourão, S. Schnell, D. Kim, H. Harada, S. Papagerakis, P. Papagerakis, Circadian rhythms regulate amelogenesis, Bone. 55 (2013) 158–165.

[216] R.S. Lacruz, J.G. Hacia, T.G. Bromage, A. Boyde, Y. Lei, Y. Xu, J.D. Miller, M.L. Paine, M.L. Snead, The circadian clock modulates enamel development, J. Biol. Rhythms. 27 (2012) 237–245.

[217] J. Tao, Y. Zhai, H. Park, J. Han, J. Dong, M. Xie, T. Gu, K. Lewi, F. Ji, W. Jia, Circadian rhythm regulates development of enamel in mouse mandibular first molar, PLoS One. 11

(2016) e0159946.

[218] L. Zheng, S. Papagerakis, S.D. Schnell, W.A. Hoogerwerf, P. Papagerakis, Expression of clock proteins in developing tooth, Gene Expr. Patterns. 11 (2011) 202–206.

[219] J.P. Simmer, P. Papagerakis, C.E. Smith, D.C. Fisher, A.N. Rountrey, L. Zheng, J.C.-C. Hu, Regulation of Dental Enamel Shape and Hardness, J. Dent. Res. 89 (2010) 1024–1038. https://doi.org/10.1177/0022034510375829.

[220] L. Zheng, L. Ehardt, B. McAlpin, I. About, D. Kim, S. Papagerakis, P. Papagerakis, The tick tock of odontogenesis, Exp. Cell Res. 325 (2014) 83–89.

[221] M. Athanassiou-Papaefthymiou, D. Kim, L. Harbron, S. Papagerakis, S. Schnell, H. Harada, P. Papagerakis, Molecular and circadian controls of ameloblasts, Eur. J. Oral Sci. 119 (2011) 35–40.

[222] R. Said, L. Lobanova, S. Papagerakis, P. Papagerakis, Calcium Sets the Clock in Ameloblasts, Front. Physiol. 11 (2020) 920.

[223] Q. Dong, Y. Wang, F. Mohabatpour, L. Zheng, S. Papagerakis, D. Chen, P. Papagerakis, Dental Pulp Stem Cells: Isolation, Characterization, Expansion, and Odontoblast Differentiation for Tissue Engineering, in: Odontogenesis, Springer, 2019: pp. 91–101.

[224] S. Sharma, D. Srivastava, S. Grover, V. Sharma, Biomaterials in tooth tissue engineering: a review, J. Clin. Diagnostic Res. JCDR. 8 (2014) 309.

[225] N. Monteiro, P.C. Yelick, Advances and perspectives in tooth tissue engineering, J. Tissue Eng. Regen. Med. (2016).

[226] C.S. Young, S. Terada, J.P. Vacanti, M. Honda, J.D. Bartlett, P.C. Yelick, Tissue engineering of complex tooth structures on biodegradable polymer scaffolds, J. Dent. Res. 81 (2002) 695–700.

[227] M.T. Duailibi, S.E. Duailibi, C.S. Young, J.D. Bartlett, J.P. Vacanti, P.C. Yelick, Bioengineered Teeth from Cultured Rat Tooth Bud Cells, J. Dent. Res. 83 (2004) 523–528. https://doi.org/10.1177/154405910408300703.

[228] S.E. Duailibi, M.T. Duailibi, W. Zhang, R. Asrican, J.P. Vacanti, P.C. Yelick, Bioengineered dental tissues grown in the rat jaw, J. Dent. Res. 87 (2008) 745–750.

[229] Z. Huang, T.D. Sargeant, J.F. Hulvat, A. Mata, P. Bringas, C. Koh, S.I. Stupp, M.L. Snead, Bioactive nanofibers instruct cells to proliferate and differentiate during enamel regeneration, J. Bone Miner. Res. 23 (2008) 1995–2006.

[230] Z. Huang, C.J. Newcomb, P. Bringas Jr, S.I. Stupp, M.L. Snead, Biological synthesis of tooth enamel instructed by an artificial matrix, Biomaterials. 31 (2010) 9202–9211.

[231] X. Chatzistavrou, R.R. Rao, D.J. Caldwell, A.W. Peterson, B. McAlpin, Y.-Y. Wang, L. Zheng, J.C. Fenno, J.P. Stegemann, P. Papagerakis, Collagen/fibrin microbeads as a delivery system for Ag-doped bioactive glass and DPSCs for potential applications in dentistry, J. Non. Cryst. Solids. 432 (2016) 143–149.

[232] N. Zhu, X. Chatzistavrou, L. Ge, M. Qin, P. Papagerakis, Y. Wang, Biological properties of modified bioactive glass on dental pulp cells, J. Dent. 83 (2019) 18–26.

[233] X. Chatzistavrou, S. Papagerakis, P.X. Ma, P. Papagerakis, Innovative approaches to regenerate enamel and dentin, Int. J. Dent. 2012 (2012).

[234] C.S. Young, H. Abukawa, R. Asrican, M. Ravens, M.J. Troulis, L.B. Kaban, J.P. Vacanti, P.C. Yelick, Tissue-engineered hybrid tooth and bone, Tissue Eng. 11 (2005) 1599–1610.

[235] W. Zhang, H. Abukawa, M.J. Troulis, L.B. Kaban, J.P. Vacanti, P.C. Yelick, Tissue engineered hybrid tooth–bone constructs, Methods. 47 (2009) 122–128.

[236] Y. Sumita, M.J. Honda, T. Ohara, S. Tsuchiya, H. Sagara, H. Kagami, M. Ueda, Performance of collagen sponge as a 3-D scaffold for tooth-tissue engineering, Biomaterials. 27 (2006) 3238–3248.

[237] W. Zhang, J. Liu, H. Wang, Z. Li, Preparation of recombinant human bone morphogenetic protein 2 decorated beta tricalcium phosphate/collagen and preliminary studies on its properties of inducing tooth formation, Zhongguo Xiu Fu Chong Jian Wai Ke Za Zhi= Zhongguo Xiufu Chongjian Waike Zazhi= Chinese J. Reparative Reconstr. Surg. 25 (2011) 149–154.

[238] S. Iwatsuki, M.J. Honda, H. Harada, M. Ueda, Cell proliferation in teeth reconstructed from dispersed cells of embryonic tooth germs in a three-dimensional scaffold, Eur. J. Oral Sci. 114 (2006) 310–317.

[239] M.J. Honda, Y. Sumita, H. Kagami, M. Ueda, Histological and immunohistochemical studies of tissue engineered odontogenesis, Arch. Histol. Cytol. 68 (2005) 89–101.

[240] M.J. Honda, Y. Shinohara, K.I. Hata, M. Ueda, Subcultured odontogenic epithelial cells in combination with dental mesenchymal cells produce enamel–dentin-like complex structures, Cell Transplant. 16 (2007) 833–847.

[241] P. Chatzistavrou, X., Papagerakis, Chapter 32- Dental enamel regeneration, in: P. Ma

(Ed.), Biomater. Regen. Med., Cambridge University Press, 2014: pp. 583–589. https://doi.org/10.1017/CBO9780511997839.038.

[242] T.A. Mitsiadis, P. Papagerakis, Regenerated teeth: the future of tooth replacement?, Regen. Med. 6 (2011) 135–139.

[243] M. Pandya, T.G.H. Diekwisch, Enamel biomimetics—fiction or future of dentistry, Int. J. Oral Sci. 11 (2019) 1–9.

[244] B.S. Ghandourah, A. Lefkelidou, R. Said, X. Chatzistavrou, S. Flannagan, C. Gonzáles-Cabezas, C.J. Fenno, L. Zheng, S. Papagerakis, P. Papagerakis, In Vitro Caries Models for the Assessment of Novel Restorative Materials, in: Odontogenesis, Springer, 2019: pp. 369–377.

[245] J. Hsiao, Y. Wang, L. Zheng, R. Liu, R. Said, L. Hadjiyski, H. Cha, T. Botero, X. Chatzistavrou, Q. Dong, In Vivo Rodent Models for Studying Dental Caries and Pulp Disease, in: Odontogenesis, Springer, 2019: pp. 393–403.

[246] S. Gronthos, M. Mankani, J. Brahim, P.G. Robey, S. Shi, Postnatal human dental pulp stem cells (DPSCs) in vitro and in vivo, Proc. Natl. Acad. Sci. 97 (2000) 13625–13630.

[247] K. Mukherjee, Q. Ruan, S. Nutt, J. Tao, J.J. De Yoreo, J. Moradian-Oldak, Peptide-Based Bioinspired Approach to Regrowing Multilayered Aprismatic Enamel, ACS Omega. 3 (2018) 2546–2557.

[248] P.C. Yelick, J.P. Vacanti, Bioengineered Teeth from Tooth Bud Cells, Dent. Clin. 50 (2006) 191–203. https://doi.org/10.1016/j.cden.2005.11.005.

[249] L. Goers, P. Freemont, K.M. Polizzi, Co-culture systems and technologies: taking synthetic biology to the next level, J. R. Soc. Interface. 11 (2014) 20140065.

[250] G.C. Padovani, V.P. Feitosa, S. Sauro, F.R. Tay, G. Durán, A.J. Paula, N. Durán, Advances in dental materials through nanotechnology: facts, perspectives and toxicological aspects, Trends Biotechnol. 33 (2015) 621–636.

[251] G. Orsini, A. Putignano, T. Mitsiadis, Advances in Craniofacial and Dental Materials Through Nanotechnology and Tissue Engineering, Front. Physiol. 10 (2019) 303.

[252] S. Huang, T. Wu, H. Yu, Biomimetics using nanotechnology/nanoparticles in dental tissue regeneration, in: Nanobiomaterials Clin. Dent., Elsevier, 2019: pp. 495–515.

[253] L. Ning, X. Chen, A brief review of extrusion-based tissue scaffold bio-printing, Biotechnol. J. (2017).

[254] N. Soltan, L. Ning, F. Mohabatpour, P. Papagerakis, X. Chen, Printability and cell viability in bioprinting alginate dialdehyde-gelatin scaffolds, ACS Biomater. Sci. Eng. (2019).

[255] F. You, X. Chen, D.M.L. Cooper, T. Chang, B.F. Eames, Homogeneous hydroxyapatite/alginate composite hydrogel promotes calcified cartilage matrix deposition with potential for three-dimensional bioprinting, Biofabrication. 11 (2018) 15015.

[256] M. Izadifar, D. Chapman, P. Babyn, X. Chen, M.E. Kelly, UV-assisted 3D bioprinting of nanoreinforced hybrid cardiac patch for myocardial tissue engineering, Tissue Eng. Part C Methods. 24 (2018) 74–88.

[257] K. Kim, C.H. Lee, B.K. Kim, J.J. Mao, Anatomically shaped tooth and periodontal regeneration by cell homing, J. Dent. Res. 89 (2010) 842–847.

[258] P. Dierickx, L.W. Van Laake, N. Geijsen, Circadian clocks: from stem cells to tissue homeostasis and regeneration, EMBO Rep. 19 (2018) 18–28.

Chapter 3. Gemini surfactant-based nanoparticles T-box1 gene delivery as novel approach to promote epithelial stem cells differentiation and 3D dental enamel formation

Fatemeh Mohabatpour[1,2], Mays Al-Dulaymi[3], Liubov Lobanova[2], Brittany Scutchings[3], Silvana Papagerakis[*1,4,6], Ildiko Badea[3], Xiongbiao Chen[*1,5], Petros Papagerakis[*1,2]

1. Division of Biomedical Engineering, University of Saskatchewan, 57 Campus Dr., S7N 5A9, SK, Canada
2. College of Dentistry, University of Saskatchewan, 105 Wiggins Rd, S7N 5E4, SK, Canada
3. College of Pharmacy and Nutrition, University of Saskatchewan, 107 Wiggins Rd, S7N 5E5, SK, Canada
4. Department of Surgery, College of Medicine, University of Saskatchewan, 107 Wiggins Rd B419, S7N 0W8, SK, Canada
5. Department of Mechanical Engineering, University of Saskatchewan, 57 Campus Dr., S7N 5A9, SK, Canada
6. Department of Otolaryngology, College of Medicine, University of Michigan, Ann Arbor, MI, USA

[*]Corresponding authors:

Petros Papagerakis, Email: petros.papagerakis@usask.ca

Xiongbiao Chen, Email: xbc719@usask.ca

Silvana Papagerakis, Email: silvana.papagerakis@usask.ca

Keywords: enamel regeneration, T-box1 gene delivery, dental stem cells, ameloblast differentiation, gemini surfactant-based nanoparticles, scaffolds, enamel defects

3.1. Abstract

Enamel is the highest mineralized tissue in the body protecting teeth from external stimuli, infections, and injuries. Enamel lacks the ability to self-repair due to the absence of enamel-producing cells in the erupted teeth. Here, we reported a novel approach to promote enamel-like tissue formation via delivery of a key ameloblast inducer, T-box1 gene, into a rat dental epithelial stem cell line, HAT-7, using non-viral gene delivery systems based on cationic lipids. We comparatively assessed the lipoplexes prepared from glycyl-lysine-modified gemini surfactants and commercially available 1,2-dioleoyl-3-trimethylammonium-propane lipids at three nitrogen- to phosphate (N/P) ratios. Our findings revealed that physico-chemical characteristics and biological activities of the gemini surfactant-based lipoplexes with the N/P ratio of 5 provide the most optimal outcomes among those examined. HAT-7 cells were transfected with T-box1 gene using the optimal formulation then cultured in both conventional 2D and hydrogel-based 3D cell culture systems of photo-cross-linkable gelatin methacrylate hydrogels. Ameloblast differentiation, mineralization, bio-enamel interface and structure and were assessed at different time points over 28 days. Our results showed that our gemini transfection system provides superior gene expression compared to the benchmark agent, while keeping low cytotoxicity levels. T-box1-transfected HAT-7 cells strongly expressed markers of secretory and maturation stages of the ameloblasts, deposited minerals, and produced enamel-like crystals when compared to control cells. Taken together, our gemini surfactant-based T-box1 gene delivery system is effective to accelerate and guide ameloblastic differentiation of dental epithelial stem cells and promote enamel-like tissue formation. These data provide foundation for future regeneration approaches towards bio-enamel fabrication with adequate biological interface to the underlying dentin tissue.

3.2. Introduction

Enamel, the external tissue layer of the dental crown, protects teeth from physical and chemical damage [1]. Defective enamel leads to high rates of tooth infection and cracking resulting in pain, fever, chronic inflammation and eventually tooth loss. Enamel is formed through amelogenesis which consists of three main stages: secretory, transition and maturation stages [1]. During the secretory phase, enamel-producing cells, the ameloblasts, secrete enamel extracellular proteins including amelogenin (AMELX), ameloblastin (AMBN) and enamelin (ENAM) into the enamel

organic matrix, which provide a scaffold that controls the formation of enamel crystals [2]. Enamel crystallization initiates via the interactions between matrix proteins and mineral ions in the gel-like enamel organic matrix [3]. Secretory ameloblasts also produce a proteinase, matrix metalloproteinase-20 (MMP-20), that cleaves or processes enamel matrix proteins in order to assist in crystal elongation [2,4]. Once the full thickness of the future enamel has formed, the transition stage, that is defined by a reduction in matrix protein secretion, takes place [5]. During the maturation stage, ameloblasts secrete kallikrein-related peptidase-4 (KLK4) that further degrades the enamel matrix proteins in order to facilitate crystal growth that increases the width and thickness of the crystals and ultimately allows for full mineralization of the enamel [1,2]. Prior to tooth eruption, the remaining ameloblasts disappear by apoptosis leaving dental enamel incapable of cell-based repair and regeneration [6].

Innovative therapeutic approaches for enamel regeneration have been explored by tissue engineering approaches, wherein cells are cultured on engineered scaffolds with the presence of signaling factors to regenerate or form enamel tissue for implantation into the body [7,8]. Dental epithelial stem cells (DESCs) are the only cellular source currently known to regenerate enamel tissue [9]. However, the stimulation of DESCs towards differentiated ameloblasts, and the acquisition of fully functional enamel, similar to native enamel, still remains challenging.

T-box transcription factor 1 is critical for normal tooth development; its alterations or absence could be responsible for DiGeorge syndrome and cause enamel defects [10]. Mouse models with T-box1 (*Tbx1*) gene deletion were shown to have severe hypoplastic incisors which completely lacked enamel due to the absence of ameloblasts. In these *Tbx1-/-* incisors, reduction in cell proliferation and in amelogenin expression levels were reported [11]. These studies suggest that *Tbx1* gene is essential for ameloblast differentiation and that *Tbx1* delivery into DESCs can prompt them toward ameloblast differentiation and enamel deposition.

Gene delivery has been employed as a potent strategy for tissue engineering and regenerative medicine applications. Using this strategy, stem cells are guided toward a precise differentiation path by expressing lineage determination factors or other tissue inductive factors. Expression in situ provides a longer exposure as compared to the exogenous addition of such signaling molecules [12]. Lipid-based carriers that are known as one of the most commonly used non-viral gene

delivery vectors [13], have offered several advantages such as simple preparation methods, the potential for being easily modified, reproducibility, low cost, and biodegradability [14,15]. Cationic lipids have been reported to interact with negatively charged DNA molecules and form positively charged complexes, lipoplexes, and facilitate cell internalization while protecting genes from nuclease degradation [16]. Gemini surfactants have gained considerable attention as cationic lipid-based gene delivery systems for *in vitro* and *in vivo* studies, as showed by our team and others, due to their advantages such as low critical micelle concentration (CMC) and lower toxicity compared to the conventional monomeric surfactants [17–19]. The structure of gemini surfactants was found to have a marked influence on particle morphology, cytotoxicity and transfection efficiency. Accordingly, we showed that glycyl-lysine-substituted gemini surfactants with 16-carbon tail showed superior gene expression and higher cell viability as compared to the counterparts with 12 and 18:1 carbon tail indicating the importance of the hydrophobic tails on the performance of the delivery systems [20]. To the best of our knowledge, no studies have been reported by means of gemini surfactants for gene delivery to promote enamel formation.

In this study, we developed lipid-based nanoparticles to deliver *Tbx1* plasmid DNA into the rat dental epithelial stem cell line (HAT-7) to 1) evaluate the effects of Tbx1 gene transfection on promoting ameloblast differentiation in vitro, 2) validate a new gene delivery method for dental epithelium cell differentiation studies. Lipoplexes were first prepared using two cationic lipids, glycyl-lysine-substituted gemini surfactants and 1,2-dioleoyl-3-trimethylammonium-propane (DOTAP) for determining the optimal formulations for *Tbx1* delivery into cells. HAT-7 cells, after being transfected with *Tbx1* encoding gene using the optimal formulation, were cultured up to 28 days in 2D and 3D, photo-cross-linkable gelatin methacrylate (GelMA) hydrogels [21], cell culture models. The effects of *Tbx1* transfection on ameloblast differentiation were examined by evaluating the expression of ameloblast differentiation markers and assessing mineralization. Our study lays down a foundation for future studies towards tissue engineering and enamel regeneration.

3.3. Material and Methods

3.3.1. Cloning and characterization of mouse *Tbx1* plasmid

Tbx1 isoform 1 polymerase chain reaction (PCR) fragment of 1,497 bps was amplified from pAAV-hSynapsin1-GCaMP6s-P2A-mRaby3-*Tbx1* (a generous gift from Dr. Thimios A. Mitsiadis, University of Zurich, Zurich, Switzerland) via *Tbx1* primers (Table 3.1) using Q5® High-Fidelity DNA Polymerase (Cat. no. M0491S, New England Biolabs, Ipswich, Massachusetts, US). Restriction digestion of pCMS-EGFP plasmid was performed with EcoRI-HF® (Cat. no. R3101S, New England Biolabs, Ipswich, Massachusetts, US) followed by gel purification. The amplified *Tbx1* fragment was then inserted into the pCMS-EGFP plasmid using Gibson Assembly® Master Mix (Cat. no. E2611S, New England Biolabs, Ipswich, Massachusetts, US) according to the manufacturer's instructions. The accuracy of the cloning was confirmed by sequencing.

3.3.2. Preparation of lipid-based nanoparticles loaded with *Tbx1* plasmid

Glycyl-lysine-modified gemini surfactant was designed as 16-7N(GK)-16, where (16) is the number of the carbon atoms in the tail region, (7) is the length of the amine modified spacer region and (GK) is the Glycyl-Lysine dipeptide attached to the amine moiety of the spacer region (the chemical name of the compound: (1,9-bis(hexadecyl)-1,1,9,9-tetramethyl-5-[Na-(glycyl)-(lysyl)]amino-1,9-nonanediammonium dichloride, tetrahydrochloride salt), and synthesized as previously described [20]. The predetermined volumes of the gemini surfactant solutions (3mM) were mixed with pCMS-*Tbx1*-EGFP plasmid (200 μg/mL) at three various N/P ratios of 2.5, 5 and 10 and incubated at room temperature for 20 min to generate pDNA/gemini surfactant (P/G) complexes. 1,2-dioleoyl-sn glycerol-3-phosphoethanolamine (DOPE, Cat. no. 850725P, Avanti Polar Lipids Inc., Alabaster, Alabama, USA) was used as helper lipids at a constant concentration of 1 mM to make final formulations of pDNA/gemini surfactant/ helper lipids (P/G/L). DOPE vesicles were prepared using sonication method as previously described [22]. As a comparison with gemini surfactants, the formulations were prepared with 1,2-dioleoyl-3-trimethylammonium-propane (DOTAP, Cat. no. 890890P, Avanti Polar Lipids Inc., Alabaster, Alabama, USA), a commercially available lipid, at the same N/P ratios of 2.5, 5 and 10 through the same steps.

Lipofectamine™2000 Transfection Reagent (Cat. no. 11668027, Invitrogen, Thermo Fisher Scientific, Waltham, Massachusetts, USA) was used as a transfection positive control at the lowest concentration recommended by the manufacturer.

3.3.3. Particle size and zeta potential measurements

Size and zeta potential of lipoplexes prepared at different N/P ratios were assessed by a Zetasizer Nano ZS instrument (Malvern Instruments, Malvern, Worcestershire, UK).

3.3.4. Morphology of lipoplex

The morphology of the gemini surfactant-based lipoplexes at the optimal N/P ratio of 5 was examined by transmission electron microscopy (TEM). 10 μL of the lipoplex suspension was placed on copper grids and left at room temperature for 10 minutes to be air-dried. Next, the remaining liquid was wicked with a kimwipe tissue paper (Kimberly-Clark Professional, Irving, Texas, US) and samples were dried at room temperature. High-resolution images were acquired with a transmission electron microscope (HT7700, Hitachi, Chiyoda, Tokyo, Japan).

3.3.5. DNA compaction and protection assays

The capacity of lipid-based nanoparticles to compact *Tbx1* pDNA and protect it from DNase enzymatic digestion was assessed using agarose gel electrophoresis. For DNA compaction assay, naked pDNA and lipoplexes were mixed with Gel Loading Dye Blue (6X) (Cat. no. B70215, New England Biolabs) and loaded into 1% agarose (Cat. no. BP160, Fisher Scientific) gel containing GelRed™ (Cat. no. 89139, Biotium, Fremont, California, USA) and immersed in 1X Tris-Acetate-EDTA (TAE) running buffer and run at 120 V for 30 minutes. For DNA protection assay, naked pDNA and lipoplexes were treated with DNase I (TURBO DNA-free™ Kit, Cat. no. AM1907, Ambion by Life Technologies, Austin, Texas, USA) at 37 °C for 30 minutes and then loaded into agarose gel. Gel was imaged using ChemiDoc MP Imaging System (17001402, BioRAD, Hercules, California, US)

3.3.6. HAT-7 cell culture and transfection

HAT-7 cells (kindly provided by Dr. Hidemitsu Harada, Iwate Medical University, Iwate, Japan) [23] were cultured as previously described [24]. The medium was changed every 48 hours. HAT-7 cells were seeded in 6-well plates at a cell density of 300,000 cells/well. After 24 hours, the growth medium

was replaced with the reduced serum medium (OptiMEM, Cat. no. 31985070, Gibco®, Invitrogen) comprising of 1% antibiotics. After 1 hour, cells were transfected with lipoplexes and incubated for 5 hours. Then, the OptiMEM containing formulations were replaced with supplemented DMEM/F12 (1:1) culture medium supplemented with 10% FBS and 1% antibiotics.

3.3.7. Cell toxicity assay

Cytotoxicity of formulations was assessed using 3-(4, 5-dimethylthiazol-2-yl)-2, 5-diphenyltetrazolium bromide (MTT) assay as we previously described [25].

3.3.8. Differentiation of HAT-7 cells

HAT-7 cells were transfected with the optimal formulations, gemini surfactant-based lipoplexes at N/P ratio of 5 and cultured for up to 28 days to undergo differentiation. The medium was changed every 48 hours.

3.3.9. Immunocytochemistry

Cells were cultured on sterile glass coverslips for 14 and 28 days and were rinsed with phosphate buffered saline (PBS) twice then fixed and permeabilized using BD Cytofix/cytoperm™ fixation/permeabilization kit (Cat. no. 554714, BD Biosciences, San Jose, California, USA). Cells were washed with PBS 3 times for 5 minutes followed by incubation in blocking buffer (PBS1x,1%BSA, 0.1%Tween 20) for 30 minutes at room temperature. Next, cells were incubated with primary antibodies including rabbit anti-AMELX (1:1000, Cat. no. ab153915, Abcam), goat anti-KLK4 (1:500, Cat. no. sc-20371, Santa Cruz Biotechnology), rabbit anti-ORAI 1 (1:100, Cat. no. 13130-1-AP, Proteintech®, Rosemont, Illinois, US) and anti-Amelotin (1:100, a generous gift from Dr. Bernhard Ganss, University of Toronto, Ontario, Canada) in blocking buffer overnight at 4℃, followed by washing with PBS 3 times for 5 minutes and incubated with secondary antibodies (1:1000) including Donkey anti-Rabbit, PE (Cat. no. 12-4739-81, Thermo Fisher Scientific), Donkey anti-Goat, Alexa Fluor 488 (Cat. no. A-11055, Thermo Fisher Scientific), Donkey anti-Rabbit, Alexa Fluor 488 (Cat. no. A-21206, Thermo Fisher Scientific) and Goat anti-Mouse, HRP (Cat. no. A28177, Thermo Fisher Scientific) in blocking buffer for 1 hour at room temperature. The cell nuclei were stained by using ProLong™ Gold antifade reagent with DAPI

(Cat. no. P36935, Invitrogen). Slides were imaged using a confocal microscope (LSM 700, Carl Zeiss, Oberkochen, Germany).

3.3.10. Gene expression

Total RNA was extracted using RNeasy Mini Kit (Cat. no. 74106, QIAGEN, GmbH, Hilden, Germany) followed by cDNA synthesis using the High-Capacity cDNA Reverse Transcription Kit (Cat. no. 4368814, Applied Biosystems^{TM}, Foster City, California, US) according to the manufacturer's instructions. mRNA expression levels of *Tbx1*, dentin sialophosphoprotein (*Dspp)*, ameloblastin (*Ambn*), enamelin (*Enam)*, kalikrein-4 (*Klk4)*, calcium release-activated calcium channel protein 1 (*Orai1),* stromal-interacting molecule (*Stim1),* alkaline phosphatase (*Alp*) genes were measured by quantitative Reverse Transcription Polymerase Chain Reaction **(**qRT-PCR) using Power SYBR^{TM} Green PCR Master Mix (Cat. No. 4367659, Thermo Fisher Scientific, Invitrogen) and designed primers (Table 3.1). The relative expression was calculated using $2^{(-\Delta\Delta Ct)}$ method and β*-actin* and *Gapdh* were used as housekeeping genes.

Table 3.3. The sequences of the primers used for qRT-PCR.

Primers	**Forward**	**Reverse**
pCMS-EGFP-Tbx1 iso-1 (for cloning)	CACTATAGGCTAGCCTCGAGATGA TCT CCGCCGTGTCTAGTC	CTCTAGAGGTACCACGCGTGCTA T CTGGGGCAGTAGTCGT
Tbx1 (for qRT-PCR)	GCCAGCAACCCCTTCGCCAA	AGTCACGGTCGAACTCGCGC
Dspp	GTGCTAAAGAACGCGAGGAC	GTCTCCATTCTGGCTCGTGT
Ambn	CAGAAGGCTCTCCACTGCAA	CCCCAAGGGTGTGGTAACAT
Enam	GATGCCCATGTGGCCTCCACCA	GCCAAATGGTGGGAATGGCTGA
Klk4	CTGGGGTACCTCATCCTTGA	CCACGGTGTAGGAGTCCTGT
Orai1	GCTCTGCTGGGTGAAGTTCT	AAGTGAACGGCAAAGACGAT
Stim1	ACTTCACTCGAGACCATGGATGTA TGCGTCCGTCTTGCC	ACTTCACTCGAGCTACTTCTTAA GAGGCTTCTTAAAGATTTTGAGC
Alp	TGATCACTCCCACGTTTTCA	CTGGGCCTGGTAGTTGTTGT
β-actin	AAGTACCCCATTGAACATGG	ATCACAATGCCTGTGGTACG
Gapdh	AACAGCAACTCCCACTCTTC	TGGTCCAGGGTTTCTTACTC

3.3.11. Alkaline phosphatase staining

After 14 and 28 days of culture, cells were fixed and permeabilized as explained above. Afterwards, alkaline phosphatase (ALP) staining was performed using SIGMAFAST™ BCIP®/NBT detection kit (Cat. no. B5655, Sigma-Aldrich) according to the manufacturer's instructions. Briefly, cells were washed with PBS three times and incubated in ALP staining solution, prepared by dissolving BCIP/NBT tablet in water, for 30 minutes at 37 °C under dark condition. Cells were rinsed with distilled water three times and visualized under a light microscope (EVOS M5000 Cell Imaging System, Thermo Fisher Scientific).

3.3.12. Von Kossa staining

Cells were fixed and permeabilized as previously described after 14 and 28 days of culture. Then, the mineral deposition was detected using von Kossa Stain Kit (Cat. no. ab150687, Abcam, Cambridge, Massachusetts, USA) according to the manufacturer's instructions.

3.3.13. Alizarin Red S staining

To evaluate mineralization potential and calcium deposition, Alizarin Red S staining was carried out. Briefly, cells were fixed and permeabilized as previously described [26] after 14 and 28 days of culture and were exposed to 2% Alizarin Red S (pH 4.2, Cat. no. sc-205998, Santa Cruz Biotechnology, Dallas, Texas, USA) for 5 minutes at room temperature, followed by rinsing with distilled water twice and visualization under the same light microscope as mentioned above.

3.3.14. Observation of cell morphology and mineral deposition in 2D cell culture models using scanning electron microscopy (SEM)

Cells grown on sterile coverslips for 14 and 28 days were washed with PBS and fixed by incubation in 2.5% glutaraldehyde (Cat.no. G6257, Sigma-Aldrich) overnight at 4℃ followed by two washes with PBS for 10 minutes at 4℃ and dehydration in graded ethanol solutions (30, 50, 60, 70, 80, 90, 95, 100%, 20 minutes for each concentration). Samples were coated with a thin layer of gold

using a sputter coater (Q150T ES, Quorum Technologies, Laughton, East Sussex, UK) and imaged under a field scanning electron microscope (SU8010, Hitachi, Chiyoda, Tokyo, Japan) with an accelerating voltage of 3kV.

3.3.15. Synthesis and characterization of GelMA

Gelatin type A from porcine skin (Cat. no. G2500, Sigma-Aldrich) was dissolved in Dulbecco's phosphate buffered saline (DPBS, SH30028.02, HyClone™) at a concentration of 10% w/v at 60 °C. After complete dissolution, the temperature was decreased to 50°C and 8% (v/v) of methacrylic anhydride (Cat. no. 276685, Sigma-Aldrich) was added into the solution dropwise (1 ml/min) and the mixture was stirred for 3 hours. The reaction was stopped by diluting the solution (5x dilution) in DPBS and the unreacted methacrylic anhydride was removed by dialysis (Seamless Cellulose Dialysis Tubing, molecular weight cut-off 12 kDa, Cat. no. S25645B, Fisher Scientific) against distilled water at 40 °C for 7 days. The solution was freeze-dried for 3 days, and the resultant white foam was kept at -80 °C until used. The synthesized GelMA was characterized by proton nuclear magnetic resonance spectroscopy (^{1}HNMR, Bruker Avance 500 MHz spectrometers, Billerica, Massachusetts, US) in deuterium oxide, and Fourier Transform Infrared (FTIR) spectroscopy by using an IlluminatIR II inVia Reflex (Smiths Detection, Danbury, Connecticut, US) equipped with an attenuated total reflectance (ATR) objective.

3.3.16. Encapsulation of *Tbx1*-transfected cells in GelMA hydrogel

GelMA solution (5% (w/v)) was prepared in PBS containing 0.5% (w/v) Irgacure 2959 (Cat. no. 410896, Sigma-Aldrich) as photo-initiator and stirred at 80°C and was then sterilized using 0.2 μm Acrodisc® Syringe Filters (Cat. no. 4612, Pall corporation) under sterile conditions. Non-transfected and *Tbx1*-transfected HAT-7 cells, 48 hours after transfection, were mixed in sterile GelMA solution (3×10^6 cells/ml). The cell-encapsulated prepolymer solutions were added to the wells of 24-well plates and exposed to UV light (365 nm) for 3 minutes. Cell-laden hydrogels were cultured in DMEM/F12 (1:1), HEPES medium supplemented with 10% FBS and 1% antibiotics and incubated at 37 °C with 5% CO_2 for up to 21 days. The medium was changed every 48 hours.

3.3.17. SEM analysis of cell-laden hydrogels

After 7, 14 and 21 days of culture, cell morphology and mineralized structures were analyzed by SEM. Cell-laden constructs were rinsed with PBS twice and fixed with 2.5% v/v glutaraldehyde for 2 hours followed by washing in PBS and distilled water three times each. Lyophilized samples were then sputter coated and imaged with gold films and imaged using the same field scanning electron microscope as previously mentioned.

3.3.18. Statistical analysis

All data are expressed as mean±standard error of the mean. Statistical analysis was done using one-way ANOVA and the post-Tukey test by GraphPad Prism 5 (GraphPad Software, San Diego, California, USA). A p value < 0.05 was considered statistically significant.

3.4. Results and Discussion

3.4.1. Physio-chemical characterization of lipoplexes

Particle size and surface charge of lipoplexes are physio-chemical characteristics that has been shown to play crucial roles in DNA condensation, colloidal stability, cellular uptake, cytotoxicity and transfection efficiency [27,28]. Both GS- and DOTAP-based lipoplexes at all N/P ratios formed particles with the mean sizes between 100 nm to 300 nm (Figure 3.1. A). Zeta potential results showed that all formulations possessed positive surface charges except for DOTAP-based nanoparticles at N/P ratio of 2.5, which revealed the zeta potential of -6.96 ±0.56 mV (Figure 3.1. B). This negative surface charge could be attributed to the inadequate neutralization of pDNA by DOTAP and the partial exposure of the pDNA molecules at the surface of lipoplexes (deficient DNA condensation), which also could result in the formation of nanoparticles with larger sizes [20,29]. An increase in zeta potential of pDNA from a negative value to a positive value demonstrated the successful formation of lipoplexes. A reduction in the size of nanoparticles is observed as a function of N/P ratio, which indicated the significance of the charge ratio in controlling the particle size [20,30]. In fact, the higher N/P ratio increased the zeta potential values and enhanced the electrostatic interactions among cationic lipids and pDNA molecules, leading to better DNA condensation and decrease in nanoparticle size. In addition, the high N/P ratios was

shown to increase the homogeneity and colloidal stability of lipoplexes owing to electrostatic repulsions among particles which could hinder the agglomeration of nanoparticles [20,30]. According to Derjaguin-Landau-Verwey-Overbeek (DLVO) theory [31], nanoparticles that possess a zeta potential between +16 and +55 mV were reported to have a high colloidal stability [32]. Among all formulations, GS-based NPs at N/P ratios of 5 and 10 and DOTAP-based NPs at N/P ratio of 10 showed the zeta potential in this range and thus were more stable. TEM image of GS-based lipoplexes at N/P ratio of 5 (Figure 3.1. C) showed the assembly of nanoparticles with bilayer morphologies and with the particle sizes consistent with those measured by DLS. Moreover, the absence of any aggregates of nanoparticle in the image revealed the stability of particles [33].

3.4.2. DNA compaction and protection assays

To evaluate the ability of formulations for binding, neutralizing and compacting DNA while identifying the optimal N/P ratios of lipoplexes, gel retardation assay was performed. Electrophoretic mobility of pDNA through the agarose gel has been found to be contingent upon its charge, size and morphology [32]. As shown in figure 3.1. D, naked pDNA migrated through the gel owing to its negative charge and appeared as bright bands. It has been reported that these bands could be corresponded with three main forms of DNA: supercoiled (lower band), which is the most bioactive form of DNA, linear (middle band) and open circular (top band), which is the less active form of DNA [34]. Once complexed within the formulations, pDNA migration was inhibited or decreased and the lipoplexes mostly remained at the origin of electrophoresis wells which could demonstrate the DNA neutralization and the complexation among lipids and pDNA as well as an increase in size [35]. The intercalation of the dye with naked pDNA has been shown to increase the fluorescence intensity of the bands on the agarose gel [36], which was lowered or prevented in lipoplexes compared to naked pDNA. The presence of bands with lower fluorescence intensity for GS-based NPs at N/P ratio of 2.5 and DOTAP-based at N/P ratios of 2.5 and 5 revealed the partial compaction of pDNA. This result is in agreement with zeta potential measurement for these ratios of NPs, which showed lower values of surface charge and uncomplete neutralization. The DNA retardation was increased for higher N/P ratios and DNA migration was fully inhibited when the N/P ratios increased to 5 and 10 for GS-based NPs and to 10 for DOTAP-based NPs, which indicated the complete complexation of pDNA conceivably owing to higher

zeta potential values. It can be concluded that GS, as compared to DOTAP, possessed superior capacity in compacting DNA since less DNA migration was observed when complexed with GS-based NPs compared with DOTAP-based NPs at the same N/P ratio.

For successful gene transfer, a gene delivery system should be able to overcome enzymatic degradation in addition to compacting and transporting DNA to the target cells; unbound DNA have been shown to be easily degraded by DNase, whereas nanoparticles revealed the potential to protect DNA from enzymatic digestions [36]. As shown in figure 3.1. D, DNase I treated-naked pDNA migrated out of the well and were completely degraded, while pDNA within formulations was not degraded by the enzyme and remained intact. This indicated that liposomes were able to protect pDNA against enzymatic digestion. The best N/P ratios of the formulations in term of condensation and protection were 5 and 10 for GS-based NPs and 10 for DOTAP-based NPs.

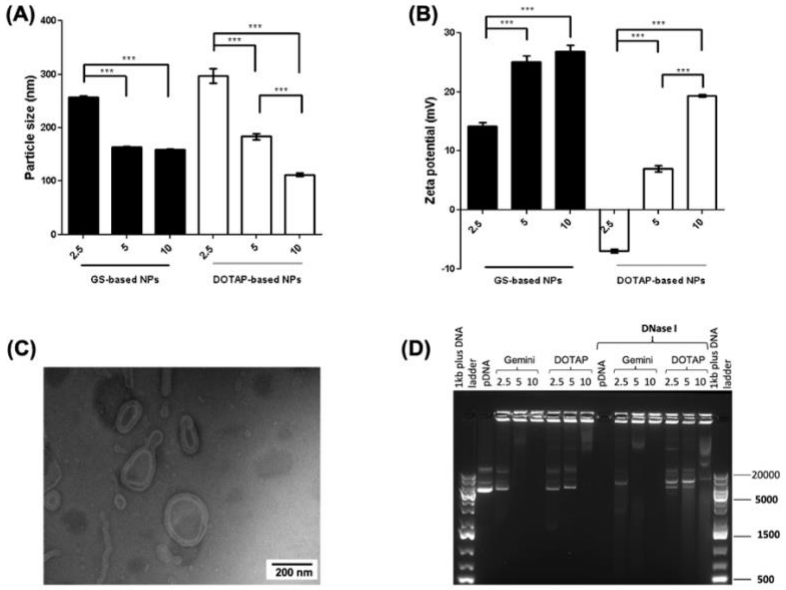

Figure 3.9. Comparative analysis of lipid-based nanoparticles based on assessment of their physico-chemical properties. (A, B) Particle size and zeta potential measured by dynamic light scattering indicated a statistically significant decrease in the size of lipoplexes and an increase in their surface charge by increasing nitrogen to phosphate (N/P) ratios in both gemini surfactant (GS)- and DOTAP-based nanoparticles (NPs). Error bars represent mean±SEM of repeats (*** $p<0.001$). Experiments were performed in triplicates. (C) Representative transmission electron microscopy (TEM) image of GS-based lipoplexes at N/P ratio of 5 showing assembly of nanoparticles with bilayer morphologies. (D) DNA compaction and protection against enzymatic digestion in lipoplexes visualized by agarose gel electrophoresis revealed the suitability of the N/P ratio of 5 and 10 for GS-based NPs and N/P ratio for 10 in DOTAP-based NPs.

3.4.3. Cytotoxicity assay

Cytotoxicity of gene delivery systems is of great importance for assessing the efficiency of the cell transfection and gene expression. To evaluate cellular toxicity of lipid-based formulations at different N/P ratios compared to Lipofectamine as a positive control, MTT assay was carried out 48 hours after cell transfection. As depicted in figure 3.2. A, cell viability was diminished by increasing N/P ratio. The N/P ratio of 10 in both GS- and DOTAP-based formulations showed the highest cytotoxicity, while the N/P ratios of 2.5 and 5 showed significantly lower cytotoxic effects. This is in agreement with other studies reporting that cytotoxicity of liposomes will increase upon increasing the amount of the cationic lipid; in fact, toxicity of cationic liposomes was found to be the result of the interactions between their positively charged head groups (quaternary ammonium in GS and trimethylammonium in DOTAP) and negatively charged molecules in cells which could disrupt cellular functions and the integrity of the cellular components [32,37]. It has been reported that once pDNA is completely neutralized by cationic surfactants or lipids, no further lipidic molecule binds to lipoplexes; the remaining lipids form free micelles or free liposomes in the environment which can compete with lipoplexes to bind or enter cells and cause toxicity in formulations with high N/P ratios [20,38].

Lipofectamine 2000, the commercially available liposome for gene delivery, showed a high level of cytotoxic effects compared to GS- and DOTAP-based formulations at all N/P ratios except ratio 10 of GS-based NPs. However, no significant difference was observed between cells transfected with empty vector (pCMS-EGFP) or *Tbx1* pDNA using lipofectamine which revealed that the toxic effects was not due to the insertion of *Tbx1* gene fragment into the pCMS-EGFP plasmid. It also showed that the expressed *TBX1* protein did not cause any toxicity.

3.4.4. Evaluation of *in vitro Tbx1* gene expression

In vitro transfection activity of lipid-based formulations was assessed by measuring *Tbx1* gene expression using qRT-PCR 48 hours after cell transfection. As shown in figure 3.2. B, the level of the up-regulation of *Tbx1* mRNA was contingent upon not only the type of the lipid composition used in the formulations but also on the N/P ratios. An increase in *Tbx1* levels was observed in cells transfected with lipoplexes carrying *Tbx1* pDNA. The transfection efficiency increased at higher N/P ratio in both GS- and DOTAP-based lipoplexes. NPs prepared at N/P ratio of 10

showed, in both GS- and DOTAP-based NPs, the highest level of *Tbx1*expression as compared with other ratios. However, the N/P ratios of 2.5 and 5 in DOTAP-based NPs did not show a significant increase in *Tbx1* gene expression compared to both control and cells which were transfected using Lipofectamine, whereas the N/P ratio of 10 in DOTAP-based NPs showed such significant increase. Additionally, GS-based NPs consistently revealed significantly higher levels of *Tbx1* mRNA expression compared to DOTAP-based NPs with the same N/P ratios ($P<0.001$) and Lipofectamine ($P<0.001$). Moreover, empty plasmid without *Tbx1* insertion (pCMS-EGFP), when delivered by using Lipofectamine, showed no increase in *Tbx1* gene expression indicating that the up-regulation observed in other groups was induced by successful delivery of *Tbx1* gene into cells mediated by lipid-based formulations.

Similar to cellular toxicity, cell internalization and transfection efficiency have been reported to be influenced by physico-chemical properties of cationic liposomes such as particle size, surface charge, morphology, stability and lipid composition [39,40]. Moreover, it has been reported that positively charged NPs displayed superior cellular interactions and a higher extent of cell internalization, which occurs through clathrin-mediated endocytosis, as compared with negatively charged NPs, which employs caveolae-mediated pathway, or neutral particles [41–43]. Higher density of positive charges on the surface of NPs was found to result in a greater level of cellular uptake with a faster speed [44]. Cationic liposomes, in particular, showed enhanced effectiveness of cellular uptake and thus greater intracellular bioavailability when they had higher positive charges [45]. As a result, the higher *Tbx1* gene expression observed in the cells treated with higher N/P ratios of both GS- and DOTAP-based NPs could be due to the higher surface charge and the smaller size of particles.

In the case of lipid composition, cationic lipids have reported to play an essential role in cellular uptake, whereas DOPE as a fusogenic lipid has shown to be involved in the fusion between lipid particles and plasma membrane, is influential for cell internalization [46]. Given the constant concentration of DOPE in all formulations, the difference observed in *Tbx1* gene expression could be only attributed to the effect of the cationic lipid content and composition.

Cellular uptake of majority of lipoplexes including DOTAP/DOPE-based lipoplexes was found to occur via clathrin-mediated endocytosis [47], while GS-based NPs were shown to be taken up through either clathrin- or caveolin-mediated endocytosis [48]. As mentioned above, GS-based NPs at all N/P ratios exhibited significantly higher levels of *Tbx1* gene expression compared to

DOTAP-based NPs and commercial Lipofectamine 2000. This finding was in agreement with other studies that showed the superior potential of gemini liposomes for *in vitro* gene transfer than DOTAP and Lipofectamine, conceivably due to a suitable balance among rigidity and fluidity of gemini lipids [49], which were found to be important parameters for wrapping pDNA and interaction with cell membrane [50,51]. The low critical micelle concentration of gemini lipids compared to the monovalent counterparts might be another possible reason for their higher transfection ability, which could be resulted from the higher stability of complexes during the delivery of gene as well [20].

According to the physico-chemical and biological characterizations of NPs, the N/P ratio 5 of GS-based NPs was selected as the optimal formulation to deliver *Tbx1* encoding genes into dental epithelial stem cells to induce ameloblast differentiation. Although the N/P ratio of 2.5 of GS-based NPs revealed the lowest cellular toxicity, it was unable to condense and protect pDNA properly and it showed a relatively low level of *Tbx1* mRNA expression. On the other hand, the N/P ratio of 10 of GS-based NPs showed a greater transfection ability, but its high level of cytotoxicity made it unfavorable for the *in vitro* cell differentiation.

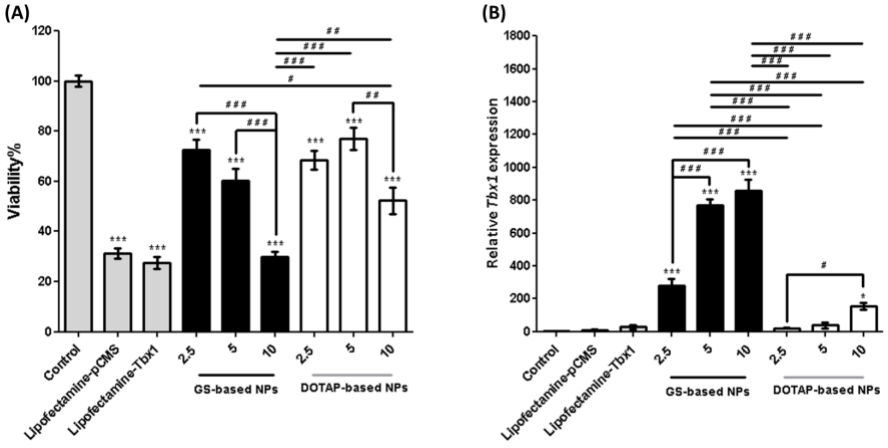

Figure 3.10. Comparative analysis of lipid-based nanoparticles at different N/P ratios and Lipofectamine, as a positive control, based on the assessment of their biological activities in HAT-7 cells transfected with Tbx1 encoding gene 48 hours after transfection. (A) Viability test performed by MTT assay showing relatively low cytotoxic effects of gemini surfactant (GS)- and DOTAP-based nanoparticles (NPs) at ratios of 2.5 and 5 compared to Lipofectamine. (B) Tbx1 mRNA expression measured by qRT-PCR which was higher in cells transfected with Tbx1 gene using GS-based NPs compared to DOTAP-based NPs and Lipofectamine. Error bars represent mean±SEM of repeats (*statistically significant results indicated in the graphs and * represents comparison vs control group and # reflects comparison among different groups determined in the graphs, ***, ### $p<0.001$, **, ## $p<0.01$, *, # $p<0.05$). Experiments were performed in triplicates.

3.4.5. Expression of ameloblast differentiation markers

To examine the effect of *Tbx1* transfection on dental epithelial stem cell differentiation, control and *Tbx1*-transfected cells were cultured for up to 28 days and the expression of ameloblast differentiation markers, including enamel matrix proteins, proteinases and calcium signalling-related markers, were assessed using immunocytochemistry (Figure 3.3) and qRT-PCR (Figure 3.4 and 5). *Tbx1* mRNA expression was significantly up regulated at days 2 ($P<0.001$), 4 ($P<0.05$), 7 ($P<0.05$), 14 ($P<0.05$); it was the highest at day 2 then decreased over time (Figure 3.4. A). This confirmed that *Tbx1* transfection successfully resulted in *Tbx1* upregulation in HAT-7 cells. At day 28, no statistically significant difference was observed between *Tbx1*-transfected cells and control. This could be due to the fact that transiently transfected cells were able to express the gene of interest only for a limited period of time. Dentin sialophosphoprotein (DSPP) is a protein expressed not only in odontoblasts but also in ameloblasts during the presecretory phase, and it plays an essential role in the development of newly-formed enamel at the dentino-enamel interface (junction) [52,53]. No significant difference was observed in *Dspp* mRNA expression in *Tbx1*-transfected cells compared to control (Figure 3.4. B). Enamel matrix proteins including AMELX, AMBN and ENAM are secreted during secretory stage of amelogenesis and undergo degradation during transition and maturation stages [54]. AMELX is the most abundant protein of the enamel (80-90% of all enamel proteins), which regulates the nucleation, growth and alignment of crystals as well as the organization of the prismatic patterns and the thickness of enamel [55–57]. Amelogenin expression was stronger in *Tbx1*-transfected cells compared to control group at the 14- ($P<0.001$) and 28-day (not statistically significant, $P>0.05$) timepoints. In addition, the level of AMELX expression decreased in *Tbx1*-transfected cells from days 14 to 28, while it increased in control cells (Fig. 3. A-C). This might suggest that *Tbx1*-transfected cells transitioned from the secretory phase to the maturation phase between these two time points while control cells were still in the secretory stage. A previous study showed that electroporation of *Tbx1* gene into the dental epithelium led to up-regulation of amelogenein expression indicating that the expression of AMELX is under control of *Tbx1* expression [10]. Thus, another possible reason for up-regulation of AMELX expression at only day 14 could be the increased expression of *Tbx1* that was observed at day 14 and not at day 28 (Figure 3.4. A). AMBN is the second abundant matrix protein after amelogenin (5-10%) and acts as a cell adhesion molecule and is needed for proliferation and

differentiation of ameloblasts [56,58,59]. The mRNA levels of ameloblastin were significantly lower in *Tbx1*-transfected cells compared to control following 2 and 4 days of culture, whereas no significant difference was observed after 7, 14 and 28 days (Figure 3.4. C). ENAM is a glycoprotein considered the largest, least abundant protein in the enamel matrix (3-5%) which regulates the aggregation of amelogenin into nanospheres and controls crystal nucleation and growth [54–56,60]. The *Enam* mRNA expression level was slightly lower in *Tbx1*-transfected cells compared to control cells; however, the difference was not statistically significant (Figure 3.4. D). Amelotin (AMTN) is another ameloblast marker that accumulates in the basal lamina layer between cells and minerals once it is secreted, and it contributes to the cell-matrix attachment [5,61,62]. It also enhances the hydroxyapatite (HAp) mineralization and controls the organization and morphology of minerals [63]. AMTN expression was reported to be up-regulated during both the transition phase [62] and the maturation stages [64]. AMTN immunostaining was negative in control group at days 14 and 28. In contrast, AMTN was expressed in *Tbx1*-transfected group at day 14 and disappeared at day 28 (Figure 3.3. D-F). No AMTN expression during maturation stage at day 28 could be detected probably due to the absence of basal lamina in *in vitro* models as compared to *in vivo* events occurring during ameloblast differentiation and enamel formation in which AMTN accumulates in basal lamina, as mentioned above. Proteinases also play a pivotal role in enamel formation through eliminating of the enamel matrix proteins which help with reaching to the high degree of enamel mineralization [65]. KLK4 is a proteolytic enzyme secreted during the transition and maturation steps of the enamel formation to degrade the partially hydrolyzed proteins in the organic matrix [54,66]. KLK4 protein expression was higher in *Tbx1*-transfected cells compared to control group at days 14 ($P<0.01$) and 28 (not statistically significant, $P>0.05$). In addition, the highest level of *Klk4* mRNA expression was observed in *Tbx1*-transfected cells at day 28, compared to other time points (Figure 3.5. A). Calcium ions (Ca^{2+}) play an essential role in enamel calcification and crystal nucleation and growth [67]. Ca^{2+} release-activated Ca^{2+} (CRAC) channels are considered the major route for Ca^{2+} influx into cells [68]. Calcium release-activated calcium channel protein 1 (ORAI1) is a protein existing in the plasma membrane that makes the pores of CRAC channels [69] and it is up-regulated during the maturation stage [70]. Once it is activated by stromal-interacting molecule (STIM1), ORAI1 enables Ca^{2+} ion influx [71]. ORAI1 protein was expressed significantly higher in *Tbx1*-transfected cells compared with control group at day 14 ($P<0.01$). The levels of expression increased in both *Tbx1*-transfected cells and

control groups at day 28 and the difference between these groups was not significant (Figure 3.3. D-F). Consistently, the *Orai1* mRNA expression in *Tbx1*-transfected cells was increased significantly from day 2 to day 7 ($P<0.01$), when the expression level was significantly higher in *Tbx1*-transfected cells compared to control cells ($P<0.01$), whereas no significant difference was observed between *Tbx1*-transfected cells and control cells at days 2, 4, 14 and 28 (Figure 3. 5. B). STIM1 is a transmembrane protein in the endoplasmic reticulum which is expressed in maturation ameloblasts and acts as a dynamic sensor for Ca^{2+} [68,72,73]. It detects the drop in the level of Ca^{2+} stored in endoplasmic reticulum and then it directly binds to ORAI1 in plasma membrane which activates Ca^{2+} ion channels in order to balance Ca^{2+} level [74,75]. A significant increase in *Stim1* mRNA expression was observed in *Tbx1*-transfected group with respect to control cells following 28 days of culture ($P<0.001$). The highest level of *Stim1* mRNA expression in *Tbx1*-transfected cells was at day 28, compared to other time points (Figure 3.5. C). Alkaline phosphate (*Alp*) is a marker of ameloblast differentiation which is indispensable for induction and progression of enamel matrix mineralization and is mainly expressed during the late stage of enamel formation [25,76,77]. The *Alp* mRNA expression was significantly up-regulated in *Tbx1*-transfected cells compared to control cells at day 4, 7, 14, while no significant difference was observed at day 2 and 28. Moreover, the *Alp* expression level was highest at day 14 with respect to other time points (Figure 3.5. D). Taken together, these results confirmed that gemini surfactant-based *Tbx1* transfection can differentially promote the expression of ameloblast differentiation markers and enhance enamel secretion, maturation and mineralization. Thus, our system could be used to guide the differentiation of dental epithelial stem cell into enamel-forming ameloblasts.

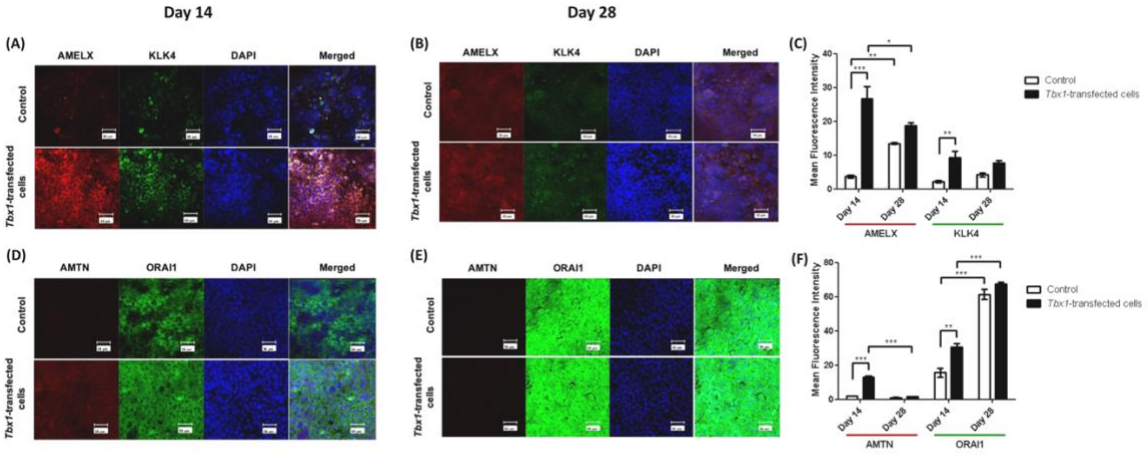

Figure 3.*11*. Immunocytochemical analysis of Tbx1-transfected HAT-7 cells compared to control cells after 14 and 28 days of culture. Transfection of HAT-7 cells with Tbx1 encoding gene significantly enhanced the levels of amelogenin (AMELX) and kalikrein-4 (KLK4) protein expression (A, B, C) and amelotin (AMTN) and calcium release-activated calcium channel protein 1 (ORAI1) protein expression (D, E, F) after 14 days of culture. No significant difference was observed in expression of AMELX, KLK4 (C), AMTN and ORAI1 (F) between control and Tbx1 transfected group at day 28. Error bars represent mean±SEM of repeats (*statistically significant results indicated in the graphs, ***p<0.001, **p<0.01, *p<0.05). Experiments were performed in triplicates. The expression of markers was quantified by measuring mean fluorescent intensity in five randomly selected areas in each image.

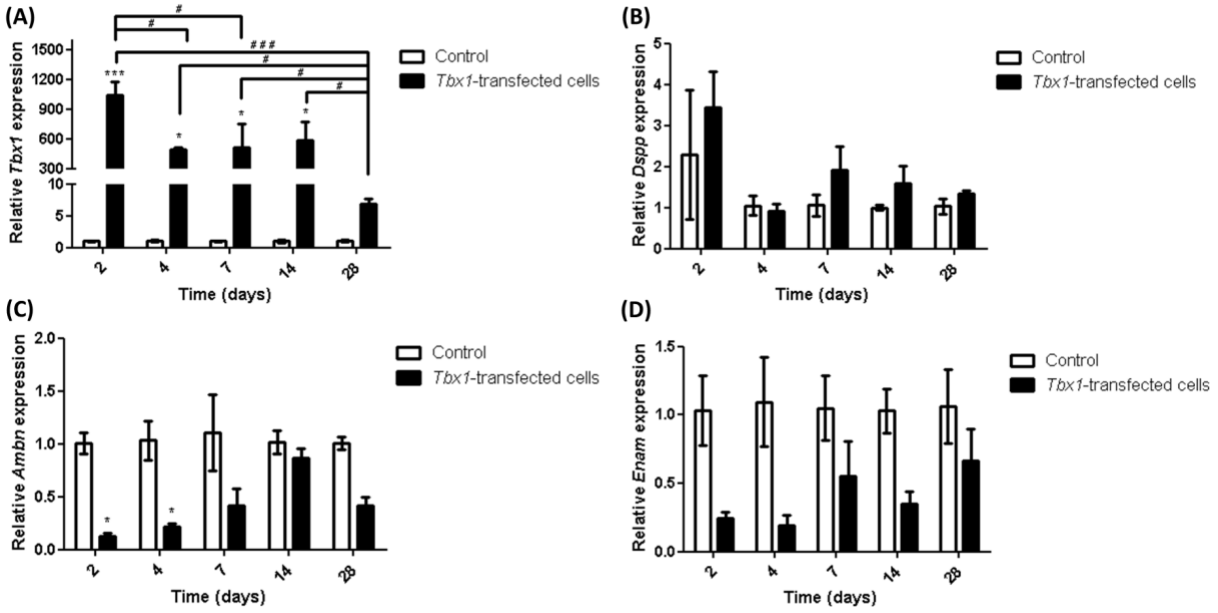

Figure 3.12. Effect of transfection of HAT-7 cells with Tbx1 encoding gene on mRNA expression of Tbx1 and secretory ameloblasts markers at different time points (days 2, 4, 7, 14 and 28) analyzed by quantitative real time polymerase chain reaction (qRT-PCR). Tbx1 mRNA expression was significantly increased at day 2, 4, 7 and 14 in Tbx1-transfected cells compared to control and the level of expression decreased overtime (A), No significant difference was observed in expression of Dspp (B) and Enam mRNA (D) between Tbx1-transfected cells and control groups. The expression of Ambn (C) was down-regulated after 2 and 4 days of culture with no significant difference at days 7, 14 and 28. Experiments were carried out in triplicates. Error bars represent mean±SEM of repeats (*statistically significant results indicated in the graphs and * represents comparison vs control group and # reflects comparison among different groups determined in the graphs, ***, ### p<0.001, **, ## p<0.01, *, # p<0.05). Tbx1, T-box1; Dspp, Dentin sialophosphoprotein; Ambn, Ameloblastin; Enam, Enamelin.

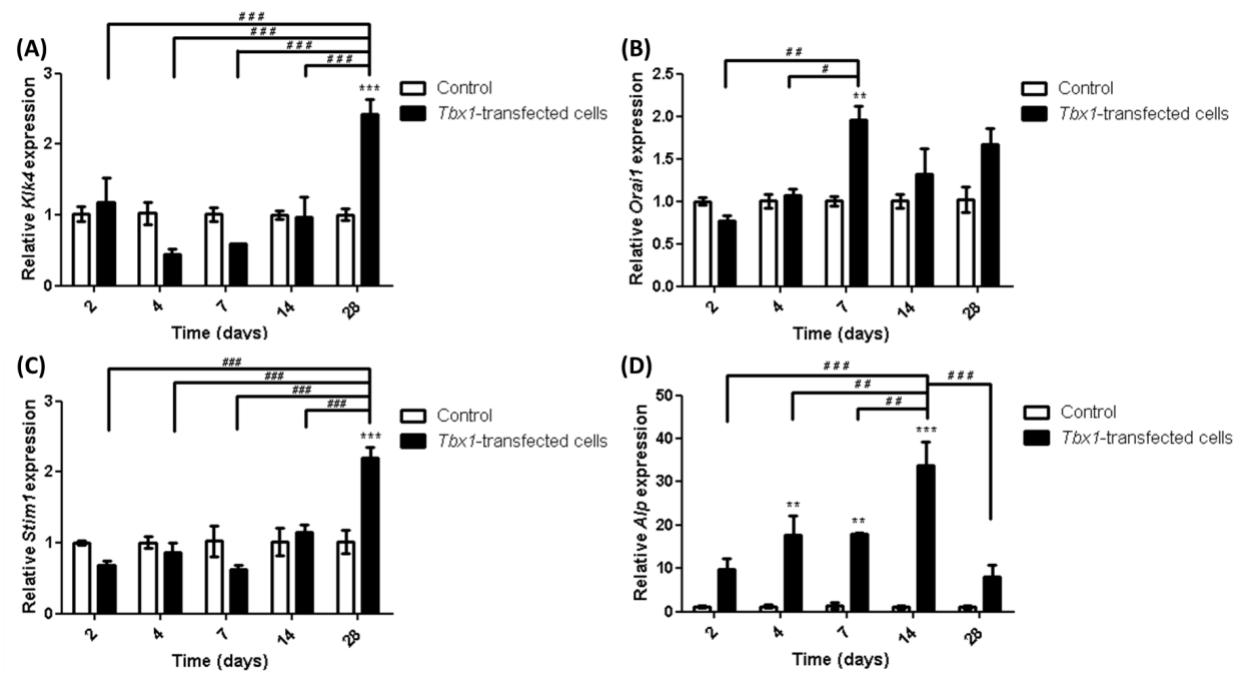

Figure 3.13. Effect of transfection of HAT-7 cells with Tbx1 encoding gene on the mRNA expression of maturation ameloblasts markers at different time points (days 2, 4, 7, 14 and 28) analyzed by quantitative real time polymerase chain reaction (qRT-PCR). Significant up-regulation of maturation markers including Klk4, at day 28; Orai1, at day 7; Stim1, at day 28; Alp, at days 4, 7, 14 shows that transfection of HAT-7 cells with Tbx1 enhances differentiation of dental epithelial stem cell into ameloblasts. Experiments were carried out in triplicates. Error bars represent mean±SEM of repeats (*statistically significant results indicated in the graphs and * represents comparison vs control group and # reflects comparison among different groups determined in the graphs, ***, ### $p<0.001$, **, ## $p<0.01$, *, # $p<0.05$). Klk4, Kalikrein-4; Stim1, Stromal-interacting molecule; Alp, Alkaline phosphate.

3.4.6. Evaluation of the effect of *Tbx1* upregulation on mineralization

To evaluate the effect of *Tbx1* transfection on mineralization, ALP, Alizarin Red S and von Kossa staining was carried out. HAT-7 cells transfected with *Tbx1* expressed higher level of ALP expression compared to non-transfected cells at days 14 and 28 (Figure 3.6. A-1, 2). It was historically suggested that ALP is involved in enamel formation to stimulate mineralization by providing the phosphate ions or by eliminating the inorganic pyrophosphate PP_i, which can have inhibitory impact on enamel mineralization. Other studies reported that stratum intermedium (SI) cells, which are situated next to ameloblasts, secreted ALP which transported phosphate ions or nutrients from blood supply to the enamel organ [78]. The higher ALP expression in *Tbx1*-transfected cells after 14 days demonstrated that mineralization started in this group earlier than

control cells, which were still in the secretory phase and expressed a very low level of ALP. In addition, transfected cells showed increased ALP expression from day 14 to day 28, which could indicate an increase in mineralization over time and the terminal differentiation of ameloblasts. HAT-7 cell line was shown to elevate ALP activity and express amelogenin and ameloblastin proteins when differentiated into ameloblast-like cells [23]. A previous study reported an increase in differentiation of HAT-7 cells, with enhanced ALP activity and greater mineralization, after being treated with a high concentration of full-length recombinant human amelogenin (rh-AMEL) [79]. Thus, this evidence suggested that the higher ALP expression in *Tbx1*-transfected cells showed increased ameloblast differentiation compared to control cells.

In addition, calcium deposition and mineralized nodule formation were assessed by Alizarin Red S (Figure 3.6. A-3, 4) and von Kossa staining (Figure 3.6. A-5, 6), respectively [80]. Positive Alizarin Red S (red) and von Kossa (black/brown) staining indicated the deposition of calcium and calcium phosphate; respectively [81], after 14 and 28 days of culture in both control and *Tbx1*-transfected cells, which increased with culture time showing the time dependent mineralization. However, the staining intensity was in a much lower extent in control cells as compared to *Tbx1*-transfected cells, and strongest staining level was observed in *Tbx1*-transfected cells at day 28. According to previous reports, the color of mineralized nodules visualized by von Kossa staining could be a determinant of the state of differentiation in osteoblasts; the semi-differentiated cells were observed to be stained in light-brown color and fully differentiated cells in dark-brown or black [82]. Accordingly, our results revealed that HAT-7 cells were semi-differentiated at day 14, while they became fully differentiated at day 28 and the proportion of fully differentiated cells were higher in *Tbx1*-transfected cells compared to control group. Mineralized nodule formation was remarkably increased in HAT-7 cells when transfected with *Tbx1* encoding gene juxtaposed with control cells after 14 and 28 days of culture. Thus, these results indicated that *Tbx1* transfection could enhance or accelerate ameloblast differentiation and mineralization of dental epithelial stem cells.

3.4.7. Observation of cell morphology and mineral deposition in 2D cell culture models

In order to observe the morphology of cells and the deposition of minerals, SEM analysis was performed at day 14 and 28. At day 14 (Figure 3.6. B-1), control and *Tbx1*-transfected HAT-7 cells

showed round or cobblestone morphologies as it was reported in a previous study [83]. In addition, the nanometer-sized amorphous globular particles, but not the mineralized nodules, were observed on the surface of the cells that seemed to be the amorphous calcium phosphate as the initial phase of crystals [84]. At day 28 (Figure 3.6. B-2), both groups deposited calcified nodules and mineralized crystals. However, the morphology of nodules was different in *Tbx1*-transfected cells compared to control group as they were more extensive, which implied the effect of *Tbx1* transfection on enhancing formation and growth of mineralized nodules by HAT-7 cells.

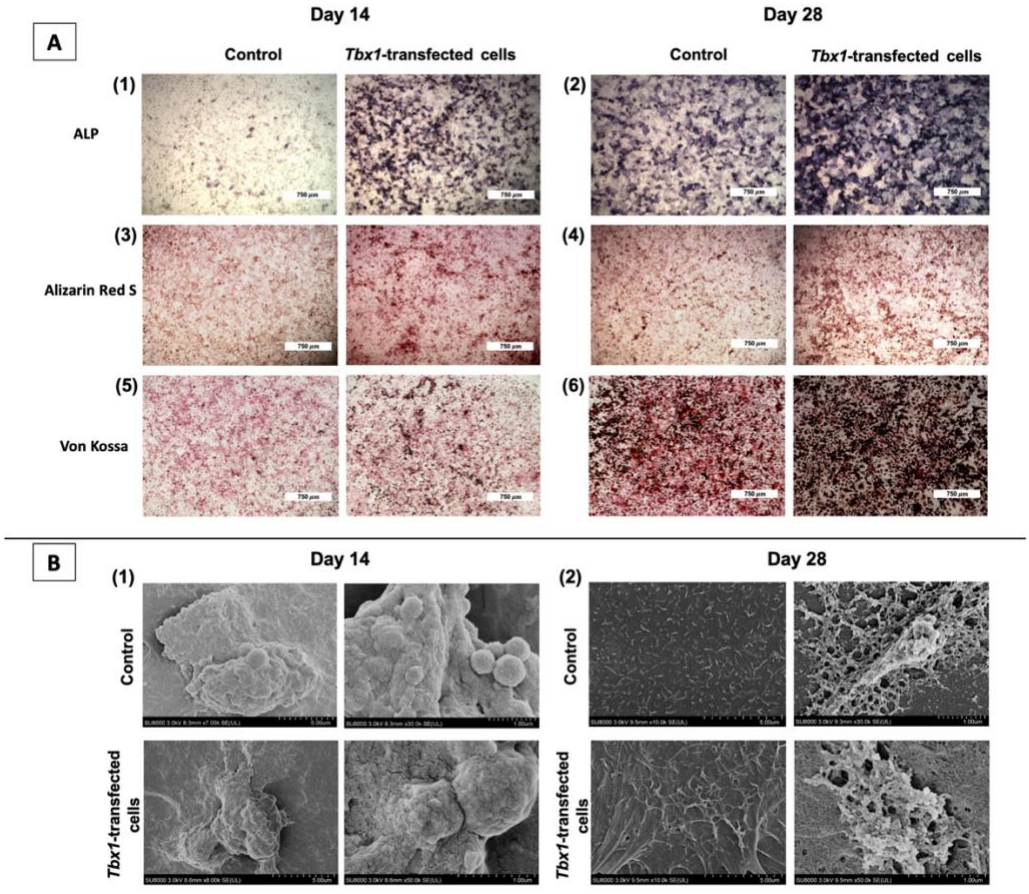

Figure 3.14. (A) alkaline phosphatase (ALP) staining and mineral deposition visualized by Alizarin Red S and von Kossa staining in control and Tbx1-transfected cells after 14 and 28 days of culture. Tbx1-transfected HAT-7 cells showed higher levels of ALP expression (1, 2) and calcium (3, 4) and calcium phosphate (5, 6) deposition than control cells, indicating the accelerated induction of ameloblast differentiation and mineralization by Tbx1 gene delivery to cells. (B) Scanning electron microscopy (SEM) images of Tbx1-transfected HAT-7 cells compared to control cells after 14 (1) and 28 (2) days of culture in conventional 2D models showed that Tbx1 transfection promoted the formation and the growth of mineralized nodules.

3.4.8. Characterization of GelMA

The successful methacryloyl-functionalization of gelatin was confirmed by FTIR-ATR and ^{1}HNMR analyses. In FTIR-ATR spectra (Figure 3.7. A), the peaks at 3297 cm^{-1}, 2934 cm^{-1}, 1082 cm^{-1} in GelMA (3276 cm^{-1}, 2938 cm^{-1} and 1080 cm^{-1} in gelatin) were associated to O-H stretching, C-H stretching and C-H bending, respectively. The peaks seen at 1523 cm^{-1} were related to C-N stretching and N-H bending. Amide I and II bands were also observed at 1631 cm^{-1} and 1523 cm^{-1} which were linked to C=O stretching and N-H bending, respectively. The changes in the C-H stretching and C-H bending regions were as a result of grafting the methacryloyl groups to the lysine groups of gelatin [85–87]. The ^{1}HNMR spectra of unmodified gelatin and GelMA are shown in figure 3.7. B. The spectrum of the GelMA exhibited two new peaks in the range of 5.3 and 5.5 ppm which were attributed to acrylic protons of methacrylate groups, and a new peak at 1.8 ppm, which was assigned to the methyl groups of grafted methacrylate groups while such signals were absent in the spectrum of the unmodified gelatin. The smaller peak observed at 2.9 ppm in GelMA spectrum compared to gelatin, revealed the functionalization of lysin groups by methacrylate groups. Therefore, the ^{1}HNMR spectra proved that the primary amino groups of gelatin has been successfully substituted with methacrylate groups [88,89].

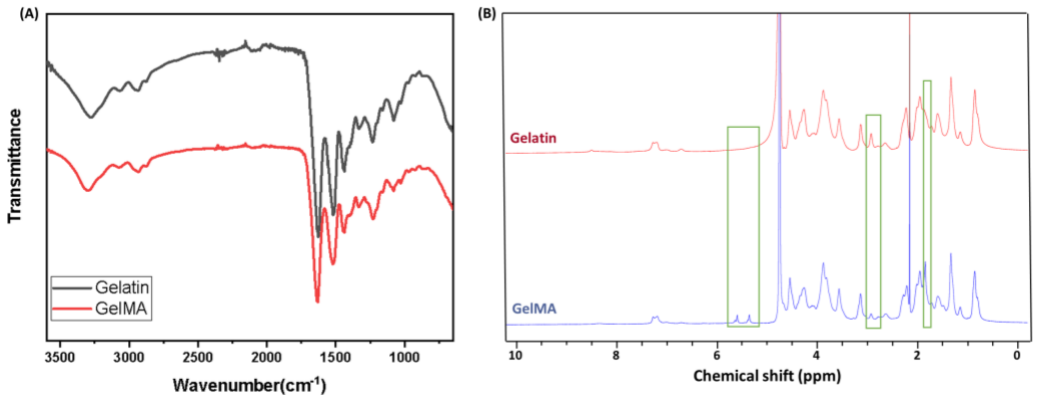

Figure 3.15. Characterization of gelatin methacrylate (GelMA) and unmodified gelatin by Fourier Transform Infrared-Attenuated Total Reflectance (FTIR-ATR) and proton nuclear magnetic resonance (^{1}HNMR) showed that gelatin is chemically modified with methacrylate groups. (A) FTIR-ATR spectra of GelMA and gelatin revealed changes in the C-H stretching and C-H bending regions at 2934 cm^{-1} and 1082 cm^{-1} which were owing to methacryloyl-functionalization (B) ^{1}HNMR spectrum of GelMA exhibited the new peaks at 5.3 and 5.3 ppm, attributed to protons of methacrylate groups, a new peak at 1.8, assigned to methyl protons of grafted methacryloyl groups, and the smaller peak at 2.9 ppm, corresponded with lysin groups functionalized with methacryloyl, confirming successful substitution of primary amines by methacrylate groups in GelMA.

3.4.9. Evaluation of the cell morphology and mineral deposition in the 3D cell culture models

To observe the morphology of the cells and crystals in 3D culture, SEM analysis was carried out on days 7, 14 and 21. Control and *Tbx1*-transfected cells encapsulated in GelMA hydrogels showed a rounded morphology at all time points (Figure 3.8). Similar observation was reported by a previous study that HAT-7 cells exhibited a round morphology when co-cultured with dental pulp stem cells in collagen I/chitosan hydrogels [90]. At day 7 (Figure 3.8. A), both control and *Tbx1* over-expressing HAT-7 cells revealed the formation of nanosized-spherical clusters of minerals on them. In addition, the ribbon-like structures with short lengths were appeared on the surface of the *Tbx1*-transfected cells at this time point, whereas such structures were not observed on the control cells. Likewise, such globular structures were observed on control and *Tbx1*-transfected cells at day 14. The ribbon-like crystals that were seen on cells over-expressing *Tbx1* had greater lengths at day 14 compared to day 7 (Figure 3.8. B). At day 21, control cells revealed the formation of rod-like crystals (Figure 3.8. C-2), while the *Tbx1*-transfected cells showed the deposition of elongated crystals with random orientations and variant morphologies including ribbon-, rod-, (Figure 3.8. C-4) and prims-like structures (Figure 3.8. D-1). However, the number of the elongated crystals were much higher in *Tbx1*-transfected cells compared to control cells. In addition, figure 3.8. D-2, 3, 4 showed the contribution of organic matrix, either from the gelatin in the GelMA hydrogel or from enamel organic matrix produced by HAT-7 cells to the elongated growth of crystals. Dental enamel mineralization has been proposed to occur in the enamel organic matrix because of the flowing steps. First, the calcium and phosphate ions are transported from ameloblasts into the matrix [91]. The initial solid phase, amorphous calcium phosphate (ACP), is spontaneously precipitated from ion clusters [92]. ACP are formed as spherical nanoparticles (20-200 nm) with a short-range order that are unstable and undergo transformation into ribbon- or plate-like octacalcium phosphate (OCP) which acts as a precursor of the apatite [91,93,94]. Subsequently, OCP crystals grow lengthwise and their morphology changes into rod- or prims-like crystals, through interactions of amelogenin with the side faces of the crystals [95,96]. Finally, OCP crystals undergo hydrolysis and are transformed into more stable apatite crystals [92]. Accordingly, it seemed that control cells were able to deposit ACP mineral phase at day 7 and 14 and OCP or apatite crystals at day 21. On the other hand, *Tbx1*-transfected cells could deposit the ACP, OCP crystals at day 7 and 14, while OCP crystal elongation and transformation into apatite

crystals occurred at day 21. It is worth mentioning that such elongated crystals were not observed in 2D culture (Figure 3.6. B), which might be due to the fact that the GelMA hydrogel could assist with crystal nucleation and growth by providing the gel like environment similar to the enamel organic matrix as previously reported [97,98]. Altogether, *Tbx1* transfection could accelerate and enhance enamel mineralization which further confirmed the results of ALP, Alizarin Red S and von Kossa staining and SEM images in 2D culture (Figure 3.6).

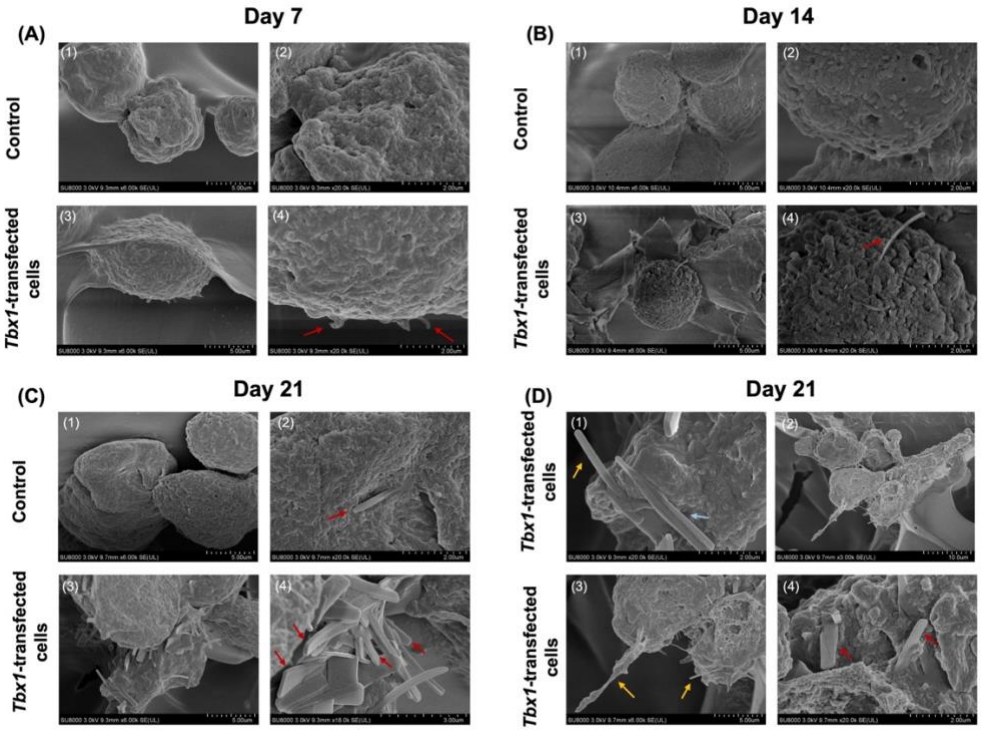

Figure 3.16. Scanning electron microscopy (SEM) images of Tbx1-transfected HAT-7 cells encapsulated in gelatin methacrylate (GelMA) hydrogel compared to control cells after 7 (A), 14 (B) and 21 (C, D) days of culture revealing that Tbx1 transfection could accelerate and promote enamel mineralization. Ribbon-, rod- and prism-like structures are shown with red, yellow and blue colored arrows, respectively.

3.5. Conclusions

In this study, we have developed and optimized a non-viral gene delivery system based on gemini surfactants as an effective tool to transfer T-box1 encoding gene into the dental epithelial stem cell line, HAT-7, in order to induce ameloblast differentiation. Our findings suggested that T-box1 gene delivery into HAT-7 cells could differentially regulate the expression of ameloblast markers

and enhance mineralization *in vitro*. Further studies including additional *in vitro* assays as well as *ex vivo* culture and in vivo implantation are needed to further evaluate the potential of this system for clinical applications. The optimized T-box1 gene delivery system presented in this study is being integrated into the co-culture with dental pulp stem cells using 3D-printed dual compartment scaffolds to combine the differentiation-inducing effect of T-box1 overexpression with epithelial-mesenchymal interactions to synergistically guide dental epithelial stem cells towards enamel-like tissue formation and appropriate interface to underlying dentin. Taken together, this work suggests that T-box1 gene delivery using gemini surfactant-based nanoparticles can be used as an efficient tool for the induction of ameloblast differentiation and enamel formation. This promising approach provides a foundation for tissue engineering approaches to repair defective enamel and might offer a translational potential for clinical restorative dentistry to improve best practices for dental caries treatments.

3.6. Acknowledgements

We would like to acknowledge the Saskatchewan Health Research Foundation (SHRF) and College of Dentistry start-up financial support (PI: PP), College of Medicine start-up funds (SP), and the University of Saskatchewan Dean's scholarship and Biomedical Engineering Devolved Scholarship (to FM). We are also grateful to Dr. Thimios A. Mitsiadis (University of Zurich, Zurich, Switzerland) and Dr. Bernhard Ganss (University of Toronto, Ontario, Canada) for providing us with pAAV-hSynapsin1-GCaMP6s-P2A-mRaby3-*Tbx1* and anti-Amelotin antibodies, respectively. Parts of this study has been presented as abstracts in 2018 AADR/CADR Annual Meeting & Exhibition (Florida, USA), 2018 IADR/PER General Session, (London, UK), 13th International Conference on the Chemistry and Biology of Mineralized Tissues (Quebec, Canada, October 2019), 2020 IADR/AADR/CADR General Session & Exhibition (Washington, D.C., USA) and 33rd Annual CSHRF August 2020.

Authors' contribution: Conceptualization, F.M, M.A, L.L, S.P, I.B, X.C, P.P; Methodology, F.M, M.A, L.L, B.S; Formal analysis, F.M, M.A, L.L; Resources, S.P, I.B, X.C, P.P; Writing-Original Draft, F.M; Writing-Review & Editing, F.M, M.A, L.L, S.P, I.B, X.C, P.P; Supervision, S.P, I.B, X.C, P.P.

3.7. References

[1] R.S. Lacruz, S. Habelitz, J.T. Wright, M.L. Paine, Dental enamel formation and implications for oral health and disease, Physiol. Rev. 97 (2017) 939–993.

[2] Q. Chu, Y. Gao, X. Gao, Z. Dong, W. Song, Z. Xu, L. Xiang, Y. Wang, L. Zhang, M. Li, Ablation of Runx2 in Ameloblasts Suppresses Enamel Maturation in Tooth Development, Sci. Rep. 8 (2018) 9594.

[3] Y. Cao, M.L. Mei, Q.-L. Li, E.C.M. Lo, C.H. Chu, Enamel prism-like tissue regeneration using enamel matrix derivative, J. Dent. 42 (2014) 1535–1542.

[4] Y. Hu, C.E. Smith, A.S. Richardson, J.D. Bartlett, J.C.C. Hu, J.P. Simmer, MMP20, KLK4, and MMP20/KLK4 double null mice define roles for matrix proteases during dental enamel formation, Mol. Genet. Genomic Med. 4 (2016) 178–196.

[5] C.E.L. Smith, J.A. Poulter, A. Antanaviciute, J. Kirkham, S.J. Brookes, C.F. Inglehearn, A.J. Mighell, Amelogenesis imperfecta; genes, proteins, and pathways, Front. Physiol. 8 (2017) 435.

[6] L. Gan, Y. Liu, D.-X. Cui, Y. Pan, M. Wan, New insight into dental epithelial stem cells: Identification, regulation, and function in tooth homeostasis and repair, World J. Stem Cells. 12 (2020) 1327.

[7] X. Chatzistavrou, S. Papagerakis, P.X. Ma, P. Papagerakis, Innovative approaches to regenerate enamel and dentin, Int. J. Dent. 2012 (2012).

[8] M.J. Honda, Y. Shinmura, Y. Shinohara, Enamel tissue engineering using subcultured enamel organ epithelial cells in combination with dental pulp cells, Cells Tissues Organs. 189 (2009) 261–267.

[9] G. Bluteau, H.U. Luder, C. De Bari, T.A. Mitsiadis, Stem cells for tooth engineering, Eur Cell Mater. 16 (2008) 9.

[10] T.A. Mitsiadis, A.S. Tucker, C. De Bari, M.T. Cobourne, D.P.C. Rice, A regulatory relationship between Tbx1 and FGF signaling during tooth morphogenesis and ameloblast lineage determination, Dev. Biol. 320 (2008) 39–48.

[11] J. Catón, H.-U. Luder, M. Zoupa, M. Bradman, G. Bluteau, A.S. Tucker, O. Klein, T.A. Mitsiadis, Enamel-free teeth: Tbx1 deletion affects amelogenesis in rodent incisors, Dev. Biol. 328 (2009) 493–505.

[12] Y.L. Fang, X.G. Chen, G. WT, Gene delivery in tissue engineering and regenerative medicine, J. Biomed. Mater. Res. Part B Appl. Biomater. 103 (2015) 1679–1699.

[13] H. Yin, R.L. Kanasty, A.A. Eltoukhy, A.J. Vegas, J.R. Dorkin, D.G. Anderson, Non-viral vectors for gene-based therapy, Nat. Rev. Genet. 15 (2014) 541–555.

[14] D. Zhi, Y. Bai, J. Yang, S. Cui, Y. Zhao, H. Chen, S. Zhang, A review on cationic lipids with different linkers for gene delivery, Adv. Colloid Interface Sci. (2017).

[15] D.A. Balazs, W.T. Godbey, Liposomes for use in gene delivery, J. Drug Deliv. 2011 (2011).

[16] C.-H. Su, Y.-J. Wu, H.-H. Wang, H.-I. Yeh, Nonviral gene therapy targeting

cardiovascular system, Am. J. Physiol. Circ. Physiol. 303 (2012) H629–H638.

[17] A. Makhlouf, I. Hajdu, I. Badea, Gemini surfactant-based systems for drug and gene delivery, in: Org. Mater. as Smart Nanocarriers Drug Deliv., Elsevier, 2018: pp. 561–600.

[18] S.D. Wettig, R.E. Verrall, M. Foldvari, Gemini surfactants: a new family of building blocks for non-viral gene delivery systems, Curr. Gene Ther. 8 (2008) 9–23.

[19] S. Ghosh, T. Chakraborty, Mixed micelle formation among anionic gemini surfactant (212) and its monomer (SDMA) with conventional surfactants (C12E5 and C12E8) in brine solution at pH 11, J. Phys. Chem. B. 111 (2007) 8080–8088.

[20] M.A. Al-Dulaymi, J.M. Chitanda, W. Mohammed-Saeid, H.Y. Araghi, R.E. Verrall, P. Grochulski, I. Badea, Di-peptide-modified Gemini surfactants as gene delivery vectors: Exploring the role of the alkyl tail in their physicochemical behavior and biological activity, AAPS J. 18 (2016) 1168–1181.

[21] S. Xiao, T. Zhao, J. Wang, C. Wang, J. Du, L. Ying, J. Lin, C. Zhang, W. Hu, L. Wang, Gelatin methacrylate (GelMA)-based hydrogels for cell transplantation: an effective strategy for tissue engineering, Stem Cell Rev. Reports. 15 (2019) 664–679.

[22] M. Foldvari, I. Badea, S. Wettig, R. Verrall, M. Bagonluri, Structural characterization of novel gemini non-viral DNA delivery systems for cutaneous gene therapy, J. Exp. Nanosci. 1 (2006) 165–176.

[23] S. Kawano, T. Morotomi, T. Toyono, N. Nakamura, T. Uchida, M. Ohishi, K. Toyoshima, H. Harada, Establishment of Dental Epithelial Cell Line (HAT-7) and the Cell Differentiation Dependent on Notch Signaling Pathway, Connect. Tissue Res. 43 (2002) 409–412. https://doi.org/10.1080/03008200290000637.

[24] L. Zheng, Y.J. Seon, M.A. Mourão, S. Schnell, D. Kim, H. Harada, S. Papagerakis, P. Papagerakis, Circadian rhythms regulate amelogenesis, Bone. 55 (2013) 158–165.

[25] L. Zheng, V. Zinn, A. Lefkelidou, N. Taqi, X. Chatzistavrou, T. Balam, J. Nervina, S. Papagerakis, P. Papagerakis, Orai1 expression pattern in tooth and craniofacial ectodermal tissues and potential functions during ameloblast differentiation, Dev. Dyn. 244 (2015) 1249–1258.

[26] Y. Wang, S. Papagerakis, D. Faulk, S.F. Badylak, Y. Zhao, L. Ge, M. Qin, P. Papagerakis, Extracellular matrix membrane induces cementoblastic/osteogenic properties of human periodontal ligament stem cells, Front. Physiol. 9 (2018) 942.

[27] M.C.P. de Lima, S. Simoes, P. Pires, H. Faneca, N. Düzgüneş, Cationic lipid–DNA complexes in gene delivery: from biophysics to biological applications, Adv. Drug Deliv. Rev. 47 (2001) 277–294.

[28] S. Simões, A. Filipe, H. Faneca, M. Mano, N. Penacho, N. Düzgünes, M. Pedroso de Lima, Cationic liposomes for gene delivery, Expert Opin. Drug Deliv. 2 (2005) 237–254.

[29] H. Song, G. Wang, B. He, L. Li, C. Li, Y. Lai, X. Xu, Z. Gu, Cationic lipid-coated PEI/DNA polyplexes with improved efficiency and reduced cytotoxicity for gene delivery into mesenchymal stem cells, Int. J. Nanomedicine. 7 (2012) 4637.

[30] J. Buck, P. Grossen, P.R. Cullis, J. Huwyler, D. Witzigmann, Lipid-based DNA therapeutics: hallmarks of non-viral gene delivery, ACS Nano. 13 (2019) 3754–3782.

[31] R. Kaur, Lysine-functionalized nanodiamonds: synthesis, characterization and potential as gene delivery agents, (2012).

[32] H. Elsana, T.O.B. Olusanya, J. Carr-Wilkinson, S. Darby, A. Faheem, A.A. Elkordy, Evaluation of novel cationic gene based liposomes with cyclodextrin prepared by thin film hydration and microfluidic systems, Sci. Rep. 9 (2019) 1–17.

[33] M.J. Limeres, M. Suñé-Pou, S. Prieto-Sánchez, C. Moreno-Castro, A.D. Nusblat, C. Hernández-Munain, G.R. Castro, C. Suñé, J.M. Suñé-Negre, M.L. Cuestas, Development and characterization of an improved formulation of cholesteryl oleate-loaded cationic solid-lipid nanoparticles as an efficient non-viral gene delivery system, Colloids Surfaces B Biointerfaces. 184 (2019) 110533.

[34] B.B.M. Garcia, O. Mertins, E.R. da Silva, P.D. Mathews, S.W. Han, Arginine-Modified Chitosan Complexed with Liposome Systems for plasmid DNA delivery, Colloids Surfaces B Biointerfaces. (2020) 111131.

[35] E. Ojeda, G. Puras, M. Agirre, J. Zarate, S. Grijalvo, R. Eritja, G. Martinez-Navarrete, C. Soto-Sánchez, A. Díaz-Tahoces, M. Aviles-Trigueros, The influence of the polar head-group of synthetic cationic lipids on the transfection efficiency mediated by niosomes in rat retina and brain, Biomaterials. 77 (2016) 267–279.

[36] B. dos Santos Rodrigues, A. Banerjee, T. Kanekiyo, J. Singh, Functionalized liposomal nanoparticles for efficient gene delivery system to neuronal cell transfection, Int. J. Pharm. 566 (2019) 717–730.

[37] Y. Kumar, K. Kuche, R. Swami, S.S. Katiyar, D. Chaudhari, P.B. Katare, S.K. Banerjee, S. Jain, Exploring the potential of novel pH sensitive lipoplexes for tumor targeted gene delivery with reduced toxicity, Int. J. Pharm. 573 (2020) 118889.

[38] P. Li, D. Liu, X. Sun, C. Liu, Y. Liu, N. Zhang, A novel cationic liposome formulation for efficient gene delivery via a pulmonary route, Nanotechnology. 22 (2011) 245104.

[39] P. Foroozandeh, A.A. Aziz, Insight into cellular uptake and intracellular trafficking of nanoparticles, Nanoscale Res. Lett. 13 (2018) 339.

[40] U.S. Huth, R. Schubert, R. Peschka-Süss, Investigating the uptake and intracellular fate of pH-sensitive liposomes by flow cytometry and spectral bio-imaging, J. Control. Release. 110 (2006) 490–504.

[41] A.A. Belanova, N. Gavalas, Y.M. Makarenko, M.M. Belousova, A. V Soldatov, P. V Zolotukhin, Physicochemical properties of magnetic nanoparticles: implications for biomedical applications in vitro and in vivo, Oncol. Res. Treat. 41 (2018) 139–143.

[42] S. Behzadi, V. Serpooshan, W. Tao, M.A. Hamaly, M.Y. Alkawareek, E.C. Dreaden, D. Brown, A.M. Alkilany, O.C. Farokhzad, M. Mahmoudi, Cellular uptake of nanoparticles: journey inside the cell, Chem. Soc. Rev. 46 (2017) 4218–4244.

[43] R. Agarwal, K. Roy, Intracellular delivery of polymeric nanocarriers: a matter of size, shape, charge, elasticity and surface composition, Ther. Deliv. 4 (2013) 705–723.

[44] R. Imani, F. Mohabatpour, F. Mostafavi, Graphene-based Nano-Carrier modifications for gene delivery applications, Carbon N. Y. (2018).

[45] Y. Li, J. Wang, Y. Gao, J. Zhu, M.G. Wientjes, J.L.-S. Au, Relationships between

liposome properties, cell membrane binding, intracellular processing, and intracellular bioavailability, AAPS J. 13 (2011) 585–597.

[46] Y. Li, L. Gao, X. Tan, F. Li, M. Zhao, S. Peng, Lipid rafts-mediated endocytosis and physiology-based cell membrane traffic models of doxorubicin liposomes, Biochim. Biophys. Acta (BBA)-Biomembranes. 1858 (2016) 1801–1811.

[47] C. Pichon, L. Billiet, P. Midoux, Chemical vectors for gene delivery: uptake and intracellular trafficking, Curr. Opin. Biotechnol. 21 (2010) 640–645.

[48] J. Singh, D. Michel, J.M. Chitanda, R.E. Verrall, I. Badea, Evaluation of cellular uptake and intracellular trafficking as determining factors of gene expression for amino acid-substituted gemini surfactant-based DNA nanoparticles, J. Nanobiotechnology. 10 (2012) 7.

[49] Y.-N. Zhao, F. Qureshi, S.-B. Zhang, S.-H. Cui, B. Wang, H.-Y. Chen, H.-T. Lv, S.-F. Zhang, L. Huang, Novel gemini cationic lipids with carbamate groups for gene delivery, J. Mater. Chem. B. 2 (2014) 2920–2928.

[50] M. Ramezani, M. Khoshhamdam, A. Dehshahri, B. Malaekeh-Nikouei, The influence of size, lipid composition and bilayer fluidity of cationic liposomes on the transfection efficiency of nanolipoplexes, Colloids Surfaces B Biointerfaces. 72 (2009) 1–5.

[51] M. Al-Dulaymi, D. Michel, J.M. Chitanda, A. El-Aneed, R.E. Verrall, P. Grochulski, I. Badea, Molecular engineering as an approach to modulate gene delivery efficiency of peptide-modified gemini surfactants, Bioconjug. Chem. 29 (2018) 3293–3308.

[52] S.-J. Park, H.-K. Lee, Y.-M. Seo, C. Son, H.S. Bae, J.-C. Park, Dentin sialophosphoprotein expression in enamel is regulated by Copine-7, a preameloblast-derived factor, Arch. Oral Biol. 86 (2018) 131–137.

[53] J.C.-C. Hu, Y. Yamakoshi, F. Yamakoshi, P.H. Krebsbach, J.P. Simmer, Proteomics and genetics of dental enamel, Cells Tissues Organs. 181 (2005) 219–231.

[54] J.D. Bartlett, Dental enamel development: proteinases and their enamel matrix substrates, ISRN Dent. 2013 (2013).

[55] A. Gupta, Dental Biochemistry, in: Compr. Biochem. Dent., Springer, 2019: pp. 595–604.

[56] J.-M. Retrouvey, M. Goldberg, S. Schwartz, Dental development and maturation, from the dental crypt to the final occlusion, in: Pediatr. Bone, Elsevier, 2012: pp. 83–108.

[57] Q. Ruan, J. Moradian-Oldak, Amelogenin and enamel biomimetics, J. Mater. Chem. B. 3 (2015) 3112–3129.

[58] S. Fukumoto, T. Kiba, B. Hall, N. Iehara, T. Nakamura, G. Longenecker, P.H. Krebsbach, A. Nanci, A.B. Kulkarni, Y. Yamada, Ameloblastin is a cell adhesion molecule required for maintaining the differentiation state of ameloblasts, J Cell Biol. 167 (2004) 973–983.

[59] P. Mazumder, S. Prajapati, S.B. Lokappa, V. Gallon, J. Moradian-Oldak, Analysis of co-assembly and co-localization of ameloblastin and amelogenin, Front. Physiol. 5 (2014) 274.

[60] B. Jayasudha, H.K. Navin, K.B. Prasanna, Enamel regeneration-current progress and challenges, J. Clin. Diagnostic Res. JCDR. 8 (2014) ZE06.

[61] Y. Gao, W. Wang, Y. Sun, J. Zhang, D. Li, Y. Wei, T. Han, Distribution of amelotin in mouse tooth development, Anat. Rec. Adv. Integr. Anat. Evol. Biol. 293 (2010) 135–140.

[62] B. Ganss, N. Abbarin, Maturation and beyond: proteins in the developmental continuum from enamel epithelium to junctional epithelium, Front. Physiol. 5 (2014) 371.

[63] N. Abbarin, S. San Miguel, J. Holcroft, K. Iwasaki, B. Ganss, The enamel protein amelotin is a promoter of hydroxyapatite mineralization, J. Bone Miner. Res. 30 (2015) 775–785.

[64] R.S. Lacruz, Y. Nakayama, J. Holcroft, V. Nguyen, E. Somogyi-Ganss, M.L. Snead, S.N. White, M.L. Paine, B. Ganss, Targeted overexpression of amelotin disrupts the microstructure of dental enamel, PLoS One. 7 (2012) e35200.

[65] Y. Yamakoshi, A.S. Richardson, S.M. Nunez, F. Yamakoshi, R.N. Milkovich, J.C. Hu, J.D. Bartlett, J.P. Simmer, Enamel proteins and proteases in Mmp20 and Klk4 null and double-null mice, Eur. J. Oral Sci. 119 (2011) 206–216.

[66] Y. Lu, P. Papagerakis, Y. Yamakoshi, J.C.-C. Hu, J.D. Bartlett, J.P. Simmer, Functions of KLK4 and MMP-20 in dental enamel formation, Biol. Chem. 389 (2008) 695–700.

[67] Y. Furukawa, N. Haruyama, M. Nikaido, M. Nakanishi, N. Ryu, M. Oh-Hora, K. Kuremoto, K. Yoshizaki, Y. Takano, I. Takahashi, Stim1 regulates enamel mineralization and ameloblast modulation, J. Dent. Res. 96 (2017) 1422–1429.

[68] I. Derler, C. Butorac, A. Krizova, M. Stadlbauer, M. Muik, M. Fahrner, I. Frischauf, C. Romanin, Authentic CRAC channel activity requires STIM1 and the conserved portion of the Orai N terminus, J. Biol. Chem. 293 (2018) 1259–1270.

[69] J. Lian, M. Cuk, S. Kahlfuss, L. Kozhaya, M. Vaeth, F. Rieux-Laucat, C. Picard, M.J. Benson, A. Jakovcevic, K. Bilic, ORAI1 mutations abolishing store-operated Ca2+ entry cause anhidrotic ectodermal dysplasia with immunodeficiency, J. Allergy Clin. Immunol. 142 (2018) 1297–1310.

[70] M.K. Nurbaeva, M. Eckstein, A. Devotta, J.-P. Saint-Jeannet, D.I. Yule, M.J. Hubbard, R.S. Lacruz, Evidence that calcium entry into calcium-transporting dental enamel cells is regulated by cholecystokinin, acetylcholine and ATP, Front. Physiol. 9 (2018) 801.

[71] M. Eckstein, R.S. Lacruz, CRAC channels in dental enamel cells, Cell Calcium. 75 (2018) 14–20.

[72] F.J. Martin-Romero, C. Pascual-Caro, A. Lopez-Guerrero, N. Espinosa-Bermejo, E. Pozo-Guisado, Regulation of calcium signaling by STIM1 and ORAI1, Calcium Signal Transduct. (2018) 1.

[73] M.K. Nurbaeva, M. Eckstein, A.R. Concepcion, C.E. Smith, S. Srikanth, M.L. Paine, Y. Gwack, M.J. Hubbard, S. Feske, R.S. Lacruz, Dental enamel cells express functional SOCE channels, Sci. Rep. 5 (2015) 15803.

[74] A. Krizova, L. Maltan, I. Derler, Critical parameters maintaining authentic CRAC channel hallmarks, Eur. Biophys. J. (2019) 1–21.

[75] J. Soboloff, B.S. Rothberg, M. Madesh, D.L. Gill, STIM proteins: dynamic calcium signal transducers, Nat. Rev. Mol. Cell Biol. 13 (2012) 549–565.

[76] X. Liu, Y. Wang, L. Zhang, Z. Xu, Q. Chu, C. Xu, Y. Sun, Y. Gao, Combination of

Runx2 and Cbfβ upregulates Amelotin gene expression in ameloblasts by directly interacting with cis-enhancers during amelogenesis, Mol. Med. Rep. 17 (2018) 6068–6076.

[77] K. Yoshizaki, L. Hu, T. Nguyen, K. Sakai, M. Ishikawa, I. Takahashi, S. Fukumoto, P.K. DenBesten, D.D. Bikle, Y. Oda, Mediator 1 contributes to enamel mineralization as a coactivator for Notch1 signaling and stimulates transcription of the alkaline phosphatase gene, J. Biol. Chem. 292 (2017) 13531–13540.

[78] J.H. Woltgens, D.M. Lyaruu, A.L. Bronckers, T.J. Bervoets, M. Van Duin, Biomineralization during early stages of the developing tooth in vitro with special reference to secretory stage of amelogenesis., Int. J. Dev. Biol. 39 (2003) 203–212.

[79] A. Takahashi, T. Morita, K. Murata, E. Minowa, A. Jahan, M. Saito, A. Tanimura, Effects of full-length human amelogenin on the differentiation of dental epithelial cells and osteoblastic cells, Arch. Oral Biol. 107 (2019) 104479.

[80] T. Kiyoshima, H. Fujiwara, K. Nagata, H. Wada, Y.F. Ookuma, M. Shiotsuka, M. Kihara, K. Hasegawa, H. Someya, H. Sakai, Induction of dental epithelial cell differentiation marker gene expression in non-odontogenic human keratinocytes by transfection with thymosin beta 4, Stem Cell Res. 12 (2014) 309–322.

[81] R.F. Cox, A. Jenkinson, K. Pohl, F.J. O'Brien, M.P. Morgan, Osteomimicry of mammary adenocarcinoma cells in vitro; increased expression of bone matrix proteins and proliferation within a 3D collagen environment, PLoS One. 7 (2012) e41679.

[82] M.D. Yazid, S.H.Z. Ariffin, S. Senafi, M.A. Razak, R.M.A. Wahab, Determination of the differentiation capacities of murines' primary mononucleated cells and MC3T3-E1 cells, Cancer Cell Int. 10 (2010) 1–12.

[83] M.G. Chavez, W. Yu, B. Biehs, H. Harada, M.L. Snead, J.S. Lee, T.A. Desai, O.D. Klein, Characterization of dental epithelial stem cells from the mouse incisor with two-dimensional and three-dimensional platforms, Tissue Eng. Part C Methods. 19 (2013) 15–24.

[84] E. Colaço, D. Brouri, C. Méthivier, L. Valentin, F. Oudet, K. El Kirat, C. Guibert, J. Landoulsi, Calcium phosphate mineralization through homogenous enzymatic catalysis: Investigation of the early stages, J. Colloid Interface Sci. 565 (2020) 43–54.

[85] T.D. Usal, D. Yucel, V. Hasirci, A novel GelMA-pHEMA hydrogel nerve guide for the treatment of peripheral nerve damages, Int. J. Biol. Macromol. 121 (2019) 699–706.

[86] K. Modaresifar, A. Hadjizadeh, H. Niknejad, Design and fabrication of GelMA/chitosan nanoparticles composite hydrogel for angiogenic growth factor delivery, Artif. Cells, Nanomedicine, Biotechnol. 46 (2018) 1799–1808.

[87] K.R. Mamaghani, S.M. Naghib, A. Zahedi, M. Mozafari, Synthesis and microstructural characterization of GelMa/PEGDA hybrid hydrogel containing graphene oxide for biomedical purposes, Mater. Today Proc. 5 (2018) 15635–15644.

[88] S. Pahoff, C. Meinert, O. Bas, L. Nguyen, T.J. Klein, D.W. Hutmacher, Effect of gelatin source and photoinitiator type on chondrocyte redifferentiation in gelatin methacryloyl-based tissue-engineered cartilage constructs, J. Mater. Chem. B. 7 (2019) 1761–1772.

[89] M. Vigata, C. Meinert, S. Pahoff, N. Bock, D.W. Hutmacher, Gelatin Methacryloyl

Hydrogels Control the Localized Delivery of Albumin-Bound Paclitaxel, Polymers (Basel). 12 (2020) 501.

[90] S. Ravindran, Y. Song, A. George, Development of three-dimensional biomimetic scaffold to study epithelial–mesenchymal interactions, Tissue Eng. Part A. 16 (2010) 327–342.

[91] M. Iijima, K. Hayashi, Y. Moriwaki, Effects of the Ca2+ and PO43− ion flow on the lengthwise growth of octacalcium phosphate in a model system of enamel crystal formation with controlled ionic diffusion, J. Cryst. Growth. 234 (2002) 539–544.

[92] J. Zhao, Y. Liu, W. Sun, H. Zhang, Amorphous calcium phosphate and its application in dentistry, Chem. Cent. J. 5 (2011) 1–7.

[93] F. Meyer, B.T. Amaechi, H.-O. Fabritius, J. Enax, Overview of calcium phosphates used in biomimetic oral care, Open Dent. J. 12 (2018) 406.

[94] M. Iafisco, L. Degli Esposti, G.B. Ramírez-Rodríguez, F. Carella, J. Gómez-Morales, A.C. Ionescu, E. Brambilla, A. Tampieri, J.M. Delgado-López, Fluoride-doped amorphous calcium phosphate nanoparticles as a promising biomimetic material for dental remineralization, Sci. Rep. 8 (2018) 1–9.

[95] M. Iijima, J. Moradian-Oldak, Control of apatite crystal growth in a fluoride containing amelogenin-rich matrix, Biomaterials. 26 (2005) 1595–1603.

[96] M. Iijima, D. Fan, K.M. Bromley, Z. Sun, J. Moradian-Oldak, Tooth enamel proteins enamelin and amelogenin cooperate to regulate the growth morphology of octacalcium phosphate crystals, Cryst. Growth Des. 10 (2010) 4815–4822.

[97] Y. Cao, M.L. Mei, Q.-L. Li, E.C.M. Lo, C.H. Chu, Agarose hydrogel biomimetic mineralization model for the regeneration of enamel prismlike tissue, ACS Appl. Mater. Interfaces. 6 (2013) 410–420.

[98] J. Zhan, Y. Tseng, J.C.C. Chan, C. Mou, Biomimetic formation of hydroxyapatite nanorods by a single-crystal-to-single-crystal transformation, Adv. Funct. Mater. 15 (2005) 2005–2010.

Chapter 4. Bioprinting of alginate- carboxymethyl chitosan scaffolds for enamel tissue engineering *in vitro*

Fatemeh Mohabatpour[1,2], Xiaoman Duan[1], Zahra Yazdanpanah[1], Ning Zhu[1,3], Silvana Papagerakis[1,4*], Xiongbiao Chen[1,5*], Petros Papagerakis[1, 2*]

[1]Division of Biomedical Engineering, University of Saskatchewan, 57 Campus Dr., S7N 5A9, SK, Canada

[2]College of Dentistry, University of Saskatchewan, 105 Wiggins Rd, Saskatoon, S7N 5E4, SK, Canada

[3]Canadian Light Source, University of Saskatchewan, 44 Innovation Blvd, Saskatoon, S7N2V3, SK, Canada

[4]Department of Surgery, College of Medicine, University of Saskatchewan, 107 Wiggins Rd, S7N 0W8, SK, Canada

[5]Department of Mechanical Engineering, University of Saskatchewan, Saskatoon, 57 Campus Dr., S7N 5A9, SK, Canada

[*]Corresponding authors:

Petros Papagerakis, petros.papagerakis@usask.ca

Xiongbiao Chen, xbc719@usask.ca

Silvana Papagerakis, silvana.papagerakis@usask.ca

Keywords: Bioprinting, bioink, enamel tissue engineering, regenerative dentistry, dental stem cells

4.1. Abstract

Tissue engineering offers a great potential in regenerative dentistry and to this end, three dimensional (3D) bioprinting has been emerging nowadays to enable the incorporation of living cells into the biomaterials (such a mixture is referred as a bioink in the literature) to create scaffolds. However, the bioinks available for scaffold bioprinting are limited, particularly for tooth tissue engineering, due to the complicated, yet compromised, printability, mechanical and biological properties simultaneously imposed on the bioinks. This paper presents our study on the development of a novel bioink from carboxymethyl chitosan and alginate for bioprinting scaffolds for enamel tissue regeneration. Carboxymethyl chitosan was used due to its antibacterial ability and superior cell interaction properties, while alginate was added to enhance the printability and mechanical properties as well as to reg2ulate the degradation rate. The bioinks with three mixture ratios of alginate and carboxymethyl chitosan (2-4, 3-3 and 4-2) were prepared, and then printed into the calcium chloride crosslinker solution (100 mM) to form a 3D structure of scaffolds. The printed scaffolds were characterized in terms of structural, swelling, degradation, and mechanical properties, followed by their in vitro characterization for enamel tissue regeneration. The results showed that the bioinks with higher concentrations of alginate were more viscous and needed higher pressure for printing; while the printed scaffolds were highly porous and showed a high degree of printability and structural integrity. The hydrogels with higher carboxymethyl chitosan ratios had higher swelling ratios, faster degradation rates, and lower compressive modulus. Dental epithelial stem cell line, HAT-7, could maintain high viability in the printed constructs after 1, 7 and 14 days of culture. HAT-7 cells were also able to maintain their round morphology and secrete alkaline phosphatase after 14 days of culture in the 3D printed scaffolds, suggesting the capacity of these cells for mineral deposition and enamel-like tissue formation. Taken together, alginate-carboxymethyl chitosan has been illustrated suitable to print scaffolds with dental stem cells for enamel tissue regeneration.

4.2. Introduction

Tooth decay or dental caries is one of the most common infectious diseases that can cause the breakdown of dental enamel [1]. The current approach to treat tooth decay includes removing the parts of the tooth affected by dental caries and replacing them with the artificial dental restoration

materials. However, given the limitations associated with dental restoration materials such as inability to mimic the structural and functional characteristics of the native dental tissue, a great deal of attention has been attracted towards developing novel alternative approaches to treat dental caries [1]. Bio-fillings that can be produced by dental stem cells could offer an ideal solution to biologically regenerate/restore the affected dental tissues [1]. Tooth tissue engineering is a new promising technique that employs three main elements of dental stem cells, scaffolds and signaling factors to produce the bioengineered dental tissues to repair the damaged teeth [2]. Among different scaffold fabrication methods, three-dimensional (3D) printing has a great potential to fabricate customized scaffolds, based on the magnetic resonance imaging or computerized tomography scans taken from the patient [3], and offers the incorporation of living cells and growth factors in the printed scaffolds [4–7]. During the process of scaffold fabrication using extrusion-based 3D printing, cells are incorporated into a biomaterial called bioinks, that are usually hydrogels, and then the cell-laden bioink is dispensed in a layer by layer fashion to fabricate constructs with the desired design [8]. Development of suitable bioinks that possess printability, and mechanical and biological properties that support cell functions such as cell attachment, proliferation and migration and the formation of new tissue is a key element to fabricate 3D printed constructs to provide a suitable microenvironment for successful applications in tissue engineering [9,10]. Bioinks also need to become crosslinked quickly, before or after printing, to retain their shape fidelity and have decent mechanical properties and degradation rate [10–12]. Various hydrogels based on biomaterials of natural (e.g. alginate, agarose, hyaluronic acid, chitosan, dextran, collagen, gelatin and fibrin) and synthetic (e.g. polyethylene glycol (PEG), PEG diacrylate (PEGDA)) origins have been used in dental tissue engineering applications [13]. However, there is a remarkable lack of hydrogel bioinks that have been primarily developed for bioprinting dental cells [14]. Thus, this study aimed to address this emerging need for bioinks for dental tissue engineering.

Chitosan is a cationic polysaccharide extracted from chitin that exhibits remarkable inherent properties such as antimicrobial and mucoadhesive characteristics and biocompatibility that make it a suitable biomaterials for various biomedical applications [15]. In particular, the antimicrobial properties of chitosan offer promises for dental applications [15,16]. In addition, the presence of positively charged amino groups in chitosan enables this polymer to interact with cell membrane

and also bind to growth factors, glycosaminoglycans and DNA [17–20]. Thus, chitosan has been reported to improve cell adhesion, proliferation, and differentiation and offers promises for biopriting and tissue engineering applications [21–23]. However, the application of chitosan hydrogels as bioinks for 3D printing applications is still under investigation [10]. Chitosan is soluble only in acidic solution that limits its application for bioprinting due to the incompatibility of cells with acidic environment [24,25]. Carboxymethyl chitosan (CMC) is a water-soluble derivative of chitosan that can be used as a bioink for cell printing. Nevertheless, CMC itself is not considered a good candidate for bioink owing to its extremely high degradation rate [25]. In addition, CMC possess poor mechanical properties, which makes the fabrication of scaffold structures challenging [26]. Several studies have attempted to develop CMC-based bioinks by blending CMC with other polymers [25]. Alginate (Alg) is a non-toxic and non-immunogenic natural polymer [27] that has been used in various biomedical applications including peptide or protein delivery [28–30], wound dressing [31] and cell encapsulation [32–34]. Alginate has been widely used in bioprinting [35–39] due to its fast gelation through ionic crosslinking in the presence of divalent ions [40]. However, alginate has shown slow degradation kinetics and limited cell interaction properties [27]. To address the limitations of alginate and carboxymethyl chitosan as a single component bioinks, we developed a novel two-component bioink composed of these two polymers with improved characteristics including good printability, proper degradation rate, enhanced mechanical properties, increased cell affinity and antibacterial properties [41]. Furthermore, similar to alginate, carboxymethyl chitosan is also able to become crosslinked with calcium ions [42]. While both alginate and carboxymethyl chitosan have been employed as bioinks alone [43,44] or in mixture with other polymers [25,45–54], the suitability of mixture of Alg and CMC as a bioink has not been studied for bioprinting, neither their applications to tooth tissue engineering. Herein, we for the first time investigated the suitability of alginate-carboxymethyl chitosan bioinks for both bioprinting and tooth tissue engineering applications. We examined the effect of the weight ratio of alginate and carboxymethyl chitosan (Alg4%-CMC2%, Alg3%-CMC3%, Alg2%-CMC4%) on structural and mechanical properties of 3D printed scaffolds as well as their swelling ability, degradation rate and biological properties for the encapsulation of a rat dental epithelial stem cell line (HAT-7) and it potential application for enamel regeneration.

4.3. Materials and methods

4.3.1. Preparation of hydrogel solutions

Medium viscosity sodium alginate powder (Cat. no. A2033, Sigma Aldrich, St. Louis, Missouri, US) and carboxymethyl chitosan powder (Cat. no. sc-358091, Santacruz Biotechnology, Dallas, Texas, USA) were dissolved in distilled water and mixed under magnet stirring at room temperature to prepare 2% (w/v) alginate-4% (w/v) carboxymethyl chitosan (Alg2%-CMC4%), 3% (w/v) alginate-3% (w/v) carboxymethyl chitosan (Alg3%-CMC3%) and 4% (w/v) alginate-2% (w/v) carboxymethyl chitosan (Alg4%-CMC2%) solutions.

4.3.2. 3D printing of alginate-carboxymethyl chitosan hydrogel

Scaffolds were designed and sliced using Magics13 Envision TEC (V13, Materialise) software and Bioplotter RP (V3, EnvisionTEC GmbH, Gladbeck, Germany) software. 31 layers of cuboid scaffolds with the latticed structure (10mm$\times$ $10mm \times 5mm$) were fabricated by using a pneumatic 3D Bioplotter (EnvisionTEC GmbH, Gladbeck, Germany) with 1 mm distance between strands and 0°-90° strand orientation. Prior to printing, the wells of 12-well plates were treated with 0.1% (w/v) polyethyleneimine (PEI, M.W. 60,000, Cot. no. J61270, Alfa Aesar, Tewksbury, MA, USA) solution and incubated in the incubator at 37 ℃ for 24 hours. Then, the PEI was removed, and 50 mM calcium chloride ($CaCl_2$, Cat. no. 223506, Sigma Aldrich) solution containing 0.1% (w/v) PEI was added to the wells. Hydrogel solutions were printed at a needle speed of 20 mm/sec and at a certain extrusion pressure (Alg2%-CMC4% for 0.2 bar, Alg3%-CMC3% for 0.4 bar, Alg4%-CMC2% for 0.7 bar) through 27-guage tapered needles with an inner diameter of 200μm in the crosslinker bath. After printing, the cross-linking bath was replaced with the fresh 100 mM $CaCl_2$. After 10 minutes, the calcium chloride solution was removed, and the scaffolds were rinsed with distilled water twice and kept in distilled water for further analysis. Strand size and pore size were measured using image J software (version 2.3.0/1.53f, NIH, Bethesda, Maryland, USA) as the strand dimeter and the space between two adjacent strands. Strand printability and pore printability were also calculated using the following equations [55]:

$$\boldsymbol{Strand\ printability} = \mathbf{1} - \frac{\boldsymbol{Ds} - \boldsymbol{Dexp}}{\boldsymbol{Ds}} \qquad (\mathbf{4.1})$$

$$\textbf{Pore printability } (Pr) = \frac{(\textbf{Pore perimeter})^2}{16 \times \textbf{pore area}} \quad (4.2)$$

4.3.3. Swelling and degradation test

The ability of the 3D printed scaffolds to uptake water was assessed by swelling test. The printed scaffolds (15 layers) were freeze-dried and were weighed to record the initial dry weight (W_{di}). The scaffolds (n=3) were immersed in phosphate buffer saline (PBS) and incubated at 37℃ and 5% CO_2. At different times (Day 1, 7, 14, 21), the samples were taken from PBS and blotted with a kimwipe tissue paper (Kimberly-Clark Professional, Irving, Texas, US) to eliminate the residual PBS and then the swollen weight was recorded (W_s). The scaffolds were freeze-dried and weighed to record the final dry weight (W_{df}). For each time points, the swelling ratio (SR) and remaining weight were calculated using the following equations:

$$\textbf{Swelling ratio } (SR) = \frac{Ws - Wdi}{Wdi} \quad (4.3)$$

$$\textbf{Remaining weight } (\%) = \frac{Wdf}{Wdi} \times 100 \quad (4.4)$$

4.3.4. Mechanical test

The mechanical properties of the 3D printed scaffolds (13 layers, 10mm$\times 10mm \times 2mm$) were assessed by uniaxial unconfined compression test using Biodynamic 5010 (BOSE, Eden Prairie, Minnesota, USA) testing machine under speed rate of 0.01 mm/s after 24 hours incubation in distilled water. The test was performed in a wet state at room temperature in the air without immersing in water during the experiment five times for each group (n=5). Samples were compressed for the maximum displacement of 70% of the scaffolds thickness. The elastic modulus was calculated by measuring the slope of the linear part of the stress-strain curves for each scaffold.

4.3.5. Microstructural evaluation of the 3D printed hydrogel scaffolds

The microstructure of the 3D printed scaffolds was assessed by scanning electron microscopy (SEM). 3D printed scaffolds were freeze-dried and then sputter coated with a chromium film using a sputter coater (Q150T ES, Quorum Technologies, Laughton, East Sussex, UK) and then imaged under a field scanning electron microscope (SU8010, Hitachi, Chiyoda, Tokyo, Japan).

4.3.6. 3D imaging using Synchrotron Radiation-based X-Ray for visualizing 3D printed hydrogel scaffolds

External geometry and porous structure of the interior of the 3D printed scaffolds were visualized by Synchrotron Radiation-based X-Ray imaging technique at the 05B1-1 beamline at the Canadian Light Source (CLS). Hydrogel scaffolds (31 layers, 10 mm×10mm×5 mm) were printed and kept in $CaCl_2$ for four days and then immersed in distilled water in a 15 ml conical centrifuge tube and fixed with Styrofoam. Then, samples were imaged using filtered white beam with a detector placed 0.2 m from the sample using the Optique Peter White Beam microscope (Lentilly, France) with the pixel size of 3.6 μm. 3000 projections were acquired during each CT scan with an exposure time of 20 milliseconds per projection. Strand and pore size were measured using 6 different images for each group of the scaffolds.

4.3.7. Cell culture

HAT-7 cells (kindly provided by Dr. Hidemitsu Harada, Iwate Medical University, Iwate, Japan) [56] were cultured in DMEM/F12 (1:1), HEPES medium (Cat. no. 11330-032, Gibco®, Invitrogen, Carlsbad, California, USA) supplemented with 10% fetal bovine serum (FBS, Cat. no. 12483-020, Gibco®, Invitrogen) and 1% antibiotic (Penicillin-Streptomycin 100X solution, 10,000 units/mL Penicillin/10,1000 μg/mL Streptomycin, Cat. no. SV30010, Hyclone™, Logan, Utah, US) and incubated at 37℃ and 5% CO_2. Medium was changed every 2 days.

4.3.8. Bioprinting of HAT-7 cell-laden hydrogel scaffolds

Alginate and carboxymethyl chitosan powders were sterilized by being exposed to UV light for 90 minutes. Then, hydrogel solutions were prepared by mixing the Alg and CMC powders in saline

solution under sterile condition. 12-well cell culture plates were coated with autoclaved PEI solution (0.1% w/v) in the incubator 24 hours prior to printing. After two passages, cells were trypsinized, counted and mixed in the sterile hydrogel solutions at a final cell density of 6×10^6 cells/ml. The cell incorporated hydrogel solutions were loaded into the bioplotter syringe and 2-3 layers of cell-laden scaffolds were printed into the autoclaved 50 mM $CaCl_2$ crosslinking bath containing 0.1% PEI. After printing, the printing bath was replaced with 100 mM $CaCl_2$ solution to further crosslink scaffolds for another 10 minutes. Then, scaffolds were rinsed with culture medium three times and immersed in culture media containing 10% FBS and 1% antibiotics and cultured in the incubator at 37℃ and 5% CO_2.

4.3.9. Assessment of cell viability using live/dead assay

Viability of HAT-7 cells within the 3D printed scaffolds were evaluated after 1, 7 and 14 days of culture using the LIVE/DEAD Cell imaging kit (Cat. no. R37601, Invitrogen, Thermo Fisher Scientific, USA) according to the manufacturer's instructions. Briefly, cell-laden scaffolds were stained with the mixed green/red dye and incubated for 15 minutes in the incubator at 37℃ and 5% CO_2, followed by imaging using fluorescent microscope (EVOS M5000 Cell Imaging System, Thermo Fisher Scientific). The number of live (green) and dead (red) cells were measured by using image J and viability was calculated by the following equation:

$$\%\textbf{Cell viability} = \frac{(\textbf{number of live cells})}{(\textbf{number of live cells} + \textbf{number of dead cells})} \quad (4.5)$$

4. 3.10. Observation of cell morphologies in 3D printed scaffolds

After 14 days of culture, the morphology of the HAT-7 cells within the 3D printed hydrogel scaffolds was observed using SEM. Cell incorporated scaffolds were washed with PBS twice and immersed in 2.5% glutaraldehyde solution prepared in PBS for 2 hours. The constructs were then rinsed with PBS and distilled water three times each. Afterwards, the scaffolds were lyophilized, and sputter coated with thin layer of chromium and imaged using the same field scanning electron microscope as previously mentioned.

4.3.11. Alkaline phosphatase staining

After 14 days of culture, 3D printed cell-laden constructs were rinsed with PBS twice and cells within the constructs were fixed and permeabilized using BD Cytofix/cytoperm™ fixation/permeabilization kit (Cat. no. 554714, BD Biosciences, San Jose, California, USA). In brief, constructs were incubated in the fixation and permeabilization solution for 30 minutes at $4°C$, followed by washing with 1× BD Perm/Wash™ buffer twice and rinsing with PBS twice. Then, alkaline phosphatase (ALP) expression in the cell-laden constructs was detected using SIGMAFAST™ BCIP®/NBT detection kit (Cat. no. B5655, Sigma-Aldrich). The staining reagent was prepared according to the manufacturer's instructions and added to the constructs and incubated for 24 hours at 37 °C under dark condition. Then, constructs were imaged using a microscope light microscope (EVOS M5000 Cell Imaging System, Thermo Fisher Scientific).

4.3.12. Statistical analysis

All data are given as mean$\pm$standard deviation. Statistical analysis was performed using one-way ANOVA followed by the post-Tukey test using GraphPad Prism 5 (GraphPad Software, San Diego, California, USA). A p value < 0.05 was considered statistically significant.

4.4. Results

4.4.1. 3D printing of alginate-carboxymethyl chitosan

To investigate the influence of alginate and carboxymethyl chitosan concentrations in hydrogel solution on printability, three different compositions including Alg2%-CMC4%, Alg3%-CMC3%, Alg4%-CMC2%, were printed using 200 μm needle at the same needle speed of 20 mm/s (figure 4.1). The total polymer concentration in the hydrogel solutions was kept constant at 6% (w/v). In addition, the crosslinker concentration and crosslinking time was kept at 100 mM and 10 minutes, respectively. It was observed that the Alg2%-CMC4% hydrogel solution required lowest extrusion pressure (0.2) to be dispensed as strands as compared to Alg3%-CMC3% and Alg4%-CMC2% hydrogel solutions that needed 0.4 and 0.7 bar dispensing pressure, respectively. This showed that the concentration of alginate polymer in the Alg-CMC blend hydrogels has a larger impact on the viscosity of the ink and thereby on the extrusion pressure required to dispense ink out of the nozzle.

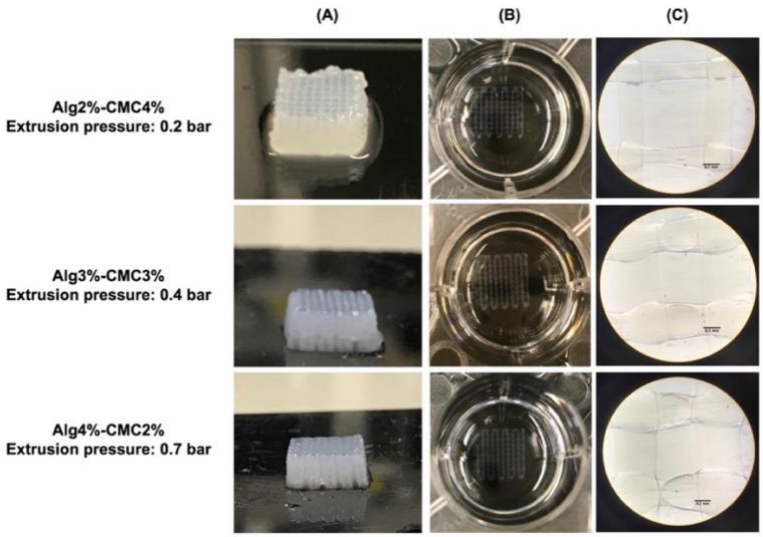

Figure 4.17. (A) Macroscopic view of 31 layers (10mm$\times$ 10$mm \times$ 5mm) of alginate-carboxymethyl chitosan (Alg-CMC) scaffolds. (B, C) Macroscopic and microscopic images of extruded strands printed using different pressure (0.2 bar for Alg2%-CMC4%, 0.4 bar for Alg3%-CMC3%, 0.7 bar for Alg4%-CMC2%) at the same needle speed of 20 mm/s.

The strand size, pore size, strand printability and pore printability of the printed strands were determined after printing two layers (figure 4.2). The strand size was found to be significantly higher ($p<0.001$) in Alg3%-CMC3% (0.570$\pm$0.035mm) and Alg4%-CMC2% (0.588 $\pm$0.029mm) scaffolds as compared to Alg2%-CMC4% (0.340$\pm$0.060 mm). However, no significant difference was observed in the strands size of Alg3%-CMC3% and Alg4%-CMC2% scaffolds. In addition, significantly smaller pore sizes ($p<0.001$) were observed in Alg3%-CMC3% (0.492$\pm$0.037mm) and Alg4%-CMC2% (0.453 $\pm$0.029mm) scaffolds as compared to Alg2%-CMC4% (0.716$\pm$0.054 mm). Although strand printability in all groups was higher than the acceptable range which was previously reported to be around 0.9-1.1 [55], their pore printability was in this range (figure 4.2. C, D).

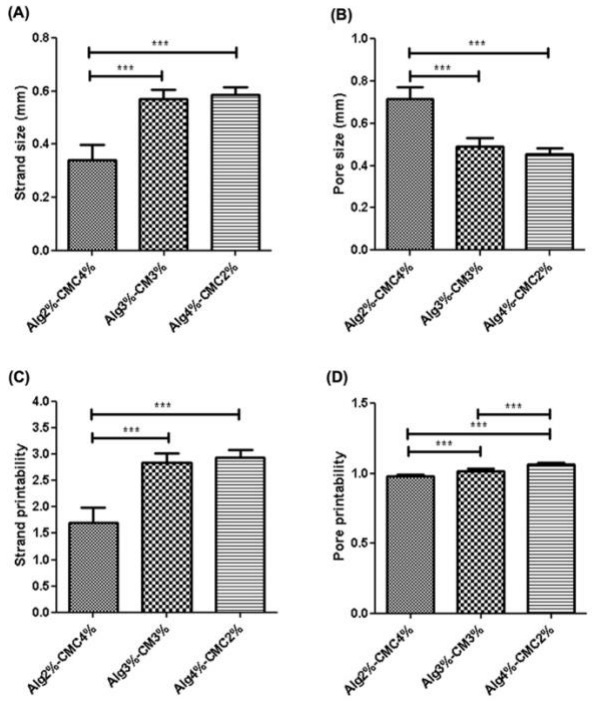

Figure 4.18. Comparative analysis of stand size (A), pore size (B), strand printability (C), pore printability (D) in 3D printed scaffolds with varying concentrations of alginate and carboxymethyl chitosan (Alg2%-CMC4%, Alg3%-CMC3%, Alg4%-CMC2%). Error bars represent mean$\pm SD$ of repeats. *Statistically significant results indicated in the graphs, ***p<0.001.

4.4.2. Microstructural evaluation of the 3D printed hydrogel scaffolds

The microstructure of the 3D printed hydrogels was observed under SEM (figure 4.3) showing that the scaffolds were printed as highly porous structures with well-defined intersections as designed. It was observed that scaffolds with higher ratios of CMC had smaller filament size and were able to maintain the pores with better square shaped morphology and large sizes during printing step.

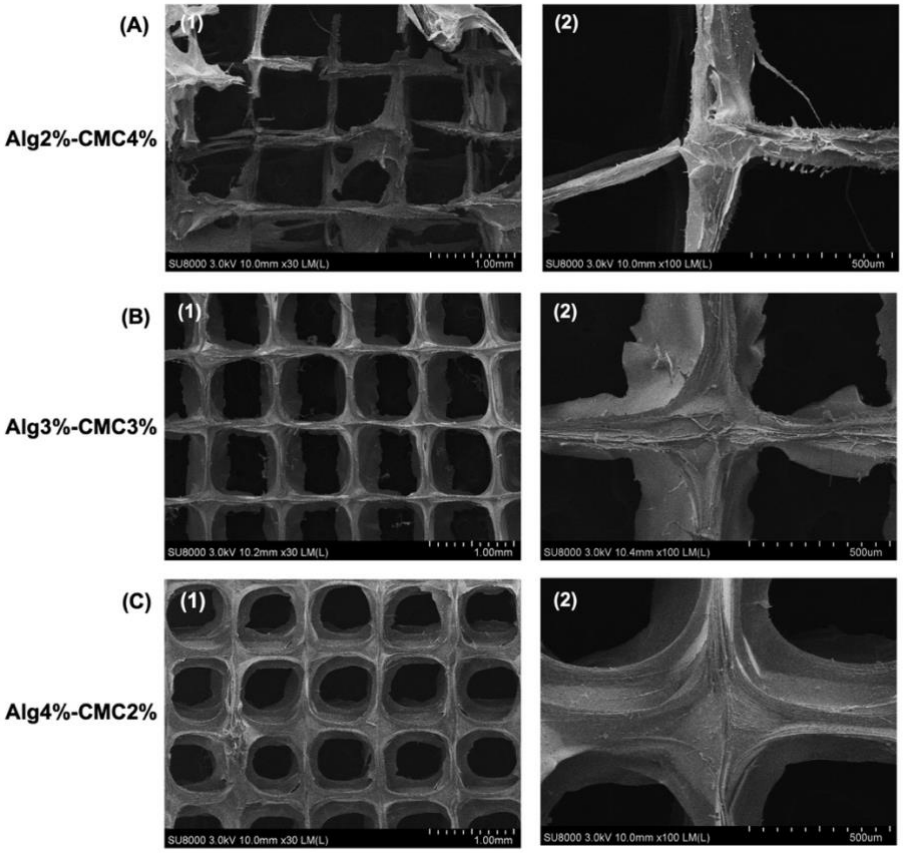

Figure 4.19. The scanning electron microscopy (SEM) of the 3D printed hydrogels at three different alginate-carboxymethyl chitosan weight ratios showed the highly porous structure of the scaffolds.

4.4.3. 3D visualization of the scaffolds using synchrotron-based X-ray imaging

The 3D structure of the 3D printed hydrogels was visualized with synchrotron-based X-ray imaging. As shown in figure 4.4. A. 1, the multilayers of the hydrogel scaffolds were successfully printed with high structural integrity and stability. Figure 4.4. A. 2 revealed the lattice internal structure of the scaffolds. Hydrogel scaffolds with higher percentage of CMC (Alg2%-CMC4% and Alg3%-CMC3%) could maintain the square-shape of pores better than Alg4%-CMC2% hydrogels which is in agreement with the SEM images. Alg4%-CMC2% hydrogels showed a significantly larger strand size compared to Alg2%-CMC4% and Alg3%-CMC3%, which occupy a larger space between strands and resulted in significantly smaller pore size (figure 4.4. B).

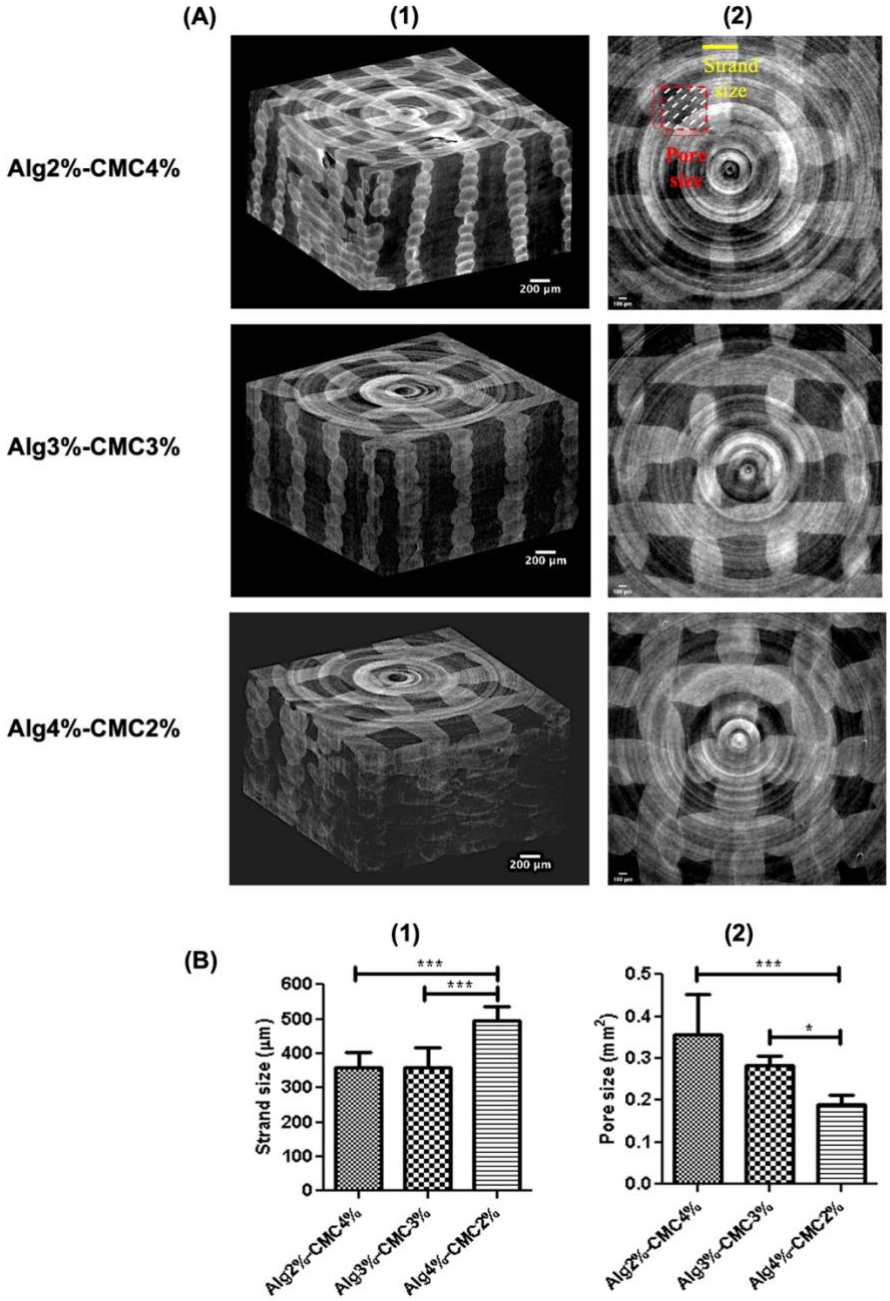

Figure 4.20. (A) 3D visualization of 3D printed hydrogels composed of three different mixture ratios of alginate to carboxymethyl chitosan (Alg-CMC) using synchrotron-based X-ray imaging (1) 3D reconstruction, (2) top view of the scaffolds. (B) Quantified structural properties of the scaffolds including strand and pore size measured form the top view images of the scaffolds using image J.

4.4.4. Swelling and degradation test

The ability of 3D printed hydrogel scaffolds to uptake water was characterized by measuring the swelling ratio at different time points. As shown in figure 4.5. A, the swelling ratio of Alg2%-CMC4% (28.12±1.282) was significantly higher ($p<0.01$) than Alg3%-CMC3% (23.47±1.249) and Alg4%-CMC2% (23.50±0.319) at day 1. At day 7, the swelling ratio of all three groups (Alg2%-CMC4%: 40.25±3.742, Alg3%-CMC3%: 40.96±1.975, Alg4%-CMC2%: 39.94±1.065) was significantly increased compared to that of the same groups at day 1 ($p<0.01$ for Alg2%-CMC4% and $p<0.001$ for Alg3%-CMC3% and Alg4%-CMC2%). However, there was no significant difference between the swelling ratios of all three groups at day 7. At day 14, the swelling ratio of Alg2%-CMC4% (35.69±1.643) was significantly lower than Alg3%-CMC3% (43.16±1.079, $p<0.01$) and Alg4%-CMC2% (39.44±1.520, $p<0.05$). The difference between swelling ratios of Alg3%-CMC3% and Alg4%-CMC2% was also significant ($p<0.05$). At day 21, Alg4%-CMC2% scaffolds showed a significantly higher ($p<0.05$) swelling ratio (43.58±0.713) compared to Alg2%-CMC4% (30.38±6.723). However, no significant difference was observed between swelling ratio of Alg3%-CMC3% (35.49±0.339) and those of two other groups. Both Alg2%-CMC4% and Alg3%-CMC3% reached to their maximum swelling ratio at day 7, however, the swelling ratio of Alg4%-CMC2% was in its highest level at day 21.

In vitro degradation of scaffolds was assessed after 1-, 7-, 14- and 21-days incubation in PBS (figure 4.5. B). At all time-points, the remaining weight in Alg2%-CMC4% was lower compared to Alg3%-CMC3% and Alg4%-CMC2% except at day 1 that no significant difference was observed between Alg2%-CMC4% and Alg3%-CMC3%. The remaining weight of Alg2%-CMC4% scaffolds was significantly ($p<0.01$) decreased from 94.1±2.33 at day 1 to 68.42±4.946 at day 14 and 69.60±8.273 at day 21. No significant difference was observed between remaining weight at day 1 and day 7 (82.55±4.930). Likewise, the remaining weight of Alg3%-CMC3% scaffolds was significantly decreased at day 21 (86.97±4.201) compared to day 1 (101.8±3.149, $p<0.001$), day 7 (94.68±1.723, $p<0.05$) and day 14 (95.23±0.204, $p<0.05$). The weight of Alg4%-CMC2% scaffolds remained unchanged during 21 days of degradation test with no significant difference between their remaining weights recorded at different time points. It can be concluded that the higher concentration of CMC lead to higher degradation rate. Figure 4.5. C shows Alg3%-

CMC3% and Alg4%-CMC2% scaffolds maintained their shape in PBS until day 21; however, Alg2%-CMC4% scaffolds were partially degraded and lost their shape to some extent.

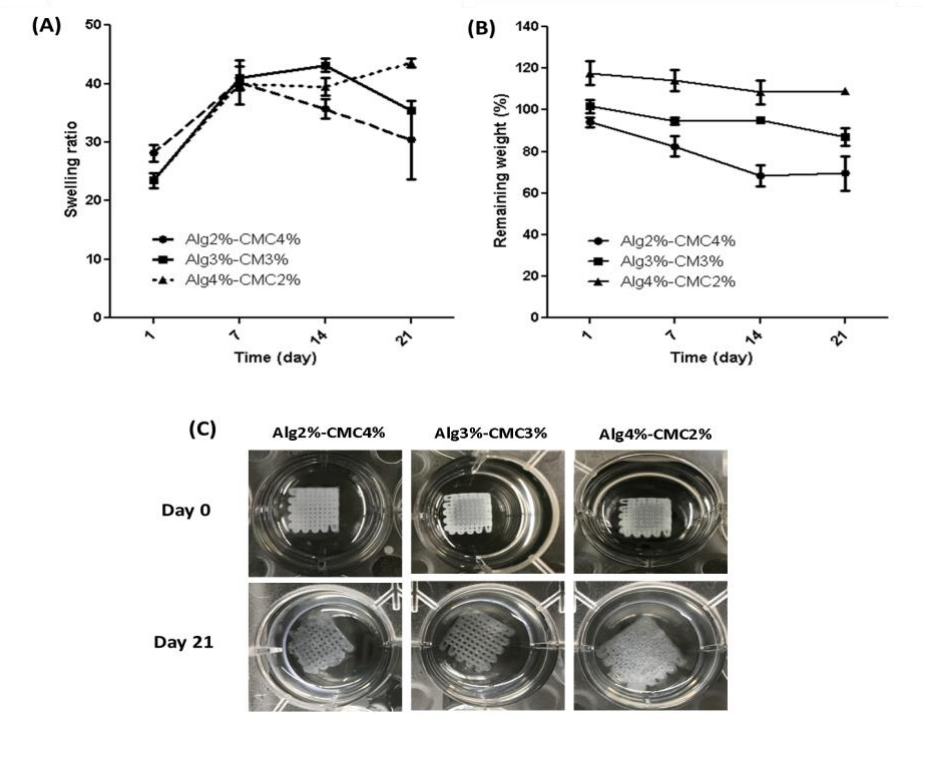

Figure 4.21. (A) swelling ratio, (B) remaining weight of 3D printed scaffolds with varying concentrations of alginate and carboxymethyl chitosan (Alg2%-CMC4%, Alg3%-CMC3%, Alg4%-CMC2%). (C) Images of the 3D printed scaffolds after being crosslinked in $CaCl_2$ solutions for 10 minutes (Day 0) and degraded scaffolds after 21 days incubation in PBS.

4.4.5. Mechanical test

To investigate the effect of alginate and carboxymethyl chitosan concentrations on mechanical performance of the 3D printed scaffolds, uniaxial mechanical test was performed. The stress-strain curves shown in figure 4.6. A indicated that the compressive stress enhanced as the content of the alginate to carboxymethyl chitosan in the ink increased. In addition, the Alg2%-CMC4% scaffolds showed the lowest Young's modulus of 6.320 ± 1.339 kPa (figure 4.6. B). By increasing the concentration of alginate and decreasing the concentration of carboxymethyl chitosan, the Young's modulus of the scaffolds significantly enhanced to 26.02 ± 3.663 kPa for Alg3%-CMC3% and 57.08 ± 6.162 kPa for Alg4%-CMC2%. Thus, it was observed that Alg4%-CMC2% exhibited the

highest elastic modulus among all three groups with 2.2- and 9-fold increase as compared to Alg3%-CMC3% and Alg2%-CMC4%, respectively.

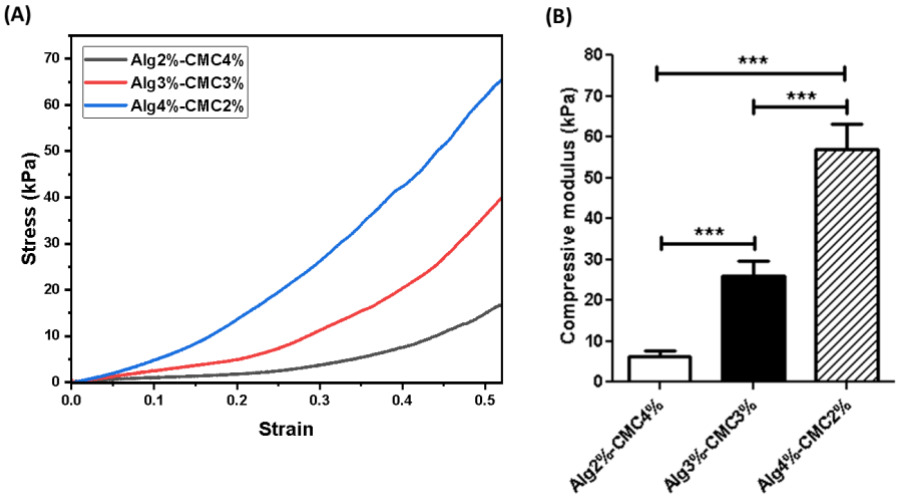

Figure 4.22. Characterization of mechanical properties of 3D printed scaffolds with three different concentrations of alginate and carboxymethyl chitosan (Alg2%-CMC4%, Alg3%-CMC3%, Alg4%-CMC2%). (A) stress-strain curves obtained from uniaxial compression test, (B) compressive modulus calculated from the slope of the linear region of the stress-strain curves showing increase in mechanical properties of the scaffolds with increase in concentration of alginate to chitosan.

4.4.6. Assessment of cell viability using live/dead assay

To investigate the compatibility of cells with hydrogel compositions and printing process, live/dead staining was carried out after 1, 7 and 14 days of in vitro culture. The viability of HAT-7 cells bioprinted in the Alg-CMC hydrogel scaffolds and representative live/dead images are shown in figure 4.7. HAT-7 cells cultured in all three groups of scaffolds revealed a high cell viability (>80%) at all time points. High percentage of cell viability in all groups of bioinks on day 1 suggests the negligible cytotoxic impact of printing process. In addition, viability of cells increased over time which can be due to the proliferation of cells in 3D printed scaffolds.

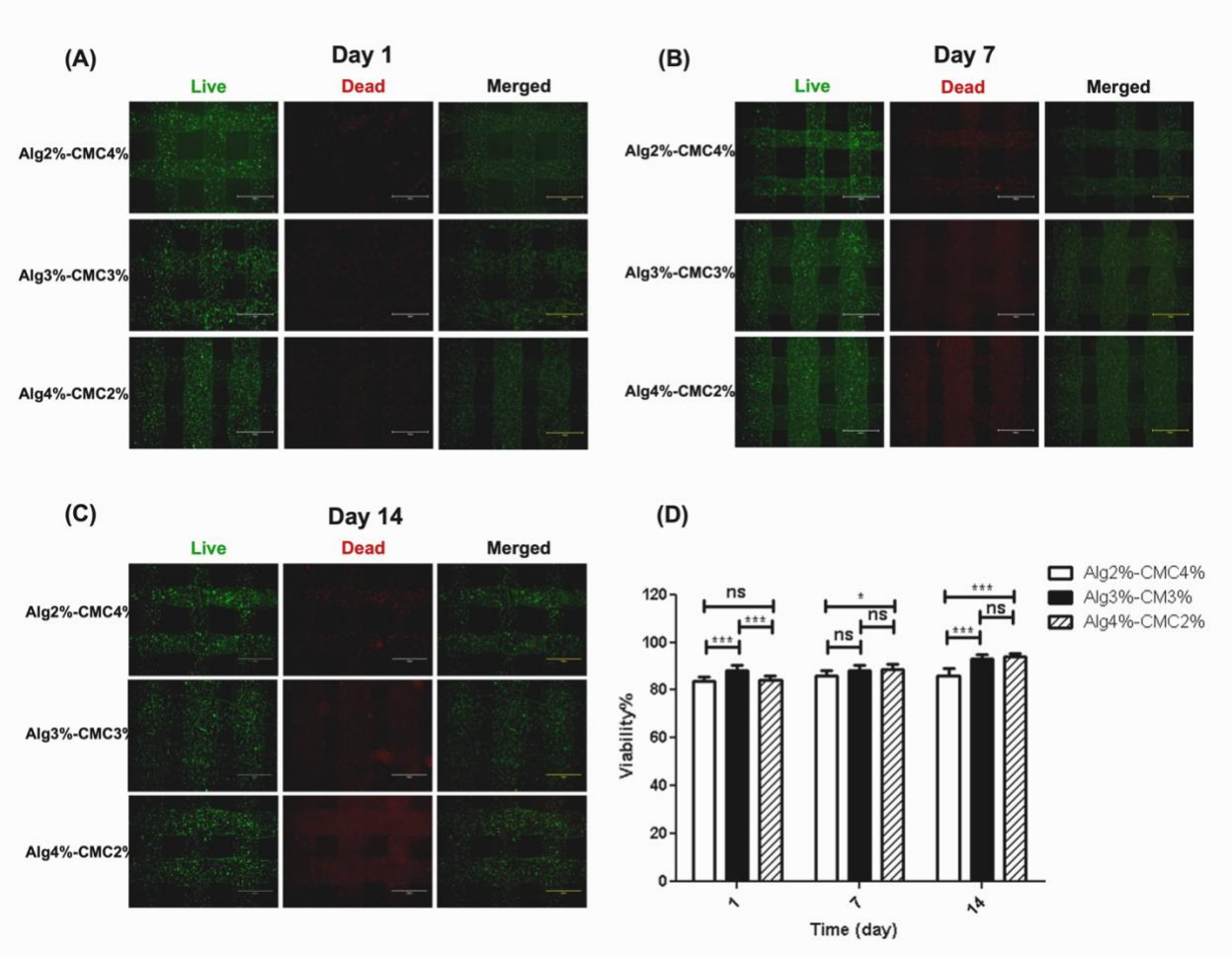

Figure 4.23. Fluorescent images of HAT-7 cells in 3D printed scaffolds with varying concentrations of alginate and carboxymethyl chitosan (Alg2%-CMC4%, Alg3%-CMC3%, Alg4%-CMC2%) after 1 (A), 7 (B) and 14 (C) days of in vitro culture examined by live-dead staining. (D) The quantitative analysis of cell viability in printed constructs at different time points.

4.4.7. ALP staining

To evaluate the capacity of HAT-7 cells for mineralization, ameloblast differentiation and enamel formation when cultured in 3D printed alginate-carboxymethyl chitosan constructs, alkaline phosphatase staining was performed. As shown in figure 4.8, a strong expression of alkaline phosphatase was detected in HAT-7 cell-laden constructs (Alg4%-CMC2%) when cultured for 14 days.

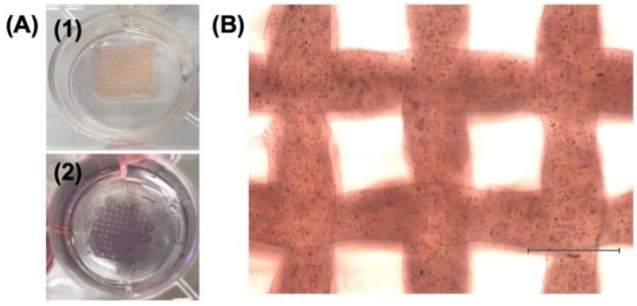

Figure 4.24. Alkaline phosphatase staining of HAT-7 cells in 3D printed alginate4%-carboxymethyl chitosan2% scaffolds after 14 days of culture.

4.4.8. SEM analysis

After 14 days of culture, cell morphology and mineral deposition in 3D printed scaffolds were assessed by SEM. As shown in figure 4.9, HAT-7 cells exhibited their normal round morphology in 3D printed scaffolds at all three different concentrations of alginate and carboxymethyl chitosan. In addition, the amorphous globular structures were observed on the cell surface, indicating the initiation of mineralization and ameloblast differentiation.

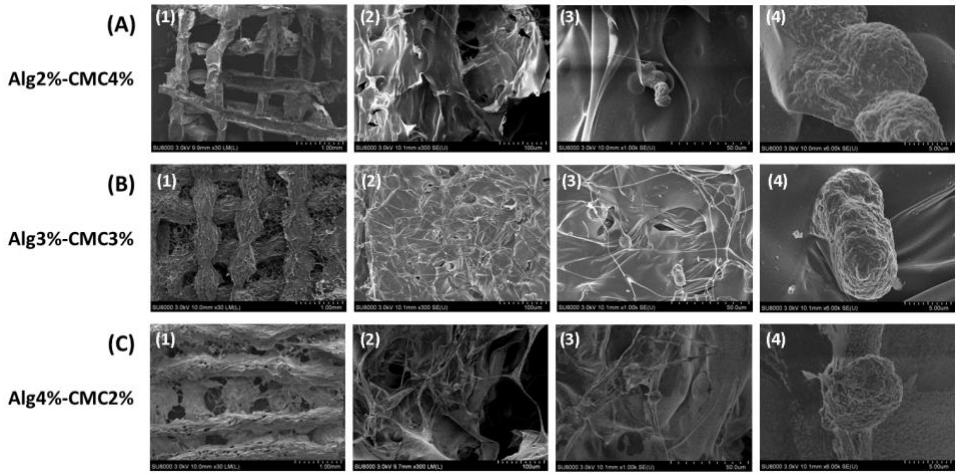

Figure 4.25. Scanning electron microscopy (SEM) images of HAT-7 cells in 3D printed scaffolds with varying concentrations of alginate and carboxymethyl chitosan: (A) Alg2%-CMC4%, (B) Alg3%-CMC3%, and (C) Alg4%-CMC2% after 14 days of in vitro culture.

4.5. Discussions

Loss of dental tissues or the whole tooth caused by factors such as tooth decay, trauma, genetic and periodontal diseases is a major health care issue that could have serious physiological and psychological impacts on those affected [57]. Regeneration of dental tissues with aesthetic and functional properties close to native tissues that can provide a permanent solution for tooth damage or loss is the ultimate goal in regenerative dentistry [1]. Tissue engineering could offer such promising solution to regenerate damaged dental tissues including enamel [1]. Scaffolds are one of the main elements for tissue engineering that need to possess desirable physical (swelling, degradation, mechanical) and biological characteristics to support the new tissue formation [58]. Extrusion based 3D bioprinting has been broadly used to create 3D tissue constructs that allows spatially controlled patterning of biomaterials and cells [59]. One of the essential factors for the successful tissue regeneration is the selection of the scaffold materials. In this study, we used alginate-carboxymethyl chitosan as a hydrogel bioink for 3D extrusion bioprinting to combine the good printability of alginate with antibacterial and biological properties of carboxymethyl chitosan that have been shown to be desirable for dental tissue applications [27,60]. Another benefit of the binary blend of alginate-carboxymethyl chitosan as the bioink is the formation of dual crosslinked hydrogels. In fact, both polymers can form hydrogel via physical crosslinking in the presence of calcium ions. In addition, the amino group of the CMC is able to form ionic bonds with carboxyl group of alginate [47,61]. The interpenetrating polymer network is formed in the dual crosslinked Alg-CMC hydrogels due to the entanglement of two polymer networks leading to the retention of both hydrogel components in the bioink [62]. The mixture ratio of these two components in the bioink was altered to find the suitable concentration in terms of printability, degradation, swelling, mechanical and biological properties. Different mixture ratios of the ink required different amount of pressure to overcome the surface tension of the hydrogel solution owing to their varying viscosities. The hydrogel solutions with higher viscosity was found to provide better extrusion uniformity and allows the printed structures to retain their shape and have higher mechanical stability, which is more favorable for printing tall and complex structures; nevertheless, they can cause increase in shear stress that can negatively influence cell survival and functions [63,64]. On the other hand, hydrogel solutions with low viscosity can cause low printability, non-uniform cell distribution and fast cell settling [64]. Among three different groups of hydrogel solutions, the one

with the lowest concentration of alginate (Alg2%-CMC4%) showed the lowest viscosity and thereby needed lowest extrusion pressure. Alg2%-CMC4% group also showed a better strand printability, smaller strand size and larger pore size. It might be due to the fact that all groups of hydrogel solutions were printed with the same speed. The speed could be adjusted for each solution to prevent extra deposition of the hydrogel and have the strands with the same range of strand diameter, pore size and strand printability. However, all groups of hydrogel solutions showed the acceptable pore printability. As discussed previously, to find the proper printing parameters, both strand and pore printability, and not only one of them, are required to be considered [55]. Another important parameter that needs to be taken into consideration when fabricating complex constructs using 3D printing is the ability to print multiple layers [44]. The alginate-carboxymethyl chitosan hydrogels with all three mixture ratios showed the ability to be printed as multilayered structures with relatively straight strands.

The SEM images of 3D printed scaffolds showed the suitability of the porous constructs for cell functions, exchange of nutrients and oxygen and tissue formation. The microstructural observation of the scaffolds was in agreement with another study showing that the addition of CMC to alginate/gelatin makes constructs with better well-defined pores [47]. In addition, the 3D structure of the full thickness of the scaffolds visualized by synchrotron-based X-ray imaging showed the structural stability and integrity of the alginate-carboxymethyl chitosan scaffolds. Swelling behavior, degradation rate and mechanical properties are the essential physical characteristics of the scaffolds that are important for successful tissue regeneration. Hydrogel solutions with higher concentration of CMC showed the higher swelling ratio, after 1 day incubation in PBS, and a faster degradation rate and lower mechanical properties. Swelling behavior of the hydrogels is a detrimental parameter for the exchange of nutrients and metabolic wastes in the hydrogel matrix [65]. The increased swelling ratio by increasing the amount of CMC in the hydrogel could be attributed to the lower crosslinking density, as a result, the mobility of the polymer chains is less restricted leading to a higher level of water retention [66]. In addition, the presence of amino groups in the constructs with higher concentration of CMC could increase the swelling capacity of the hydrogel [67]. Degradation rate of the scaffolds needs to be long enough to provide supports for cell growth and extracellular matrix secretion and then the hydrogels need to be gradually degraded after tissue formation [47,68]. It was also previously reported that the degradation rate

of the alginate-carboxymethyl gels is contingent upon the swelling ratio in a fashion that gels with higher swelling ratio forms a polymer network that is less compact with ionic crosslinking and have a faster degradation rate [69]. In addition, CMC was found to have an very high degradation rate which can cause faster degradation of the hydrogel scaffolds with higher amount of CMC [25]. Mechanical properties of hydrogels is another important parameter that allows the scaffold to maintain their shape and greatly influences tissue regeneration and cell behaviours such as viability, spreading, proliferation, and differentiation [14,47,70]. Mechanical properties of the hydrogels depend on the crosslinking density, the type of crosslinking mechanism, the nature of the polymer [71]. Additionally, strand diameter and porosity of 3D printed scaffolds affect mechanical properties in a way that scaffolds with thicker strands have lower porosity and higher mechanical properties [4]. The mechanical properties of scaffolds with higher amount of CMC (Alg2%-CMC4%) was significantly lower as compared to two other groups, which can be due to the inherently poor mechanical properties of pure CMC [72], a lower degree of crosslinking, less tight polymeric network, and smaller strand size and higher porosity. In addition to the structural integrity and mechanical stability, 3D bioprinted scaffolds should be able to support printed cells to maintain their normal morphology, viability, and functionality (including cell attachment, proliferation, differentiation, and matrix production) [73,74]. Live/dead assay results showed that all groups of 3D bioprinted scaffolds could support the viability and possibly proliferation of HAT-7 cells with minor cytotoxic effect from printing process. Nature of the polymer, polymer concentration, the type of crosslinker, crosslinking time, crosslinker concentration, cell type and density, shear stress during printing process, which depends on several factors such as needle size and extrusion pressure, were found to have significant impacts on cell survival/damage [4,33,75,76]. In this study, the type and concentration of crosslinker, crosslinking time, cell type and density, needle size were kept constant. Although the bioprinted scaffolds with higher concentration of alginate (Alg3%-CMC3% and Alg4%-CMC2%) needed a higher extrusion pressure to be extruded, they did not show a lower cell viability as compared to Alg2%-CMC4%. Previous studies have reported the use of multi-component bioinks containing alginate and carboxymethyl chitosan for bioprinting of different cell types including human neural stem cells [48], bone marrow mesenchymal stem cells [47,51], and pluripotent stem cells [52], human osteogenic sarcoma cells [49]. Another study showed that Alg-CMC hydrogel scaffolds that were fabricated by Ca^{2+} crosslinking, without being 3D printed, and then seeded with cells could support

cell growth and proliferation for neural tissue engineering applications [42]. However, no study investigated the potential of the Alg-CMC-based hydrogels for fabrication of 3D bioprinted dental stem cells-laden constructs. SEM images revealed that Alg-CMC bioink could provide a favorable environment for HAT-7 cells to retain their round morphology and attach to the scaffolds and be guided towards mineralization and differentiation, which are essential for the enamel-like tissue formation. This is in agreement with a previous study reporting the round morphology of the HAT-7 cells when co-cultured with dental pulp stem cells in biphasic scaffolds composed of chitosan-collagen I hydrogels where their viability and proliferation were supported [77]. ALP staining of bioprinted HAT-7 cells further confirmed the mineralization potential of Alg-CMC bioink.

4.6. Conclusions

Development of bioinks that fulfill the requirements (printability, mechanical and biological properties) for successful 3D cell printing is greatly required, particularly for tooth tissue engineering. In this study, a novel bioink was successfully developed by combining desirable biological and antibacterial characteristics of carboxymethyl chitosan with excellent printability and proper mechanical and degradation properties of alginate for potential use in enamel regeneration. Alginate and carboxymethyl chitosan were mixed in three ratios and were printed using 3D extrusion printing while being crosslinked in calcium chloride crosslinker solution. Our findings showed that alginate-carboxymethyl chitosan blend hydrogels have good printability, suitable swelling ability, degradation rate and mechanic al properties and were able to provide a favorable microenvironment for dental epithelial stem cell line, HAT-7, to maintain their viability and functional properties. The highly porous structure of the scaffolds showed their ability to facilitate diffusion of nutrients and wastes. Further studies on in vitro culture of cell-laden scaffolds in differentiation media could validate the suitability of the alginate-carboxymethyl chitosan bioink for dental enamel tissue regeneration. Taken together, we suggest that alginate-carboxymethyl chitosan is a promising candidate to be used as bioink for enamel tissue engineering.

Acknowledgments

We would like to acknowledge the Saskatchewan Health Research Foundation (SHRF) and College of Dentistry start-up financial support (PI: PP), College of Medicine start-up funds (SP), Natural Science and Engineering Research Council (NSERC) of Canada (to XC), and the University of Saskatchewan Dean's scholarship and Biomedical Engineering Devolved Scholarship (to FM). Part of the research described in this paper was performed at the Canadian Light Source, a national research facility of the University of Saskatchewan, which is supported by the Canada Foundation for Innovation (CFI), the Natural Sciences and Engineering Research Council (NSERC), the National Research Council (NRC), the Canadian Institutes of Health Research (CIHR), the Government of Saskatchewan, and the University of Saskatchewan. Authors would like to thank Adam Web, Adam McInnes, and Ibrahim Hoja for their help with synchrotron imaging.

Authors' contribution: Conceptualization, F.M, N.Z, S.P, X.C, P.P; Methodology, F.M, X.D, Z.Y, N.Z; Formal analysis, F.M, X.D; Resources, S.P, X.C, P.P; Writing-Original Draft, F.M; Writing-Review & Editing, F.M, N.Z, S.P, X.C, P.P; Supervision, N.Z, S.P, X.C, P.P.

References

[1] G.M. Ahmed, E.A. Abouauf, N. AbuBakr, C.E. Dörfer, K.F. El-Sayed, Tissue Engineering Approaches for Enamel, Dentin, and Pulp Regeneration: An Update, Stem Cells Int. 2020 (2020).

[2] S. Gupta, C. Sharma, A.K. Dinda, A.K. Ray, N.C. Mishra, Tooth tissue engineering: Potential and pitfalls, in: J. Biomimetics, Biomater. Tissue Eng., Trans Tech Publ, 2011: pp. 59–81.

[3] J. Park, S.J. Lee, H.H. Jo, J.H. Lee, W.D. Kim, J.Y. Lee, A. Su, Fabrication and characterization of 3D-printed bone-like β-tricalcium phosphate/polycaprolactone scaffolds for dental tissue engineering, J. Ind. Eng. Chem. 46 (2017) 175–181.

[4] L. Ning, X. Chen, A brief review of extrusion-based tissue scaffold bio-printing, Biotechnol. J. (2017).

[5] D.X.B. Chen, Extrusion Bioprinting of Scaffolds, in: Extrus. Bioprinting Scaffolds Tissue

Eng. Appl., Springer, 2019: pp. 117–145.

[6] Y. Delkash, M. Gouin, T. Rimbeault, F. Mohabatpour, P. Papagerakis, S. Maw, X. Chen, Bioprinting and In Vitro Characterization of an Eggwhite-Based Cell-Laden Patch for Endothelialized Tissue Engineering Applications, J. Funct. Biomater. 12 (2021) 45.

[7] Z. Fu, S. Naghieh, C. Xu, C. Wang, W. Sun, X. Chen, Printability in extrusion bioprinting, Biofabrication. 13 (2021) 33001.

[8] H.M. Butler, E. Naseri, D.S. MacDonald, R.A. Tasker, A. Ahmadi, Optimization of starch-and chitosan-based bio-inks for 3D bioprinting of scaffolds for neural cell growth, Materialia. 12 (2020) 100737.

[9] D. Williams, P. Thayer, H. Martinez, E. Gatenholm, A. Khademhosseini, A perspective on the physical, mechanical and biological specifications of bioinks and the development of functional tissues in 3D bioprinting, Bioprinting. 9 (2018) 19–36.

[10] M. Rajabi, M. McConnell, J. Cabral, M.A. Ali, Chitosan hydrogels in 3D printing for biomedical applications, Carbohydr. Polym. (2021) 117768.

[11] J. Adhikari, M.S. Perwez, A. Das, P. Saha, Development of hydroxyapatite reinforced alginate–chitosan based printable biomaterial-ink, Nano-Structures & Nano-Objects. 25 (2021) 100630.

[12] J. Liu, L. Sun, W. Xu, Q. Wang, S. Yu, J. Sun, Current advances and future perspectives of 3D printing natural-derived biopolymers, Carbohydr. Polym. 207 (2019) 297–316.

[13] D.G. Morrison, R.E. Tomlinson, Leveraging advancements in tissue engineering for bioprinting dental tissues, Bioprinting. (2021) e00153.

[14] A. Athirasala, A. Tahayeri, G. Thrivikraman, C.M. França, N. Monteiro, V. Tran, J. Ferracane, L.E. Bertassoni, A dentin-derived hydrogel bioink for 3D bioprinting of cell laden scaffolds for regenerative dentistry, Biofabrication. 10 (2018) 24101.

[15] F. Croisier, C. Jérôme, Chitosan-based biomaterials for tissue engineering, Eur. Polym. J. 49 (2013) 780–792.

[16] M. Kmiec, L. Pighinelli, M.F. Tedesco, M.M. Silva, V. Reis, Chitosan-Properties and Applications in Dentistry, Adv Tissue Eng Regen Med Open Access. 2 (2017) 35.

[17] Y. Zhang, X. Cheng, J. Wang, Y. Wang, B. Shi, C. Huang, X. Yang, T. Liu, Novel chitosan/collagen scaffold containing transforming growth factor-β1 DNA for periodontal tissue engineering, Biochem. Biophys. Res. Commun. 344 (2006) 362–369.

[18] P.R. Sivashankari, M. Prabaharan, Prospects of chitosan-based scaffolds for growth factor release in tissue engineering, Int. J. Biol. Macromol. 93 (2016) 1382–1389.

[19] P.A. Williams, K.T. Campbell, H. Gharaviram, J.L. Madrigal, E.A. Silva, Alginate-Chitosan Hydrogels Provide a Sustained Gradient of Sphingosine-1-Phosphate for Therapeutic Angiogenesis, Ann. Biomed. Eng. 45 (2017) 1003–1014.

[20] S. Sharma, D. Srivastava, S. Grover, V. Sharma, Biomaterials in tooth tissue engineering: a review, J. Clin. Diagnostic Res. JCDR. 8 (2014) 309.

[21] M. Sahranavard, A. Zamanian, F. Ghorbani, M.H. Shahrezaee, A critical review on three dimensional-printed chitosan hydrogels for development of tissue engineering, Bioprinting. 17 (2020) e00063.

[22] A. Sadeghianmaryan, S. Naghieh, Z. Yazdanpanah, H.A. Sardroud, N.K. Sharma, L.D. Wilson, X. Chen, Fabrication of chitosan/alginate/hydroxyapatite hybrid scaffolds using 3D printing and impregnating techniques for potential cartilage regeneration, Int. J. Biol. Macromol. (2022).

[23] A. Sadeghianmaryan, S. Naghieh, H.A. Sardroud, Z. Yazdanpanah, Y.A. Soltani, J. Sernaglia, X. Chen, Extrusion-based printing of chitosan scaffolds and their in vitro characterization for cartilage tissue engineering, Int. J. Biol. Macromol. 164 (2020) 3179–3192.

[24] K.Y. Lee, D.J. Mooney, Alginate: properties and biomedical applications, Prog. Polym. Sci. 37 (2012) 106–126.

[25] H.M. Butler, E. Naseri, D.S. MacDonald, R.A. Tasker, A. Ahmadi, Investigation of rheology, printability, and biocompatibility of N, O-carboxymethyl chitosan and agarose bioinks for 3D bioprinting of neuron cells, Materialia. 18 (2021) 101169.

[26] T. Jiang, J. Zhao, S. Yu, Z. Mao, C. Gao, Y. Zhu, C. Mao, L. Zheng, Untangling the response of bone tumor cells and bone forming cells to matrix stiffness and adhesion ligand density by means of hydrogels, Biomaterials. 188 (2019) 130–143.

[27] E. Axpe, M.L. Oyen, Applications of alginate-based bioinks in 3D bioprinting, Int. J. Mol. Sci. 17 (2016) 1976.

[28] P. Zhai, X.B. Chen, D.J. Schreyer, An in vitro study of peptide-loaded alginate nanospheres for antagonizing the inhibitory effect of Nogo-A protein on axonal growth, Biomed. Mater. 10 (2015) 45016.

[29] F. Yasmin, X. Chen, B.F. Eames, Effect of process parameters on the initial burst release of protein-loaded alginate nanospheres, J. Funct. Biomater. 10 (2019) 42.

[30] P. Zhai, X.B. Chen, D.J. Schreyer, PLGA/alginate composite microspheres for hydrophilic protein delivery, Mater. Sci. Eng. C. 56 (2015) 251–259.

[31] H.R. Bakhsheshi-Rad, Z. Hadisi, A.F. Ismail, M. Aziz, M. Akbari, F. Berto, X.B. Chen, In vitro and in vivo evaluation of chitosan-alginate/gentamicin wound dressing nanofibrous with high antibacterial performance, Polym. Test. 82 (2020) 106298.

[32] S. Qiao, Y. Zhao, C. Li, Y. Yin, Q. Meng, F.-H. Lin, Y. Liu, X. Hou, K. Guo, X. Chen, An alginate-based platform for cancer stem cell research, Acta Biomater. 37 (2016) 83–92.

[33] L. Ning, A. Guillemot, J. Zhao, G. Kipouros, X. Chen, Influence of Flow Behavior of Alginate–Cell Suspensions on Cell Viability and Proliferation, Tissue Eng. Part C Methods. 22 (2016) 652–662.

[34] L. Ning, Y. Xu, X. Chen, D.J. Schreyer, Influence of mechanical properties of alginate-based substrates on the performance of Schwann cells in culture, J. Biomater. Sci. Polym. Ed. 27 (2016) 898–915.

[35] N. Soltan, L. Ning, F. Mohabatpour, P. Papagerakis, X. Chen, Printability and cell viability in bioprinting alginate dialdehyde-gelatin scaffolds, ACS Biomater. Sci. Eng. (2019).

[36] S. Naghieh, M.D. Sarker, E. Abelseth, X. Chen, Indirect 3D bioprinting and characterization of alginate scaffolds for potential nerve tissue engineering applications, J. Mech. Behav. Biomed. Mater. 93 (2019) 183–193.

[37] M.D. Sarker, S. Naghieh, A.D. McInnes, L. Ning, D.J. Schreyer, X. Chen, Bio-fabrication of peptide-modified alginate scaffolds: Printability, mechanical stability and neurite outgrowth assessments, Bioprinting. 14 (2019) e00045.

[38] M. Sarker, X.B. Chen, Modeling the flow behavior and flow rate of medium viscosity alginate for scaffold fabrication with a three-dimensional bioplotter, J. Manuf. Sci. Eng. 139 (2017) 81002.

[39] M. Izadifar, P. Babyn, M.E. Kelly, D. Chapman, X. Chen, Bioprinting Pattern-Dependent Electrical/Mechanical Behavior of Cardiac Alginate Implants: Characterization and Ex Vivo Phase-Contrast Microtomography Assessment, Tissue Eng. Part C Methods. 23

(2017) 548–564.

[40] S. Naghieh, M.R. Karamooz-Ravari, M.D. Sarker, E. Karki, X. Chen, Influence of crosslinking on the mechanical behavior of 3D printed alginate scaffolds: Experimental and numerical approaches, J. Mech. Behav. Biomed. Mater. 80 (2018) 111–118.

[41] J. Sun, H. Tan, Alginate-based biomaterials for regenerative medicine applications, Materials (Basel). 6 (2013) 1285–1309.

[42] Y. Bu, H.-X. Xu, X. Li, W.-J. Xu, Y. Yin, H. Dai, X. Wang, Z.-J. Huang, P.-H. Xu, A conductive sodium alginate and carboxymethyl chitosan hydrogel doped with polypyrrole for peripheral nerve regeneration, RSC Adv. 8 (2018) 10806–10817.

[43] L. Ning, N. Betancourt, D.J. Schreyer, X. Chen, Characterization of cell damage and proliferative ability during and after bioprinting, ACS Biomater. Sci. Eng. 4 (2018) 3906–3918.

[44] Y. He, S. Derakhshanfar, W. Zhong, B. Li, F. Lu, M. Xing, X. Li, Characterization and application of carboxymethyl chitosan-based bioink in cartilage tissue engineering, J. Nanomater. 2020 (2020).

[45] M. Yao, Q. Zou, W. Zou, Z. Xie, Z. Li, X. Zhao, C. Du, Bifunctional scaffolds of hydroxyapatite/poly (dopamine)/carboxymethyl chitosan with osteogenesis and anti-osteosarcoma effect, Biomater. Sci. 9 (2021) 3319–3333.

[46] A. Rajaram, D. Schreyer, D. Chen, Bioplotting alginate/hyaluronic acid hydrogel scaffolds with structural integrity and preserved schwann cell viability, 3D Print. Addit. Manuf. 1 (2014) 194–203.

[47] J. Huang, H. Fu, Z. Wang, Q. Meng, S. Liu, H. Wang, X. Zheng, J. Dai, Z. Zhang, BMSCs-laden gelatin/sodium alginate/carboxymethyl chitosan hydrogel for 3D bioprinting, Rsc Adv. 6 (2016) 108423–108430.

[48] Q. Gu, E. Tomaskovic-Crook, R. Lozano, Y. Chen, R.M. Kapsa, Q. Zhou, G.G. Wallace, J.M. Crook, Functional 3D neural mini-tissues from printed gel-based bioink and human neural stem cells, Adv. Healthc. Mater. 5 (2016) 1429–1438.

[49] W.E.G. Müller, E. Tolba, H.C. Schröder, M. Neufurth, S. Wang, T. Link, B. Al-Nawas, X. Wang, A new printable and durable N, O-carboxymethyl chitosan–Ca 2+–polyphosphate complex with morphogenetic activity, J. Mater. Chem. B. 3 (2015) 1722–1730.

[50] E. Naseri, C. Cartmell, M. Saab, R.G. Kerr, A. Ahmadi, Development of N, O-

carboxymethyl chitosan-starch biomaterial inks for 3D printed wound dressing applications, Macromol. Biosci. (2021) 2100368.

[51] M. Neufurth, S. Wang, H.C. Schröder, B. Al-Nawas, X. Wang, W.E.G. Müller, 3D bioprinting of tissue units with mesenchymal stem cells, retaining their proliferative and differentiating potential, in polyphosphate-containing bio-ink, Biofabrication. (2021).

[52] Q. Gu, E. Tomaskovic-Crook, G.G. Wallace, J.M. Crook, 3D bioprinting human induced pluripotent stem cell constructs for in situ cell proliferation and successive multilineage differentiation, Adv. Healthc. Mater. 6 (2017) 1700175.

[53] F. You, X. Chen, D.M.L. Cooper, T. Chang, B.F. Eames, Homogeneous hydroxyapatite/alginate composite hydrogel promotes calcified cartilage matrix deposition with potential for three-dimensional bioprinting, Biofabrication. 11 (2018) 15015.

[54] F. You, X. Wu, X. Chen, 3D printing of porous alginate/gelatin hydrogel scaffolds and their mechanical property characterization, Int. J. Polym. Mater. Polym. Biomater. 66 (2017) 299–306.

[55] S. Naghieh, M.D. Sarker, N.K. Sharma, Z. Barhoumi, X. Chen, Printability of 3D printed hydrogel scaffolds: Influence of hydrogel composition and printing parameters, Appl. Sci. 10 (2020) 292.

[56] S. Kawano, T. Morotomi, T. Toyono, N. Nakamura, T. Uchida, M. Ohishi, K. Toyoshima, H. Harada, Establishment of Dental Epithelial Cell Line (HAT-7) and the Cell Differentiation Dependent on Notch Signaling Pathway, Connect. Tissue Res. 43 (2002) 409–412. https://doi.org/10.1080/03008200290000637.

[57] F.O. Costa, E.J.P. Lages, L.O.M. Cota, T.C.M. Lorentz, R. V Soares, J.R. Cortelli, Tooth loss in individuals under periodontal maintenance therapy: 5-year prospective study, J. Periodontal Res. 49 (2014) 121–128.

[58] N. Monteiro, P.C. Yelick, Dental tissue engineering, in: Princ. Regen. Med., Elsevier, 2019: pp. 907–921.

[59] Y.S. Zhang, G. Haghiashtiani, T. Hübscher, D.J. Kelly, J.M. Lee, M. Lutolf, M.C. McAlpine, W.Y. Yeong, M. Zenobi-Wong, J. Malda, 3D extrusion bioprinting, Nat. Rev. Methods Prim. 1 (2021) 1–20.

[60] G. Tang, Z. Tan, W. Zeng, X. Wang, C. Shi, Y. Liu, H. He, R. Chen, X. Ye, Recent advances of chitosan-based injectable hydrogels for bone and dental tissue regeneration,

Front. Bioeng. Biotechnol. 8 (2020) 1084.

[61] Y. Hu, Z. Zhang, Y. Li, X. Ding, D. Li, C. Shen, F. Xu, Dual-Crosslinked Amorphous Polysaccharide Hydrogels Based on Chitosan/Alginate for Wound Healing Applications, Macromol. Rapid Commun. 39 (2018) 1800069.

[62] M. Tavakol, E. Vasheghani-Farahani, S. Hashemi-Najafabadi, The effect of polymer and CaCl 2 concentrations on the sulfasalazine release from alginate-N, O-carboxymethyl chitosan beads, Prog. Biomater. 2 (2013) 1–8.

[63] H. Chen, F. Fei, X. Li, Z. Nie, D. Zhou, L. Liu, J. Zhang, H. Zhang, Z. Fei, T. Xu, A facile, versatile hydrogel bioink for 3D bioprinting benefits long-term subaqueous fidelity, cell viability and proliferation, Regen. Biomater. 8 (2021) rbab026.

[64] D. Chimene, R. Kaunas, A.K. Gaharwar, Hydrogel bioink reinforcement for additive manufacturing: a focused review of emerging strategies, Adv. Mater. 32 (2020) 1902026.

[65] S. Mishra, F.J. Scarano, P. Calvert, Entrapment of Saccharomyces cerevisiae and 3T3 fibroblast cells into blue light cured hydrogels, J. Biomed. Mater. Res. Part A. 100 (2012) 2829–2838.

[66] Y.-H. Lin, H.-F. Liang, C.-K. Chung, M.-C. Chen, H.-W. Sung, Physically crosslinked alginate/N, O-carboxymethyl chitosan hydrogels with calcium for oral delivery of protein drugs, Biomaterials. 26 (2005) 2105–2113.

[67] S. Potiwiput, H. Tan, G. Yuan, S. Li, T. Zhou, J. Li, Y. Jia, D. Xiong, X. Hu, Z. Ling, Dual-crosslinked alginate/carboxymethyl chitosan hydrogel containing in situ synthesized calcium phosphate particles for drug delivery application, Mater. Chem. Phys. 241 (2020) 122354.

[68] G.A. Paredes Juárez, M. Spasojevic, M.M. Faas, P. de Vos, Immunological and technical considerations in application of alginate-based microencapsulation systems, Front. Bioeng. Biotechnol. 2 (2014) 26.

[69] Y. Hu, J. Peng, L. Ke, D. Zhao, H. Zhao, X. Xiao, Alginate/carboxymethyl chitosan composite gel beads for oral drug delivery, J. Polym. Res. 23 (2016) 1–10.

[70] X. Lu, Z. Ding, F. Xu, Q. Lu, D.L. Kaplan, Subtle Regulation of Scaffold Stiffness for the Optimized Control of Cell Behavior, ACS Appl. Bio Mater. 2 (2019) 3108–3119.

[71] X. Lv, Y. Liu, S. Song, C. Tong, X. Shi, Y. Zhao, J. Zhang, M. Hou, Influence of chitosan oligosaccharide on the gelling and wound healing properties of injectable hydrogels based

on carboxymethyl chitosan/alginate polyelectrolyte complexes, Carbohydr. Polym. 205 (2019) 312–321.

[72] Y. Gao, X. Zhang, X. Jin, Preparation and properties of minocycline-loaded carboxymethyl chitosan gel/alginate nonwovens composite wound dressings, Mar. Drugs. 17 (2019) 575.

[73] L. Ning, 3D Bioprinting Tissue Scaffolds with Living Cells for Tissue Engineering Applications, (2018).

[74] R.F. Pereira, P.J. Bártolo, 3D bioprinting of photocrosslinkable hydrogel constructs, J. Appl. Polym. Sci. 132 (2015).

[75] R. Pugliese, B. Beltrami, S. Regondi, C. Lunetta, Polymeric Biomaterials for 3D Printing in Medicine: An Overview, Ann. 3D Print. Med. (2021) 100011.

[76] A. GhavamiNejad, N. Ashammakhi, X.Y. Wu, A. Khademhosseini, Crosslinking strategies for 3D bioprinting of polymeric hydrogels, Small. 16 (2020) 2002931.

[77] S. Ravindran, Y. Song, A. George, Development of three-dimensional biomimetic scaffold to study epithelial–mesenchymal interactions, Tissue Eng. Part A. 16 (2010) 327–342.

Chapter 5. Self-cross-linkable oxidized alginate-carboxymethyl chitosan hydrogels as an injectable cell carrier for dental enamel regeneration *in vitro*

Fatemeh Mohabatpour[1,2], Zahra Yazdanpanah[1], Silvana Papagerakis[1,3], Xiongbiao Chen[1,4*], Petros Papagerakis[1, 2*]

[1]Division of Biomedical Engineering, University of Saskatchewan, 57 Campus Dr., Saskatoon, S7N 5A9, SK, Canada

[2]College of Dentistry, University of Saskatchewan, 105 Wiggins Rd, Saskatoon, S7N 5E4, SK, Canada

[3]Department of Surgery, College of Medicine, University of Saskatchewan, 107 Wiggins Rd, Saskatoon, S7N 0W8, SK, Canada

[4]Department of Mechanical Engineering, University of Saskatchewan, 57 Campus Dr., Saskatoon, S7N 5A9, SK, Canada

[*]Corresponding authors:

Petros Papagerakis, petros.papagerakis@usask.ca

Xiongbiao Chen, xbc719@usask.ca

Silvana Papagerakis, silvana.papagerakis@usask.ca

Keywords: in situ forming injectable hydrogels, enamel regeneration, regenerative dentistry, dental stem cells

5.1. Abstract

Injectable hydrogels, as a carrier, offer great potential to incorporate cells or growth factors for dental tissue regeneration. Notably, development of injectable hydrogels with appropriate structures and properties has been a challenging task, leaving many to be desired in terms of cytocompatibility, antibacterial and self-healing properties, and the ability to support dental stem cell functions. This paper presents our study on the development of a self-cross-linkable hydrogel composed of oxidized alginate and carboxymethyl chitosan, and its characterization, as a cell carrier to incorporate dental epithelial cell line (HAT-7 cells), for dental enamel regeneration *in vitro*. Oxidized alginate was synthesized with 60% theoretical oxidation degree using periodate oxidation and characterized by Fourier Transform Infrared spectroscopy and proton nuclear magnetic resonance spectroscopy and UV-Vis absorption spectroscopy. Then, hydrogels were prepared at three varying weight ratios of oxidized alginate to carboxymethyl chitosan (4:1, 3:1 and 2:1) through Schiff base reactions, which was confirmed by Fourier Transform Infrared spectroscopy. The hydrogels were characterized in terms of gelation time, swelling ratio, structural, injectability, self-healing, antibacterial properties, and *in vitro* characterization for enamel regeneration. The results indicated that hydrogels with higher ratio of oxidized alginate had faster gelation time and lower swelling ability. Hydrogels formed highly porous structures and were able to be injected through a 20-gauge needle without clogging. The injected broken pieces of the hydrogels could be rapidly reformed into a single piece, showing the self-healing property of the hydrogels. The hydrogels also showed antibacterial properties against two cariogenic bacterial: *Streptococcus mutans* and *Streptococcus sobrinus*. HAT-7 cellsshowed a high viability in the hydrogels which was not affected by the extrusion pressure during injection. Also, HAT-7 cells encapsulated in the hydrogels showed alkaline phosphatase production and mineral deposition and maintained their round morphology after 14 days of *in vitro* culture. In summary, this study has illustrated that the oxidized alginate-carboxymethyl chitosan hydrogels could be used as injectable a cell carrier for dental enamel tissue engineering.

5.2. Introduction

Dental caries is the most common oral disease caused by microbial biofilm which results in enamel damage and demineralization, cavity formation and tooth destruction [1,2]. Loss of enamel

forming cells, ameloblasts, after tooth eruption causes enamel to have no capacity to self-regenerate [3]. Thus, developing innovative approaches to regenerate dental enamel are needed to tackle the loss of dental enamel tissue [4]. Tissue engineering has shown a remarkable promise as a therapeutic option in restorative dentistry to regenerate damaged or lost dental tissues [5,6]. Tooth tissue engineering employs three main elements including dental stem cells, scaffolds, and growth factors to reconstruct new dental tissues that resemble the structure and function of the native tissue [5,7,8]. Scaffolds are frameworks that guide cells to grow into the desired tissue and growth factors modulate cellular activities. Scaffolds ideally require to be biocompatible and have a controllable biodegradability and mimic the extracellular matrix of the natural tissues and provide 3D environments for cells that facilitate cell attachment, proliferation, and differentiation [9,10]. Dental enamel is developed through amelogenesis process during which enamel crystals are grown in a gel-like organic matrix secreted by ameloblasts [11]. Hydrogels have been used as models for enamel mineralization due to their capacity to mimic the *in vivo* enamel matrix and they have shown to promote regrowth of enamel crystals and to form enamel-like structures [12,13].

Injectable hydrogels have shown a great potential as cell carriers or delivery systems for biomolecules in regenerative medicine and cancer treatment [14–17]. Injectable hydrogels can be formed in situ and have beneficial properties over pre-formed hydrogels, that are shaped before being applied to the target site, given the morphology, size, and complexity of the dental tissues' structures [18–20]. These advantages include the minimally invasive procedure for applying injectable hydrogels to the defected site leading to reduced risk of infection and decreased patient discomfort, their capacity to fill defects with irregular shapes; they also facilitate the incorporation of cells and growth factors into the hydrogel solution prior to injection [18–20]. An injectable hydrogel system contains hydrophilic polymers of natural or synthetic origins which undergo in situ gelation, via physical or chemical crosslinking methods, and form three dimensional networks that can absorb a large amount of water or biological fluids [21,22]. Although physical crosslinking such as ionic or thermo gelation occurs in a milder condition, physically crosslinked hydrogels often suffer from low mechanical properties [23]. Chemical crosslinking takes place via chemical reactions that form covalent bonds in the polymeric network such as photo-polymerization or enzyme polymerization and develops hydrogels with more stability, slower degradation rate, and

higher mechanical properties [23–25]. The photo-initiators and UV light that are used during photo-polymerization can have cytotoxic effects and cause cell death [26]. Chemical crosslinkers such as glutaraldehyde are highly toxic to cells that could limit their applications for developing in situ forming injectable hydrogels [27]. The Schiff-base reaction is a chemical crosslinking mechanism that occurs between aldehyde and amino groups of polymers [28]. As this reaction does not involve any chemical crosslinker or other external stimulation, it is considered non-toxic to cells [27,29]. Also, the conventional injectable hydrogels lack the ability of quick restoration and protecting loaded cells from the damage caused by mechanical forces; as a result, they can lose their functionality and structural integrity [30]. On the other hand, the dynamic Schiff base crosslinking confers self-healing properties to the hydrogels which allow them to spontaneously recover following damage and protect cells from the damage associated with the injection pressure or other external mechanical forces [30,31]. Therefore, a new generation of in situ forming hydrogels that possess both injectability and self-healing properties has been developed to better address the requirements for biomedical applications [30,32]. Although the injectable hydrogel with self-healing ability have been used for drug/cell delivery [30,33–36] and wound healing [37,38], their application as dental cell carriers has not yet been investigated for the regeneration of dental tissues. As inspired, this study aimed to develop alginate-based injectable hydrogels as a cell carrier for dental enamel regeneration.

Alginate is a natural anionic polysaccharide that has been widely used in dental impression and tissue engineering applications owing to its appealing biocompatibility and its ability to be gelled under mild conditions in the presence of divalent cations [14,17,39]. However, alginate has low cell attachment properties and low degradation rate [40]. Alginate can be modified through oxidation reaction using periodate that converts the hydroxyl groups in the backbone of alginate to aldehyde groups [14,17,41]. Oxidized alginate has reported to have higher biocompatibility and faster degradation in aqueous environments [40,42]. In addition, oxidized alginate is capable of self-crosslinking with amino containing polymers such as gelatin and carboxymethyl chitosan through Schiff base reaction to generate in situ forming hydrogels [41,42]. Carboxymethyl chitosan is a water-soluble derivative of chitosan that has antibacterial activity, high biocompatibility and cell interaction properties, which make them suitable for tissue regeneration applications [43–46].

Oxidized alginate and carboxymethyl chitosan have been reported to undergo self-crosslinking process through Schiff base reaction upon mixing allowing them to form covalently crosslinked hydrogels, that are more stable compared to ionically-crosslinked hydrogels, with injectable, self-healing and antibacterial properties [29,47]. This defined the basis of this study to develop an injectable self-healing hydrogel composed of oxidized alienate and carboxymethyl chitosan for dental enamel regeneration. First, oxidized alginate was synthesized using sodium meta periodate, followed by chemical characterization and oxidation degree determination. Then, the hydrogels were prepared at three different weight ratios of oxidized alginate to carboxymethyl chitosan. The properties of hydrogels were evaluated in terms of gelation time, swelling ratio, chemical and morphological characterizations. Also, the injectability, self-healing and antibacterial properties of the hydrogels were assessed. The suitability of self-cross-linkable hydrogels for enamel regeneration was evaluated by the encapsulation and in vitro culture of dental epithelial stem cell line, HAT-7, followed by assessment of cell viability, cell morphology and mineral formation in the cell-laden hydrogels.

5.3. Materials and methods

5.3.1. Synthesis of oxidized alginate

Oxidized alginate was synthesized according to a previously reported protocol [48,49]. Two gram of sodium alginate powder (Cat. no. A2033, Sigma-Aldrich, St. Louis, Missouri, US) was dispersed in 10 mL ethanol. Then, 1.28 g of sodium metaperiodate (Cat.no. 20504, Thermo Fisher Scientific, Waltham, Massachusetts, USA) was dissolved in 10 mL water (the molar ratio of sodium periodate to repeating units of alginate=0.6 to produce oxidized alginate with 60% theoretical degree of oxidation) and added to the alginate dispersion drop by drop and was continuously stirred at room temperature in the dark for 6 hours. The reaction stopped by adding 2 mL ethylene glycol (Cat. no. 324558, Sigma-Aldrich) and stirred for another 30 minutes. The mixture was then dialyzed against water using Seamless Cellulose Dialysis Tubing (molecular weight cut-off 12 kDa, Cat. no. S25645B, Fisher Scientific) with several changes of water. The oxidized alginate solution was freeze-dried for 3 days and kept at 4 °C until used. To characterize the composition of oxidized alginate and unmodified alginate, Fourier Transform Infrared (FTIR) spectroscopy was performed by using an IlluminatIR II inVia Reflex (Smiths Detection, Danbury,

Connecticut, US) equipped with an attenuated total reflectance (ATR) objective. The successful synthesis of oxidized alginate was confirmed by proton nuclear magnetic resonance spectroscopy (^{1}HNMR, Bruker Avance 500 MHz spectrometers, Billerica, Massachusetts, US). Oxidized alginate and alginate were dissolved in deuterium oxide and were transferred into NMR tubes and the spectra were taken at room temperature.

5.3.2. Determination of oxidation degree

The oxidation degree of synthesized oxidized alginate was determined by UV-Vis absorption spectroscopy [50]. The 20% (w/v) potassium iodide (KI, Cat. no. P4101, Fisher Scientific) and 1% (w/v) starch solutions (Cat. no. S516, Fisher Scientific) in buffer phosphate (pH7) were mixed in 1:1 volume ratio to prepare the indicator solution. One mL of oxidation reaction mixture prior to adding ethylene glycol was diluted to 250 mL distilled water. Three mL of diluted solution was added to 1.5 mL of indicator solution and then 0.5 mL of distilled water was added to the solution. The absorbance of the diluted solution was measured at 486 nm to determine the concentration of the sodium metaperiodate in the sample using the standard curve created for sodium periodate solutions. The consumed amount of the periodate was calculated by subtracting the amount of sodium periodate before and after oxidation reaction. The oxidation degree (OD) of alginate was calculated using the following equation [51]:

$$\text{OD}\ (\%) = \frac{m_w \times n}{m} \times 100 \qquad (5.1)$$

M_w is the molecular weight of the repeating units of sodium alginate that is equal to 198 g/mol. m is the initial amount of sodium alginate (g). n is the amount of sodium periodate (mol). To calculate the theoretical oxidation degree, the initial amount of sodium periodate (mol) is considered as n, while for the actual oxidation degree n is considered as the consumed amount of sodium (mol).

5.3.3. Self-cross-linkable Hydrogel formation

Three different concentrations of oxidized alginate (10%, 15% and 20% (w/v)) and a 7.5% (w/v) carboxymethyl chitosan (CMC, Cat. no. sc-358091, Santacruz Biotechnology, Dallas, Texas, USA) solutions were prepared in phosphate buffered saline (PBS) separately under stirring at room temperature. Then, each concentration of oxidized alginate solutions was gently mixed with

carboxymethyl chitosan solution at a fixed volume ratio of 60:40 (v/v%) to obtain hydrogel solutions with three different weight ratios of 4:1, 3:1 and 2:1 (table 1). Hydrogel solutions were then placed in 37 °C to allow gelation through self-crosslinking occurs.

Table 5.4. Labels for different hydrogel groups based on their compositions.

Label	Weight ratio		Final concentration (w/v%)		Total polymer concentration (w/v%)
	OAlg	CMC	OAlg	CMC	
OAlg:CMC (4:1)	4	1	12	3	15
OAlg:CMC (3:1)	3	1	9	3	12
OAlg:CMC (2:1)	2	1	6	3	9

5.3.4. Gelation time

Gelation time of self-crosslinked oxidized alginate/carboxymethyl chitosan was determined by the tube inversion method [30]. Briefly, hydrogel solutions with the compositions described above were prepared in 15 mL glass vials and placed in 37 °C. Gelation of hydrogels were monitored by inverting the tube at 37 °C and the gelation time was recorded when hydrogel solutions stopped flowing.

5.3.5. Chemical characterization of self-crosslinked hydrogels

To evaluate the crosslinking between oxidized alginate and carboxymethyl chitosan, FTIR spectroscopy was performed using the hydrogel sample with highest concentration of oxidized alginate (OAlg:CMC (4:1)). Briefly, hydrogel samples were prepared as described before and were crosslinked at 37 °C according to the gelation time measured by tube inversion test and then was instantly placed in -80 °C and lyophilized for 24 hours. The spectra of lyophilized hydrogels were recorded using the same instrument as previously mentioned and were compared with oxidized alginate and carboxymethyl chitosan.

5.3.6. Swelling test

Crosslinked hydrogels were immersed in PBS solution and allowed to completely swell. After incubating and equilibrating the samples at 37 °C for 24 hours, hydrogels were removed, and swollen weights (W_s) were measured, and samples were dried under vacuum and dry weights were measured (W_d). Swelling ratio was calculated according to the following equation:

$$\text{Swelling ratio} = (W_s - W_d)/ W_d \quad (5.2)$$

5.3.7. Microstructural observation of the self-cross-linkable hydrogels

The morphology of the hydrogels was analyzed scanning electron microscopy (SEM). The self-crosslinked hydrogels were lyophilized at -50 °C and placed on the aluminum stubs and sputter coated with a thin layer of gold using a sputter coater (Q150T ES, Quorum Technologies, Laughton, East Sussex, UK). Samples were imaged under vacuum using a field scanning electron microscope (SU8010, Hitachi, Chiyoda, Tokyo, Japan).

5.3.8. Injectability and self-healing assays

The injectability of the hydrogels was assessed using a previously reported method [52,53]. The hydrogel with OAlg:CMC ratio of 2:1 was chosen as an example. OAlg and CMC solutions were added to a 5 mL glass vial and vortexed to obtain a homogenous mixture and allowed the sol-gel transition occurs. After gelation, the disk-shaped hydrogel was loaded into a 3 mL syringe and was injected through a 20-gauge needle to write four letters “ABCD” on a glass microscope slide. In addition, the hydrogels were injected into a 10 mL beaker and then after injection, the beaker containing the injected hydrogel was kept at 37 °C for 10 minutes to allow hydrogels to be self-healed. The photos of the one single piece of hydrogel were taken to record the self-healing property. The stability of the self-healed hydrogels was assessed by immersing them in PBS.

5.3.9. Antibacterial properties

To assess the antibacterial properties of the OAlg-CMC hydrogels, the inhibition zone test [54] was performed using two common cariogenic bacteria found in dental plaque biofilm, *Streptococcus mutans* and *Streptococcus sobrinus.* Both bacterial strains were incubated in

Bacto™ Brain Heart Infusion broth (BHI, 237500, Becton, Dickinson and Company (BD), New Jersey, United States) at 37 °C overnight to obtain the bacterial suspensions. Then, 200 μL of bacterial suspensions (*Streptococcus mutans*, 10^6 CFU/mL and *Streptococcus sobrinus*, 10^9 CFU/mL) were uniformly spread on the surface of agar plates (BBL™ Brain Heart Infusion Agar, Cot.no. 211065 BD), followed by placing 200 μL of hydrogel samples at all three OAlg:CMC ratios. After incubation for 24 hours at 37 °C, the inhibition zones were measured using image J software (version 2.3.0/1.53f, NIH, Bethesda, Maryland, USA).

5.3.10. In vitro evaluations of self-cross-linkable hydrogels

5.3.10.1. Cell culture

HAT-7 cells (kindly provided by Dr. Hidemitsu Harada, Iwate Medical University, Iwate, Japan) [55] were cultured in DMEM/F12 (1:1), HEPES medium (Cat. no. 11330-032, Gibco®, Invitrogen, Carlsbad, California, USA) supplemented with 10% fetal bovine serum (FBS, Cat. no. 12483-020, Gibco®, Invitrogen) and 1% antibiotic (Penicillin-Streptomycin 100X solution, 10,000 units/mL Penicillin/10,1000 μg/mL Streptomycin, Cat. no. SV30010, Hyclone™, Logan, Utah, US) in a humidified incubator. Medium was changed every 2-3 days.

5.3.10.2. Cell encapsulation in self-cross-linkable hydrogels

Oxidized alginate and carboxymethyl chitosan powder were sterilized by being exposed to UV light for 90 minutes. Then, oxidized alginate (10%, 15% and 20% (w/v)) and 7.5% (w/v) carboxymethyl chitosan solutions were prepared in PBS separately under stirring under sterile condition. HAT-7 cells were sub-cultured twice, counted and then resuspended in the 7.5% carboxymethyl chitosan solutions. Cell-containing CMC solution were mixed with oxidized alginate solutions at a volume ratio of 40:60 (v/v%) to obtain hydrogel solutions with weight ratios of 4:1, 3:1 and 2:1 and a final cell density of 400,000 cells/mL for live dead assay and 6×10^6 cells/mL for alkaline phosphatase and alizarin red S staining and SEM analysis. Hydrogel solutions were inserted in the wells of cell culture plates and kept in 37 °C to be crosslinked through Schiff base reaction. Next, culture media supplemented with 10% FBS and 1% antibiotics was added to the cell-laden hydrogels and kept in the incubator. Medium was changed every 2-3 days.

5.3.10.3. Cell viability assessment

To investigate the effect of hydrogel composition and extrusion pressure during injection on cell viability, live/dead assay was performed using the LIVE/DEAD Cell imaging kit (Cat. no. R37601, Invitrogen, Thermo Fisher Scientific, USA) according to the manufacturer's instructions at days 0, 1 and 3. Briefly, 50 microliters of the hydrogel encapsulating HAT-7 cells were either injected to the wells of the 96 well cell culture plates using 20-gauge needles or mixed in the wells of 96 well plates with pipette tips. After 2, 24 and 72 hours of culture at 37 °C, cell-laden hydrogels were washed with PBS and stained with the mixed green/red dye. After 15 minutes incubation at room temperature, constructs were imaged using fluorescent microscope (EVOS M5000 Cell Imaging System, Thermo Fisher Scientific). The number of live (green) and dead (red) cells were quantified by using image J software and viability was calculated by the following equation:

$$\%\textbf{Cell viability} = \frac{(\textbf{number of live cells})}{(\textbf{number of live cells} + \textbf{number of dead cells})} \qquad (\mathbf{5.3})$$

5.3.10.4. Alkaline phosphatase staining

HAT-7 cells were cultured within oxidized alginate-carboxymethyl chitosan hydrogels for 14 days and then stained by alkaline phosphatase staining (ALP) to detect the expression of alkaline phosphatase as a marker of ameloblast differentiation. Cell-laden constructs were rinsed with PBS twice and cells encapsulated in the hydrogels were fixed and permeabilized using BD Cytofix/cytoperm™ fixation/permeabilization kit (Cat. no. 554714, BD Biosciences, San Jose, California, USA) by incubating the constructs in the fixation and permeabilization solution for 30 minutes at 4 $°C$. Cell-encapsulated hydrogels were washed with 1× BD Perm/Wash™ buffer and then with PBS, twice each. Then, alkaline phosphatase expression in cell-laden constructs was detected using SIGMAFAST™ BCIP®/NBT detection kit (Cat. no. B5655, Sigma-Aldrich). The ALP staining reagent was prepared by dissolving 1 tablet from SIGMAFAST™ BCIP®/NBT detection kit (Cat. no. B5655, Sigma-Aldrich) in 10 mL of distilled water as instructed by the manufacturer. Cell-laden constructs were incubated in ALP staining reagent at 37 °C under dark condition for 24 hours. Cell-encapsulated hydrogels were then visualized under a microscope light microscope (EVOS M5000 Cell Imaging System, Thermo Fisher Scientific).

5.3.10.5. Alizarin red S staining

After 14 days of culture, HAT-7-encapsulated oxidized alginate-carboxymethyl chitosan hydrogels were stained with alizarin red S staining to assess mineralization and calcium deposition. Cells within the hydrogels were fixed and permeabilized as previously described. Then, 2% Alizarin red S (pH 4.2, Cat. no. sc-205998, Santa Cruz Biotechnology, Dallas, Texas, USA) was added to cell-laden constructs and incubated for 5 minutes at room temperature. Cell-laden hydrogels were then rinsed with distilled water twice and imaged using the same light microscope as mentioned above.

5.3.10.6. Observation of cell morphologies in the self-crosslinked hydrogels

After 14 days of culture, the morphology of cells and the mineral deposition in the self-crosslinked hydrogels were examined by scanning electron microscopy (SEM). Cell encapsulated hydrogels with all three oxidized alginate to carboxymethyl chitosan weight ratios were rinsed with PBS twice and fixed with 2.5% v/v glutaraldehyde in PBS for 2 hours. After washing with PBS and distilled water, three times each, samples were kept at -80 °C and then freeze-dried. The lyophilized call-laden hydrogels were sputter coated with a chromium film with a sputter coater and imaged using the same scanning electron microscope as previously mentioned.

5.3.11. Statistical analysis

All data are presented as mean$\pm$standard deviation and were analyzed statistically using one-way ANOVA and the post-Tukey test by GraphPad Prism 5 (GraphPad Software, San Diego, California, USA). A p value < 0.05 was considered statistically significant.

5.4. Results

5.4.1. Synthesis of oxidized alginate

Sodium alginate was synthesized through oxidation reaction using sodium metaperiodate. During this reaction, hydroxyl groups on carbons 2 and 3 (C2 and C3) present in the monomeric units of unmodified alginate are oxidized which leads to the cleavage of C2-C3 bond and the formation of

aldehyde groups in each oxidized repeating units [50]. The synthesized oxidized alginate was characterized by FTIR and ^{1}HNMR. FTIR spectra of unmodified alginate and oxidized alginate (shown in figure 5.1) exhibited the characteristic peaks at 1605 and 1405 cm^{-1} which are attributed to asymmetric and symmetric stretching modes of carboxyl groups, respectively [56].The broad peak appeared at 3267 cm^{-1} in the spectrum of alginate is corresponded to stretching vibration of hydroxyl groups (-OH), which became weaker and narrower in the spectrum of oxidized alginate [49]. The peaks at 815 and 1078 cm^{-1} in the spectrum of alginate are related to symmetrical C-O-C stretching that were reduced in the spectrum of oxidized alginate [56]. In addition, the new peak related to symmetric vibration of aldehyde groups was not observed at 1735 cm^{-1} in the FTIR spectrum of oxidized alginate [56].

The ^{1}H NMR spectrum of oxidized alginate showed two new signals at 5.3 and 5.6 pp which are assigned to the hemiacetalic protons that confirms the successful synthesis of oxidized alginate (figure 5.2) [57]. The new signal at 4.2 ppm in the spectrum of oxidized alginate is correlated to the proton of the oxidized guluronic acid unit in the backbone of the polymer [57].

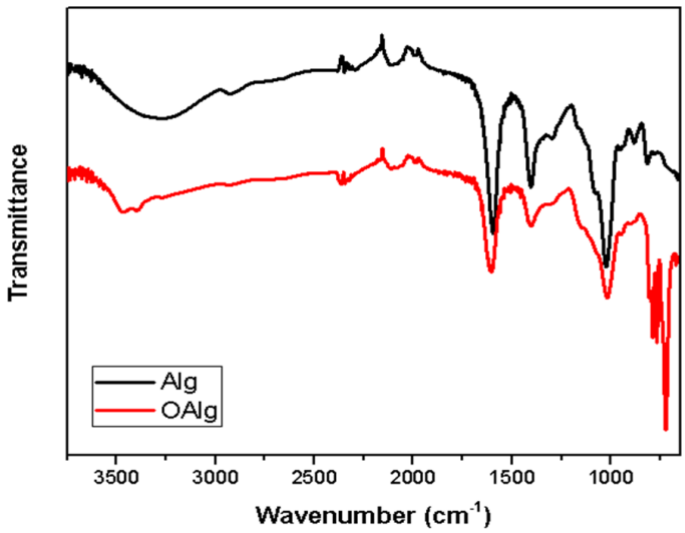

Figure 5.26. Fourier Transform Infrared-Attenuated Total Reflectance (FTIR-ATR) of alginate and synthesized oxidized alginate highlighted the modification of alginate by the addition of aldehyde groups.

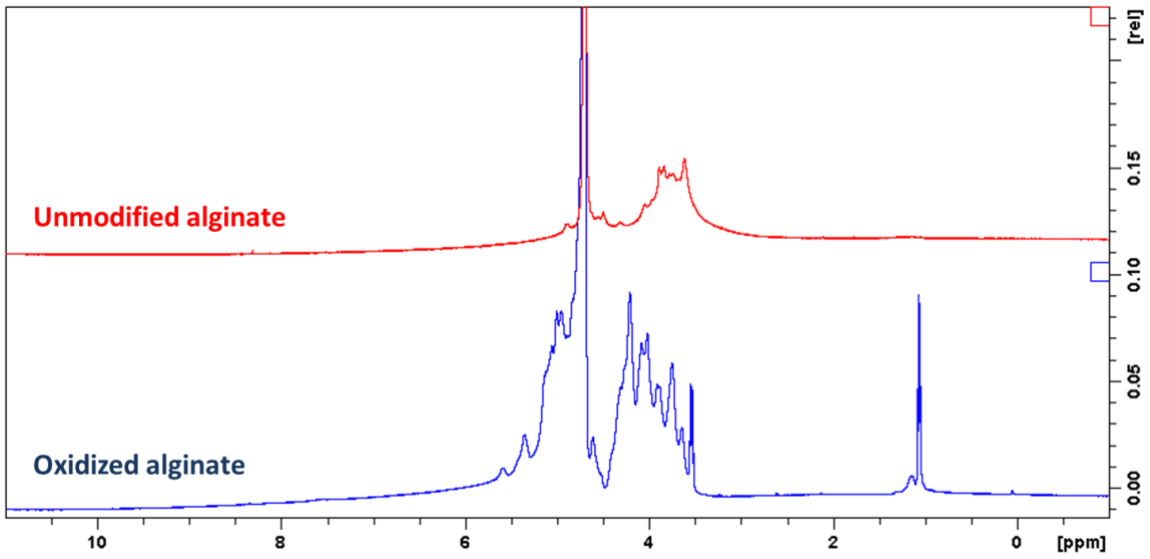

Figure 5.27. Proton nuclear magnetic resonance spectroscopy (^{1}H NMR) spectrum of alginate and synthesized oxidized alginate further confirmed the successful synthesis of oxidized alginate.

5.4.2. Determination of oxidation degree

After oxidation reaction, the oxidation degree was determined to be 59.33% by measuring the quantity of consumed sodium periodate using UV-vis absorption spectroscopy.

5.4.3. Self-cross-linkable hydrogel formation

The chemical crosslinking of hydrogels through Schiff base reaction was assessed by FTIR. As shown in figure 5.3, the peak at 1729 cm^{-1} is related to the free aldehyde groups in oxidized alginate that was not appeared in the FTIR spectrum of oxidized alginate shown in figure 5.1. A new peak was observed at 1621 cm^{-1} in the spectrum of OAlg-CMC hydrogels which is related to Schiff base C=N bonds [58] that was merged with the C=O stretching vibrations of carboxylate in carboxymethyl chitosan observed at 1586 cm^{-1} [59].

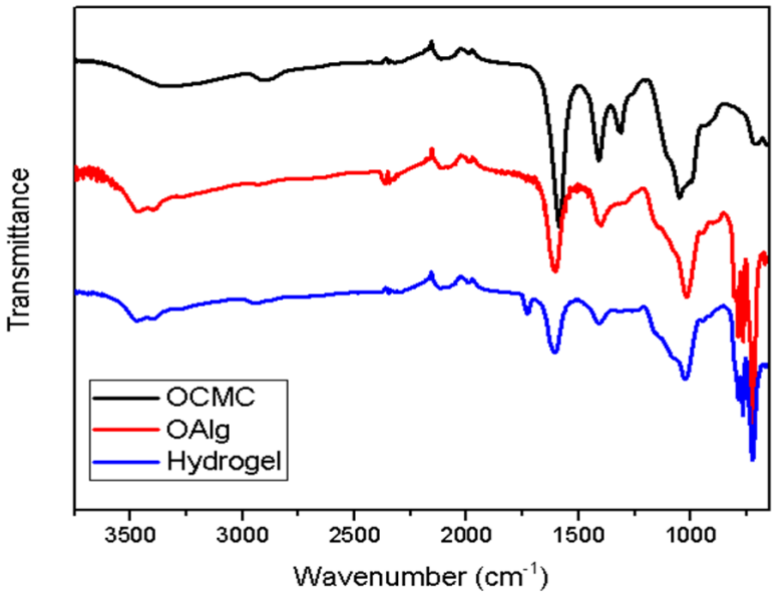

Figure 5.28. Chemical characterization of self-crosslinked oxidized alginate-carboxymethyl chitosan hydrogel with the weight ratio of 4:1 using Fourier Transform Infrared-Attenuated Total Reflectance (FTIR-ATR) showed the imine bond formation as a result of Schiff base reactions.

5.4.4. Gelation time

Gelation time is considered the required time for hydrogels to form and complete crosslinking [60]. Figure 5.4. A shows gelation time of self-crosslinked hydrogels for various weight ratio of oxidized alginate and carboxymethyl chitosan. The higher weight ratio of oxidized alginate in the hydrogel led to a shorter gelation time. The gelation time was decreased from 4.7 min for OAlg:CMC (2:1) ratio to 2.3 min for OAlg:CMC (4:1), which could be due to the higher concentration of aldehyde groups for Schiff base reaction which accelerates the crosslinking reaction and gel formation. Hydrogels with quick gelation time are crucial for clinical application of injectable hydrogels as they can facilitate filling the defected region [60].

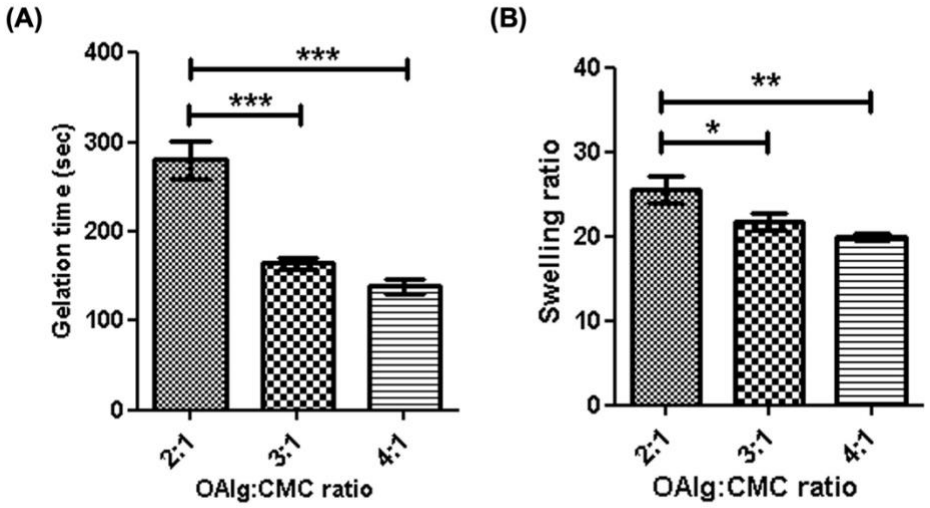

Figure 5.29. (A) Gelation time and (B) swelling ratios of self-crosslinked oxidized alginate-carboxymethyl chitosan hydrogels. Increase in weight ratios of oxidized alginate to carboxymethyl chitosan decreased the gelation time and swelling ratio of the hydrogels. Error bars represent mean$\pm SD$ of repeats (*statistically significant results indicated in the graphs, ***p<0.001, **p<0.01, *p<0.05). Experiments were performed in triplicates.

5.4.5. Swelling test

The quantity of water absorbed into the self-crosslinked hydrogels was determined by swelling test after 24 hours incubation in PBS. As shown in figure 5.4. B, swelling ratio significantly decreased by increasing the weight ratio of oxidized alginate and carboxymethyl chitosan. The swelling ratio of hydrogels is contingent upon crosslinking density in a manner that hydrogels with higher crosslinking density have lower swelling ratio [61]. The higher weight ratio of oxidized alginate provides more available aldehyde groups to react with amino groups for Schiff-base reaction which lead to formation of more imine bonds and thus increase in crosslinking density, which lowered the swelling ratio [61]..

5.4.6. Morphological observation of self-crosslinked hydrogels

Cross-sectional morphology of the hydrogels observed under SEM showed interconnected and porous structures with the pores on the micron scale (figure 5.5). The hydrogels with higher ratio

of OAlg showed smaller pore sizes, higher porosity, and a less homogenous distribution of pore size.

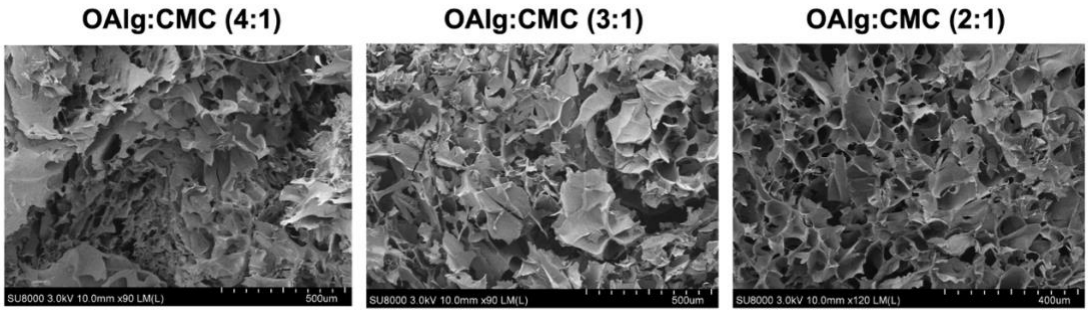

Figure 5.30. Scanning electron microscopy (SEM) images of self-crosslinked oxidized alginate-carboxymethyl chitosan hydrogels at three different weight ratios after lyophilization showed the highly porous structure of the hydrogels.

5.4.7. Injectability and self-healing assays

To test the ability of the self-cross-linkable hydrogels for potential applications as injectable cell delivery systems, hydrogels, after gelation (figure 5.6. A, B, C), were extruded through a 20-gauge needle. As shown in figure 5.6. D, the four letters “ABCD” were successfully drawn using the hydrogels. In addition, figure 5.6. E demonstrates that OAlg-CMC hydrogels were able to be injected through the 20-gauge needle into the 10 mL glass beaker without clogging. After 10 minutes, the pieces of the injected hydrogels could be recovered rapidly through re-crosslinking, which resulted in the re-formation of a single piece hydrogel (figure 5.6. F, G). In addition, the self-healed hydrogels could maintain their structure when immersed in PBS (figure 5.6. H).

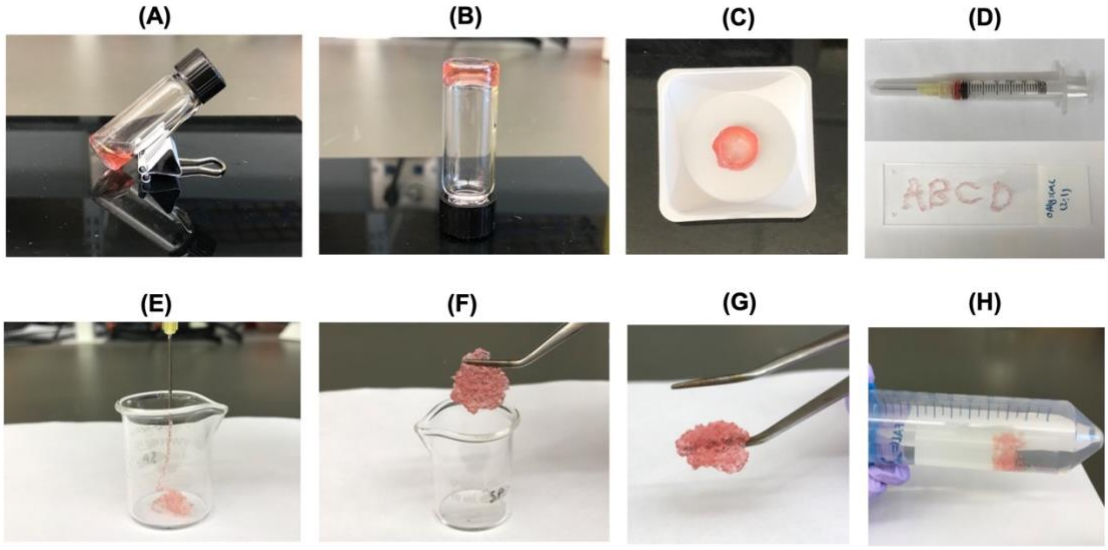

Figure 5.31. The injectability and self-healing assessments of the self-cross-linkable hydrogels at oxidized alginate to carboxymethyl chitosan weight ratios of 2:1. (A, B) The sol-gel transition of the hydrogel. (C, D) The formed disk-shaped hydrogel was placed in a 3 mL syringe and used as ink to draw the letters "ABCD" (E) Hydrogels were able to be extruded through the 20-gauge needle without clogging into a 10 mL beaker. (F, G) The injected hydrogel fragments were self-healed and reformed a single piece after 10 minutes incubation at 37 °C. (H) Immersion of the self-healed hydrogel in PBS that shows the stability and integrity of the hydrogel after self-healing.

5.4.8. Assessment of antibacterial properties

Antibacterial properties of the hydrogels were assessed against *Streptococcus mutans and Streptococcus sobrinus* by measuring the inhibition zone in which no bacterial growth was observed. As shown in figure 5.7, hydrogels at all OAlg:CMC ratios showed the growth inhibition against both *Streptococcus mutans* and *Streptococcus sobrinus*. Hydrogels with the OAlg:CMC weight ratio of 3:1 exhibited a significantly larger inhibition zone compared to the weight ratio of 4:1 and 2:1which indicates the higher antibacterial effects of this groups towards *Streptococcus mutans* (figure 5.7. A). However, no significant difference was observed between three different groups of hydrogels against *Streptococcus sobrinus* (figure 5.7. B).

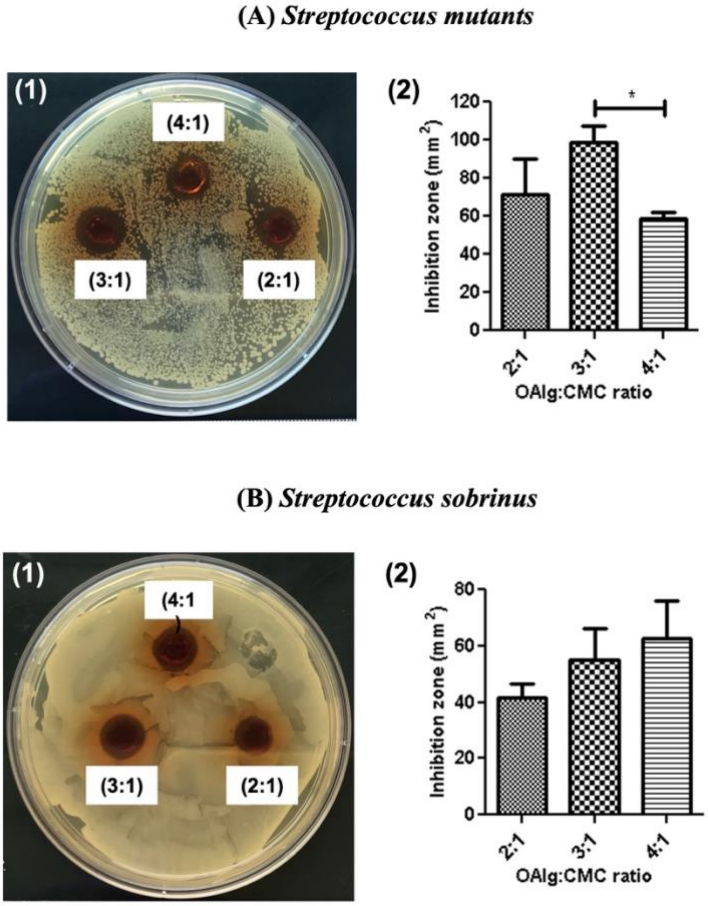

Figure 5.32. The assessment of antibacterial activity of self-crosslinked hydrogels at three different weight ratios of oxidized alginate to carboxymethyl chitosan. Hydrogels showed the inhibition of bacterial growth against (A) Streptococcus mutans and (B) Streptococcus sobrinus. Error bars represent mean$\pm SD$ of repeats (*statistically significant results indicated in the graphs, *p<0.05). Experiments were performed in triplicates.

5.4.9. Live/dead assay

The viability of HAT-7 cells in the OAlg-CMC hydrogels was assessed using live/dead assays after 0, 1 and 3 days. HAT-7 cells loaded hydrogels were injected through a 20-gauge needle in a 96 well plate. As shown in figure 5.8, the extruded hydrogel pieces were self-healed and became one piece hydrogel. Both non-injected and injected HAT-7 cells showed a high cell viability over 80% indicating the cytocompatibility of the self-crosslinked hydrogels and no negative effect of extrusion pressure during injection on cell survival at all three time points.

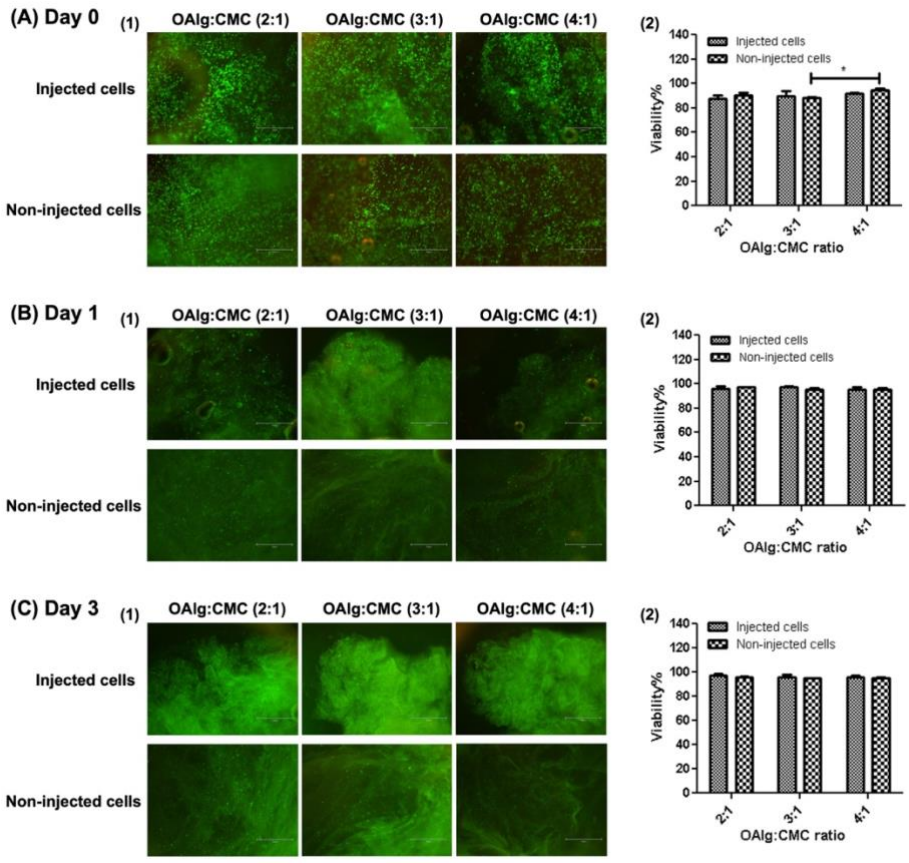

Figure 5.33. Live/dead staining of HAT-7 cells encapsulated in self-crosslinked oxidized alginate-carboxymethyl chitosan hydrogels at different time points (Days 0, 1 and 3) showed no significant difference in the viability of the injected cells compared to non-injected cells. Error bars represent mean$\pm SD$ of repeats (*statistically significant results indicated in the graphs, *p<0.05). Experiments were performed in triplicates.

5.4.10. Mineralization assays

After 14 days of culture, the capacity of HAT-7 cells cultured in self-crosslinked hydrogels to differentiate into enamel-producing ameloblasts and deposit calcium was assessed by alkaline phosphatase and alizarin red S staining, respectively. As shown in figure 5.9. B, C, cell encapsulated in self-cross-linkable hydrogels with all three different OAlg-CMC weight ratios stained positive with ALP and alizarin red S. However, no significant difference was observed between the three groups of hydrogels.

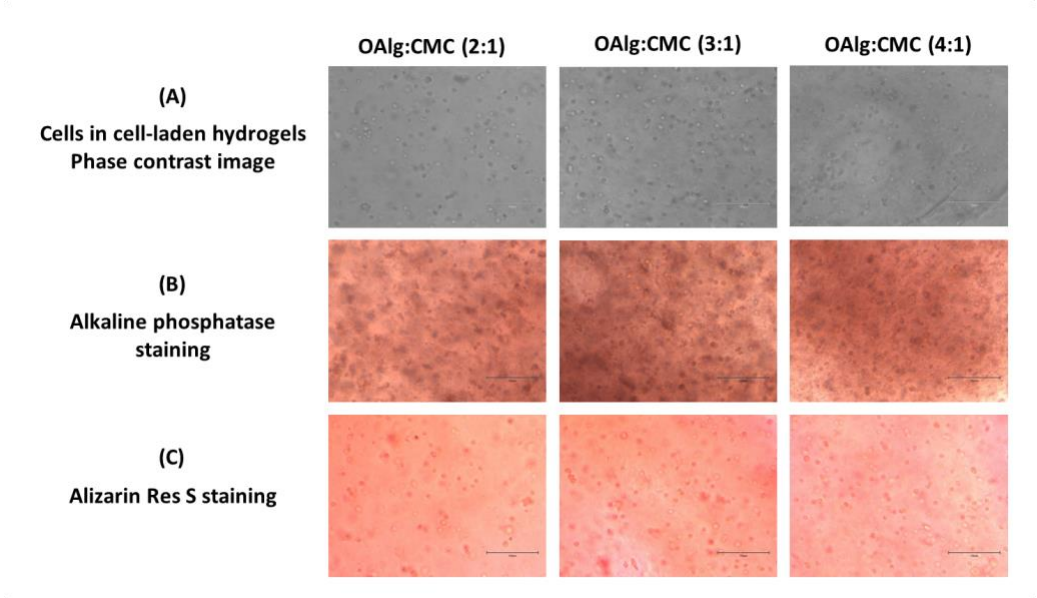

Figure 5.34. In vitro culture of the dental epithelial stem cell line (HAT-7) in self-crosslinked oxidized alginate-carboxymethyl chitosan hydrogels with three weight ratios of 2:1, 3:1 and 4:1 for 14 days. (A) Observation of cell morphology in cell-laden hydrogels using optical microscopy. (B) Alkaline phosphatase and (C) Alizarin red S staining of HAT-7 cells in self-crosslinked hydrogels, indicating the initiation of mineralization and ameloblast differentiation.

5.4.11. SEM analysis of cell-laden hydrogels

The morphology of the HAT-7 cells cultured in self-crosslinked hydrogels for 14 days was observed by SEM analysis. As shown in figure 5.10. A, B, HAT-7 cells maintained their round morphology in self-crosslinked hydrogels after 14 days of culture. Moreover, figure 5.10. B1-3 showed the appearance of ribbon-like structures and rod-like crystals on the surface of HAT-7 cells. These observed mineralized structures could indicate that HAT-7 cells started to differentiate into ameloblast.

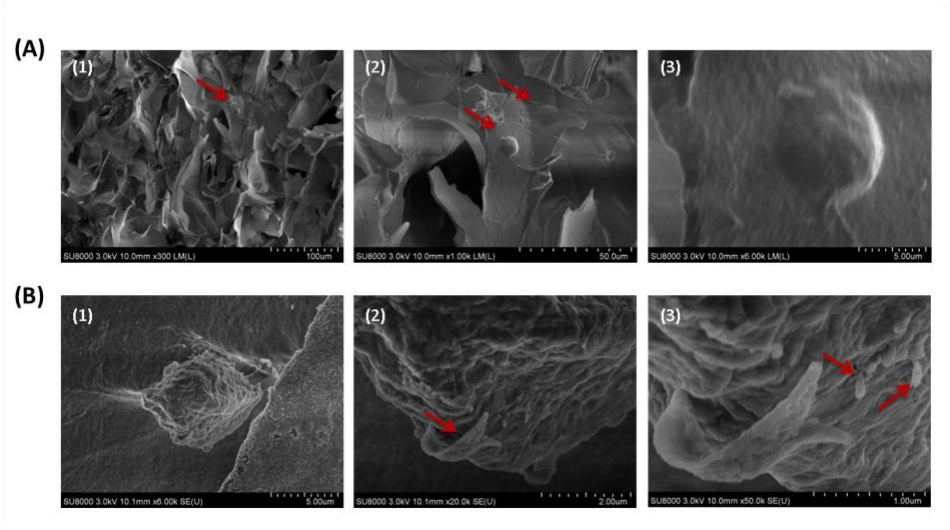

Figure 5.35. Scanning electron microscopy (SEM) images of HAT-7 cells encapsulated in self-cross-linkable oxidized alginate-carboxymethyl chitosan hydrogel with weight ratio of 2:1(A1-3) and 4:1 (B1-3) after 14 days of in vitro culture showed the round morphology of HAT-7 cells and initiation of the mineral formation. (2) and (3) are the magnified image of (1) and (2).

5.5. Discussion

Recent advances in the field of tissue engineering offer remarkable promises for the invention of innovative treatment options in dentistry to regenerate lost or diseased dental tissues [62,63]. Selection of biomaterials, stem cells, and growth factors, as well as the scaffold design, have a critical impact on the clinical outcome of the regenerative therapies [62]. In situ forming hydrogels have become one of the promising scaffold platforms for dental tissue regeneration due to their beneficial characteristics such as minimally invasiveness filling the irregular-shaped defects [18]. One of the chemical crosslinking reactions to produce the injectable hydrogel systems is based on Schiff base reactions [64]. This reversible chemical reaction occurs upon mixing the aqueous solutions of two polymers, one of which contains aldehyde groups and the other has amine functional groups, and form imine bonds [64,65]. Schiff base reaction enables the possibility of in situ gelling process under physiological condition that is highly desirable [65]. Schiff base crosslinking avoids the use of any additional external crosslinking agents, which often exhibit cytotoxic effects and could be released to the body as the hydrogel degrades [66]. In addition, the generation of non-toxic products as a result of this reactions further ensures the suitable biocompatibility of hydrogels formed through Schiff base reactions [65]. One of the concerns

associated with hydrogel scaffolds is that their structural and functional integrity is prone to be ruptured under destructive factors such as external mechanical forces or chemical erosion, which may lead to the need for frequent replacement [67,68]. Schiff base reaction-based hydrogels possess intrinsic self-healing properties due to the dynamic crosslinking networks which allow them to self-repair when they are exposed to destructive factors; thus, they improve patients' convenience [67–69]. Due to this unique property, when the imine linkages in the hydrogel network are broken, the amino groups on the disrupted site reacts with the available aldehyde groups that are in contact with them and form Schiff-base bonds again quickly [65]. The injectable hydrogels that are self-healable can repair any damage exerted to the hydrogel quickly, which support and protect encapsulated cells and drugs, while in the injectable hydrogels that do not have this characteristic, the damage from mechanical forces can disrupt the in situ crosslinking [65]. Some of the commonly used polymers for the formation of Schiff base reaction-based hydrogels include oxidized alginate/gelatin or collagen [49,70–72], oxidized alginate/carboxymethyl chitosan [29,73–76], oxidized hyaluronic acid/gelatin [77], oxidized hyaluronic acid/glycol chitosan [78] oxidized dextran/gelatin [79]. The present study aimed to develop in situ forming hydrogels composed of oxidized alginate and carboxymethyl chitosan and investigate their suitability for the use as dental stem cell carriers for enamel tissue regeneration. Although self-cross-linkable oxidized alginate-carboxymethyl chitosan hydrogels were previously developed for different applications including wound healing, drug delivery and bone tissue engineering [29,73–76], this is the first study on its application for dental tissue regeneration. The first step was to modify alginate through periodate oxidation to have aldehyde functional groups required for Schiff base crosslinking. The periodate as the oxidant cleaves the vicinal glycols in the alginate backbone to form dialdehyde groups and generate oxidized alginate; one molecule of sodium meta-periodate was reported to be consumed per α-glycol group [80]. Several factors have been reported to affect the oxidation reaction which include periodate/alginate ratio, alginate concentration, reaction medium, reaction time [56,81]. Increase in the periodate/alginate ratio and alginate concentration were found to increase the degree of oxidation [50,56]. The aqueous solutions of alginate, even at low concentrations, have very high viscosity and produce the small quantity of oxidized alginate, whereas alginate dispersion in ethanol-water reaction medium was found to be able to produce large quantity of oxidized alginate with higher reaction yield and lower volume of the solvent [48,81]. In addition, the oxidized alginate synthesized in ethanol-water mixture showed a higher

crosslinking efficiency for hydrogel formation with amino group containing polymers [81]. The degree of oxidation was reported to be increased as the time of the oxidation reaction increases in a manner that the increase in degree of oxidation is fast in the beginning of the reaction and then the reaction becomes slow in both water and ethanol/water as reaction media [49,81]. According to these studies, 6 hours reaction time is enough for having a high yield of oxidation reaction. In this study, sodium alginate was oxidized by sodium periodate (the molar ratio of sodium periodate to repeating units of alginate=0.6) in ethanol-water (1:1) mixture for 6 hours. FTIR characterization revealed that the characteristic peaks of alginate at 1605 and 1405 cm^{-1} are still present in the spectrum of oxidized alginate indicating that the oxidation reaction has not influence the carboxyl groups in the backbone of alginate [56]. The narrower OH stretching peak in the spectrum of oxidized alginate showed the contribution of the hydroxyl group in the oxidation reaction [49]. The reduced symmetrical C-O-C stretching in the spectrum of oxidized alginate compared to alginate showed the cleavage of the alginate chains as a result of oxidation reaction [56]. The absence of new peak ascribed to aldehyde groups could be due to the reaction between free aldehyde groups and hydroxyl groups of neighboring uronic acid subunits which results in hemiacetal formation as previously reported in other studies [56,82]. The appearance of new signals in the ^{1}H NMR spectrum of oxidized alginate at 4.2, 5.3 and 5.6 ppm further confirmed the modification of alginate with aldehyde groups [57]. The oxidation degree is defined as the number of C2-C3 bonds that are cleaved and converted to aldehyde groups [83]. Two major approaches have been used to determine the oxidation degree of alginate [84]. Here, the degree of oxidation was calculated by the method that involves measuring the consumption of the sodium periodate in the oxidation reaction. The actual oxidation degree was 59.33% which is in the similar range reported in previous studies [40,50]. In the next step, hydrogels were prepared by mixing the aqueous solutions of oxidized alginate and carboxymethyl chitosan followed by incubation at 37 °C. The kinetics of crosslinking through Schiff base reaction were found to be contingent upon the pH, temperature and the type and content of amine and aldehyde groups in the polymers [35,85]. The properties of the hydrogel depends on the oxidation degree, and the ratio of aldehyde- to amino-containing polymers [35,48,86]. Thus, in this study, we aimed to modulate the properties of the hydrogels including gelation time, swelling ability by varying OAlg:CMC ratios. Chemical composition of self-crosslinked hydrogels with the Alg:CMC ratio of 4:1, that was expected to have higher crosslinking density and thus showing stronger peak related to Schiff base linkages,

was investigated using FTIR. The appearance of a new peak at 1621 cm^{-1} representing the imine bonds indicated the successful Schiff base crosslinking [58]. The observation of the peaks corresponded to aldehyde groups at 1729 cm^{-1} in the spectrum of the hydrogel, and not in the spectrum of oxidized alginate, could be due to the difference in the moisture content of the samples, as previously reported in other studies [84]. Gelation time is one of the most essential aspect of injectable hydrogels that need to be taken into consideration [35]. It should be slow enough to allow the homogenous mixing of cells or biomolecules and fast enough to prevent the hydrogel precursor to move away from the injection site [35,87]. In this work, the gelation time were 280.7$\pm$ 21.08, 164.3$\pm$6.028 and 138.3$\pm$7.638 for hydrogels with OAlg:CMC ratios of 2:1, 3:1 and 4:1, respectively. All hydrogels showed relatively short gelation time that are believed to be beneficial for clinical applications and provide convenience for patients and clinicians [85]. The hydrogel with OAlg:CMC ratio of 4:1 was found to have the fastest gelation time, which could be due to the higher aldehyde content and thus higher crosslinking density compared to hydrogels with OAlg:CMC ratio of 3:1 and 2:1. Swelling ratio is another essential aspect of hydrogels which shows the ability of hydrogels to absorb body fluids and to allow the diffusion of nutrients and metabolites [88]. The composition and crosslinking of the hydrogel are the factors affecting the swelling ability of hydrogels [89]. In this study, the hydrogels with highest ratio of oxidized alginate showed the lowest swelling ratio. This finding is in consistent with previous reports showing that Schiff base reaction-based hydrogels with higher aldehyde content provide more crosslinking sites which hinder water absorption into the hydrogel network structure which lead to decrease in the swelling ratio [86].

Porosity, pore size and interconnectivity are the important morphological characteristics of tissue engineering scaffolds which influence the migration and proliferation of cells as well as tissue formation [90,91]. SEM images showed the highly porous structures of hydrogels which indicates the ability of hydrogels to support tissue formation. The high pore interconnectivity of the hydrogels that was observed in the images suggested facilitating the exchange of nutrients [27]. In addition, the pore size of the hydrogels are in the range of the size of the most mammalian cells, on the micron scale, which suggests the suitability of the hydrogels for supporting cell proliferation [92]. The wider range of porosity distribution and smaller pore size observed in hydrogels with

higher concentration of OAlg could be attribute to faster gelation time and higher crosslinking density.

The injectability test of the hydrogels showed their potential to be used to encapsulate cells homogenously and to be directly injected to the defect site [53]. The self-healing assays of the hydrogels confirmed the spontaneous ability of the OAlg-CMC hydrogels to repair themselves quickly once they are fractured under external forces which help them to keep their structural stability and mechanical strength [53].

The zone inhibition test revealed the antibacterial activity of the OAlg-CMC hydrogels at all three different mixture ratios towards *Streptococcus mutans* and *Streptococcus sobrinus*, that are known as two main bacterial that contribute to the enamel demineralization [93]. The antibacterial activity of the hydrogels could be attributed to the presence of chitosan and Schiff base reaction. The previous studies have reported the antibacterial and antibiofilm activities against cariogenic microorganisms including *Streptococcus mutans* and *Streptococcus sobrinus* [94,95]. The antibacterial effect of chitosan is due to the electrostatic interactions between the positive charges of amino groups in chitosan and the negatively charged bacterial walls [96]. In addition, it was found Schiff base reactions significantly increased the antimicrobial effects of chitosan [54,97].

The live/dead assay revealed that self-cross-linkable hydrogels provide a favorable 3D environment for cell survival without cytotoxic effects. No decrease in the viability of cells within the injected hydrogels was observed compared to hydrogels that were formed by mixing the hydrogel components in the wells without injection. This was in agreement with other studies reporting no cell damage after being extruded in self-healing injectable carboxyethyl chitosan and oxidized alginate from a syringe through the 21-gauge needle [30]. It was previously reported that although oxidized alginate has slight cytotoxic effect compared to alginate, the crosslinking of OAlg with CMC decreased the cellular toxicity due to the consumption of free aldehyde groups in OAlg in the crosslinking reactions [74].

Alkaline phosphatase is known as a marker of enamel matrix mineralization [98] that was found to be expressed in all groups of self-crosslinked hydrogels after 14 days of culture indicating their ability in supporting differentiation and function of dental epithelial stem cells. The HAT-7 cells

encapsulated in all groups of the self-cross-linkable hydrogels were stained positively with alizarin red S which is a common technique for detection of the calcium deposition [99]. The absence of the difference in the intensity of ALP and alizarin red S staining between the three groups of hydrogels might be due to the absence of differentiation inducing factors in growth media. SEM images of HAT-7 cells encapsulated in self-crosslinked hydrogels after 14 days of in vitro culture showed the ability of these cells to retain their normal round morphology inside the hydrogels. This is consistent with another study that reported the round morphology of HAT-7 cells in chitosan-collagen I hydrogels [100]. In addition, the formation of rod- and ribbon-like structures on the cell surface observed in the SEM images further confirmed the initiation of mineralization and differentiation of dental epithelial stem cells which is in agreement with the ALP and alizarin red staining results. Together, SEM images and ALP and alizarin red staining results demonstrated the ability of self-crosslinked hydrogels to support mineralization and enamel-like tissue formation.

5.6. Conclusions

Injectable hydrogels have a great application potential in the field of dental tissue regeneration. However, the conventional hydrogel-based cell carrier systems are often made from toxic crosslinkers and are prone to be damaged during injection or under mechanical forces leading to cell death or loss. In this work, injectable self-healing hydrogels were prepared by Schiff-base self-crosslinking reactions between aldehyde groups in oxidized alginate and amino groups in carboxymethyl chitosan and characterized to study their suitability for enamel tissue engineering application. The properties of the hydrogels were tuned by changing the oxidized alginate to carboxymethyl chitosan weight ratio. Hydrogels were quickly formed under five minutes which make them suitable for clinical applications. The gelation time and swelling degree of the hydrogels decreased as the weight ratio of oxidized alginate to carboxymethyl chitosan increased. The highly porous structure of the hydrogels suggested their ability to support cell migration and proliferation and to facilitate nutrient exchange. The self-cross-linkable hydrogels showed the self-healing ability after injection due to their dynamic imine bonds. The antibacterial performance of the hydrogels against cariogenic bacteria showed their potential to be used as cell carrier system and decrease the risk of bacterial infection during the tissue regeneration. Dental epithelial stem cell line, HAT-7 cells, maintained highly viable when encapsulated and injected within the self-

cross-linkable hydrogels, which suggested the suitability of the hydrogels for cell delivery vehicle and injection cell therapy. In addition, the self-cross-linkable hydrogels were able to support HAT-7 cells to maintain their round morphology and deposit minerals. Further studies are required to investigate the differentiation and mineralization of HAT-7 cells cultured in the self-cross-linkable hydrogels in the presence of differentiation media. Moreover, ex vivo and in vivo studies could be done to evaluate the suitability of the in situ forming hydrogels for clinical applications.

Acknowledgments

Authors would like to acknowledge the Saskatchewan Health Research Foundation (SHRF) and College of Dentistry start-up financial support (PI: PP), College of Medicine start-up funds (SP), Natural Science and Engineering Research Council (NSERC) of Canada (to XC), and the University of Saskatchewan Dean's scholarship and Biomedical Engineering Devolved Scholarship (to FM).

Authors' contribution: Conceptualization, F.M, S.P, X.C, P.P; Methodology, F.M, Z.Y; Formal analysis, F.M; Resources, S.P, X.C, P.P; Writing-Original Draft, F.M; Writing-Review & Editing, F.M, S.P, X.C, P.P; Supervision, S.P, X.C, P.P.

References

[1] D. Kim, J.P. Barraza, R.A. Arthur, A. Hara, K. Lewis, Y. Liu, E.L. Scisci, E. Hajishengallis, M. Whiteley, H. Koo, Spatial mapping of polymicrobial communities reveals a precise biogeography associated with human dental caries, Proc. Natl. Acad. Sci. 117 (2020) 12375–12386.

[2] W. Qiu, Y. Zhou, Z. Li, T. Huang, Y. Xiao, L. Cheng, X. Peng, L. Zhang, B. Ren, Application of antibiotics/antimicrobial agents on dental caries, Biomed Res. Int. 2020 (2020).

[3] M. Binder, L.C. Biggs, M.S. Kronenberg, P. Schneider, I. Thesleff, A. Balic, Novel strategies for expansion of tooth epithelial stem cells and ameloblast generation, Sci. Rep. 10 (2020) 1–11.

[4] M.J. Honda, Y. Shinmura, Y. Shinohara, Enamel tissue engineering using subcultured

enamel organ epithelial cells in combination with dental pulp cells, Cells Tissues Organs. 189 (2009) 261–267.

[5] M. Yazdanian, A.H. Arefi, M. Alam, K. Abbasi, H. Tebyaniyan, E. Tahmasebi, R. Ranjbar, A. Seifalian, A. Yazdanian, Decellularized and biological scaffolds in dental and craniofacial tissue engineering: a comprehensive overview, J. Mater. Res. Technol. (2021).

[6] X. Chatzistavrou, S. Papagerakis, P.X. Ma, P. Papagerakis, Innovative approaches to regenerate enamel and dentin, Int. J. Dent. 2012 (2012).

[7] V. Rosa, A. Della Bona, B.N. Cavalcanti, J.E. Nör, Tissue engineering: from research to dental clinics, Dent. Mater. 28 (2012) 341–348.

[8] Q. Dong, Y. Wang, F. Mohabatpour, L. Zheng, S. Papagerakis, D. Chen, P. Papagerakis, Dental Pulp Stem Cells: Isolation, Characterization, Expansion, and Odontoblast Differentiation for Tissue Engineering, in: Odontogenesis, Springer, 2019: pp. 91–101.

[9] G. Li, T. Zhou, S. Lin, S. Shi, Y. Lin, Nanomaterials for craniofacial and dental tissue engineering, J. Dent. Res. 96 (2017) 725–732.

[10] D.X.B. Chen, Extrusion Bioprinting of Scaffolds, in: Extrus. Bioprinting Scaffolds Tissue Eng. Appl., Springer, 2019: pp. 117–145.

[11] Z. Fang, M. Guo, Q. Zhou, Q. Li, H.M. Wong, C.Y. Cao, Enamel-like tissue regeneration by using biomimetic enamel matrix proteins, Int. J. Biol. Macromol. (2021).

[12] M.T. Duailibi, S.E. Duailibi, F.M.L. Dantas, P.C. Yelick, Scaffolds that promote enamel remineralization, in: Handb. Tissue Eng. Scaffolds Vol. One, Elsevier, 2019: pp. 545–562.

[13] K. Mukherjee, Q. Ruan, D. Liberman, S.N. White, J. Moradian-Oldak, Repairing human tooth enamel with leucine-rich amelogenin peptide–chitosan hydrogel, J. Mater. Res. 31 (2016) 556–563.

[14] R. Fang, W. Tian, X. Chen, Synthesis of injectable alginate hydrogels with muscle-derived stem cells for potential myocardial infarction repair, Appl. Sci. 7 (2017) 252.

[15] S. Qiao, Y. Zhao, C. Li, Y. Yin, Q. Meng, F.-H. Lin, Y. Liu, X. Hou, K. Guo, X. Chen, An alginate-based platform for cancer stem cell research, Acta Biomater. 37 (2016) 83–

92.

[16] R. Fang, S. Qiao, Y. Liu, Q. Meng, X. Chen, B. Song, X. Hou, W. Tian, Sustained co-delivery of BIO and IGF-1 by a novel hybrid hydrogel system to stimulate endogenous cardiac repair in myocardial infarcted rat hearts, Int. J. Nanomedicine. 10 (2015) 4691.

[17] X. Bai, R. Fang, S. Zhang, X. Shi, Z. Wang, X. Chen, J. Yang, X. Hou, Y. Nie, Y. Li, Self-cross-linkable hydrogels composed of partially oxidized alginate and gelatin for myocardial infarction repair, J. Bioact. Compat. Polym. 28 (2013) 126–140.

[18] B. Chang, N. Ahuja, C. Ma, X. Liu, Injectable scaffolds: Preparation and application in dental and craniofacial regeneration, Mater. Sci. Eng. R Reports. 111 (2017) 1–26.

[19] W. Toh, Injectable hydrogels in dentistry: Advances and promises, Austin J. Dent. 1 (2014) 1001.

[20] H.J. Haugen, P. Basu, M. Sukul, J.F. Mano, J.E. Reseland, Injectable Biomaterials for Dental Tissue Regeneration, Int. J. Mol. Sci. 21 (2020) 3442.

[21] K. Wang, Z. Han, Injectable hydrogels for ophthalmic applications, J. Control. Release. 268 (2017) 212–224.

[22] L. Yu, J. Ding, Injectable hydrogels as unique biomedical materials, Chem. Soc. Rev. 37 (2008) 1473–1481.

[23] A.A. Amini, L.S. Nair, Injectable hydrogels for bone and cartilage repair, Biomed. Mater. 7 (2012) 24105.

[24] C. Liu, Q. Zhang, S. Zhu, H. Liu, J. Chen, Preparation and applications of peptide-based injectable hydrogels, RSC Adv. 9 (2019) 28299–28311.

[25] Q.V. Nguyen, J.H. Park, D.S. Lee, Injectable polymeric hydrogels for the delivery of therapeutic agents: A review, Eur. Polym. J. 72 (2015) 602–619.

[26] R. Jin, L.S.M. Teixeira, P.J. Dijkstra, C.A. Van Blitterswijk, M. Karperien, J. Feijen, Enzymatically-crosslinked injectable hydrogels based on biomimetic dextran–hyaluronic acid conjugates for cartilage tissue engineering, Biomaterials. 31 (2010) 3103–3113.

[27] Z. Naghizadeh, A. Karkhaneh, A. Khojasteh, Self-crosslinking effect of chitosan and gelatin on alginate based hydrogels: injectable in situ forming scaffolds, Mater. Sci. Eng.

C. 89 (2018) 256–264.

[28] A.P. Mathew, S. Uthaman, K.-H. Cho, C.-S. Cho, I.-K. Park, Injectable hydrogels for delivering biotherapeutic molecules, Int. J. Biol. Macromol. 110 (2018) 17–29.

[29] L. Ma, W. Su, Y. Ran, X. Ma, Z. Yi, G. Chen, X. Chen, Z. Deng, Q. Tong, X. Wang, Synthesis and characterization of injectable self-healing hydrogels based on oxidized alginate-hybrid-hydroxyapatite nanoparticles and carboxymethyl chitosan, Int. J. Biol. Macromol. 165 (2020) 1164–1174.

[30] Z. Wei, J. Zhao, Y.M. Chen, P. Zhang, Q. Zhang, Self-healing polysaccharide-based hydrogels as injectable carriers for neural stem cells, Sci. Rep. 6 (2016) 37841.

[31] S. Talebian, M. Mehrali, N. Taebnia, C.P. Pennisi, F.B. Kadumudi, J. Foroughi, M. Hasany, M. Nikkhah, M. Akbari, G. Orive, Self-healing hydrogels: the next paradigm shift in tissue engineering?, Adv. Sci. 6 (2019) 1801664.

[32] N. Pathan, P. Shende, Strategic conceptualization and potential of self-healing polymers in biomedical field, Mater. Sci. Eng. C. 125 (2021) 112099.

[33] A.H. Pandit, N. Mazumdar, K. Imtiyaz, M.M. Alam Rizvi, S. Ahmad, Self-healing and injectable hydrogels for anticancer drug delivery: A study with multialdehyde gum arabic and succinic anhydride chitosan, ACS Appl. Bio Mater. 3 (2020) 8460–8470.

[34] H. Xu, L. Zhang, J. Cai, Injectable, self-healing, β-chitin-based hydrogels with excellent cytocompatibility, antibacterial activity, and potential as drug/cell carriers, ACS Appl. Bio Mater. 2 (2018) 196–204.

[35] S. Lü, C. Gao, X. Xu, X. Bai, H. Duan, N. Gao, C. Feng, Y. Xiong, M. Liu, Injectable and self-healing carbohydrate-based hydrogel for cell encapsulation, ACS Appl. Mater. Interfaces. 7 (2015) 13029–13037.

[36] Y. Li, Y. Zhang, F. Shi, L. Tao, Y. Wei, X. Wang, Modulus-regulated 3D-cell proliferation in an injectable self-healing hydrogel, Colloids Surfaces B Biointerfaces. 149 (2017) 168–173.

[37] J. Qu, X. Zhao, Y. Liang, T. Zhang, P.X. Ma, B. Guo, Antibacterial adhesive injectable hydrogels with rapid self-healing, extensibility and compressibility as wound dressing for joints skin wound healing, Biomaterials. 183 (2018) 185–199.

[38] K. Wang, R. Dong, J. Tang, H. Li, J. Dang, Z. Zhang, Z. Yu, B. Guo, C. Yi, Exosomes laden self-healing injectable hydrogel enhances diabetic wound healing via regulating macrophage polarization to accelerate angiogenesis, Chem. Eng. J. 430 (2022) 132664.

[39] S. Naghieh, M.D. Sarker, N.K. Sharma, Z. Barhoumi, X. Chen, Printability of 3D printed hydrogel scaffolds: Influence of hydrogel composition and printing parameters, Appl. Sci. 10 (2020) 292.

[40] H. Baniasadi, S. Mashayekhan, S. Fadaoddini, Y. Haghirsharifzamini, Design, fabrication and characterization of oxidized alginate–gelatin hydrogels for muscle tissue engineering applications, J. Biomater. Appl. 31 (2016) 152–161.

[41] N. Soltan, L. Ning, F. Mohabatpour, P. Papagerakis, X. Chen, Printability and cell viability in bioprinting alginate dialdehyde-gelatin scaffolds, ACS Biomater. Sci. Eng. (2019).

[42] F. Ding, S. Wu, S. Wang, Y. Xiong, Y. Li, B. Li, H. Deng, Y. Du, L. Xiao, X. Shi, A dynamic and self-crosslinked polysaccharide hydrogel with autonomous self-healing ability, Soft Matter. 11 (2015) 3971–3976.

[43] Z. Shariatinia, Carboxymethyl chitosan: Properties and biomedical applications, Int. J. Biol. Macromol. 120 (2018) 1406–1419.

[44] A. Sadeghianmaryan, S. Naghieh, Z. Yazdanpanah, H.A. Sardroud, N.K. Sharma, L.D. Wilson, X. Chen, Fabrication of chitosan/alginate/hydroxyapatite hybrid scaffolds using 3D printing and impregnating techniques for potential cartilage regeneration, Int. J. Biol. Macromol. (2022).

[45] A. Sadeghianmaryan, S. Naghieh, H.A. Sardroud, Z. Yazdanpanah, Y.A. Soltani, J. Sernaglia, X. Chen, Extrusion-based printing of chitosan scaffolds and their in vitro characterization for cartilage tissue engineering, Int. J. Biol. Macromol. 164 (2020) 3179–3192.

[46] H.R. Bakhsheshi-Rad, A.F. Ismail, M. Aziz, M. Akbari, Z. Hadisi, M. Omidi, X. Chen, Development of the PVA/CS nanofibers containing silk protein sericin as a wound dressing: In vitro and in vivo assessment, Int. J. Biol. Macromol. 149 (2020) 513–521.

[47] L. Fan, X. Pan, Y. Zhou, L. Chen, W. Xie, Z. Long, H. Zheng, Preparation and

characterization of crosslinked carboxymethyl chitosan–oxidized sodium alginate hydrogels, J. Appl. Polym. Sci. 122 (2011) 2331–2337.

[48] B. Sarker, D.G. Papageorgiou, R. Silva, T. Zehnder, F. Gul-E-Noor, M. Bertmer, J. Kaschta, K. Chrissafis, R. Detsch, A.R. Boccaccini, Fabrication of alginate–gelatin crosslinked hydrogel microcapsules and evaluation of the microstructure and physico-chemical properties, J. Mater. Chem. B. 2 (2014) 1470–1482.

[49] F. You, X. Wu, M. Kelly, X. Chen, Bioprinting and in vitro characterization of alginate dialdehyde–gelatin hydrogel bio-ink, Bio-Design Manuf. 3 (2020) 48–59.

[50] C.G. Gomez, M. Rinaudo, M.A. Villar, Oxidation of sodium alginate and characterization of the oxidized derivatives, Carbohydr. Polym. 67 (2007) 296–304.

[51] A. Mousavi, S. Mashayekhan, N. Baheiraei, A. Pourjavadi, Biohybrid oxidized alginate/myocardial extracellular matrix injectable hydrogels with improved electromechanical properties for cardiac tissue engineering, Int. J. Biol. Macromol. 180 (2021) 692–708.

[52] W. Huang, Y. Wang, Z. Huang, X. Wang, L. Chen, Y. Zhang, L. Zhang, On-demand dissolvable self-healing hydrogel based on carboxymethyl chitosan and cellulose nanocrystal for deep partial thickness burn wound healing, ACS Appl. Mater. Interfaces. 10 (2018) 41076–41088.

[53] W. Huang, Y. Wang, Y. Chen, Y. Zhao, Q. Zhang, X. Zheng, L. Chen, L. Zhang, Strong and rapidly self-healing hydrogels: Potential hemostatic materials, Adv. Healthc. Mater. 5 (2016) 2813–2822.

[54] H. Li, F. Cheng, X. Wei, X. Yi, S. Tang, Z. Wang, Y.S. Zhang, J. He, Y. Huang, Injectable, self-healing, antibacterial, and hemostatic N, O-carboxymethyl chitosan/oxidized chondroitin sulfate composite hydrogel for wound dressing, Mater. Sci. Eng. C. 118 (2021) 111324.

[55] S. Kawano, T. Morotomi, T. Toyono, N. Nakamura, T. Uchida, M. Ohishi, K. Toyoshima, H. Harada, Establishment of Dental Epithelial Cell Line (HAT-7) and the Cell Differentiation Dependent on Notch Signaling Pathway, Connect. Tissue Res. 43 (2002) 409–412. https://doi.org/10.1080/03008200290000637.

[56] Z. Emami, M. Ehsani, M. Zandi, R. Foudazi, Controlling alginate oxidation conditions for making alginate-gelatin hydrogels, Carbohydr. Polym. 198 (2018) 509–517.

[57] J. Park, J. Nam, H. Yun, H.-J. Jin, H.W. Kwak, Aquatic polymer-based edible films of fish gelatin crosslinked with alginate dialdehyde having enhanced physicochemical properties, Carbohydr. Polym. 254 (2021) 117317.

[58] Y. Wu, L. Yuan, N. Sheng, Z. Gu, W. Feng, H. Yin, Y. Morsi, X. Mo, A soft tissue adhesive based on aldehyde-sodium alginate and amino-carboxymethyl chitosan preparation through the Schiff reaction, Front. Mater. Sci. 11 (2017) 215–222.

[59] M. Kurniasih, T. Cahyati, R.S. Dewi, Carboxymethyl chitosan as an antifungal agent on gauze, Int. J. Biol. Macromol. 119 (2018) 166–171.

[60] T.-P. Nguyen, B.-T. Lee, Fabrication of oxidized alginate-gelatin-BCP hydrogels and evaluation of the microstructure, material properties and biocompatibility for bone tissue regeneration, J. Biomater. Appl. 27 (2012) 311–321.

[61] H. Liao, H. Zhang, W. Chen, Differential physical, rheological, and biological properties of rapid in situ gelable hydrogels composed of oxidized alginate and gelatin derived from marine or porcine sources, J. Mater. Sci. Mater. Med. 20 (2009) 1263–1271.

[62] W. Wang, M. Dang, Z. Zhang, J. Hu, T.W. Eyster, L. Ni, P.X. Ma, Dentin regeneration by stem cells of apical papilla on injectable nanofibrous microspheres and stimulated by controlled BMP-2 release, Acta Biomater. 36 (2016) 63–72. https://doi.org/https://doi.org/10.1016/j.actbio.2016.03.015.

[63] K.A. Fukushima, M.M. Marques, T.K. Tedesco, G.L. Carvalho, F. Gonçalves, H. Caballero-Flores, S. Morimoto, M.S. Moreira, Screening of hydrogel-based scaffolds for dental pulp regeneration—a systematic review, Arch. Oral Biol. 98 (2019) 182–194.

[64] F. Lee, K.H. Bae, M. Kurisawa, Injectable hydrogel systems crosslinked by horseradish peroxidase, Biomed. Mater. 11 (2015) 14101.

[65] C. Mo, L. Xiang, Y. Chen, Advances in Injectable and Self-healing Polysaccharide Hydrogel Based on the Schiff Base Reaction, Macromol. Rapid Commun. 42 (2021) 2100025.

[66] D.N. Heo, M.A. Alioglu, Y. Wu, V. Ozbolat, B. Ayan, M. Dey, Y. Kang, I.T. Ozbolat, 3D

bioprinting of carbohydrazide-modified gelatin into microparticle-suspended oxidized alginate for the fabrication of complex-shaped tissue constructs, ACS Appl. Mater. Interfaces. 12 (2020) 20295–20306.

[67] Q. Li, C. Liu, J. Wen, Y. Wu, Y. Shan, J. Liao, The design, mechanism and biomedical application of self-healing hydrogels, Chinese Chem. Lett. 28 (2017) 1857–1874.

[68] X. Yang, P. Li, W. Tang, S. Du, M. Yu, H. Lu, H. Tan, X. Xing, A facile injectable carbon dot/oxidative polysaccharide hydrogel with potent self-healing and high antibacterial activity, Carbohydr. Polym. 251 (2021) 117040.

[69] J. Xu, Y. Liu, S. Hsu, Hydrogels based on Schiff base linkages for biomedical applications, Molecules. 24 (2019) 3005.

[70] R. Resmi, J. Parvathy, A. John, R. Joseph, Injectable self-crosslinking hydrogels for meniscal repair: A study with oxidized alginate and gelatin, Carbohydr. Polym. 234 (2020) 115902.

[71] S. Zhu, X. Yu, S. Xiong, R. Liu, Z. Gu, J. You, T. Yin, Y. Hu, Insights into the rheological behaviors evolution of alginate dialdehyde crosslinked collagen solutions evaluated by numerical models, Mater. Sci. Eng. C. 78 (2017) 727–737.

[72] X. Li, X. Kong, Z. Zhang, K. Nan, L. Li, X. Wang, H. Chen, Cytotoxicity and biocompatibility evaluation of N, O-carboxymethyl chitosan/oxidized alginate hydrogel for drug delivery application, Int. J. Biol. Macromol. 50 (2012) 1299–1305.

[73] H. Chen, X. Xing, H. Tan, Y. Jia, T. Zhou, Y. Chen, Z. Ling, X. Hu, Covalently antibacterial alginate-chitosan hydrogel dressing integrated gelatin microspheres containing tetracycline hydrochloride for wound healing, Mater. Sci. Eng. C. 70 (2017) 287–295.

[74] X. Li, Y. Weng, X. Kong, B. Zhang, M. Li, K. Diao, Z. Zhang, X. Wang, H. Chen, A covalently crosslinked polysaccharide hydrogel for potential applications in drug delivery and tissue engineering, J. Mater. Sci. Mater. Med. 23 (2012) 2857–2865.

[75] B. Ren, X. Chen, S. Du, Y. Ma, H. Chen, G. Yuan, J. Li, D. Xiong, H. Tan, Z. Ling, Injectable polysaccharide hydrogel embedded with hydroxyapatite and calcium carbonate for drug delivery and bone tissue engineering, Int. J. Biol. Macromol. 118 (2018) 1257–

1266.

[76] X. Li, S. Chen, B. Zhang, M. Li, K. Diao, Z. Zhang, J. Li, Y. Xu, X. Wang, H. Chen, In situ injectable nano-composite hydrogel composed of curcumin, N, O-carboxymethyl chitosan and oxidized alginate for wound healing application, Int. J. Pharm. 437 (2012) 110–119.

[77] T. Hozumi, T. Kageyama, S. Ohta, J. Fukuda, T. Ito, Injectable hydrogel with slow degradability composed of gelatin and hyaluronic acid cross-linked by schiff's base formation, Biomacromolecules. 19 (2018) 288–297.

[78] H. Park, S.W. Kim, J.W. Lee, K.Y. Lee, Injectable hydrogels prepared from partially oxidized hyaluronate and glycol chitosan for chondrocyte encapsulation, Carbohydr. Polym. 157 (2017) 1281–1287.

[79] S. Guan, K. Zhang, L. Cui, J. Liang, J. Li, F. Guan, Injectable gelatin/oxidized dextran hydrogel loaded with apocynin for skin tissue regeneration, Mater. Sci. Eng. C. (2021) 112604.

[80] B. Balakrishnan, A. Jayakrishnan, Self-cross-linking biopolymers as injectable in situ forming biodegradable scaffolds, Biomaterials. 26 (2005) 3941–3951.

[81] B. Balakrishnan, S. Lesieur, D. Labarre, A. Jayakrishnan, Periodate oxidation of sodium alginate in water and in ethanol–water mixture: a comparative study, Carbohydr. Res. 340 (2005) 1425–1429.

[82] R. Rajalekshmi, A.K. Shaji, R. Joseph, A. Bhatt, Scaffold for liver tissue engineering: Exploring the potential of fibrin incorporated alginate dialdehyde–gelatin hydrogel, Int. J. Biol. Macromol. 166 (2021) 999–1008.

[83] E. Höglund, Production of dialdehyde cellulose and periodate regeneration: Towards feasible oxidation processes, (2015).

[84] S. Reakasame, A.R. Boccaccini, Oxidized alginate-based hydrogels for tissue engineering applications: a review, Biomacromolecules. 19 (2018) 3–21.

[85] E. Astudillo-Ortiz, P.S. Babo, R.L. Reis, M.E. Gomes, Evaluation of Injectable Hyaluronic Acid-Based Hydrogels for Endodontic Tissue Regeneration, Materials (Basel). 14 (2021) 7325.

[86] J. Liu, J. Li, F. Yu, Y. Zhao, X. Mo, J. Pan, In situ forming hydrogel of natural polysaccharides through Schiff base reaction for soft tissue adhesive and hemostasis, Int. J. Biol. Macromol. 147 (2020) 653–666.

[87] G. Jalani, D.H. Rosenzweig, G. Makhoul, S. Abdalla, R. Cecere, F. Vetrone, L. Haglund, M. Cerruti, Tough, In-Situ Thermogelling, Injectable Hydrogels for Biomedical Applications, Macromol. Biosci. 15 (2015) 473–480.

[88] G.-W. Oh, S.-C. Kim, T.-H. Kim, W.-K. Jung, Characterization of an oxidized alginate-gelatin hydrogel incorporating a COS-salicylic acid conjugate for wound healing, Carbohydr. Polym. 252 (2021) 117145.

[89] P. Chuysinuan, P. Nooeaid, T. Thanyacharoen, S. Techasakul, P. Pavasant, K. Kanjanamekanant, Injectable eggshell-derived hydroxyapatite-incorporated fibroin-alginate composite hydrogel for bone tissue engineering, Int. J. Biol. Macromol. 193 (2021) 799–808.

[90] B. Sarker, W. Li, K. Zheng, R. Detsch, A.R. Boccaccini, Designing porous bone tissue engineering scaffolds with enhanced mechanical properties from composite hydrogels composed of modified alginate, gelatin, and bioactive glass, ACS Biomater. Sci. Eng. 2 (2016) 2240–2254.

[91] K. Kim, A. Yeatts, D. Dean, J.P. Fisher, Stereolithographic bone scaffold design parameters: osteogenic differentiation and signal expression, Tissue Eng. Part B Rev. 16 (2010) 523–539.

[92] L. Zhang, J. Liu, X. Zheng, A. Zhang, X. Zhang, K. Tang, Pullulan dialdehyde crosslinked gelatin hydrogels with high strength for biomedical applications, Carbohydr. Polym. 216 (2019) 45–53.

[93] S.-J. Ahn, B.-S. Lim, S.-J. Lee, Prevalence of cariogenic streptococci on incisor brackets detected by polymerase chain reaction, Am. J. Orthod. Dentofac. Orthop. 131 (2007) 736–741.

[94] Z. Abedian, N. Jenabian, A.A. Moghadamnia, E. Zabihi, H. Tashakorian, M. Rajabnia, F. Sadighian, A. Bijani, Antibacterial activity of high-molecular-weight and low-molecular-weight chitosan upon oral pathogens, J. Conserv. Dent. JCD. 22 (2019) 169.

[95] A. Aliasghari, M.R. Khorasgani, S. Vaezifar, F. Rahimi, H. Younesi, M. Khoroushi, Evaluation of antibacterial efficiency of chitosan and chitosan nanoparticles on cariogenic streptococci: an in vitro study, Iran. J. Microbiol. 8 (2016) 93.

[96] D.R. Perinelli, L. Fagioli, R. Campana, J.K.W. Lam, W. Baffone, G.F. Palmieri, L. Casettari, G. Bonacucina, Chitosan-based nanosystems and their exploited antimicrobial activity, Eur. J. Pharm. Sci. 117 (2018) 8–20.

[97] S.M. Anush, B. Vishalakshi, B. Kalluraya, N. Manju, Synthesis of pyrazole-based Schiff bases of Chitosan: Evaluation of antimicrobial activity, Int. J. Biol. Macromol. 119 (2018) 446–452.

[98] K. Yoshizaki, L. Hu, T. Nguyen, K. Sakai, M. Ishikawa, I. Takahashi, S. Fukumoto, P.K. DenBesten, D.D. Bikle, Y. Oda, Mediator 1 contributes to enamel mineralization as a coactivator for Notch1 signaling and stimulates transcription of the alkaline phosphatase gene, J. Biol. Chem. 292 (2017) 13531–13540.

[99] C.A. Gregory, W.G. Gunn, A. Peister, D.J. Prockop, An Alizarin red-based assay of mineralization by adherent cells in culture: comparison with cetylpyridinium chloride extraction, Anal. Biochem. 329 (2004) 77–84.

[100] S. Ravindran, Y. Song, A. George, Development of three-dimensional biomimetic scaffold to study epithelial–mesenchymal interactions, Tissue Eng. Part A. 16 (2010) 327–342.

Chapter 6. Conclusions and future perspectives

6.1. Concluding remarks

Tissue engineering, as a rapidly developing field, holds a great potential for the regeneration of dental tissues. The commonly used clinical treatments for the repair of tooth damage or loss have several limitations. Briefly, synthetic materials used as dental fillings lack the vital properties of native dental tissues. There are still a number of research issues that need to be addressed in order to create the scaffolds and/or constructs that resemble both structural and functional features of the native enamel. Currently, there is a lack of bioink that have good printability, and favorable mechanical and biological characteristics, and injectable hydrogels with self-healing, antibacterial properties that are designed for the regeneration of dental enamel. A large number of transcription factors and growth factors have been identified to be essential for natural tooth development. However, the efficiency of genes encoding such signalling molecules to induce ameloblast differentiation and enamel formation has not yet been fully explored. The gene delivery systems that have been specifically designed for the transfer of genes encoding siglaning factors for the regeneration of dental tissues are limited. By addressing some of the issues, this study aimed to develop methods for enamel regeneration *in vitro* based on gene therapy and tissue engineering principles. The main conclusions drawn from this study are summarized below:

- Physicochemical and biological characteristics of lipid/pDNA complexes (or lipoplexes) could be optimized by varying the ratio of cationic lipid nitrogen to pDNA phosphate (N/P ratio). Both gemini surfactant- and DOTAP-based nanoparticles with higher N/P ratios have shown smaller particle size, more positive surface charge, better DNA compaction and protection, superior transfection efficiency (resulting in higher *Tbx1* mRNA expression) but also higher cytotoxicity.
- Gemini surfactant-based lipoplexes showed higher level of *Tbx1* upregulation compared to DOTAP-based lipoplexes.
- Based on the physicochemical and biological characterization of lipoplexes, gemini surfactant-based lipoplexes with a N/P ratio of 5 was found to provide high level of *Tbx1* upregulation with relatively low cytotoxicity and thus was selected as the optimal

formulation to transfer *Tbx1*gene into dental epithelial stem cells to induce ameloblast differentiation.

- *Tbx1* gene delivery to dental epithelial stem cells using optimized gemini surfactant-based nanoparticles could promote more robust ameloblast differentiation by regulating the expression of the ameloblast markers and enhancing mineral deposition.
- The gelatin methacrylate hydrogel-based 3D culture systems were able to support calcium, deposition and formation of mineralized nodules and elongated crystals which may be due to mimicking the gel-like environment that exist during the mineralization of the native enamel.
- The novel two-component bioink composed of alginate and carboxymethyl chitosan was printed as multilayer scaffolds with highly porous structures. Among the three mixture ratios, the ones with higher concentrations of alginate were more viscous and needed higher pressure to be extruded. The 3D printed hydrogel scaffolds with higher carboxymethyl chitosan ratios had higher swelling ratios, faster degradation rates, and lower compressive modulus. Alginate-carboxymethyl chitosan scaffolds supported both high cell viability, with negligible cytotoxic effect of printing process, and the initiation of mineralization and ameloblast differentiation.
- In situ forming hydrogels were prepared by mixing oxidized alginate and carboxymethyl chitosan hydrogels solutions. The weight ratios of oxidized alginate to carboxymethyl chitosan (OAlg:CMC) were found to play an important role in physicochemical properties of scaffolds. Hydrogels with higher OAlg:CMC ratios had faster gelation time and lower swelling ratio. The OAlg-CMC hydrogels showed injectability, self-healing properties and could inhibit the growth of cariogenic bacteria. Injectable OAlg-CMC hydrogels could also support cell viability as well as the initiation of mineralization and ameloblast differentiation.
- All hydrogel-based scaffolds that were characterized in this work, gelatin methacrylate, 3D printed alginate-carboxymethyl chitosan and in situ forming oxidized alginate/carboxymethyl chitosan hydrogels, could provide a favorable environment for cells and support dental epithelial stem cell functions.

6.2. Directions for future work

By extending the present research, the following studies would be of interest and promising for future work in this field.

- The physico-chemical characterization of lipoplexes that was carried out in this study could determine the essential requirements for the design of an efficient gene delivery system. In the future, additional characterizations such as the assessment of colloidal stability of lipoplexes in salt- and serum-containing media, pDNA loading efficiency, the evaluation of pDNA conformational change and condensation by circular dichroism spectroscopy and atomic force microscopy, may provide further information about other properties of the lipoplexes.
- The biological characterization of lipoplexes that was performed in this study could provide information about the cytotoxicity and mRNA expression of the target gene after transfection that allowed the selection of the optimal formulation. In the future, the biological characteristics of lipoplexes could be further evaluated with the investigation of cellular uptake and subcellular distribution of the lipoplexes.
- The extensive in vitro assessment of ameloblast differentiation and mineral deposition after *Tbx1* transfection that was carried out in this study could provide basic evidence about the formation of enamel-like tissue. In the future, the quantitative evaluation of mineralization level using Raman spectroscopy, energy dispersive spectroscopy, X-ray micro-computed tomography or synchrotron X-ray imaging, could further verify the promoting effect of *Tbx1* upregulation on enamel mineralization. In addition, the evaluation of cell proliferation after transfection could provide additional information about the effect of *Tbx1* upregulation on other dental epithelial stem cell functions.
- There are a wide range of transcription and growth factors involved in ameloblast differentiation and enamel formation. In this study we only considered investigated the effect of *Tbx1* gene. To overcome this limitation and better mimic natural enamel development, a combination of transcription for growth factors could be used to induce enamel secretion in dental epithelial stem cells.
- In this study, the gelatin methacrylate hydrogels were used for 3D culture of *Tbx1* transfected-dental epithelial stem cells based on the parameters found in papers such as the

polymer concentration and UV exposure time. Further characterization of hydrogels including the assessment of mechanical properties, degradation rate, swelling behavior, the effect of UV exposure time or polymer concentration on cell functions is recommended.

- The physico-chemical characterization of the 3D printed alginate-carboxymethyl chitosan and in situ forming oxidized alginate-carboxymethyl chitosan hydrogels that was conducted in this study determined some of the essential properties of the scaffolds as cell carriers. In the future, additional characterizations including more comprehensive printability tests for 3D printed alginate-carboxymethyl chitosan hydrogels to obtain structures with the same range of strand and pore size that more closely resemble the designed structure, rheological evaluation of the hydrogels and mechanical test under a dynamic condition is recommended.
- The biological characterization of 3D printed alginate-carboxymethyl chitosan hydrogels and the in situ forming alginate-carboxymethyl chitosan that was carried out in this thesis could provide the basic information about the suitability of these hydrogel-based scaffolds for enamel regeneration. Additional *in vitro* assays are required to further study the behavior of dental epithelial stem cells such as proliferation, differentiation, and mineralization in the hydrogels. In addition, the cell-laden hydrogel scaffolds were cultured in growth media in this study. It is highly recommended to study enamel-like tissue formation within the hydrogel constructs in the presence of differentiation media.
- The stiffness of the hydrogels was found to have an important regulatory effect on stem cells differentiation. It is recommended to investigate how cell behavior such as proliferation, ameloblast differentiation and mineralization is affected by matrix stiffness and to find a hydrogel system with the optimum stiffness for enamel formation.
- Hydrogels without cells can be used as control groups for ALP and alizarin Red S staining of cell-laden hydrogels.
- In this dissertation, 3D printed scaffolds were fabricated from hydrogels alone which inherently have poor mechanical properties, structural stability, and integrity. Combining hydrogels with other thermoplastic polymers such as polycaprolactone (PCL) that possess high mechanical properties could overcome this limitation. PCL provides the mechanical and structural strength for the structure and hydrogels allows the incorporation of cells and growth factors in the 3D printed PCL/hydrogel structures.

- The epithelial-mesenchymal interactions were found to be vital for the development of dental enamel and whole tooth. Thus, it is recommended to investigate the ameloblast differentiation of dental epithelial stem cells co-cultured with dental pulp stem cells in a 3D printed dual compartment scaffold that are separated with a nanofibrous membrane that allows cell-cell communication without cell migration.
- Combination of boosting dental epithelial stem cells with *Tbx1* gene delivery and encapsulating the *Tbx1*-transfected cells in the hydrogel with optimum stiffness, and co-culture with dental pulp stem cells in a dual compartment scaffold could allow the production of optimum enamel formation *in vitro*.
- HAT-7 cells that have been used in this study is a dental epithelial cell line derived from rat. The duration of tooth development in rodents is different from humans which might affect the concentration of *Tbx1,* and the duration required for ameloblast differentiation and mineralization. To overcome these difficulties, dental epithelial stem cells derived from human can be used to better optimize *Tbx1* gene delivery system and hydrogel-based cell carriers.
- The clinical feasibility of enamel tissue engineering might be challenging due to the available cell sources for dental epithelial cells that can be expanded and yield a sufficient number of cells.
- Finally, the results obtained from this dissertation are promising for the development of enamel-like tissue *in vitro*. However, *in vitro* models do not closely mimic the complications of the *in vivo* conditions. Thus, the evaluation of the regenerative potential of the optimized Tbx1-gene delivery system and hydrogel-based scaffolds in animal models or even in vivo caries models could provide the correlation between in vitro and in vivo studies and assess clinical relevance. The long-term goal of this work will be to directly transplant the *Tbx1*-transfected cells to fill cavity and/or repair a enamel defect or to fabricate bio-enamel generated in the lab and integrated into a specialized scaffold with regenerative potential that can be placed into the patient's tooth and fill a cavity.